INSIGHTS INTO THE BEHAVIOUR OF HYDROPHOBICALLY MODIFIED ETHOXYLATED URETHANE POLYMERS IN SOFT AND HARD COLLOID FORMULATION

MERVAT SHAFIK SOLYMAN IBRAHIM

A thesis submitted in partial fulfilment of the requirements of the University of Greenwich for the Degree of Doctor of Philosophy

March 2018

DECLARATION

I certify that the work contained in this thesis, or any part of it, has not been accepted in substance for any previous degree awarded to me, and is not concurrently being submitted for any degree other than that of Doctor of Philosophy being studied at the University of Greenwich. I also declare that this work is the result of my own investigations, except where otherwise identified by references and that the contents are not the outcome of any form of research misconduct.

…………………………………………….. Mervat S. Ibrahim (Candidate)

………………………………………….. Date

………………………………………….. Professor P. C. Griffiths (Supervisor)

………………………………………….. Date

………………………………………….. Dr. B. D. Alexander (Supervisor)

………………………………………….. Date

ACKNOWLEDGEMENTS

Firstly, I would like to express my sincere gratitude to my first supervisor Prof. Peter Griffiths for the continuous support of my Ph.D study, for his patience, motivation, and immense knowledge. I'm very grateful for Dr Bruce Alexander, my second supervisor, for the discussion that we had which incentivised me to widen my research from various perspectives. My supervisors guidance helped me in all the time of research and writing of this thesis.

Besides my University supervisors, I would like to thank the AkzoNobel supervisory team: Dr Martin Murray, Dr Agnieszka Szczygiek and Dr Beth Green for their insightful comments, encouragement.

I thank my fellow labmates, Omar and Leesa for the stimulating discussions in the group meeting. Also, I thank my friends especially Leesa, Karifa, Hana, Voula, Rob, Ionut, Wasiu, Elody, and Ruw for the moral support, hangouts, and for all the fun we have had in the last three years.

Last but not the least, I would like to thank my family: my parents, sister and cousins for their endless love and support.

ABSTRACT

Hydrophobically modified ethoxylated urethane polymers (HEUR) are used as viscosity modifiers in various formulations, *e.g.* cosmetics, paints. The HEURS show a complex behaviour in solution owing to the interaction between the hydrophobic segments present in the polymer and other formulation components. Since HEUR containing formulations are complex and multi-component, binary mixtures of HEURs with other formulation components *e.g.* surfactant, particles and oil were initially examined. The study was then expanded to model ternary formulations - polymer/ sodium dodecylsulphate (SDS)/latex and polymer/SDS/oil. The main techniques used here were nuclear magnetic resonance and small-angle neutron scattering.

The HEUR showed evidence of strong interaction with SDS, where the SDS interacts both with the polymer hydrophilic and hydrophobic segments. The effect of varying the HEUR architecture on the behaviour of polymer in solution and the interaction with SDS has been explored by studying three different polymers, C_6-L-$(EO_{100}$-L$)_9$-C_6, C_{10}-L-$(EO_{200}$-L$)_4$-C_{10}, and C_{18}-L-$(EO_{200}$-L$)_7$-C_{18} . It has been concluded that the linkers play an important role in the behaviour of the polymer, where the polymer that possess more linkers show higher viscosity and lower diffusion coefficient at fixed concentration.

The key polymer investigated here C_6-L-$(EO_{100}$-L$)_9$-C_6 showed weak adsorption to a hydrophobic (polystyrene-butylacrylate) latex. Decreasing the hydrophobicity of the particles turned off the adsorption of the polymer. The addition of SDS to the polymer/latex mixture further weakened the polymer adsorption to the hydrophobic latex. It was therefore concluded that the polymer/SDS interaction was stronger than polymer/latex interaction.

Finally, the three same polymers with different architectures were used to stabilise a model emulsion dodecane in water in which the oil droplets were stabilised in the polymer network. The addition of SDS to the emulsion shows a synergistic effect for the oil solubilisation. Evidence of SDS interaction with the polymer in the emulsion has been observed. This work developed insights into the interaction of the HEUR in model formulation by highlighting the key interactions and factors in the formulation.

CONTENTS

.

FIGURES

xvii

xxi

xxii

TABLES

List of Abbreviations and Symbols

This is a list of the most commonly used abbreviations in this thesis, followed by a list of the symbols used.

16-DSE	16-doxyl-stearic acid methyl ester
AA-BA-PSL	acrylic acid stabilised butylacrylate-polystyrene latex
ANS	8-Anilinonaphthalene-1-sulfonic acid
AT	associative thickeners
BA-MMAL	butylacrylate-methylmethacrylic acid latex
BA-PSL	butylacrylate-styrene latex
C^*	critical overlap concentration
$C_{12} E_6$	hexaethylene glycol monododecyl
CAC	critical aggregation concentration
CD	cyclodextrin
CMC	critical micelle concentration
CPCl	cetylpyridinum chloride
DLS	dynamic light scattering
D_s	self-diffusion coefficient
DTAB	dodecyltrimethylammonium bromide
EPR	electron-paramagnetic resonance
$H_{12}MDI$	4,4'-diisocyanatodicyclohexylmethane
HASE	hydrophobically modified alkali swellable polymers
HDI	hexamethylene diisocyanate
HEURs	hydrophobically modified ethoxylated urethane polymers
HM-EHEC	hydrophobically modified ethylhydroxyethyl cellulose
HM-HEC	hydrophobically modified hydroxyethyl cellulose
HMPs	hydrophobically modified polymers

MAA-MMAL	methylmethacrylate-methacrylic acid latex
MA-BAL	methylacrylate-butylacrylate latex
MDI	4,4'-methylene diphenyl diisocyanate
MS	molar substitution
n.d.	not determined
N_{agg}	aggregation number
NMR	nuclear magnetic resonance
NPE10	nonylphenol (10) ethoxylate
PCS	photon correlation spectroscopy
PDI	polydispersity index
PEO	poly(ethylene oxide)
PEOM	hydrophobically modified poly(ethylene oxide)
PS-BAL	polystyrene-butylacrylate latex
PSL	polystyrene latex
PVP	polyvinylpyrrolidone
R_{2sp}	specific relaxation rate
RF	radio frequency
R_H	hydrodynamic radius
SANS	small-angle neutron scattering
SAXS	small-angle X-ray scattering
SDS	sodium dodecylsulphate
SLD	scattering length density
TICT	twisted intramolecular charge transfer
UV	ultraviolet spectroscopy
η_r	relative viscosity
Δ	diffusion time
$\Delta\rho$	difference in SLD of sample and solvent
B_{inc}	incoherent background
D_{min}	minimum diffusion cofficient
D_r	relative diffusion cofficient
G	field gradient

γ	surface tension
$I(Q)$	scattered intensity
k	gradient parameter
$P(Q)$	form factor
Q	wavevector
$S(Q)$	structure factor
V_{max}	maximum viscosity
T_1	spin-lattice relaxation
T_2	spin-spin relaxation
β	β parameter
δ	gradient pulse duration
τ	relaxation time

Chapter 1. Introduction

1. Introduction

1.1. Associative thickeners in solution

1.1.1. Classification of associative polymers

Hydrophobically modified polymers (HMPs) are water-soluble polymers comprising hydrophilic backbones into which hydrophobic chains have been chemically incorporated. They are often classified as end-capped (telechelic) or comb-like, depending on the location of these hydrophobic groups (1). Also known as associative thickeners (ATs), there are three common families of HMPs: hydrophobically-modified polyacrylate thickeners (HASE), a group of cellulose derivatives, and hydrophobically modified poly(ethylene oxide) (2).

HASE polymers consist of a polyacrylate backbone, with hydrophobic macro-monomers distributed along the polymer backbone. The polymer exists as an insoluble latex dispersed in an aqueous medium at low pH. Upon raising the pH, the polymer chains expand as a result of electrostatic repulsion of the negative charges on the polymer backbone. The polymer becomes water-soluble, but its hydrophobic groups self-associate. The concentration of charges along the backbone and the ionic strength of the solution significantly affects the rheological behaviour (3). Hydrophobically modified cellulose derivatives consist of long-chain cellulose derivatives to which small amounts of hydrophobic substituents are grafted. The rigidity of the polymer backbone and the association in solution contribute to the viscosifying ability of this family (4).

By far, the most widely studied family of associative thickeners is the hydrophobically modified poly(ethylene oxide). The hydrophobic modification of poly(ethylene oxide) (PEO) based polymers can be by direct incorporation of an aliphatic alcohol, alkyl phenyl, or fluorocarbon group as the end-groups. These polymers are known as hydrophobically modified poly(ethylene oxide) (PEOM) (5). A urethane linker can be used to attach the hydrophobic end-group to the PEO backbone or link the PEO segments to each other as well as the hydrophobic end-group to the backbone. These polymers are known as hydrophobically modified ethoxylated urethane (HEUR) (1). Telechelic polymers can be modified with the hydrophobic group at one end to be mono-functionalised or both ends to be di-functionalised (6).

Chapter 1. Introduction

1.1.2. Aggregation of associative thickeners in solution

The presence of hydrophobic regions in the HMPs structure induces a complex, concentration-dependent set of *inter-* and *intra-*molecular associations, dependent on factors such as the length of the hydrophilic backbone and the number, length, and distribution of the hydrophobic groups. The concentration at which hydrophobic aggregates of the polymer are formed is called critical aggregation concentration (CAC) (7).

In di-functionalised telechelic polymers below the critical aggregation concentration (CAC), polymers adopt the so-called loop, bridge, and closed loop conformations. At the CAC, flower micelles are formed. Above the CAC, flower micelles tend to associate into super-bridges, super-loops, dangling ends, and hence clusters of flower micelles are formed (Figure 1.1). Further increase in the concentration forces the flower micelles to overlap and reach the critical overlap concentration (C^*). Above C^*, upon further increase of the concentration, a network structure is formed (8–14).
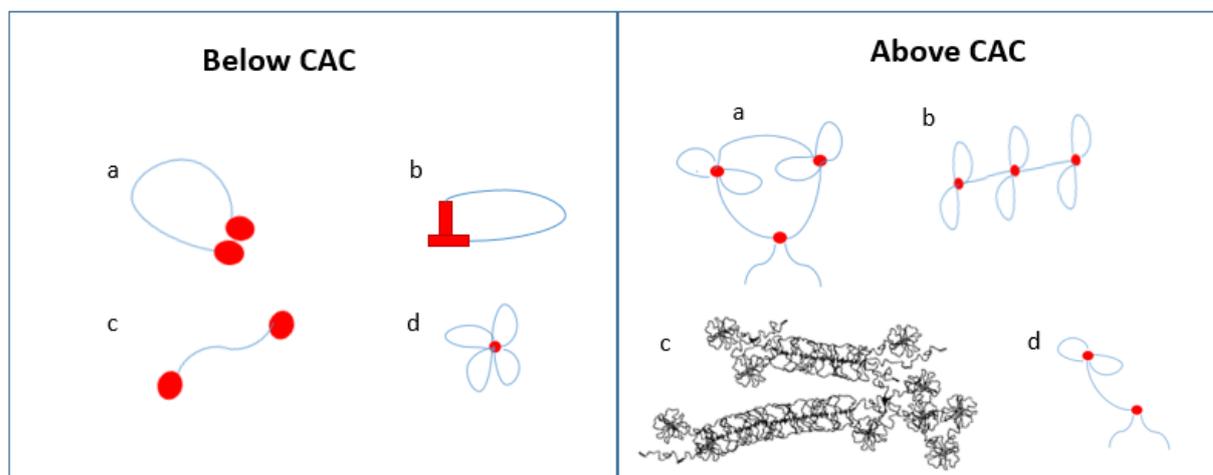
Figure 1.1. The conformation of di-functionalised telechelic polymers below the CAC in: a) loop, b) closed loop, c) bridge, d) flower micelle, and above CAC in a) super-loops, b) and c) super-bridge, and d) dangling ends reproduced from (8–10).

Yekta *et al.* used fluorescence spectroscopy to determine the CAC of two di-functionalised PEOMs denoted as PEOM-20-12, and PEOM-20-16 where the first number is the molecular weight of the polymer in kg mol^{-1} and the second number is the length of the hydrophobic end-group (11). Pyrene was used as a fluorescence probe, where it has five vibronic peaks. The ratio of the pyrene I/III peak was used as a polarity index where water has a I/III ratio of 1.8-1.9 and non-polar solvent 0.9. The CAC was

Chapter 1. Introduction

taken at the onset of the I/III ratio change. The I/III ratio decreases as a function of PEOM concentration due to the presence of hydrophobic aggregates. The PEOM-20-16 shows lower CAC relative to PEOM-20-12 due to the increase in hydrophobicity which, in turn, enhances the formation of flower micelles at low concentration (11).

Xu *et al.* conducted a quenching fluorescence experiment using HEUR-51-16 to determine the aggregation number (N_{agg}) of hydrophobic end-groups per micelle (15). The N_{agg} of the HEUR is 22 ± 2 hydrophobic end-groups, which remains constant at HEUR concentration from 0.1-1.2 wt%. Persson *et al.* suggested that the N_{agg} of $C_{12}EO_{200}C_{12}$ (PEOM-10-12) studied by electron-paramagnetic resonance (EPR) is 31 ± 6 over a range of polymer concentration varied from 0.2 to 5 wt% (5). Over these concentrations, the local viscosity and micro-polarity of the samples investigated are invariant suggesting that the structure of the hydrophobic aggregates stays unchanged in those concentration ranges. The non-telechelic polymers usually have smaller N_{agg} values. A comb-like C_{16} hydrophobically modified hydroxyethylcellulose (HM-HEC), with roughly five pendent hydrophobes per chain of molecular weight 250,000 g mol^{-1}, has N_{agg} equivalent to three hydrophobes per aggregate (16).

Dynamic light scattering (DLS) was used to study the telechelic polymers (PEOM-20-12) association mode (17). The studies divided the association mode into two steps. The first step is closed association forming the flower-like micelles, and the second step is open associations corresponds to the formation of clusters.

Above the polymer critical overlap concentration (C^*), as the flower micelles get closer to each other, cubic order is formed, leading to a correlation peak in small-angle neutron scattering (SANS) curves for PEOM-32-16 (18). This correlation peak disappears as the flower-like micelles interpenetrate at even higher concentrations and the PEOM behaviour resemble the parent semi-dilute PEO behaviour. However, if the PEO chains are matched in 7.7 % D_2O/H_2O mixture, the hydrophobic aggregates are shown to maintain their organization. Some papers reported the co-existence of a lamellar phase with the cubic phase of PEOM at higher concentrations (19,20).

1.1.3. Solution behaviour of associative thickeners

Abrahmsen-Alami *et al.* studied the response of the diffusion coefficient of PEOM-20-16 at 20 °C to the increases in the concentration within the one phase region and 25 °C for PEOM-20-12 (21). The diffusion coefficient measured by diffusion nuclear magnetic

resonance (NMR) decreases as a function of the polymer concentration due to the increase in the aggregate size and interaction between them. The self-diffusion coefficient of PEOM-20-16 is slower than PEOM-20-12. A phase transition is observed in the diffusion curve at C^* of the two polymers. Below the CMC, the signal decay as a function of gradient parameters curves fit a single exponential model (single diffusion coefficient is extracted), indicating a single diffusive rate; however, at the CAC and higher concentrations, the curves fit to a stretched model (generally used for polydisperse sample where single diffusion is extracted and polydispersity of the sample is noted) due to the polydispersity of the aggregates. The polydispersity of the aggregates above the CMC was reported by some authors for various telechelic e.g. Persson *et al.* for PEOM-10-12, Urema *et al.* for HEUR-51-16, Walderhaug *et al.* for PEOM-6-[8-18] and Choi *et al.* for HEUR-35-8, HEUR-35-12, and HEUR-35-18 (22–25). Choi *et al.* reported two phase transitions for HEUR-3-18, the first phase transition is indicative of CAC and a second one for C^* (24).

The decrease in diffusion coefficient as a function of telechelic polymer concentration is reflected by a rapid increase in low-shear viscosity of polymer solution. Beaudoin *et al.* compared the viscosity of parent PEO-32 to mono- and di-functionalised PEOM-32-16 (6). The viscosity of mono-functionalised PEO is higher than that of the parent PEO polymer due to the formation of micelles above the CAC. The di-functionalised PEO shows a significantly higher viscosity than the parent and mono-functionalised PEO due to the formation of micelles and bridging of polymer chains between the formed micelles. Some factors such as length of the hydrophobic end-group (25) and PEO backbone (1) affects the HEUR viscosity. Below C^*, the viscosity of telechelic polymers increases as hydrophobic end-group chain length increases due to the formation of hydrophobic aggregates at lower concentration (26,27).

The increase in viscosity as a function of C-chain length above C^* is correlated to the increase of the residence time of the hydrophobes in the hydrophobic aggregate and hence, the strength of cross-linking points increases (1). Factors that weaken the strength of network structure, *e.g.* decrease in number or strength of cross-link points, leads to a significant decrease in viscosity. The addition of cyclodextrins to AT solutions encapsulates the hydrophobic end-groups and prevent their association, leading to a decrease in the number of cross-linking points (28–30). The addition of a water-miscible solvent such as methanol shortens the residence time of crosslinks and reduces the

strength of cross-linking points (31). The length of PEO segment affects the behaviour of the polymer at fixed C-chain length. The telechelic with smaller PEO shows lower CAC, higher N_{agg}, and increased number of junction points, hence higher low-shear viscosity. In terms of rheology, a less elastic network is formed and shorter relaxation times are observed (32).

In addition to the length of C-chain (33), molar substitution (MS) of the hydrophobes in non-telechelic polymers affects the AT solution viscosity. Low MS of hydrophobes are directly proportional to viscosity as a result of the *inter*-molecular association between molecules that forms the network structure. However, *intra*-molecular association is observed at high molecular substitution showing a negative correlation to viscosity and can lead to decreasing solubility of the polymer in water. In addition, the random distribution of the hydrophobes along the polymer backbone shows better viscosity enhancement relative to blockier structures at a fixed polymer concentration (1).

1.1.4. Rheological behaviour of associative thickeners

In terms of rheology, some HEUR show a nonlinear shear profile. A Newtonian region at low shear, followed by shear thickening at moderate shear, and shear thinning behaviour at high shear is observed (34,35). Early reports explained the shear thickening region by deformation of the bridging polymer molecules by stretching at moderate shear followed by fragmentation of the clusters into smaller aggregates at high shear, reflected by shear thinning behaviour (11). Tam *et al.* extensively studied the behaviour of HEUR-35-16 at 2 wt% (above C^*) in solution where the three shear-dependent behaviours of the polymer are observed; Newtonian (region N), shear thickening (region TK), and shear thinning (Figure 1.2) (36). The shear thinning region is divided into three regions denoted as TN1, TN2, and TN3 (Figure 1.2).
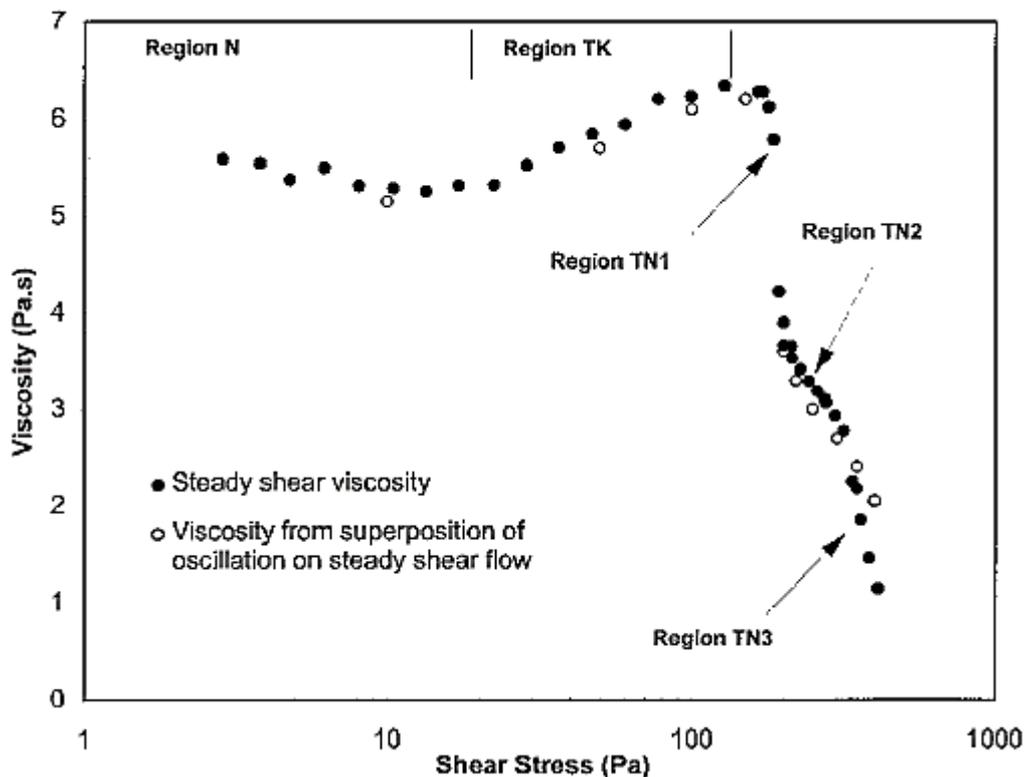
Figure 1.2. Viscosity versus shear stress measured at 25 °C for HEUR-35-16 at 2.0 wt % concentration reproduced from Tam *et al.*(36).

The shear thickening region is postulated to be due to rearrangement of polymer clusters where the flower-like micelles that are not incorporated in the super-loop structure (as shown in Figure1.1) are incorporated under shear, increasing the number of cross-linking points (Figure 1.3 (a)). At TN1 and TN2 the new super-loop arrangement in the shear thickening region is maintained with an increase of hydrophobes exit rate from the hydrophobic aggregates, hence a slight decrease in shear-dependent viscosity is observed. At TN3 the viscosity significantly decreases due to fragmentation of the super-loop structure into smaller aggregates and the increase in exit rate of the hydrophobes from hydrophobic aggregate (Figure 1.3 (b)) (36).
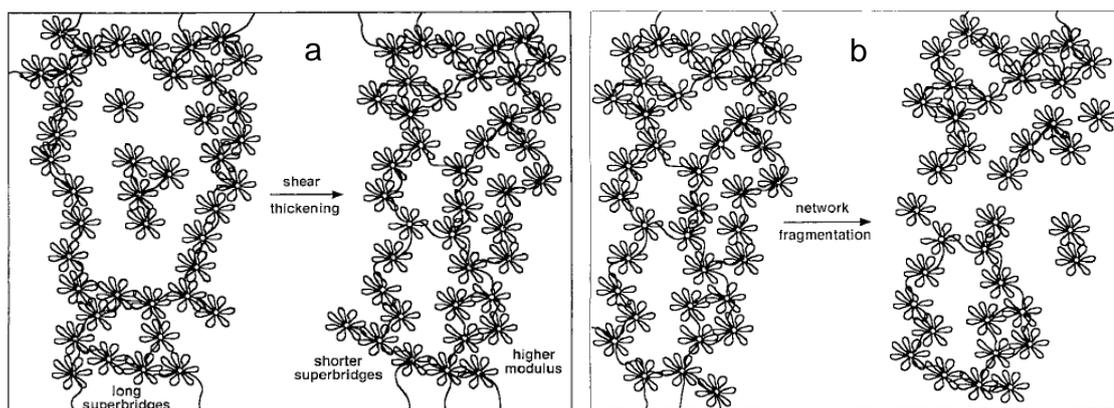
Figure 1.3. Illustration of the effect of shear on the super-loop arrangement of HEUR-35-16 at 2 wt% reproduced from Tam *et al.*(36).

Although some studies have suggested a Maxwell model for relaxation (only one relaxation rate is observed for the polymer hydrophobes) of linear hydrophobic end-group of telechelic polymers (8,36), more recent studies suggest a dual relaxation behaviour arising from the Rouse relaxation time (relaxation of the individual polymer chains which is not incorporated in the hydrophobic aggregates of the polymer) and from the network relaxation time (37). The model predicts that this network relaxation time depends on the concentration, molecular weight of the chains, length of the hydrophobic end-groups, and aggregation number of the micelles. The dual relaxation is reported for spiropyran functionalised HEUR (38).

Suzuki *et al.* studied HEUR-48-16 where a concentration-dependent relaxation model is postulated. In the dilute regime ($C_{polymer} < C^*$), the relaxation fits to a Maxwell model (39); however, in the concentrated regime ($C_{polymer} > C^*$), a broadened non-Maxwell relaxation is observed. In addition, the shear thickening behaviour observed at moderate shear in the rheological profile of HEURs disappears at $C_{polymer} > C^*$. The rheological behaviour of the polymer in the dilute and concentrated regimes is correlated to polymer arrangement in solution. In the dilute regime, a sparse network is formed due to the bridging of HEUR chains between the flower micelles. The shear thickening behaviour in the dilute regime at moderate shear is correlated to the orientation of dissociated chains. When the strands re-associate in the shear direction the stretching penalty on the re-associating strand is decreased and thickening at moderate shear is observed. At high shear, the dissociation/re-association balance is shifted to the dissociation side, hence shear thinning behaviour is noted.

Chapter 1. Introduction

In the concentrated regime, chain entanglement occurs and a dense network is formed. The HEUR chains behave as the HEUR network strands that show only dissociation/re-association at the ends and network dynamics are somehow close to that of the homopolymer. This was discussed here earlier in Beaudoin *et al.* SANS experiment conclusions (18). The HEUR chains orientation in the concentrated regime are therefore less important and hence the shear thickening region at moderate shear is absent (39,40).

Ianniruberto *et al.* proposed a different mechanism for the shear thickening behaviour of HEUR at moderate shear (41). The shear thickening in the dilute regime is explained by forcing the flower micelles to interpenetrate one another at moderate shear, bearing in mind that at this concentration the flower micelles are intact and well separated. The absence of the shear thickening behaviour at moderate shear in the concentrated regime is explained by the interpenetration of micelles and the flower micelles are reduced due to the increased number of bridges in this concentration regime.

The relaxation of non-telechelic associative polymers shows a broad distribution of relaxation times (3,42,43). With non-telechelic associative polymers, a shear thickening region is not necessarily present. Only shear thinning is observed, and sometimes a Newtonian plateau cannot be detected in the accessible range of shear rates (44,45).

The interesting rheological behaviour of ATs widens their applications in various industries. In the cosmetic industry, ATs are used in cleanser formulation to reduce irritation due to the formation of complexes with the surfactants (46). Hydrophobically modified pectin (HM-pectin) is used in the food industry as an emulsifier and foaming additive (47). ATs are used as rheology modifiers in the paint and cosmetics industries (48,49).

Recently, research is directed towards the synthesis of novel HEURs. Wang *et al.* synthesised a C_{12} and C_{16} two tail end-functionalised hydrophobes at each end. The functionalisation with two tails significantly enhances the thickening properties of HEUR due to the formation of stronger cross-link points (50). Aggregation of HEUR can be stimuli-responsive by using functionalised end-group, where the hydrophobicity of end-group is altered upon exposure to stimuli which induce or reverse the formation of hydrophobic aggregates (51). Functionalisation of hydrophobic end-group with azobenzene imparts a sensitivity of aggregates to ultra-violet (UV) and visible light exposure (51). Similarly, functionalisation of HEUR with a ferrocene end-group renders the hydrophobic aggregates sensitive to redox reaction (52). Functionalisation of HEUR

Chapter 1. Introduction

with two tails each is sensitive to different stimuli can turn the HEUR sensitive to multiple stimuli. Du *et al.* synthesised a UV/visible and redox-responsive HEUR by functionalisation of HEUR with 3-(6-ferrocenyhexyloxyl)-5-(6-azobenzenehexyloxy) benzyl alcohol at each end (53). The functionalisation of HEUR with stimuli-responsive end-groups broaden the applications of HEUR to include the electronic, and fabrication of soft materials. Given the various applications of ATs in different formulations that contain surfactants, *e.g.* cosmetics and paints, it is necessary to study the interaction of ATs with surfactants.

1.2. Interaction of associative thickeners with surfactants

The phase behaviour of the polymer/surfactant mixture and a wide range of physicochemical properties qualifies the system for versatile applications. Polymer/surfactant systems are mainly used to control the rheological profile and stabilise dispersions in many industries, *e.g.* food, cosmetics, household formulation and drug delivery (54).

Alami *et al.* studied the diffusion of PEO and PEOM-20-12 at 1 wt% as a function of the non-ionic surfactant hexaethyelene glycol monododecyl ($C_{12}E_6$) by DLS (55). The diffusion of PEO in presence of the surfactant does not change, indicative of the absence of interaction between the non-ionic surfactant and PEO. The diffusion of PEOM as a function of the $C_{12}E_6$ concentration decreases to a minimum (D_{min}) due to the formation of mixed hydrophobic aggregates which enhance the polymer network structure. At higher surfactant concentration the self-diffusion coefficient of PEOM-20-12 increases to reach the value of the parent PEO/$C_{12}E_6$ mixtures as a result of the solubilisation of the polymer hydrophobic end-groups in surfactant micelles, hence the polymer network structure is broken.

From quenching fluorescence results, the PEOM-22-12/$C_{12}E_6$ mixed micelles showing D_{min} have four polymer end-groups per micelle (55). The inverse trend of the diffusion curve as a function of surfactant concentration is observed for the viscosity of PEOM-20-12 as a function of $C_{12}E_6$ concentration. A typical viscosity curve for ATs as a function of surfactant concentration is observed for PEOM-22-12/$C_{12}E_6$ mixtures, where the viscosity increases to a maximum value (V_{max}) and then decreases. The viscosity increases due to strengthening of the polymer network structure and decreases as the structure is broken to smaller aggregates. The V_{max} is shifted to higher surfactant concentration than

Chapter 1. Introduction

D_{min} due to the formation of larger clusters or strengthening the network of the polymer. The number of polymer hydrophobic end-groups in mixed micelles formed at V_{max} is estimated to be two polymers (55).

The diffusion behaviour and distribution of 2.5 wt% PEOM-10-12 and the anionic surfactant SDS, cationic surfactant dodecyltrimethylammonium bromide (DTAB), and non-ionic surfactant octaethyelene glycol monododecyl ($C_{12}E_8$) surfactants were reported by Persson *et al.* (22). The distribution of the polymer diffusion in the absence of surfactants is very broad due to polymer polydispersity. The addition of surfactants narrows the diffusion distribution of the polymer, as the number of bridging polymer molecules increase at the expense of looping ones. Therefore the homogenization of PEOM/surfactant mixtures occurs. At high SDS concentration, as the PEOM hydrophobes are solubilised in the SDS micelle, their effect is annulled and distribution of the diffusion coefficients becomes similar to the parent PEO/SDS mixture. The effect of SDS on the position of the PEOM diffusion peak is more significant than that of DTAB or $C_{12}E_8$. This can be correlated to the ability of SDS to interact with the hydrophobic end-groups of the PEOM as well as PEO backbone (56–59); however, DTAB and $C_{12}E_6$ interact only with the former.

The effect of the surfactant hydrophobicity on the diffusion of the polymer reported by Almai *et al.* was studied by measuring the diffusion of 0.5 wt% PEOM-20-12 as a function of $C_{12}E_6$, $C_{12}E_8$, and $C_{12}E_{23}$ (55). Increasing the surfactant hydrophobicity affected the position and depth of D_{min}. The more hydrophilic surfactant shifts the D_{min} to lower surfactant concentration and the peak is less deep. Therefore, the larger aggregates of the PEOM-20-12/non-ionic surfactants are formed for the more hydrophobic surfactant.

The viscosity and diffusion of 1 wt% HEUR-51-16, PEO-40 was reported by Zhang *et al.* as a function of DTAB concentration and compared to SDS (60). The viscosity of HEUR-51-16 shows a typical viscosity curve for ATs as a function of surfactant. V_{max} in DTAB occurs at higher surfactant concentration relative to SDS (Figure 1.4). Diffusion of HEUR as a function of SDS and DTAB show the same but inverted trend as viscosity where surfactant concentration at which V_{max} occurs, the D_{min} is observed (Figure 1.5). These observations disagree with Alami *et al.* where V_{max} is shifted to higher surfactant concentration relative to D_{min}, this can be due to the use of a different class of surfactant (non-ionic). Interaction of SDS with HEUR increases the number of hydrophobic aggregates and decreases the average separation between the domains. Further

increase of the surfactant concentration results in breakage of the polymer network reflected by a decrease in viscosity and increase in self-diffusion coefficient. The viscosity of parent PEO-40 increases and diffusion decreases as a function of SDS, those properties are barely changing in the presence of DTAB. The binding isotherms of surfactants to PEO and HEUR were plotted from diffusion data where DTAB shows the lowest affinity to both polymer and affinity of surfactants is higher to HEUR than parent PEO polymer.
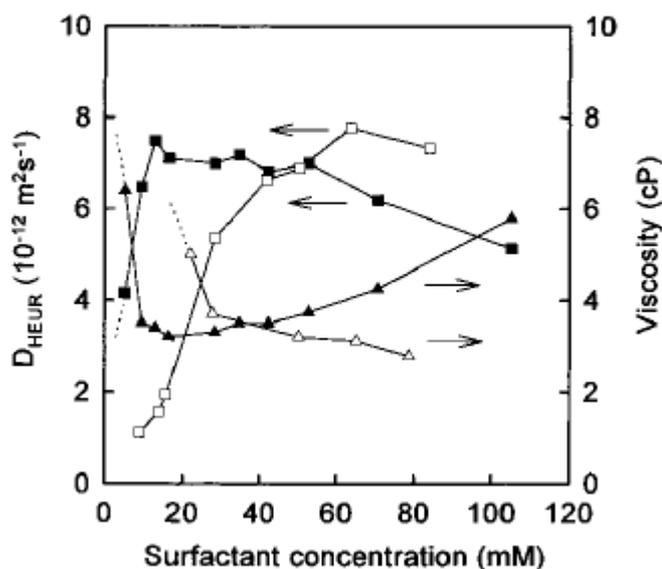
Figure 1.4. Self-diffusion coefficient and viscosity of HEUR-51-16 in presence of SDS (closed symbols) and DTAB (open symbols) reproduced from Zhang *et al.* (60).
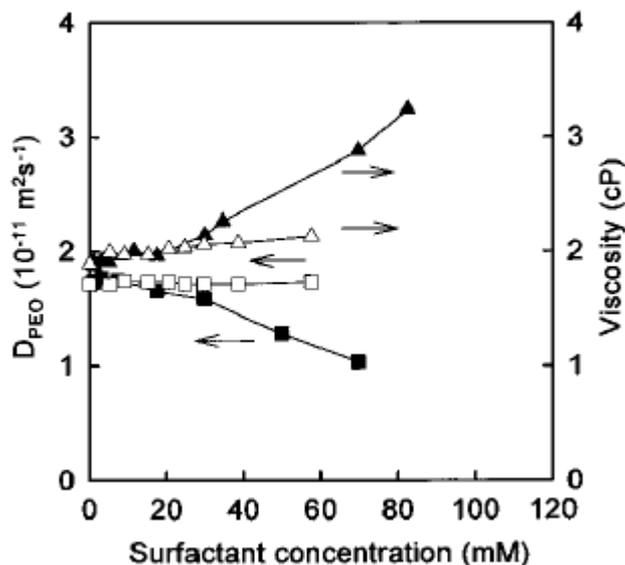
Figure 1.5. Self-diffusion coefficient and viscosity of PEO-40 in presence of SDS (closed symbols) and DTAB (open symbols) reproduced from Zhang *et al.* (60).

Hulden studied the effect of varying PEO molecular weight of C_{18} HEUR on low-shear viscosity as a function of SDS and non-ionic surfactant nonylphenol (10) ethoxylate (NPE10) concentrations (32). Typical low-shear viscosity curve of HEUR as a function of surfactant is observed. However, decreasing the HEUR molecular weight or C-chain length shifts the viscosity peak to higher surfactant concentration. The magnitude of viscosity maximum is greater for longer C-chain and lower molecular weight PEO. In the non-ionic NPE10 case, the lower molecular weight PEO and longer C-chain length of the HEUR show increase in viscosity which plateaus at higher surfactant concentration.

Kim *et al.* reported typical viscosity plots for HEUR-35-16, HEUR-35-16, and HEUR-35-22 as a function of the concentration of non-ionic surfactant $C_{18}E_{20}$ (61). In contrast to Hulden, increasing the C-chain length does not affect the position of V_{max} as a function of surfactant concentration. The HEUR show shear thinning behaviour in the presence and absence of surfactant. As the surfactant concentration increases, the shear at which shear thinning behaviour starts shifts to a lower shear rate. The shear rate at which shear thinning behaviour occurs is correlated to the inverse of the relaxation time, therefore as surfactant concentration increases, the relaxation time of the hydrophobes increase (62). Annable *et al.* suggest a distribution of the hydrophobes relaxation for PEOM-36-16/SDS mixtures (62). On the other hand, PEOM-20-16 in the absence of surfactants, and PEOM-20-16/non-ionic surfactant NPE10 mixtures fits to Maxwell relaxation model. The viscosity

Chapter 1. Introduction

and relaxation time of PEOM/NPE6 mixtures show higher viscosity and longer hydrophobe relaxation time (τ, is the reciprocal of the chain disengagement rate) relative to PEOM/NPE6 mixture, where NPE6 has low water solubility, whilst NPE10 is water soluble surfactant.

Spin-spin relaxation time (T_2), of SDS in presence of PEO-40, HEUR-51-16 and in absence of polymer reported by Zhang *et al.* was measured by NMR (60). T_2 is sensitive to changes in spectral density for slow motion, such as changes that occur as a result of surfactant aggregation changes. T_2 decreases as a function of surfactant concentrations in absence of polymer. T_2 for SDS in SDS/PEO mixtures abruptly increases at 4.5 mM and decreases at higher SDS concentration. The same behaviour is observed in the presence of HEUR, however, the increase in the SDS T_2 is less intense. At low SDS concentration, the increase in the T_2 is correlated to lateral diffusion of SDS molecules within SDS-micelle bound to PEO. The authors expect the N_{agg} of polymer-SDS bound micelle to be half that of free SDS micelle. The DTAB T_2 values are hardly changing in presence of PEO. However, the T_2 decreases at low concentration of DTAB (20 mM) in presence of HEUR as DTAB partition in HEUR/DTAB mixed micelles which is part of large polymer clusters. At higher DTAB concentration, as the network structure is broken, T_2 of DTAB decreases and resembles that of surfactant in presence and absence of PEO.

The surface tension (γ) of 0.5 wt% HEUR-19-18 and HEUR-19-15 as a function of SDS concentration is reported by Hulden (32). The γ log SDS concentration curves for the two polymers show two break points T_1 (in some texts is referred to as CAC_1, concentration at which the surfactant starts to interact with the polymer) and T_2 (sometimes equated to CAC_2, concentration at which the surfactant starts to form pure free micelles after polymer saturation) at 5 and 63 mM SDS, respectively. T_1 reflects the beginning of the interaction of SDS with the polymer; however, the viscosity data indicates the presence of interaction between HEUR and SDS at SDS concentration lower than T_1. The SDS molecules binds to existing HEUR hydrophobic aggregates in an uncooperative manner (occurs when more than one SDS monomer binding to the existing hydrophobic aggregate of the polymer, this process is slow as the binding of more than one charged species to the aggregates is unfavourable) below T_1. T_2 reflect the saturation of the polymer with the surfactant and the formation of free surfactant micelles, hence the surfactant surface tension in the presence and absence of polymer overlap. The surface tension curve of 0.5 wt% HEUR-19-18 and HEUR-19-15 as a function of NPE10 shows only one break

Chapter 1. Introduction

point T_2 at 1.8 and 1.9 mM per 5 g of polymer for HEUR-19-18 and HEUR-19-15, respectively. Above T_2, the surface tension curve in the presence and absence of polymer overlap, suggesting the formation of free micelles above T_2 in solution. NPE10 hydrophobe ratio to that of the polymer at T_2 is 3.5 and 3.7 for HEUR-19-18 and HEUR-19-15, respectively, close to the ratio obtained at viscosity maximum (5.2 ± 0.9). This might suggest that above T_2 re-arrangement between HEUR/surfactant mixed micelles and pure surfactant micelles occurs.

Dai *et al.* reported a lower T_1 value for HEUR and SDS than that for PEO/SDS mixtures due to the increase in polymer hydrophobicity (63). T_1 for the HEUR/SDS mixtures is independent of HEUR concentration or molecular weight, for molecular weight higher than 17,000 g mol^{-1}. CAC$_2$ is not affected by the molecular weight of HEUR, but shifts to higher SDS concentration at higher HEUR concentration.

The hydrophobicity of PEOM-10-12/SDS and PEOM-10-12/$C_{12}E_8$ mixed aggregates reported by Persson *et al.* was studied by EPR using 16-doxylstearic acid methyl ester (16-DSE) as a probe, where polymer concentration is held constant (2.5 wt%) (5). The polarity of PEOM10-12/SDS mixed aggregates increases at low SDS concentration at a molar ratio of SDS to PEOM-10-12 of 3:1. Increasing the molar ratio to 6:1 decreases the polarity of the mixed aggregate. Various factors may attribute to the change in PEOM/SDS mixed micelles polarity such as the effect of charged head group and associated counter ion, change in aggregate size, and interaction between SDS with PEO backbone. The polarity of PEOM-10-12/$C_{12}E_8$ decreases as a function of surfactant concentration. This can be explained by the growth of hydrophobic aggregates and shielding ability of PEO segment to the hydrophobic core from exposure to water. The addition of $C_{12}E_8$ moves the polarity from polymer-like aggregates towards surfactant micelles. Since the surfactant interacts only with the hydrophobic end groups of the polymer, the effect of the interaction of the non-ionic surfactant $C_{12}E_6$ on the composition of hydrophobic aggregates of PEOM-20-12 was studied by quenching fluorescence. Increasing the concentration of $C_{12}E_6$ decreases the number of polymer hydrophobic end-groups in the mixed aggregates; however, the overall number of hydrophobes in the mixed micelles insignificantly changed (55).

Liao *et al.* presented the effect of SDS interaction on HEUR/cyclodextrin inclusion complex (29). SDS interacts with cyclodextrin (CD) to set the HEUR hydrophobes free in solution, hence the viscosity increases. At higher SDS concentration, the molecules

interact with HEUR and typical viscosity curve for HEUR/SDS is observed with V_{max} moved to higher SDS concentration than in absence of cyclodextrin. V_{max} in HEUR/SDS in presence of alpha-cyclodextrin (α-CD) has a value (9.2 Pa.s) close to HEUR/SDS mixture (11.2 Pa.s), in presence of beta-cyclodextrin (β-CD) lower V_{max} (6 Pa.s) is reported. To conclude, in the presence of SDS HEUR/β-CD mixtures show partial recovery whereas HEUR/α-CD mixtures exhibit relatively full recovery.

1.3. Interaction of polymer/surfactant/particles

The effect of surfactant on polymer adsorption to particle surfaces has been studied in various systems; homopolymer adsorption to various particles is discussed here, whereas a review of HMP adsorption to latices is presented in Chapters 3 and 4. The addition of surfactant to polymer/particle mixtures can: (1) enhance the polymer adsorption, *e.g.* SDS/PVP/alumina at low SDS concentrations (64); (2) compete with the polymer for the adsorption sites, *e.g.* NPE8/polyvinylpyrrolidone (PVP)/silica (65); (3) lead to adsorption of the polymer/surfactant complex on the particle, which finally desorbs at high surfactant concentration due to a competing solution complexation, *e.g.* PEO/SDS/silica (66).

Esumi *et al.* studied the interaction of PVP and alumina particles where weak interaction was observed (64). The adsorption isotherm of 0.8 g dm^{-3} PVP and 5 g of alumina in presence of at 4 and 10 mM SDS was studied. The PVP/SDS mixtures adsorb on the alumina surface enhancing the polymer adsorption on the particle at 4 mM SDS. Esumi *et al.* suggested that the SDS monomers bind to the particle surface through electrostatic interaction, the polymer associate to the SDS monomers through hydrophobic interaction. At high SDS concentration, it is postulated that SDS monomers adsorb to the alumina surface rather than PVP-SDS complex, which prefers to be in the bulk.

Rachas *et al.* studied the non-ionic surfactant NPE8, PVP and silica interaction where competitive adsorption of surfactant and polymer to the particle surface occurs (65). The PVP and NPE8 adsorb to the silica surface. To study the competitive adsorption of polymer and surfactant the adsorption isotherm of silica/PVP in a range of NPE8 concentrations was studied. The silica, PVP, and NPE8 were mixed overnight, spun down and the concentration of the PVP in the supernatant was measured colourimetrically. The amount of polymer adsorbed was plotted as a function of equilibrium PVA. The addition of NPE8 to silica/PVP mixture results in partial desorption of PVA, at 1000 ppm of NPE8

complete desorption of PVP occurred. In this experiment, the PVP and silica concentrations were held constant at 340 ppm and 2 % (w/v), respectively.

PEO/SDS/silica is one of the most studied systems, many techniques have been used to study their interaction. The PEO of molecular weight 100,000 g mol^{-1} adsorbs to the silica surface and the polymer adsorbed layer thickness is around 4.2 ± 0.2 nm as measured by DLS. The DLS, and scattering curves indicate an increase in the thickness of PEO adsorbed layer on silica as a function of SDS, above the CMC of the surfactant, due to repulsive forces between the adsorbed SDS/PEO complexes. The addition of NaCl increases the adsorbed amount due to screening of charges and the adsorbed layer thickness decreases (66,67).

Cattoz *et al.* studied the effect of SDS addition on PVP adsorbed layer on silica surface by DLS, solvent relaxation NMR, and SANS (68). The PVP strongly adsorbs to the silica particles. The conformation of the polymer at the particle interface is concentration dependent. At low PVP concentration, the PVP adopts a flat conformation, whereas loops (polymer segments extended in solution between two adsorbed polymer segments on a particle) and tails (the free polymer segments at the end adsorbed polymer chain on a particle) form at higher polymer concentrations until surface saturation is attained at 1 mg m^{-2} of PVP. The addition of SDS increases the overall size of the mixture resulting from interchain repulsion and stretching of the adsorbed polymer layer as a result of complexation with SDS. Solvent relaxation NMR shows a decrease in near polymer concentration (trains). The SANS data confirms complete desorption of PVP/SDS complex from silica surface at higher SDS concentration.

1.4. Aim

The aim of this project is to develop unique insights into the interactions of the associative thickeners in multi-component formulations by elucidating the key interactions and controlling factors, focusing on the effect of latex particles on the HEUR/surfactant interaction. This, in turn, should allow a sounder scientific basis for the approach to formulation and, in terms of wider impact, should provide essential information to help guide the future development of thickener and latex chemistries.

Chapter 1. Introduction

1.5. Thesis in context

In this thesis, the characterisation of ternary mixture (HEUR/SDS/latex) is built upon an understanding of the different binary interaction (HEUR/SDS and HEUR/latex). Chapter 2, therefore, focuses on HEURs/surfactant mixtures where HEURs with different architectures studied in dilute and concentrated regimes as a function of SDS concentration. Chapter 3 studies the polymer/particle interaction and Chapter 4 focuses on the effect of latex particle on the polymer/surfactant interaction. The work is extended in Chapter 5 to soft colloids where dodecane droplets are stabilised by polymer and polymer surfactant mixtures. Chapter 6, highlights the conclusions drawn from each chapter and recommendations for future work. The supporting figures, theory of the techniques and purity of the materials used are discussed in the Appendices.

1.6. References

1. Karlson, L. Hydrophobically modified polymers rheology and molecular associations. Ph.D. Thesis, University of Lund. **2002**.

2. Huldun, M. Hydrophobically modified urethane-ethoxylate (HEUR) associative thickeners 1. Rheology of aqueous solutions and interactions with surfactants. *Colloids Surfaces A Physicochem.* **1994**;*82*(3):263–277.

3. English RJ. Solution rheology of a hydrophobically modified alkali-soluble associative polymer. *J Rheol.* **1997**;*41*(2):427-444.

4. Thuresson K, Lindman B, Nystrom B. Effect of hydrophobic modification of a nonionic cellulose derivative on the interaction with surfactants phase behaviour ans association. *J Phys Chem B.* **1997**;*101*(97):6450–6459.

5. Persson K, Bales BL. EPR study of an associative polymer in solution: determination of aggregation number and interactions with surfactants. *J Chem Soc Faraday Trans.* **1995**;*91*(17):2863-2870.

6. Beaudoin E, Hiorns RC, Borisov O, Francois J. Association of hydrophobically end-capped poly(ethylene oxide). 1. Preparation of polymers and characterization of critical association concentrations. *Langmuir.* **2003**;*19*(6):2058–2066.

7. Rubinstein M, Dobrynin AV. Solutions of assosiative polymers. *Trip.* **1997**;*5*(6): 181–186.

8. Annable T, Buscall R, Ettelaie R, Whittlestone D. The rheology of solutions of associating polymers: comparison of experimental behaviour with transient network theory. *J. Rheol.* **1992**;*37*:695-726.

9. Annable T, Buscall R, Ettelaie R. Network formation and its consequences for the physical behaviour of associating polymers in solution. *Colloids Surfaces A Physicochem Eng Asp.* **1996**;*11*:97-116.

10. Paeng KW, Kim B, Kim E, Sohn D. Aggregation processes of hydrophobically modified polethylene oxide. *Bull Korean Chem Soc.* **2000**;*21*:623-627.

11. Yekta A, Xu B, Duhamel J, Adiwidjaja H, Winnik MA. Fluorescence studies of associating polymers in water - determination of the chain-end aggregation number and a model for the association process. *Macromolecules.* **1995**;*28*(4):956–966.

12. Gourier C, Beaudoin E, Duval M, Sarazin D, Maître S, François J. A Light scattering study of the association of hydrophobically alpha- and alpha, omega-end-capped poly(ethylene oxide) in water. *J Colloid Interface Sci.* **2000**;*230*(1):41–52.

13. Lafleche F, Durand D, Nicolai T. Association of adhesive spheres formed by hydrophobically end-capped PEO.1. Influence of the presence of single end-capped PEO. *Macromolecules.* **2003**;*36*(4):1331–1340.

14. Maechling-Strasser C, Clouet F, Francois J. Hydrophobically end-capped polyethylene-oxide urethanes: 2. Modelling their association in water. *Polymer.* **1992**;*33*(5):1021–1025.

15. Xu B, Yekta A, Li L, Masoumi Z, Winnik MA. The functionality of associative polymer networks: the association behavior of hydrophobically modified urethane-ethoxylate (HEUR) associative polymers in aqueous solution. *Colloids Surfaces A Physicochem Eng Asp.* **1996**;*112*(2-3):239–250.

16. Panmai S, Prud'homme RK, Peiffer DG, Jockusch S, Turro NJ. Interactions between hydrophobically modified polymers and surfactants: a fluorescence study. *Langmuir,* **2002**;*18*(10):3860–3864.

17. Gourier C, Beaudoin E, Duval M, Sarazin D, Maître S, François J. A Light scattering study of the association of hydrophobically alpha- and alpha, omega-end-capped poly(ethylene oxide) in water. *J Colloid Interface Sci.* **2000**;*230*(1):41–52.

18. Beaudoin E, Lapp A, Hiorns RC, Grassl B, François J. Neutron scattering of hydrophobically modified poly(ethylene oxide) in aqueous solutions in the presence of latex particles. *Polymer*. **2002**;*43*(9):2677–2689.

19. François J, Maitre S, Rawiso M, Sarazin D, Beinert G, Isel F. Neutron and X-ray scattering studies of model hydrophobically end-capped poly(ethylene oxide) aqueous solutions at rest and under shear. *Colloids Surfaces A Physicochem Eng Asp*. **1996**;*112*(2–3):251–65.

20. Abrahmsen-Alami S, Alami E, Francois J. The lyotropic cubic phase of model associative polymers : small-angle X-ray scattering (SAXS), differential scanning calorimetry (DSC), and turbidity measurements. *J Colloid Interface Sci*. **2000**;*179*(1):20–33.

21. Abrahmsen-Alami S, Stilbs P. NMR self-diffusion of associative polymers in aqueous solution: the influence of the hydrocarbon end-chain length on the polymer transport dynamics in single-and two-component mixtures. *J Colloid Interface Sci*. **1997**;*189*(1):137–143.

22. Persson K, Griffiths PC, Stilbs P. Self-diffusion coefficient distributions in solutions containing hydrophobically modified water-soluble polymers and surfactants. *Polymer*. **1996**;*37*(2):253–261.

23. Uemura Y, Macdonald PM. Associating polymer binding to polystyrene latex. *Macromolecules*. **1996**;*29*(1):63–69.

24. Choi J, Sohn D, Lee Y, Cheong C. Self-diffusion of hydrophobically end-capped polyethylene oxide urethane resin by using pulsed-gradient spin echo NMR spectroscopy. *Macromol Res*. **2003**;*11*(6):444–450.

25. Walderhaug H, Hansen FK, Abrahmsén S, Persson K, Stilbs P. Associative thickeners. NMR self-diffusion and rheology studies of aqueous solutions of hydrophobically modified poly(oxyethylene) polymers. *J Phys Chem*. **1993**;*97*(31):8336–8342.

26. Barmar M, Barikani M, Kaffashi B. Steady shear viscosity study of various HEUR models with different hydrophilic and hydrophobic sizes. Colloids *Surfaces A Physicochem Eng Asp*. **2005;***253*(1–3):77–82.

27. Lundberg DJ, Brown RG, Glass JE, Eley RR. Synthesis, characterization, and

solutionr Rheology of model hydrophobically-modified, water-soluble ethoxylated urethanes. *Langmuir.* **1994**;*10*(9):3027–3034.

28. Liao D, Dai S, Tam KC. Rheological properties of hydrophobic ethoxylated urethane (HEUR) in the presence of methylated β-cyclodextrin. *Polymer.* **2004**;*45*(25):8339–8348.

29. Liao D, Dai S, Tam KC. Influence of anionic surfactant on the rheological properties of hydrophobically modified polyethylene-oxide/cyclodextrin inclusion compex. *J Rheol.* **2009**;*53*(2):293-308.

30. Horsky J, Mikesova J, Quadrat O, Snuparek J. The effect of (2-hydroxypropyl)-beta-cyclodextrin on rheology of hydrophobically end-capped poly(ethylene glycol) aqueous solutions. *J Rheol.* **2004**;*48*(1):23–38.

31. Kaneda I, Koga T, Tanaka F. Rheological properties of physical gel formed by hydrophobically modified urethane ethoxylate (HEUR) associative polymers in methanol-water mixtures. *Rheol Acta.* **2012**;*51*(1):89–96.

32. Hulden M. Hydrophobically modified urethane-ethoxylate (HEUR) associative thickeners 2. Interaction with latex. *Colloids Surfaces A Physicochem Eng Asp.* **1994**;*88*(2–3):207–221.

33. Tan H, Tam KC, Tirtaatmadja V, Jenkins RD, Bassett DR. Extensional properties of model hydrophobically modified alkali-soluble associative (HASE) polymer solutions. J *Nonnewton Fluid Mech.* **2000**;*92*(2–3):167–185.

34. Pellens L, Gamez Corrales R, Mewis J. General nonlinear rheological behavior of associative polymers. *J Rheol.* **2004**;*48*(2):379.

35. Kaffashi B, Barmar M, Eyvani J. The steady state and dynamic rheological properties of telechelic associative polymer solutions. *Colloids Surfaces A Physicochem Eng Asp.* **2005**;*254*(1–3):125–130.

36. Tam KC, Jenkins RD, Winnik M a, Bassett DR. A structural model of hydrophobically modified urethane-ethoxylate (HEUR) associative polymers in shear flows. *Macromolecules.* **1998**;*31*(98):4149–4159.

37. Tripathi A, Tam KC, McKinley GH. Rheology and dynamics of associate polymer solutions in shear and extension: theory and experiments. *Macromolecules.*

2006;*39*(5):1981–1999.

38.   Dong R, Peng J, Chang X, Zhang Q, Hong L, Ren B. Rheology of a spiropyran functionalized hydrophobically modified ethoxylated urethane in aqueous solution. *J Rheol*. **2017**;*61*(1):107-116.

39.   Suzuki S, Uneyama T, Inoue T, Watanabe H. Nonlinear rheology of telechelic associative polymer networks: Shear thickening and thinning behavior of hydrophobically modified ethoxylated urethane (HEUR) in aqueous solution. *Macromolecules*. **2012**;*45*(2):888–898.

40.   Suzuki S, Uneyama T, Watanabe H. Concentration dependence of nonlinear rheological properties of hydrophobically modified ethoxylated urethane aqueous solutions. *Macromolecules*. 2013;*46*(9):3497–3504.

41.   Ianniruberto G, Marrucci G. New interpretation of shear thickening in telechelic associating polymers. *Macromolecules*. **2015**;*48*(15):5439–5449.

42.   Heitz C, Prud'Homme RK, Kohn J. A new strictly alternating comblike amphiphilic polymer based on PEG. 2. Associative behavior of a high molecular weight sample and interaction with SDS. *Macromolecules*. **1999**;*32*(20):6658–6667.

43.   Ng W, Tam K, Jenkins R. Rheological properties of methacrylic acid/ethyl acrylate co-polymer: comparison between an unmodified and hydrophobically modified system. *Polymer*. **2001**;*42*(1):249–259.

44.   Tirtaatmadja V, Tam KC, Jenkins RD. Superposition of oscillations on steady shear flow as a technique for investigating the structure of associative polymers. *Macromolecules*. **1997**;*30*(5):1426–1433.

45.   Mewis J, Kaffashi B, Vermant J, Butera RJ. Determining relaxation modes in flowing associative polymers using superposition flows. *Macromolecules*. **2001**;*34*(5):1376–1383.

46.   Draelos Z, Hornby S, Walters RM, Appa Y. Hydrophobically modified polymers can minimize skin irritation potential caused by surfactant-based cleansers. *J Cosmet Dermatol*. **2013**;*12*(4):314–321.

47.   Dickinson E. Hydrocolloids as emulsifiers and emulsion stabilizers. *Food Hydrocoll*. **2009**;*23*(6):1473–1482.

48. Winnik MA, Yekta A. Associative polymers in aqueous solution. *Curr Opin Colloid Interface Sci.* **1997**;*2*(4):424–436.

49. Mcmahon ML. Part A: the use of nonionic associative polymers for the thickening and emulsifying of personal care products. Part B: The synthesis of Manganese sod mimetic for reactive coatings. MSc thesis, The Faculty of California Polytechnic State Unity. **2011**.

50. Wang F, Peng J, Dong R, Chang X, Ren B, Tong Z. Highly efficient hydrophobically modified ethoxylated urethanes (HEURs) end-functionalized by two-tail dendritic hydrophobes : Synthesis, solution rheological behavior, and thickening in latex. *Colloids Surfaces A Physicochem Eng Asp.* **2016**;*502*:114–120.

51. Du Z, Ren B, Chang X, Dong R, Peng J, Tong Z. Aggregation and rheology of an azobenzene-functionalized hydrophobically modified ethoxylated urethane in aqueous solution. *Macromolecules.* **2016;***49*(13):4978–4988.

52. Chang X, Du Z, Hu F, Cheng Z, Ren B, Fu S, Tong Z. A ferrocene-functionalized hydrophobically modified ethoxylated urethane : Redox-responsive controlled self-assembly and rheological behavior in aqueous solution. *Langmuir.* **2016;***32*(46):12137–12145.

53. Du Z, Ren B, Chang X, Dong R, Tong Z. An end-bifunctionalized hydrophobically modified ethoxylated urethane model polymer: multiple stimuli-responsive aggregation and rheology in aqueous solution. *Macromolecules.* **2017**;*50*(4):1688–1699.

54. Guzmán E, Llamas S, Maestro A, Fernández-peña L, Akanno A, Miller R, Ortega F, Rubio RG. Polymer–surfactant systems in bulk and at fluid interfaces.*Adv Colloid Interface Sci.* **2016**;*233*:38–64.

55. Alami E, Almgren M, Brown W. Interaction of hydrophobically end-capped poly(ethylene oxide) with nonionic surfactants in aqueous solution. Fluorescence and light scattering studies. *Macromolecules.* **1996**;*29*(14):5026–5035.

56. Brown W, Fundin J, Miguel MG. Poly(ethylene oxide)-sodium dodecyl sulfate interactions studied using static and dynamic light scattering. *Macromolecules.* **1992**;*25*(26):7192–7198.

57. Smitter LM, Guedez JF, Muller AJ, Saez AE. Interactions between poly(ethylene

oxide) and sodium dodecyl sulfate in elongational flows. *J Colloid Interface Sci.* **2001**;*236*(2):343–353.

58.   Jones MN. The interaction of sodium dodecyl sulfate with polyethylene oxide. *J Colloid Interface Sci.* **1967**;*23*(1):36–42.

59.   Francois J, Dayantis J, Sabbadin J. Hydrodynamical behaviour of the poly (ethylene oxide)-sodium dodecylsulphate complex. *Eur Polym J.* **1985**;*21*(2):165–174.

60.   Zhang K, Xu B, Winnik MA, Macdonald PM. Surfactant interactions with HEUR associating polymers. *J Phys Chem.* **1996**;*100*(23):9834–9841.

61.   Kim D, Kim J, Oh S, Kim J, Han S, Chung DJ, Suh K. Effects of nonionic surfactant on the rheological property of associative polymers in complex formulations. *Polymer.* **2007;***48*(13):3817–3821.

62.   Annable T, Buscall R, Ettelaie R. Influence of surfactants on the rheology of associating polymers in solution. *Langmuir.* **1994**;*10*(4):1060–1070.

63.   Dai S, Tam KC, Wyn-Jones E, Jenkins RD. Isothermal titration calorimetric and electromotive force studies on binding interactions of hydrophobic ethoxylated urethane and sodium dodecyl sulfate of different molecular masses. *J Phys Chem B.* **2004**;*108*(16):4979–4988.

64.   Esumi K, Iitaka M, Torigoe K. Kinetics of simultaneous adsorption of poly(vinylpyrrolidone) and sodium dodecyl Sulfate on aumina particles. *J Colloid Interface Sci.* **2000**;*232*(1):71–75.

65.   Rachas I, Tadros TF, Taylor P. The displacement of adsorbed polymer from silica surfaces by the addition of a nonionic surfactant. *Colloids Surfaces A Physicochem Eng Asp.* **2000**;*161*(2):307–319.

66.   Flood C, Cosgrove T, Qiu D, Espidel Y, Howell I, Revell P. Influence of a surfactant and electrolytes on adsorbed polymer layers. *Langmuir.* **2007**;*23*(5):2408–2413.

67.   Flood C, Cosgrove T, Espidel Y, Howell I, Revell P. Effects of surfactants and electrolytes on adsorbed layers and particle stability. *Langmuir.* **2008**;*24*(14):7323–7328.

68.   Cattoz B, Cosgrove T, Crossman M, Prescott SW. Surfactant-mediated desorption

of polymer from the nanoparticle interface. *Langmuir.* **2012**;*28*(5):2485–2492.

Polymer	Structure
PEOM-20-12	di-functionalised end-capped hydrophobically modified polyethylene oxide polymer ($C_{12}EO_{450}C_{12}$), the molecular weight is 20,000 g mol^{-1}, and the hydrophobic end-group is a C_{12} chain. ◀—(EO)$_x$—▶ where ▬ is the EO units, ▶ is the hydrophobic end-group, and x is the number of EO units.
PEOM-20-16	di-functionalised end-capped hydrophobically modified polyethylene oxide polymer ($C_{16}EO_{450}C_{16}$), the molecular weight is 20,000 g mol^{-1}, and the hydrophobic end-group is a C_{16} chain.
HEUR-51-16	di-functionalised end-capped hydrophobically modified ethoxylated-urethane polymer, the molecular weight is 51,000 g mol^{-1}, and the hydrophobic end-group is a C_{16} chain. ◀—■—EO—■—▶ where ▬ is the EO units, ■ is the urethane linker, and ▶ is the hydrophobic end-group.

$C_{12}EO_{200}C_{12}$ (PEOM-10-12)	di-functionalised end-capped hydrophobically modified polyethylene oxide polymer ($C_{12}EO_{200}C_{12}$), the molecular weight is 10,000 g mol^{-1}, and the hydrophobic end-group is a C_{12} chain.
PEOM-32-16	di-functionalised end-capped hydrophobically modified polyethylene oxide polymer ($C_{16}EO_{700}C_{16}$), the molecular weight is 32,000 g mol^{-1}, and the hydrophobic end-group is a C_{16} chain.
PEOM-6-[8-18]	di-functionalised end-capped hydrophobically modified polyethylene oxide polymer ($C_6EO_{180-400}C_6$), the molecular weight is varied between 8,000 to 18,000 g mol^{-1}, and the hydrophobic end-group is a C_6 chain.
HEUR-35-8	di-functionalised end-capped hydrophobically modified ethoxylated-urethane polymer, the molecular weight is 35,000 g mol^{-1}, and the hydrophobic end-group is a C_8 chain.
HEUR-35-12	di-functionalised end-capped hydrophobically modified ethoxylated-urethane polymer, the molecular weight is 35,000 g mol^{-1}, and the hydrophobic end-group is a C_{12} chain.
HEUR-35-18	di-functionalised end-capped hydrophobically modified ethoxylated-urethane polymer, the molecular weight is 35,000 g mol^{-1}, and the hydrophobic end-group is a $C1_8$ chain.
PEO-32	homopolymer, polyethylene oxide with a molecular weight of 32,000 g mol^{-1}.

Mono-functionalised PEOM-32-16	mono-functionalised end-capped hydrophobically modified polyethylene oxide polymer ($C_{16}EO_{700}C_{16}$), the molecular weight is 32,000 g mol^{-1}, and the hydrophobic end-group is a C_{16} chain.
di-functionalised PEOM-32-16	di-functionalised end-capped hydrophobically modified polyethylene oxide polymer ($C_{16}EO_{700}C_{16}$), the molecular weight is 32,000 g mol^{-1}, and the hydrophobic end-group is a C_{16} chain.
HEUR-35-16	di-functionalised end-capped hydrophobically modified ethoxylated-urethane polymer, the molecular weight is 35,000 g mol^{-1}, and the hydrophobic end-group is a C_{16} chain.
PEOM-22-12	di-functionalised end-capped hydrophobically modified polyethylene oxide polymer ($C_{12}EO_{500}C_{12}$), the molecular weight is 32,000 g mol^{-1}, and the hydrophobic end-group is a C_{12} chain.
PEO-40	homopolymer, polyethylene oxide with a molecular weight of 40,000 g mol^{-1}.
HEUR-35-22	di-functionalised end-capped hydrophobically modified ethoxylated-urethane polymer, the molecular weight is 35,000 g mol^{-1}, and the hydrophobic end-group is a C_{22} chain.
PEOM-36-16	di-functionalised end-capped hydrophobically modified polyethylene oxide polymer ($C_{16}EO_{800}C_{16}$), the molecular weight is 36,000 g mol^{-1}, and the hydrophobic end-group is a C_{16} chain.
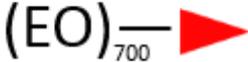
HEUR-19-18	di-functionalised end-capped hydrophobically modified ethoxylated-urethane polymer, the molecular weight is 19,000 g mol^{-1}, and the hydrophobic end-group is a C$_{18}$ chain.
HEUR-19-15	di-functionalised end-capped hydrophobically modified ethoxylated-urethane polymer, the molecular weight is 19,000 g mol^{-1}, and the hydrophobic end-group is a C$_{15}$ chain.

Table 1.1. List of the polymer structures listed in Chapter 1.

_____

2. Interaction of hydrophobically modified ethoxylated urethane (HEUR) polymers and sodium dodecylsulphate (SDS) in solution

2.1. Abstract

Hydrophobically modified ethoxylated urethane polymers (HEURs) are widely used to control the rheological profile of formulated particulate dispersions. However, HEURs, sometimes interact with other components in the formulation, in particular surfactants, leading to substantial and undesirable perturbations in rheological behaviour. Surface tension, rheology, fluorescence, electron paramagnetic resonance (EPR), small-angle neutron scattering (SANS) and pulsed-gradient spin-echo nuclear magnetic resonance (PGSE-NMR) have been employed to quantify how molecular-level interactions between HEURs and sodium dodecylsulphate (SDS) define the macroscopic behaviour of the polymers/surfactant mixture. Three different HEUR polymers from the Acrysol range were studied: RM2020E, with formula (where L = urethane linker, C_n = hydrophobic end-group chain length, EO = ethylene oxide) C_6-L-(EO$_{100}$-L)$_9$-C$_6$, RM8W C_{10}-L-(EO$_{200}$-L)$_4$-C$_{10}$, and RM12W C_{18}-L-(EO$_{200}$-L)$_7$-C$_{18}$ have been studied at both $C_{polymer} < C^*$ (critical overlap concentration) and $C_{polymer} > C^*$. Below C^*, monomeric anti-cooperative and micellar cooperative binding of SDS were detected, leading to observations of polymer conformational changes as a function of SDS concentration. Above C^* the two SDS binding mechanisms, as well as the polymer conformational changes, have been observed to shift to higher SDS concentration. There is a complex balance between polymer molecular weight, ethylene oxide segment size, and therefore the number of urethane linkers, coupled with the size of the hydrophobic end-groups. The insights gained in this work attempt to define macroscopic and nanoscale structure-property relationship of HEURs/SDS interaction.

Chapter 2. HEUR/SDS interaction

2.2.   Introduction

The properties of associative thickeners was discussed in Chapter 1, this chapter focuses on hydrophobically modified ethylene oxide telechelic polymers, and hydrophobically modified ethoxylated-urethane (HEUR). HEURs are widely used to control the rheological profile of formulated particulate dispersions.

The presence of hydrophobic regions in the HMP structure induces a complex, concentration-dependent set of *inter-* and *intra*-molecular associations, dependent on factors such as the length of the hydrophilic backbone and the number, length, and distribution of the hydrophobic groups. Below the critical overlap concentration (C^*), end-capped HMPs adopt the so-called loop, bridge, closed loop conformations as well as forming flower micelles (Figure 1.1). At concentrations above the overlap concentration, they tend to associate into super-bridges, super-loops, dangling ends, and hence form networks of flower micelles (Figure 1.1) (1–6). Most of the published papers in this area are focused on the flower micelle forming HMPs as these are the prevailing structures in real applications.

Various techniques have been used to characterise the hydrophobic aggregates of model system of hydrophobically modified PEO (PEOM) $C_nEO_mC_n$. The number of polymer end-groups (or polymer chains) aggregating per micelle (N_{agg}) can be detected using quenching fluorescence, electron-paramagnetic resonance (EPR) and small-angle neutron scattering (SANS) techniques. EPR has been used to determine the N_{agg} of $C_{12}EO_{200}C_{12}$ using 16-doxyl-stearic methyl ester (16-DSE) as a probe, the polymer N_{agg} is 31 ± 6. Microviscosity and effective relative permeability, which is correlated to the polarity of the polymer aggregates, have been determined as well, showing no change as a function of $C_{12}EO_{200}C_{12}$ concentration (7).

Fluorescence experiments have been employed to determine the N_{agg} of PEOM $C_{16}EO_{100}C_{16}$ (4). The CAC of $C_{16}EO_{100}C_{16}$ is 0.001 wt%. The polymer forms spherical hydrophobic aggregates each consisting of 10 ± 1 chain loops. Over a wide range of concentration, N_{agg} 22 ± 2 per micelle, reflective of the insensitivity of the flower micelle size to concentration. Francois and co-workers found, using SANS and small-angle X-ray scattering (SAXS), that the core size of PEOM increases at very high concentrations (8,9). The scattering from the PEO in the flower micelle shows at least one broad peak at small Q value and a second one that appears as a shoulder at high-Q value. These

peaks indicate a liquid-like order that is temperature and concentration dependent. These diffraction patterns are characteristic of a cubic phase (5,10).

The polymer arrangement changes as a function of polymer concentration. Bridges are formed between the flower micelles as the polymer concentration increases to form secondary aggregates, clusters, of a specific size (11). The mean number of bridge-forming chains per micelle increases linearly as a function of polymer concentration and a network structure is formed (11,12). The network structure has been studied as a function of shear by Richey *et al.* who synthesised a HEUR polymer with a pyrene group attached to the hydrophobic end group (13). The fluorescence was recorded throughout the shearing process. The intensity ratio remains constant as a function of shearing, though the rheology experiment shows a shear thinning behaviour. The unchanged pyrene probe intensity confirms that the shear thinning behaviour is not accompanied by a change in the polymer micellar structures, and that the shear thinning behaviour is correlated to the breakage of the bridges connecting the hydrophobic aggregates.

The interaction between sodium dodecylsulphate (SDS) and HMPs affect some properties of the polymer such as viscosity, self-diffusion coefficient, hydrophobicity, and size of the hydrophobic aggregates (7,14,15). In the HEUR and PEOM series of polymers, the SDS interacts with two sites in the polymer: the hydrophobic end-group, and the PEO backbone. The interaction of SDS with the hydrophobes forms polymer/SDS mixed hydrophobic aggregates, whereas a bead and necklace structure is formed as a result of SDS interaction with PEO, as well documented in the literature (16–19).

The effect of SDS on the viscosity of HEUR solutions has been reported previously; in general, the viscosity increases to a maximum at a characteristic SDS concentration before decreasing. The SDS concentration at which this maximum occurs shifts to a lower SDS concentration for polymers with a longer hydrophilic backbone or hydrophobic end groups (14,20,21). A similar behaviour has been observed for other HMPs (22–24).

The local structure has been probed by several techniques such as EPR to characterise the polarity of the hydrophobic aggregate of $C_{12}EO_{200}C_{12}$ with increasing SDS concentration (7) and diffusion NMR to measure the self-diffusion coefficient. The results demonstrate the formation of larger aggregates with increasing SDS concentration (25,26).

Chapter 2. HEUR/SDS interaction

This study focuses on correlating the macroscopic and microscopic properties of SDS and HEUR systems using a range of techniques with particular focus on polymer concentrations both below and above the critical overlap concentration (C^*). Three polymers with different hydrophobic and EO chain lengths are explored to understand how the molecular structure of the polymer impacts on its interaction with SDS, thereby manifesting the bulk characteristics.

2.3. Materials and methods

2.3.1. Materials

Hydrophobically modified ethoxylated urethane (HEUR) polymers are generally synthesised in two steps: (a) reaction between poly(ethylene glycol) (PEG) and the urethane linker, 4,4'-diisocyanatodicyclohexylmethane (H_{12}MDI) is used for the polymers studied here, through step polymerization technique that yields an ethoxylated urethane pre-polymer and subsequently (b) reacting this prepolymer with alcohol to provide the hydrophobic end caps (Figure 2.1) (27,28).
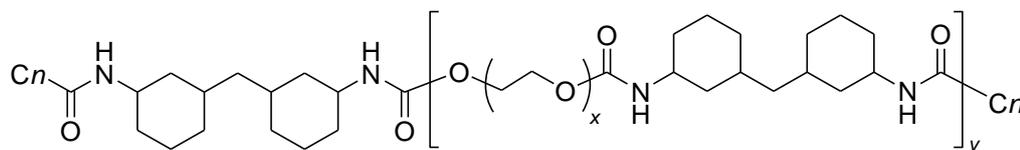
Figure 2.1. General structure of HEURs studied here, where Cn is the hydrophobic end-group, x number of EO unit, y number of polyurethane segments.

The samples employed here were all gifts from Dow. These polymers are schematically denoted C_n-L-(EO$_x$-L)$_y$-C$_n$ where C_n denotes the length of the hydrophobic end group and L is a urethane linker, x is the number of ethylene oxide units per segment, and y is the number of segments per polymer. Therefore RM2020E is C_6-L-(EO$_{100}$-L)$_9$-C$_6$, RM8W C_{10}-L-(EO$_{200}$-L)$_4$-C$_{10}$, and RM12W C_{18}-L-(EO$_{200}$-L)$_7$-C$_{18}$ (Figure 2.2). The three polymers were purified from cyclodextrin before use as described in Appendix D, Section D.1. Sodium dodecylsulphate (SDS) (Aldrich, no impurity observed (Figure D.8) deuterated sodium dodecylsulphate (d_{25}-SDS) (ISIS deuteration facility), Hydroin buffer pH 9 (Aldrich), deionized water (Purite Select deionizer) and deuterium oxide (Aldrich, purity 99.9%) were used as received.

RM2020E, C_6-L-$(EO_{100}$-L$)_9$-C_6, $\smile\!\!\sim$ is 100 EO units, $\blacksquare$ H_{12}MDI linker, and $\sim\!\!\frown$ C_6 hydrophobic end group

RM8W, C_{10}-L-$(EO_{200}$-L$)_4$-C_{10}, $\smile\!\!\sim$ is 200 EO units, $\blacksquare$ H_{12}MDI linker, and $\sim\!\!\frown$ C_{10} hydrophobic end group

RM12W, C_{18}-L-$(EO_{200}$-L$)_7$-C_{18} $\smile\!\!\sim$ is 200 EO units, $\blacksquare$ H_{12}MDI linker, and $\smile\!\!\sim$ C_{18} hydrophobic end group

	RM2020E, C_6-L-$(EO_{100}$-L$)_9$-C_6, is a —100 EO units, $\blacksquare$ is a H12MDI linker, and $\blacktriangleright$ is a C_6 hydrophobic end-group.
	RM8W, C_{10}-L-$(EO_{200}$-L$)_4$-C_{10}, — is a 200 EO units, $\blacksquare$ is a H12MDI linker, and $\blacktriangleright$ is a C_{10} hydrophobic end-group.
	RM12W, C_{18}-L-$(EO_{200}$-L$)_7$-C_{18} — is a 200 EO units, $\blacksquare$ is a H12MDI linker, and $\blacktriangleright$ is a C_{18} hydrophobic end-group
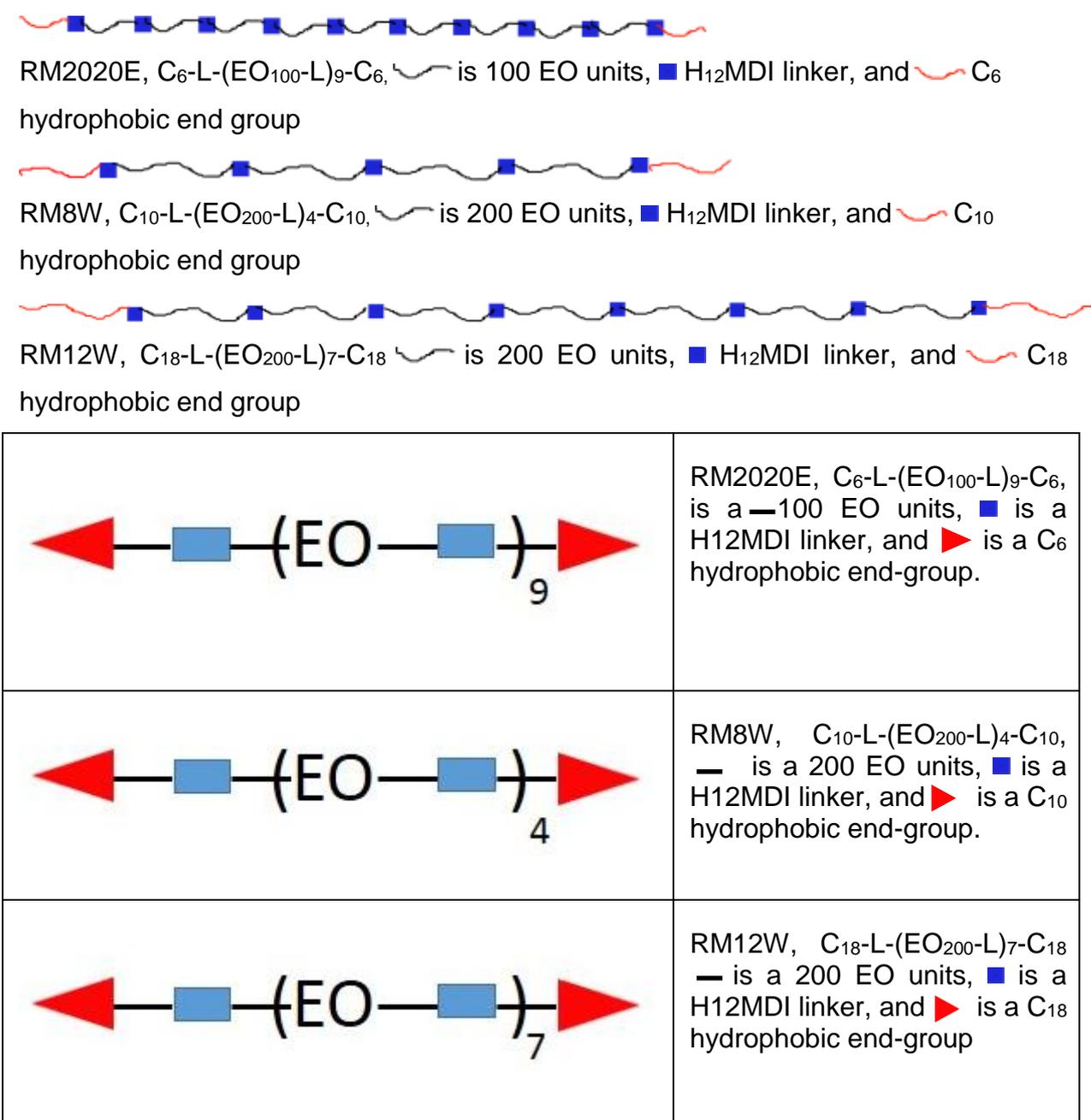
Figure 2.2. Schematic illustration for the HEUR polymers studied in this Chapter.

2.3.2. Methods

All samples were prepared in Hydroin buffer at pH 9 (pH checked by Orion Star A111 pH meter), the buffer ionic strength is 100 mM. The pH and ionic strength were controlled as these are known to strongly influence the formulation behaviour. All measurements were carried out at a temperature of 25 ± 0.5°C. The error bars in the graphs, excluding the scattering graphs, represent repeats of measurement on two sets of samples and repeats of the measurement on the same sample.

Chapter 2. HEUR/SDS interaction

2.3.2.1. Rheology

Shear profiles were recorded on a Malvern GEM 200 rheometer using a cone and plate geometry (4/40) calibrated against silicone oil with a sample volume of 1.5 mL. Shear profiles were recorded at 25 °C for a shear range of 0.1-1000 s^{-1}, with an integration time of 5 s, and delay time of 5 s.

2.3.2.2. Pulsed-Gradient Spin-Echo Nuclear Magnetic Resonance (PGSE-NMR)

Polymers and surfactants were dissolved in Hydroin buffered deuterium oxide (D_2O), pH 9. Experiments were carried out at 25 °C on a 400 MHz Bruker FT NMR spectrometer. A stimulated echo sequence was used, in which the diffusion time (Δ) was set to 800 ms, the duration of the gradient pulses (δ) was held constant at 1 ms and their intensity (G) varied from 5 - 800 G cm^{-1}. Typically, 16 scans were accumulated over 32 gradient steps. Self-diffusion coefficients were extracted by fitting the peak intensities (I) to Equation 2.1 for the peaks at 3.75 ppm (EO) where I_0 is signal intensity in absence of gradient pulses, D_s the diffusion coefficient, γ the gyromagnetic ratio of protons (29,30).

$$I = I_0\, e^{-D_s \gamma^2 G^2 \delta^2 \left(\Delta - \frac{\delta}{3}\right)}$$ Equation 2.1

2.3.2.3. Surface tension

The surface tension of aqueous polymers/surfactant solutions was measured at 25 °C using a maximum bubble pressure tensiometer (SITA Science online t60), calibrated with deionized water. Samples were prepared in Hydroin buffered water, pH 9. Bubble lifetimes of 10 seconds were used to ensure full equilibration.

2.3.2.4. Fluorescence

For all samples, 8-anilinonaphthalene-1-sulphonic acid (ANS) was first dissolved in Hydroin buffered water (pH 9) at a concentration of 2.5 x 10^{-5} M. All samples were then prepared from this ANS stock solution and measured after 24 hours of preparation. Measurements were performed on a Horiba Jobin Yvon Fluoromax-4 spectrophotometer at 25 °C in a semi-micro quartz cell. The excitation frequency was set to 380 nm, and the excitation spectrum recorded over wavelength range 400-600 nm (31).

2.3.2.5. Electron-paramagnetic Resonance (EPR)

EPR spectra of the water-insoluble spin-probe 16-doxyl-stearic acid methyl ester (16-DSE) solubilised into hydrophobic domains have been examined as a function of SDS and HEUR polymer concentrations. A range of SDS concentrations were mixed with the polymer at two concentrations, 7 wt% (twice the overlap concentration C^*) and 1 wt% (half the overlap concentration C^*) of the C_6-L-(EO_{100}-L)$_9$-C_6. A concentration of 3 µg/mL of 16-DSE was used in HEUR, SDS and blend samples. The probe samples were mixed for 24 hours in a hula- mixer before measurement.

The nitroxide free radical exhibits three lines in the spectrum, the separation of the lines is dependent on polarity sensed by the spin-probe, whilst the line shapes are dependent on the viscosity and temperature of the samples. EPR spectra were recorded at 25 °C on a CMS 8400 ADANI EPR spectrometer, centre field set to 337.4 mT, sweep width 6 mT, amplitude 70 uT, power attenuation 12 dB, gain value 1, gain order 3, sweep time 50 s. Each EPR spectrum is an average of four scans.

2.3.2.6. Neutron Scattering

SANS measurements were carried out at 25 °C on the SANS2D instrument (ISIS spallation Neutron Source, Oxfordshire, UK). Neutrons wavelengths spanning 2-14 Å were used to access a Q range of 0.002 to 3 Å^{-1} (Q = 4π sin(θ/2)/λ) (32) with a fixed sample-detector distance of 4 and 2.4 m for the rear and front detector, respectively. Temperature control was achieved through the use of a thermostatted circulating bath pumping fluids through the base of the sample changer, which allowed the experiment to be run at 25 ± 0.5 °C. Samples were contained in UV-spectrophotometer grade 1 mm path length quartz cuvettes (Hellma). The scattering data were normalized for the sample transmission and the incident wavelength distribution, corrected for instrumental and sample backgrounds using a quartz cell filled with D_2O (this also removes the incoherent instrumental background arising from vacuum windows), and corrected for the linearity and efficiency of the detector response using the instrument specific software package. The data were put onto an absolute scale using a well characterised, partially deuterated polystyrene blend standard sample. The intensity of the scattered radiation, $I(Q)$, as a function of the wave vector, Q, is given by Equation 2.2:

$$I(Q) = N_p V_P^2 \Delta\rho^2 P(Q)S(Q) + B_{inc} \hspace{2cm} \text{Equation 2.2}$$

where V_p is the volume of the scattering species, N_p the number of scattering species, $\Delta\rho$ the difference between the neutron scattering length density of the scattering species and the solvent, $P(Q)$ describes the morphology of the scattering species and, $S(Q)$ describes the spatial arrangement of the scatterers in solution, B_{inc} incoherent background.

2.3.3. Programs

All the graphs here were plotted using SigmaPlot 8 (33). The illustrative diagrams were drawn using INKSCAPE 0.91 (34). The chemical structures were drawn using CS ChemDraw std 5.0.

The scattering data was fitted using the Fish program, available to download from the STFC website (35). Fish program is a sophisticated program developed by R. Heenan for analysis of small-angle scattering data.

The EPR data was analysed by Lowfit software developed by Bales group (36). The program calculates the separation between the EPR peaks as well as fitting the Voigt shaped peaks to extract the polarity and rotation correlation coefficient sensed by the probe, hence the aggregate hydrophobicity and microviscosity can be described.

2.4. Results and discussion

2.4.1. Behaviour of HEUR and SDS in solution

2.4.1.1. Behaviour of HEUR in solution

The behaviour of the three HEURs denoted as C_6-L-$(EO_{100}$-L$)_9$-C_6, C_{10}-L-$(EO_{200}$-L$)_4$-C_{10}, and C_{18}-L-$(EO_{200}$-L$)_7$-C_{18} was studied as a function of their concentration. The surface activity of the polymers is measured by surface tension. The changes in the viscosity and size of the polymer aggregates as a function of polymer concentrations are then presented. The analysis of the polymer hydrophobic aggregates is studied by fluorescence and EPR. Finally, various SANS contrasts are presented for the polymer/SDS blends. These three polymers were nominated by AkzoNobel with more focus on C_6-L-$(EO_{100}$-L$)_9$-C_6. For this reason, all experimental data for C_6-L-$(EO_{100}$-L$)_9$-C_6 is presented in this chapter whilst some data of the other two polymers is moved to Appendix A. Only the comparison of the datasets and results will be discussed here.

2.4.1.1.1. Surface activity of the polymers

The surface tension of the polymer was measured as a function of polymer concentration (Figure 2.3). The three polymers show weak surface activity, but their surface activity increases monotonically with $C_{polymer}$.
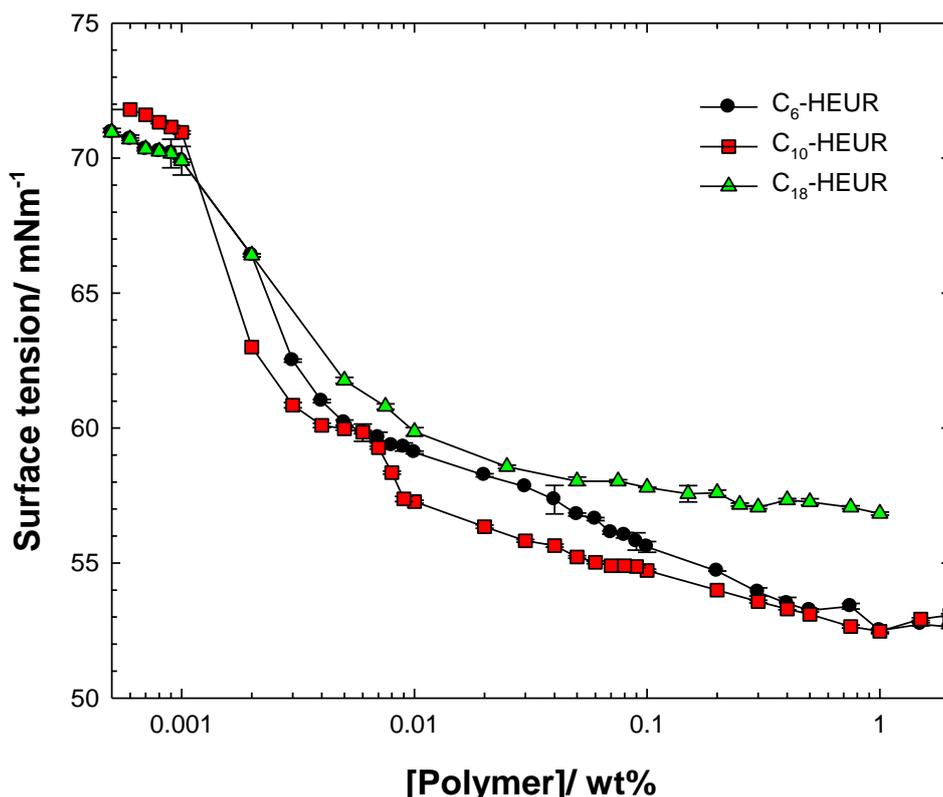
Figure 2.3. Surface tension (γ) of C_6-L-(EO$_{100}$-L)$_9$-C$_6$ (circles), C$_{10}$-L-(EO$_{200}$-L)$_4$-C$_{10}$ (squares), and C$_{18}$-L-(EO$_{200}$-L)$_7$-C$_{18}$ (triangles) as a function of HEUR concentration. Measurements were carried out at 25 °C, pH 9, and ionic strength 100 mM. The solid lines are guides for the eye. The error bars are the standard deviation of three measurements for the same sample and a second set of samples.

2.4.1.1.2. Solution behaviour of the HEURs

The viscosity and self-diffusion coefficients (D_s) of the three polymers were measured as a function of polymer concentration. The viscosity of the polymers as a function of its concentration shows a very subtle increase at low concentration followed by an abrupt increase in viscosity starting at 3 wt% for C_6-L-(EO$_{100}$-L)$_9$-C$_6$ and C$_{10}$-L-(EO$_{200}$-L)$_4$-C$_{10}$ and 0.5 wt% for C$_{18}$-L-(EO$_{200}$-L)$_7$-C$_{18}$ (Figure 2.4). The concentration at which the viscosity starts to increase significantly is known as the critical overlap concentration (C^*).
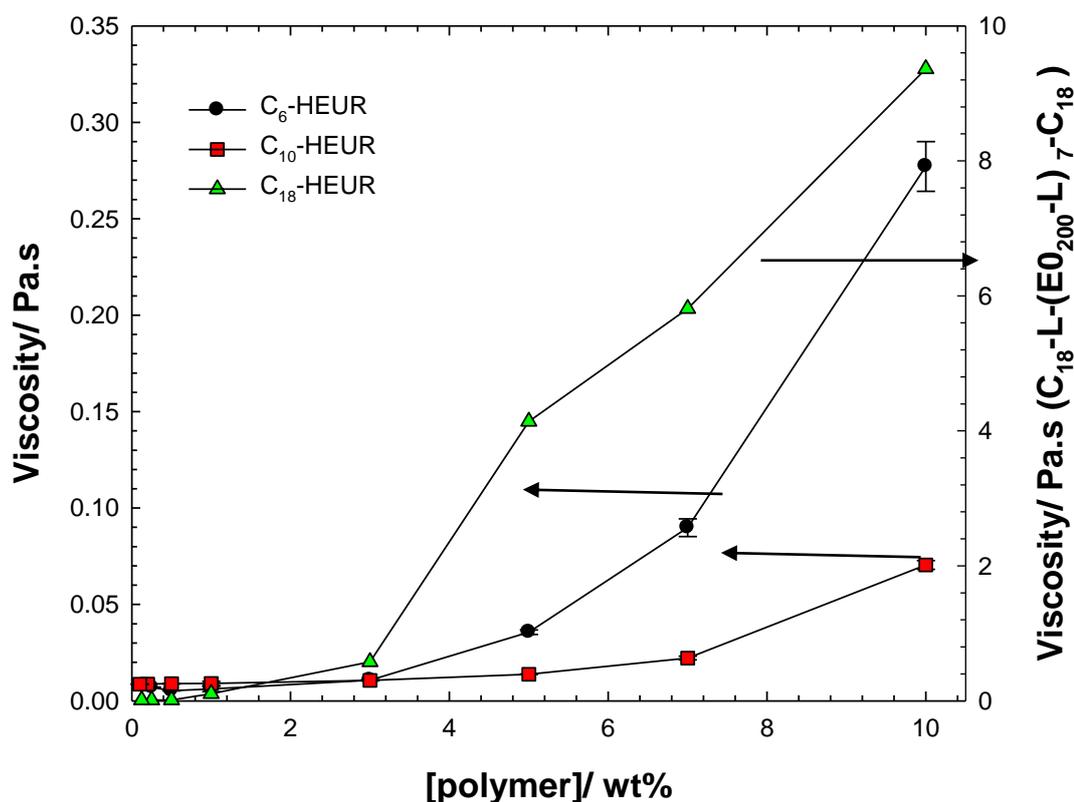
Figure 2.4. Viscosity of C$_6$-L-(EO$_{100}$-L)$_9$-C$_6$ (circles) at shear rate 0.1 s^{-1}, C$_{10}$-L-(EO$_{200}$-L)$_4$-C$_{10}$ (squares), and C$_{18}$-L-(EO$_{200}$-L)$_7$-C$_{18}$ (triangles) as a function of polymer concentration. Measurements were carried out at 25 °C, pH 9, and ionic strength 100 mM. The solid lines are guides for the eye. The error bars are the standard deviation of three measurements for the same sample and a second set of samples.

The self-diffusion coefficients (D_s) of the polymer decreases as a function of its concentration, reflective of the formation of larger aggregates (Figure 2.5). Below the polymer overlap concentration, the D_s is sensitive to molecular weight and is mirrored by viscosity changes but this order is broken for systems above the overlap concentration.
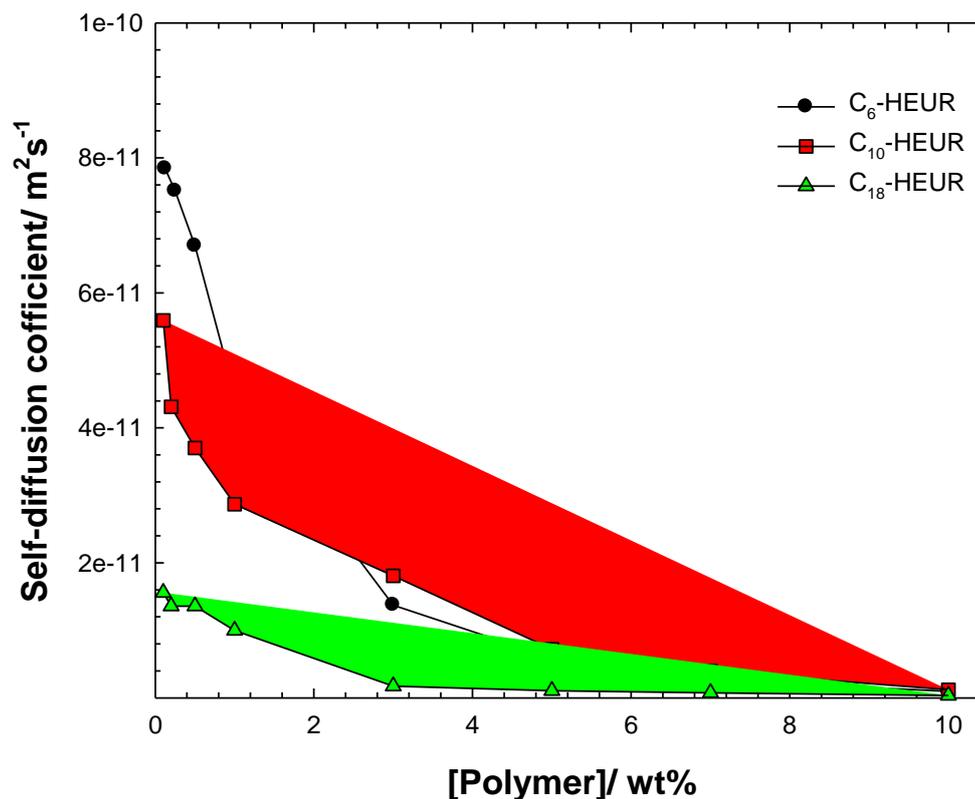
Figure 2.5. Self-diffusion coefficient of C_6-L-(EO_{100}-L)$_9$-C_6 (circles), C_{10}-L-(EO_{200}-L)$_4$-C_{10} (squares), and C_{18}-L-(EO_{200}-L)$_7$-C_{18} (triangles) as a function of polymer concentration. Measurements were carried out at 25 °C, pH 9, and ionic strength 100 mM. The solid lines are guides for the eye. The error bars are the standard deviation of three measurements for the same sample and a second set of samples.

The changes in the viscosity and D_s of the polymer can be correlated to the changes in the arrangement of the polymer as a function of its concentration in solution. Below the C^*, the viscosity slightly increases and D_s decreases as the HEUR polymer tend to associate in the form of flower micelles in solution (29,37). The flower micelles are then linked together forming clusters or sparse network as described by Suzuki *et al.* (38). Above C^*, a dense polymer network structure is formed, where viscosity significantly increases and D_s decreases. Abrahmsen-Alami *et al.* reported the decrease of D_S for PEOM-20-16 (recall the first number is the molecular weight of the polymer in kg mol^{-1} and the second number is the hydrophobic end-group C-chain length) and PEOM-20-18 as a function of polymer concentration, where a phase transition is observed around C^* (29). The comparison between the three polymers here is not straightforward given that

more than one parameter is varied, the end-group chain length, length of PEO segments, number and distribution of urethane linkers.

2.4.1.1.3. Characterisation of the HEUR aggregates

In the ANS fluorescence experiment, variation in the structure and composition of the hydrophobic domain leads to changes in the measured ANS intensity as the fluorescence yield is sensitive to the interaction between the two organic rings in the ANS molecule, a factor that is sensitive to both polarity and fluidity of the probe location. The ANS intensity in water is very low, however in the presence of hydrophobic aggregate ANS is solubilised and higher intensity is observed. The ANS intensity increases due to changes in viscosity of the sample (31).
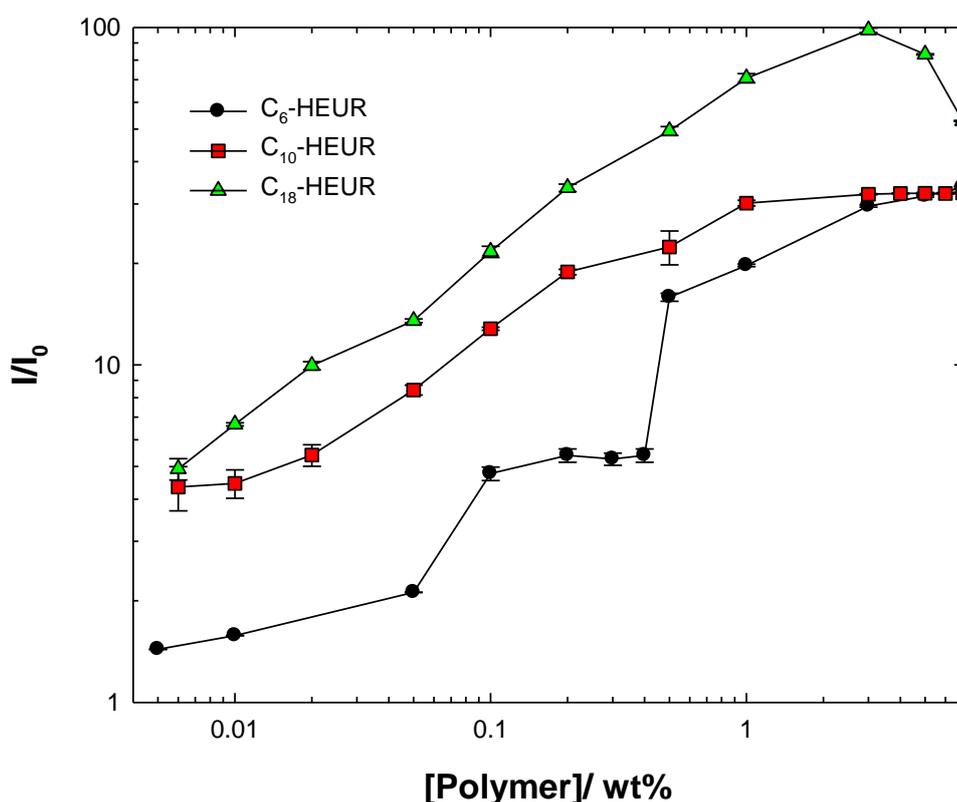
Figure 2.6. ANS intensity of C_6-L-(EO$_{100}$-L)$_9$-C_6 (circles), C_{10}-L-(EO$_{200}$-L)$_4$-C_{10} (squares), and C_{18}-L-(EO$_{200}$-L)$_7$-C_{18} (triangles) as a function of polymer concentration. Measurements were carried out at 25 °C, pH 9, and ionic strength 100 mM. The solid lines are guides for the eye. The error bars are the standard deviation of three measurements for the same sample and a second set of samples.

Chapter 2. HEUR/SDS interaction

The measured ANS intensities in the presence of polymer and/ or surfactant (I) is normalized to the intensity of ANS in water (I_0) to factor out any subtle changes in solubility or degradation of ANS itself. The ANS intensity increases with C_6-L-$(EO_{100}$-L$)_9$-C_6 concentration with an unusual discontinuity around 0.05, and 0.4 wt% (Figure 2.6). The increase in the intensity is due to partitioning of ANS in the hydrophobic aggregate and the breakpoints may be correlated to the structure of the formed aggregates *i.e.* flower micelles, clusters of flower micelles.

Broadly, similar observations are made for the other two polymers (Figure 2.6). There is a decrease in the ANS intensity at high C_{18}-L-$(EO_{200}$-L$)_7$-C_{18} concentrations, this may be explained by the rearrangement of the hydrophobes to form smaller or less hydrophobic aggregates at higher concentrations. Generally, there is a trend in the ANS intensity across the three polymers, where the ANS intensity in the presence of C_{18}-L-$(EO_{200}$-L$)_7$-C_{18} > C_{10}-L-$(EO_{200}$-L$)_4$-C_{10} > C_6-L-$(EO_{100}$-L$)_9$-C_6. This may be correlated to the variation in the C-chain length, where the longer the chain length the higher the ANS intensity observed.

EPR is another technique that is used to study the hydrophobic aggregates of polymer, surfactants and polymer/surfactant blends (39–41). Since, the 16-doxyl-stearic acid methyl ester (16-DSE) is a water-insoluble, it does not give any EPR signal in water. In presence of hydrophobic aggregates, the probe is solubilised in the aggregate and an EPR signal is observed for the probe (7). The changes in the peak separation and broadness are reflective of the polarity and rotation correlation coefficient sensed by the probe, respectively. The rotation correlation coefficient may be correlated to the microviscosity of the aggregates. The 16-DSE signal in the presence of C_6-$(EO_{100}$-L$)_9$-C_6 hydrophobic aggregates show changes in the polarity and microviscosity as a function of its concentration (Figure 2.7). Similar conclusions may be drawn from the C_{18}-L-$(EO_{200}$-L$)_7$-C_{18} (Figure A.1) as a function of its concentration but not for the C_{10}-L-$(EO_{200}$-L$)_4$-C_{10} (Figure A.2), though these data are much noisier, both facts are indicative of the absence of polymer-dominated hydrophobic domains of sufficient size to solubilise the probe. It is interesting that this corresponds to the polymer system with fewest urethane linkers, suggesting that this signal arises from a urethane-rich micro-domain, or that the urethane linkers are important in forming domains of some size.
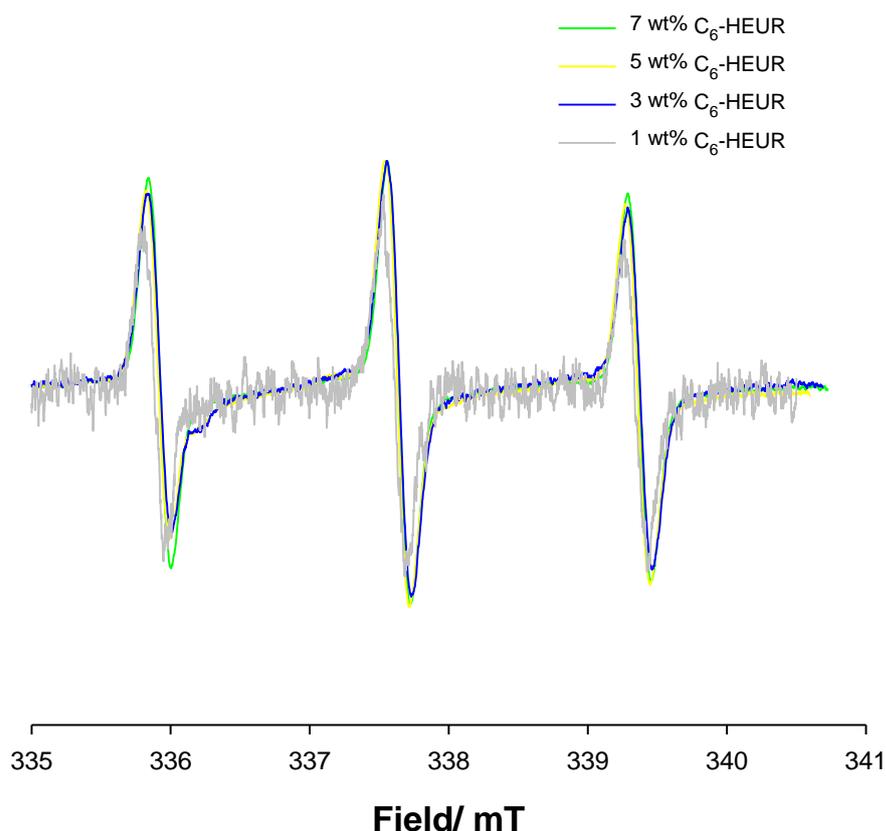
Figure 2.7. EPR spectrum for 16-DSE in the presence 1 of (grey line), 3 (blue line), 5 (yellow line), and 7 (green line) wt% C_6-L-$(EO_{100}$-L$)_9$-C_6. Measurements were carried out at 25 °C, pH 9, and ionic strength 100 mM.

The raw data of C_6-L-$(EO_{100}$-L$)_9$-C_6 were fitted using Lowfit program to extract the polarity and rotation correlation coefficient for the polymer as a function of its concentration. The rotation correlation time and polarity sensed by the probe decreases by increasing concentration of C_6-L-$(EO_{100}$-L$)_9$-C_6. The decrease in the rotation correlation coefficient indicates an increase of the microviscosity of the aggregates. The decrease in the hyperfine coupling constant (A_0) is correlated to the decrease of the polarity sensed by probe, hence more hydrophobic aggregates are formed. These findings contradict with the findings of Persson *et al.* where a PEOM-10-12 was studied as a function of each concentration where the microviscosity and the polarity of the polymer were invariant over a concentration range varied from 0.25 to 5 wt% (7). However, the polymer used in this study are different in architecture due to the presence of the urethane linkers.
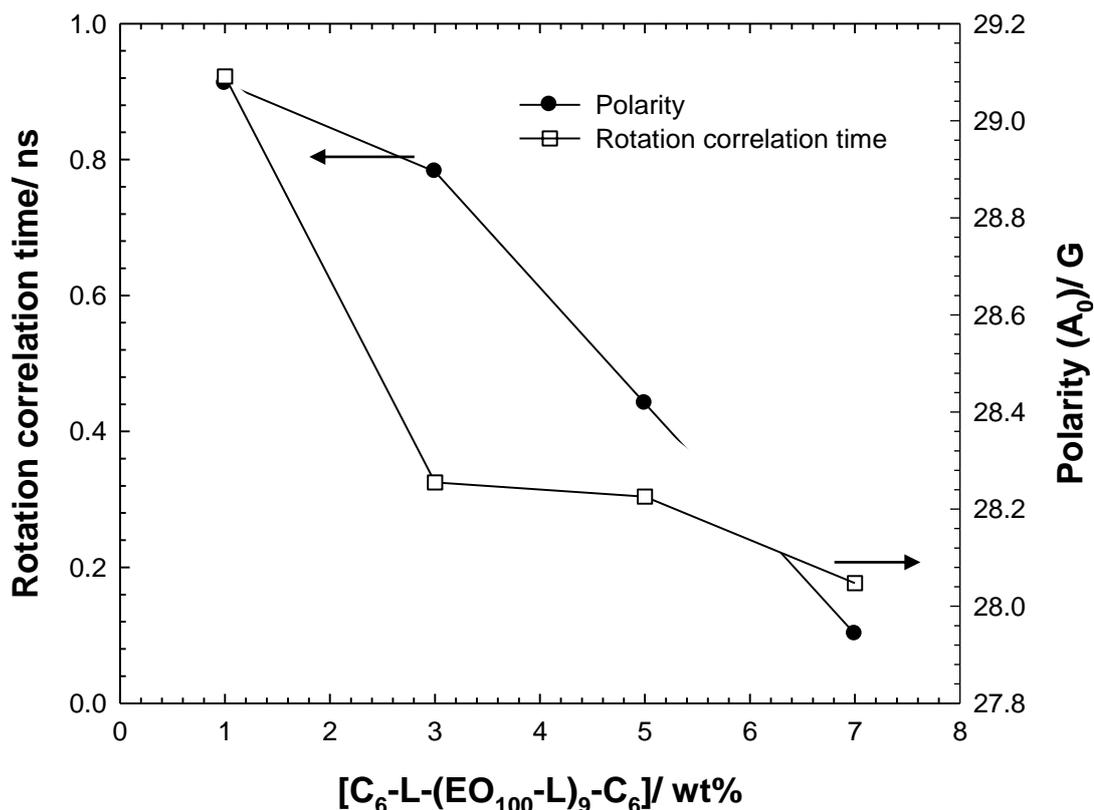
Figure 2.8: Rotation correlation time (squares) and polarity (circles) of 16-DSE solubilised in C_6-L-(EO_{100}-L)$_9$-C_6 solutions as a function of HEUR concentration. Measurements were carried out at 25 °C, pH 9, and ionic strength 100 mM.

2.4.1.1.4. SANS from HEURs

The scattering intensity of the polymers was measured as a function of Q vector at two polymer concentrations, 1 and 7 wt% (Figure 2.9). The C_6-L-(EO_{100}-L)$_9$-C_6 shows a surfactant-like scattering around mid-Q (0.02 $Å^{-1}$) at 1 wt% reflecting the structure of the aggregates of the hydrophobic groups present within the polymer. The scattered intensity at low-Q increases as a function of polymer concentration. In addition, the scattering peak observed at mid Q (this feature might be more aptly described as a shoulder but the term "peak" will be used to highlight the comparison with surfactant scattering) becomes more defined. The peak at mid-Q observed in C_6-L-(EO_{100}-L)$_9$-C_6 seems to be shifted to lower Q range in the C_{10}-L-(EO_{200}-L)$_4$-C_{10}, and C_{18}-L-(EO_{200}-L)$_7$-C_{18} case due to the formation of larger aggregates (Figures A.3 and A.4). Generally, similar conclusions may be drawn from the scattering curves of the other two polymers.
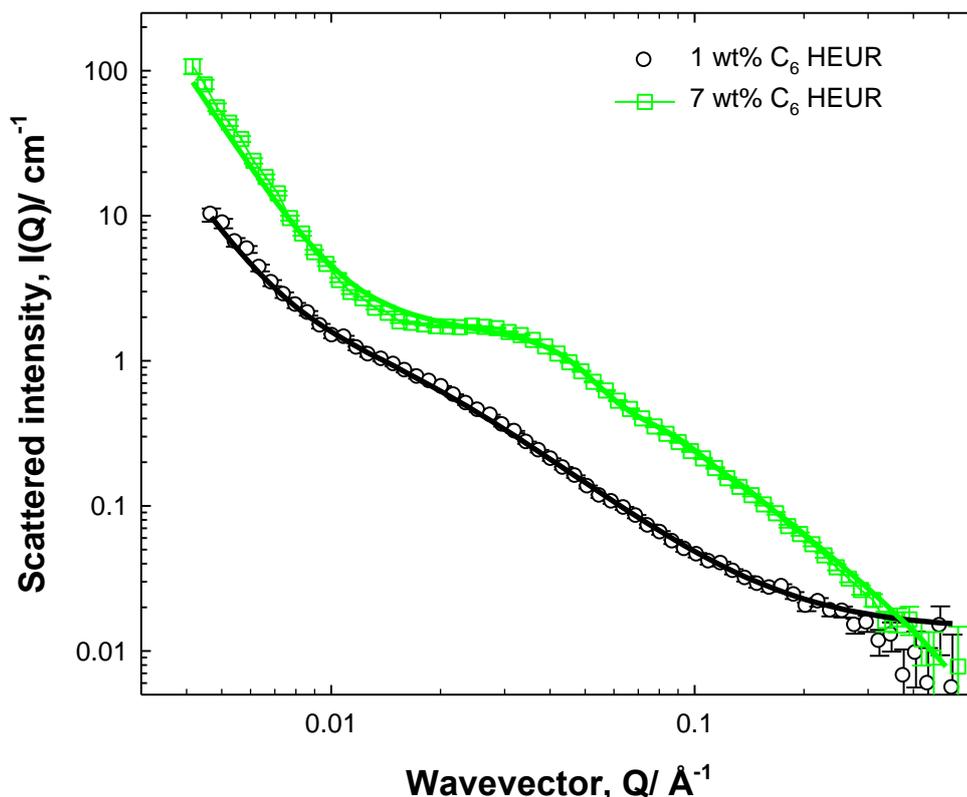
Figure 2.9. Small-angle neutron scattering from h-C_6-L-(EO_{100}-L)$_9$-C_6/D_2O at 1 (circles) and 7 (rectangles) wt% polymer. Measurements were carried out at 25 °C, pH 9 and ionic strength 100 mM. The solid lines are fit for sphere and gel model described later in this section. Key fitting parameters value are presented in Table 2.2.

Similar systems for pure PEOM and HEUR have been fitted to a polydisperse sphere model (9,10). However, this model does not capture the features of the data presented here, especially the low-Q data points. The steepness of the scattering curve at low-Q suggests the presence of large structures which can be correlated to the sparse network structure postulated by Suzuki *et al.* for telechelic polymers below $C,^*$ due to the connection of flower micelles *via* bridging polymer chains (38). Therefore, terms that describe network structure should be added to capture all the scattering curves features. Saffer *et al.* used a two correlation length network model to describe two-phase net-like mesh structure formed by cross-linked PEG gels (42), these systems are very close to the system used here. Therefore, the scattering has been modeled using a compound model, comprising several components: a solid sphere model to reflect the micelle scattering and a two correlation length model to reflect the polymeric network described by Equation 2. 3:

Chapter 2. HEUR/SDS interaction

$$\frac{\partial \sigma}{\partial \Omega}(Q) = N_p V_p^2 (\Delta\rho)^2 . \left(\left(\frac{4}{3}\pi R^3 \frac{[sin(QR) - QRcos(QR)]}{(QR)^3} * S(q) \right) \right) + \frac{I_1}{(1+Q^2\xi^2)} + \frac{I_2}{(1+Q^2A^2)^2} + B_{inc}$$

Equation 2. 3

Where N_p is the number of scattering species V_p the volume of scatterers , $\Delta\rho$ the difference of scattering length density between molecules and solvent, R the radius of the sphere, Q the wavevector, $S(q)$ sphere structure factor, I_1 the Lorentzian term, ξ the shorter length scale, I_2 the Debye-Bueche term, and A longer length scale, B_{inc} inchoherent background. The description of each term of the fitting parameters is illustrated in Table 2.1, the calculated parametres and those obtained from the fit are higlighted.

Solid spherical particles model	
Intensity of radius term	Schultz distribution scale is proportional to the total dispersed volume.
Radius (Å)	radius of the sphere.
Hayter-Penfold charged sphere model	
e	charge (electrons) per sphere,
Debye screening length (Å^{-1})	calculated from Hydroin buffer ionic strength (100 mM) and SDS concentration using the following equations: $$I = 0.5 \sum_i Z_i^2 C_i$$ where *I* is the ionic strength of the solution, z_i *the* valence of the ion *i*, c_i the concentration (M). $$K^{-1} = \left(\frac{k_B T \epsilon_0 \epsilon}{2 q^2 N_A I} \right)^{0.5}$$ or $$K^{-1} = \frac{0.3}{\sqrt{I}}$$ where K^{-1} is the Debye screening length, k_B Boltzmann constant, T absolute temperature, ϵ_0 permittivity of

	vacuum, ϵ dielectric constant of solvent, q elementary charge, N_A Avogadro's number, I ionic strength. The last equation is valid for water at room temperature (43).
Volume fraction	<u>calculated</u> from concentration of the dispersed polymer and/or surfactant.
Peaks and network functions (Gels) - Lorentzian plus Debye-Beuche;	
I_1	Lorentzian term
ξ (Å)	screening length for a semi-dilute solution c > c*, in a good solvent is the average mesh size of a transient network.
I_2	Debye-Beuche term
A (Å)	decay length for inhomogeneities of correlation function.

Table 2.1. The description of the models and fitting parameters used to describe the SANS data in this thesis.

The sphere term would capture the radius of the hydrophobic HEUR aggregates, SDS micelle (studied in Section 2.3.1.2), or HEUR/SDS mixed aggregates (studied in Section 2.3.2). The structure factor of the sphere is represented by the charge density (*e*) per SDS micelle or the HEUR/SDS mixed micelle and inverse the Debye screening length (K^{-1}). In the network model, which was adopted from Saffer *et al.* paper (42) two correlation lengths are considered which may describe a shorter length scale $'\xi'$ which define the mesh size of the network and the longer length scale '*A*' which may be correlated to the distance between the inhomogenous centres of the system (Figure 2.10). However, the correlation length values extracted from the fit for the polymers studied here suggested that the shorter length scale may describe gel network structure fluctuation, wherease the longer length scale is out of the instrument range *e.g.* polymer network. In the fitting process the clalculated terms where the volume fraction, and Debye screening length, whereas the radius of the sphere and the two network correlation length scales. The model developed captures many of the features observed in the experimental data, and

is based on literature precedence of similar systems. As with any model that hasn't been used before to fit these specific systems, care must be taken to over interpret any derived parameter without first justifying the use of the model. Generally speaking the parameters extracted from the model are consistent with similar systems in a broader sense, though there may be challenges associated with ascribing a specific parameter to a molecular characteristic. Notwithstanding this caveat the fits describe the data fully across the wide range of sample characteristic. Further validation of the fitting approach is born out in the contrast variation experiments.
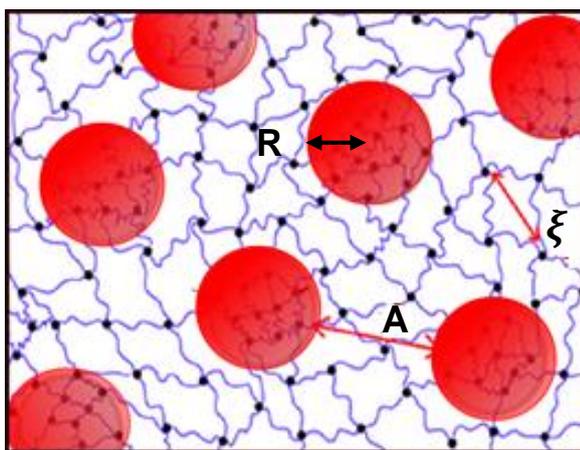
Figure 2.10. Sphere and network model illustrating the key parameters in the model; R is the sphere radius, A is Debye-Bueche length and ξ is Lorentzian length scale. The figure has been derived and manipulated to describe our system from Saffer *et al.* paper (42).

The fitting parameters of C_6-L-$(EO_{100}$-L$)_9$-C_6 are presented in Table 2.2. At 7 wt% C_6-L-$(EO_{100}$-L$)_9$-C_6, The size of the polymer aggregates become more defined and the fit is more sensitive to the changes in the sphere radius parameter. The shorter length scale becomes smaller and the longer length scale becomes larger. The changes in the length scales may be explained by the formation of the network with a smaller mesh size in the dense network structure, however, the distance between the hydrophobic aggregates is bigger may be due to the conversion of polymer looping chains to bridges. Similar conclusions can be drawn from the fit of the other two polymers, the key parameters from the fit are presented in Table A.1 and A.2 in Appendix A for C_{10}-L-$(EO_{200}$-L$)_4$-C_{10}, and C_{18}-L-$(EO_{200}$-L$)_7$-C_{18}, respectively. The sensitivity of the fit to the parameters is presented in the Appendix (Figures A.5 to A.8).

Fit parameters/ Units	1 % HEUR	7 % HEUR
Intensity of radius term	n.d.	1.8×10^{-6}
Radius (Å)	n.d.	62 ± 2
e	n.d.	n.d.
K^{-1} (Å)	n.d.	n.d.
φ	0.01	0.07
I_1	1.78	1.7
ξ (Å)	75 ± 2	20 ± 1
I_2	247	7190
A (Å)	455 ± 5	672 ± 10

Table 2.2. SANS key parameters from the sphere and network model for C_6-L-(EO_{100}-L)$_9$-C_6 at $C_{polymer}$ = 1 and 7 wt%.

2.4.1.2. SDS behaviour in solution

2.4.1.2.1. Critical micelle concentration and aggregates of pure SDS
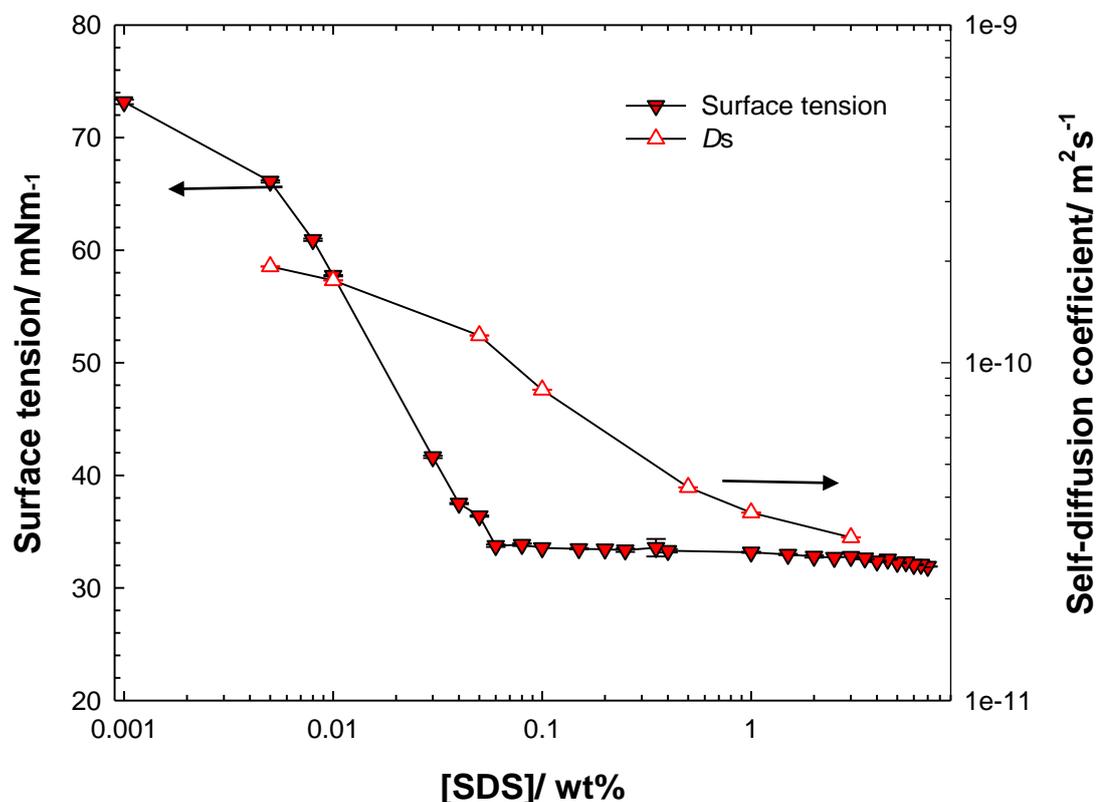
Figure 2.11. Surface tension (γ) (red inverted triangles) and self-diffusion coefficient (white triangles) of SDS as a function of its concentration. Measurements were carried out at 25 °C, pH 9, and ionic strength 100 mM. The solid lines are guides for the eye. The error bars are the standard deviation of three measurements for the same sample and a second set of samples.

For the simple anionic surfactant SDS in buffered H_2O, the surface tension and diffusion data show the expected clear breakpoint at 0.06 wt% (2 mM) (Figure 2.11) in good agreement with literature values pertaining to the prevailing values of pH and ionic strength (44).
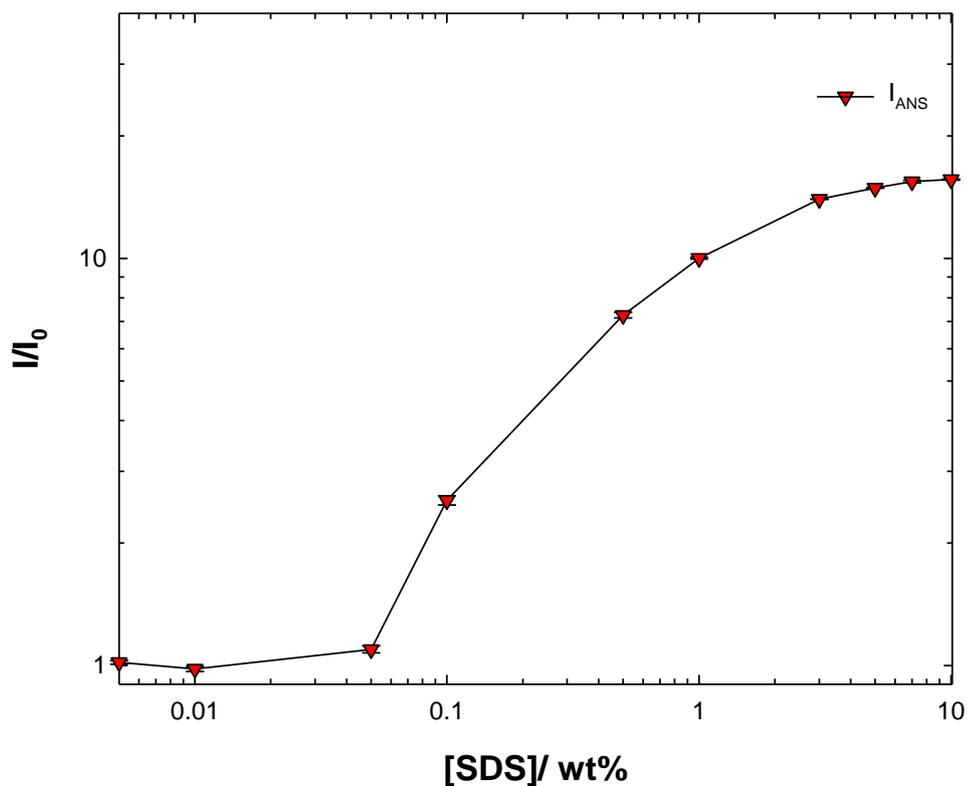
Figure 2.12. ANS fluorescence intensity as a function of SDS concentration. Measurements were carried out at 25 °C, pH 9 and ionic strength 100 mM. The solid line is a guide for the eye. The error bars are the standard deviation of three measurements for the same sample and a second set of samples.

In the ANS fluorescence data, SDS shows the expected substantial increase in the measured intensity at the CMC, 0.05 wt% (in a reasonable agreement with the surface tension data, 0.06 wt%) (Figure 2.12).
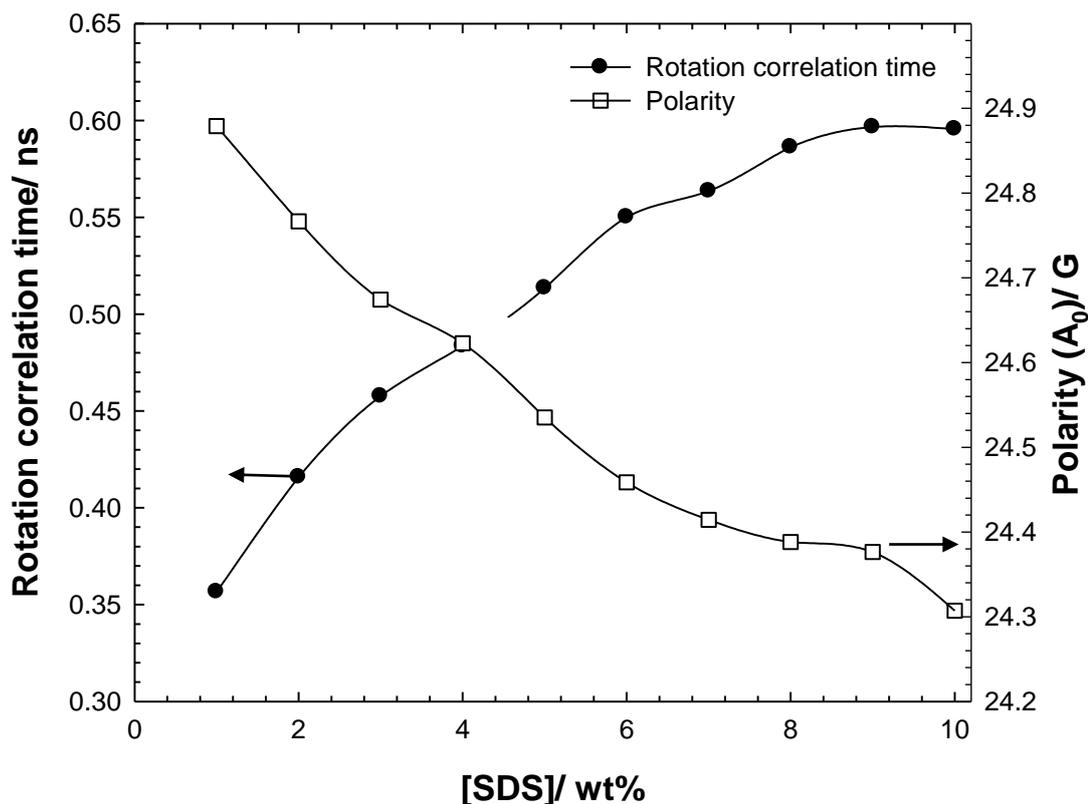
Figure 2.13. Rotation correlation time (circles) and polarity (squares) of 16-DSE solubilised in SDS solutions as a function of SDS concentration. Measurements were carried out at 25 °C, pH 9, and ionic strength 100 mM.

In the EPR experiment, the 16-DSE signal was measured as a function of SDS concentration. The raw data is presented in Appendix A (Figure A.9). The extracted polarity and rotation correlation coefficients are presented in (Figure 2.13). The rotation correlation time increases as a function of SDS. In contrast, however, the A_0 decreases with increasing SDS concentration. The changes in the rotation correlation coefficient and polarity of SDS as a function of its concentration agrees with the data reported by Griffiths *et al.* for pure SDS as a function of its concentration in simple H_2O (*i.e.* not buffered) (41).
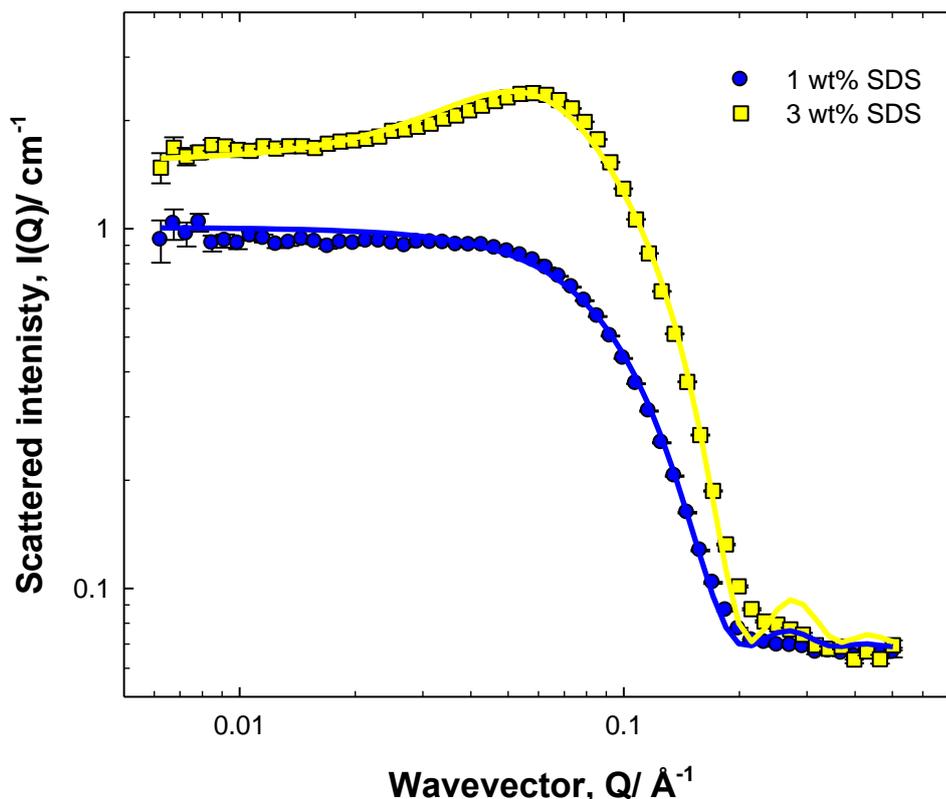
Figure 2.14. Small-angle neutron scattering from 1 (blue circles), and 3 (yellow squares) wt% h-SDS. Measurements were carried out at 25 °C, pH 9, and ionic strength 100 mM. The solid lines are charged sphere fit. Key fitting parameters value are presented in Table A.3.

The scattered intensity of the SDS was measured in Hydroin buffered D_2O (Figure 2.14). The SDS scattering shows a concentration-dependent increase in the scattered intensity at mid Q, reflective of micellar scattering. However, at low-Q there is a decrease in the scattered intensity due to the structure factor. The data were fitted to a Hayter-Penfold charged sphere model, Table 2.1 where the radius of the sphere at both SDS concentrations is 20 ± 2 Å. The key parameters from the fit are presented in the Appendix, Table A.3.

2.4.2. HEURs/SDS interaction

The interaction of the anionic surfactant SDS was studied with three HEURs denoted as C_6-L-$(EO_{100}$-L$)_9$-C_6, C_{10}-L-$(EO_{200}$-L$)_4$-C_{10}, and C_{18}-L-$(EO_{200}$-L$)_7$-C_{18}. The three polymers were quantified at two polymer concentrations, $C_{polymer}$, spanning the critical overlap concentration (C^*) of C_6-L-$(EO_{100}$-L$)_9$-C_6, $C^* = 3$ wt%, *viz* $C_{polymer} = 1$ wt% and $C_{polymer} = 7$

wt%. For consistency, similar concentrations were used for the other two polymers. The more concentrated system is then presented which has been less studied. The surface tension data is presented first, where the concentrations at which SDS begins to bind to the polymer (in the dilute regime) and polymer saturation with SDS are noted. The interaction of the polymer with the surfactant results in changes in the bulk viscosity and polymer diffusion, therefore the polymer viscosity and self-diffusion coefficient are studied as a function of SDS. The changes in the polymer hydrophobic aggregates composition are studied by fluorescence and EPR. Finally, a series of contrast-match experiments are presented to study the arrangement of the polymer and surfactant in the polymer/surfactant blends.

2.4.2.1. Polymer/surfactant interactions below the polymer critical overlap concentration (C*)

2.4.2.1.1. Surface tension measurements for HEUR, SDS, and HEUR/SDS blends
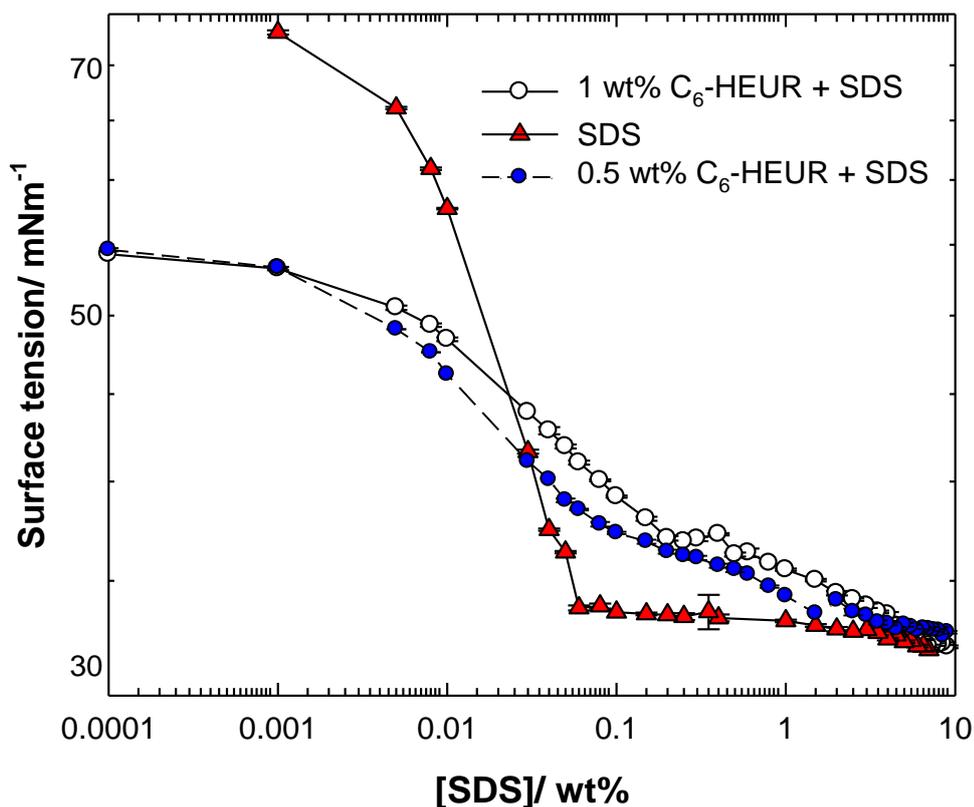
Figure 2.15. Surface tension (γ) as a function of SDS concentration in the absence (red triangles) and presence of 0.5 (blue circles) and 1 (white circles) wt% C_6-L-(EO_{100}-L)$_9$-C_6. Measurements were carried out at 25 °C, pH 9, and ionic strength 100 mM. The solid lines are guides for the eye. The error bars are the standard deviation of three measurements for the same sample and a second set of samples.

Figure 2.15 presents the surface tension data for the SDS, and C_6-L-(EO_{100}-L)$_9$-C_6/SDS mixture, for $C_{polymer}$ = 0.5 and 1 wt%. In a typical γ-ln *C* curve for non-hydrophobically modified polymer/surfactant blends, the surface tension generally shows two break points, CAC_1 (critical aggregation concentration) and CAC_2. CAC_1 corresponds to the onset of cooperative binding of the surfactant to the polymer and usually lies below the CMC of pure surfactant. CAC_2 corresponds to the onset of formation of free non-bound surfactant micelles and is higher than CMC of pure surfactant (45).
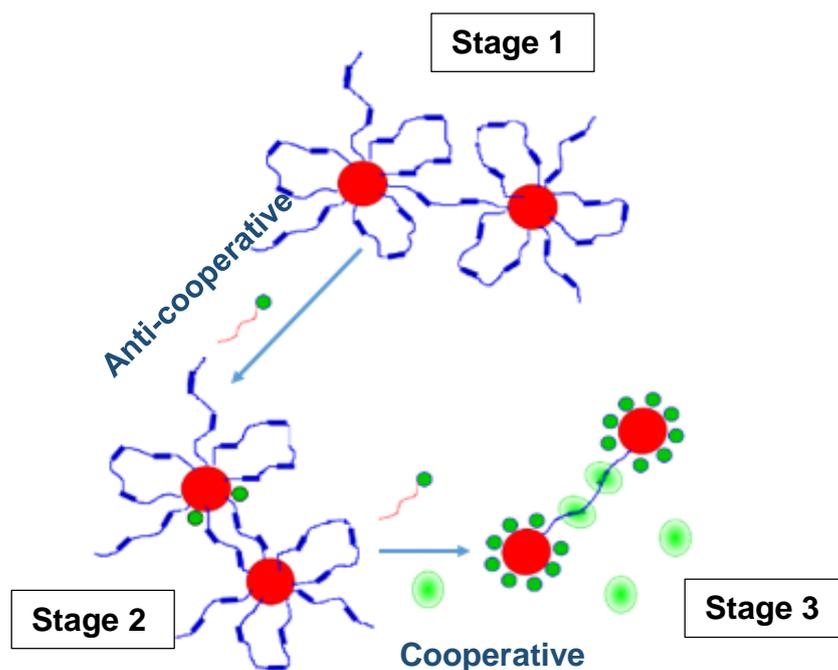
Figure 2.16. Illustrative diagram for the two mechanisms of SDS binding to the HEUR polymer where $\multimap$ **is the SDS unimer and** $\circ$ **the SDS micelle.**

The HEUR/surfactant data are rather different. As may be seen in Figure 2.15, for HEUR (1 wt%)/SDS blend there are indeed two break points observed: $CAC_1 = 0.3$ wt% and $CAC_2 = 7$ wt% SDS. These two points are shifted to **lower** values when the polymer concentration is **reduced** *viz* for $C_{polymer} = 0.5$ wt%, $CAC_1 = 0.15$ wt% and $CAC_2 = 4$ wt%. Further, both CAC_1 values are greater than the CMC of pure SDS. These observations indicate that the HEUR/surfactant interaction is an anti-cooperative one, with (monomeric) binding of discrete surfactant molecules to the polymer hydrophobic aggregates before interacting cooperatively (micellar binding) with the backbone at higher surfactant concentrations (Figure 2.15). Thus, the feature representing CAC_1 is shifted to values greater than the CMC of pure SDS, when the hydrophobes are present, because of the reduced apparent activity of the surfactant. Generally, the anti-cooperative binding reflects the binding of charged surfactant monomer to already existing hydrophobic aggregate, the presence of more than one charged species in the aggregates is unfavorable, and hence this process is slow. Cooperative binding reflects the binding of surfactant micelle to polymer and this process is fast and favorable, as in the case of charge surfactant and neutral polymer, the polymer interaction with the micelle tends to reduce the electrostatic repulsive forces between the head groups.
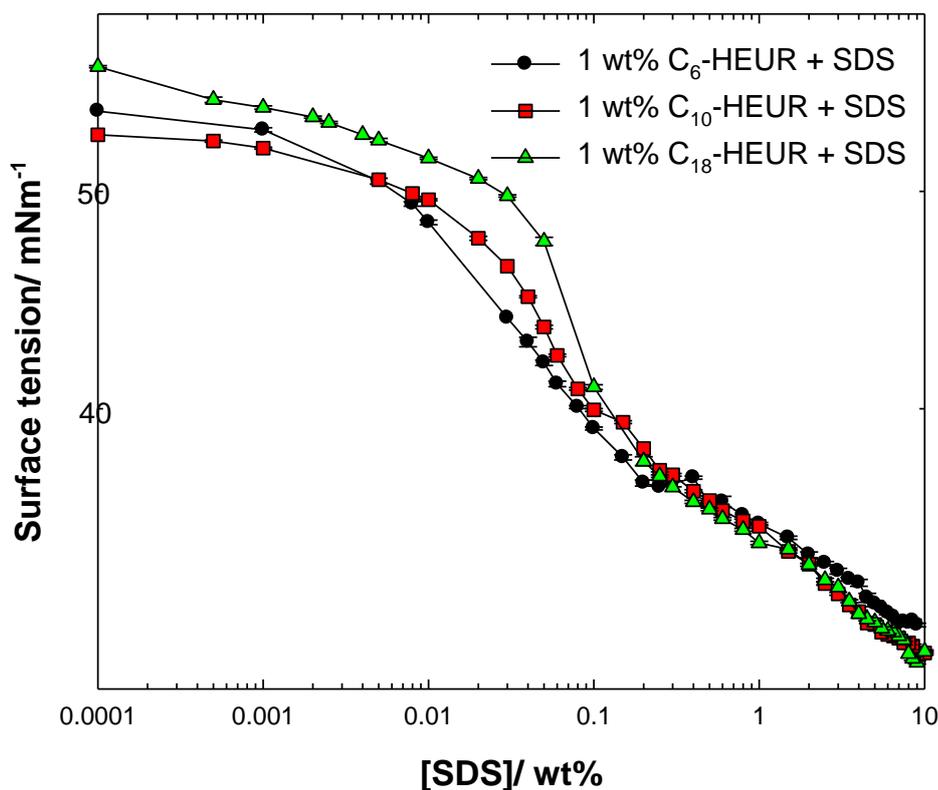
Figure 2.17. Surface tension (γ) of 1 wt% C_6-L-(EO$_{100}$-L)$_9$-C_6 (circles), C_{10}-L-(EO$_{200}$-L)$_4$-C_{10} (squares), and C_{18}-L-(EO$_{200}$-L)$_7$-C_{18} (triangles) as a function of SDS concentration. Measurements were carried out at 25 °C, pH 9, and ionic strength 100 mM. The solid lines are guides for the eye. The error bars are the standard deviation of three measurements for the same sample and a second set of samples.

Hulden measured the surface tension for HEUR-19-18 and HEUR-19-15 (recall the first number in the code is the molecular weight of the polymer and second number is the C-chain length) as a function of SDS concentration (14). CAC$_1$ and CAC$_2$ reported are 5 mM and 63 mM for the two polymers. Hulden CMC values are lower than the values reported for the three polymers studied here (10.4 mM). This can be explained by the different architectures of the polymers used in this study. The polymers used here have more urethane linkers distributed along the backbone, increasing the hydrophobic nature of the polymers, compared to those used by Hulden. Further, the polymers used in Hulden's study possess hexamethylene diisocyanate (HDI), present at the ends, and two distributed along the hydrophilic backbone at equal distances from each other. This observation reinforces the hypothesis that the urethane linkers present along the

backbone, as well as the hydrophobic aggregates, interact with the SDS monomer, hence CAC_1 concentration shifted to higher SDS concentration.

Dai *et al.* reported the CAC_1 and CAC_2 for a range of C_{16} HEUR polymers with various molecular weights (18-100 kg mol^{-1}) with SDS measured by isothermal titration calorimetry. The CAC_1 and CAC_2 are reported to be independent of the molecular weight of the polymer (46). Hulden illustrated the independence of C-chain length on CAC_1 and CAC_2, by measuring the surface tension of HEUR-19-18 and HEUR-19-15 as a function of SDS concentration (14). Here, the surface tension data demonstrates also very little dependence on the polymer structure over this relatively narrow range explored (factors of 2 in the number of urethane linkers and end groups at this fixed polymer concentration) (Figure 2.17).

2.4.2.1.2. Solution behaviour of HEUR/SDS mixtures in polymer dilute regime

Further evidence for the interaction at these low concentrations of SDS is presented in Figure 2.18, where there are changes in the viscosity (and self-diffusion coefficient) of the polymer at SDS concentrations below the CAC_1 (0.3 wt%).
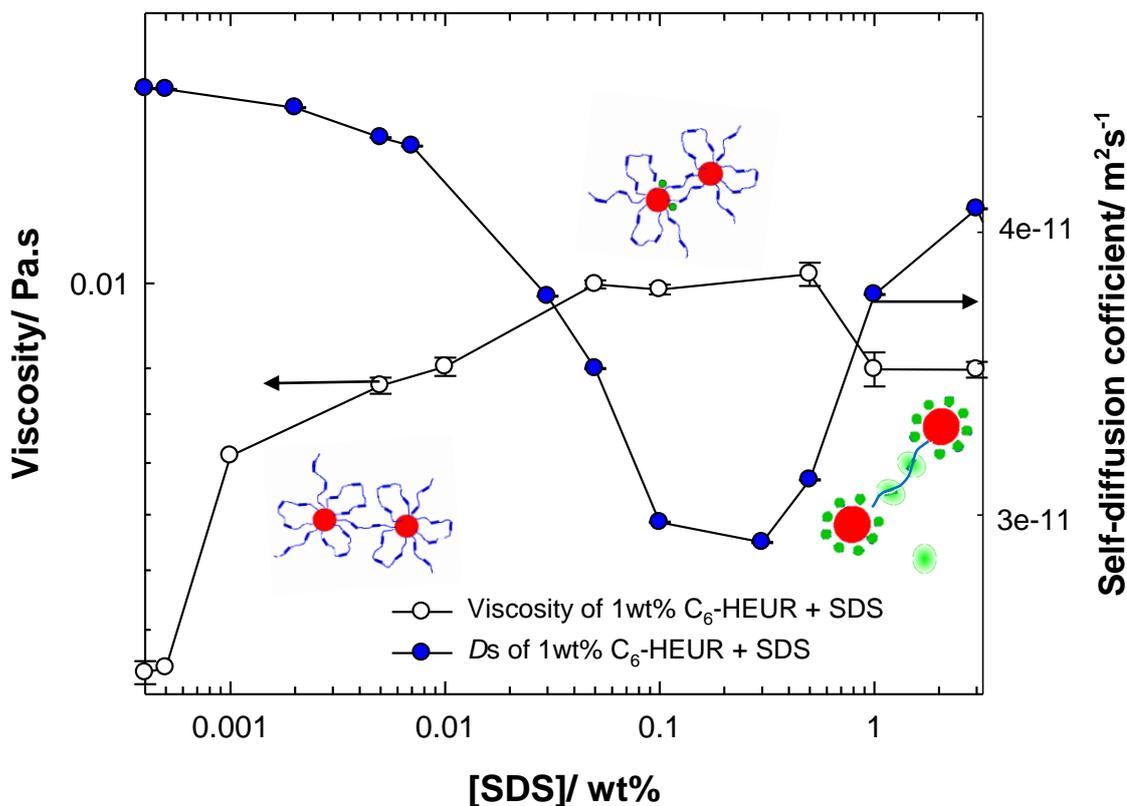
Figure 2.18. Viscosity (white circles) at shear rate 0.1 s^{-1} and self-diffusion coefficient (blue circles) of aqueous solutions of 1 wt% C$_6$-L-(EO$_{100}$-L)$_9$-C$_6$/SDS mixtures as a function of SDS concentration. Measurements were carried out at 25 °C, pH 9, and ionic strength 100 mM. The solid lines are guides for the eye. The error bars are the standard deviation of three measurements for the same sample and a second set of samples.

The viscosity and self-diffusion coefficient have been measured for solutions with C$_{polymer}$ = 1 wt% over a range of SDS concentrations. Viscosity and self-diffusion data are generally complementary to each other, an increase in viscosity is reflected by a decrease in the self-diffusion coefficient. The behaviour becomes more complex with increasing SDS concentration; the viscosity increases, attains a plateau then decreases before finally increasing at very high SDS concentrations. The self-diffusion coefficient, therefore, follows a very similar but an inverted profile. This complex behaviour reflects the balance of *intra-* and *inter*-molecular polymer association that is changed by the addition of SDS. The larger changes in viscosity at lower SDS concentration are due to the monomeric, anti-cooperative binding of SDS onto the polymer hydrophobic aggregates. The SDS monomeric binding is hypothesised to facilitate the adoption of a more extended conformation of the polymer by turning loops into bridges (26) (Figure

2.16, Stage 2). However, at high SDS concentration, the HEUR hydrophobes are solubilised in the SDS micelles and the sparse network structure is lost (Figure 2.16, stage 3).

The viscosity and D_s trends presented here agree with the literature. Zhang *et al.* reported a similar viscosity and diffusion behaviour for 1 wt% HEUR-15-16 as a function of SDS concentration (15). Generally, the increase in viscosity (and decrease in self-diffusion coefficient) with increasing surfactant concentration reflects the number and composition of mixed micelles of SDS and hydrophobic end-groups, as this defines the strength of the polymer network. The network is generally strengthened by increasing the residence time of the polymeric end-groups within such micelles or increasing the number of cross-links by increasing the number of hydrophobic aggregates, or conversion of loop-forming polymer chains to bridges (14,37). In the literature, it is postulated that at low SDS concentration, where the viscosity increases and the diffusion decreases, the SDS forms more mixed aggregates with the polymer hydrophobes of smaller size (15), hence the sparse network formed at this concentration is strengthened. At higher SDS concentration, the polymer hydrophobes are solubilised in SDS micelles which annul the presence of the hydrophobes. As a result, the network structure is broken and the HEUR behaves as PEO/SDS mixtures (15,26).
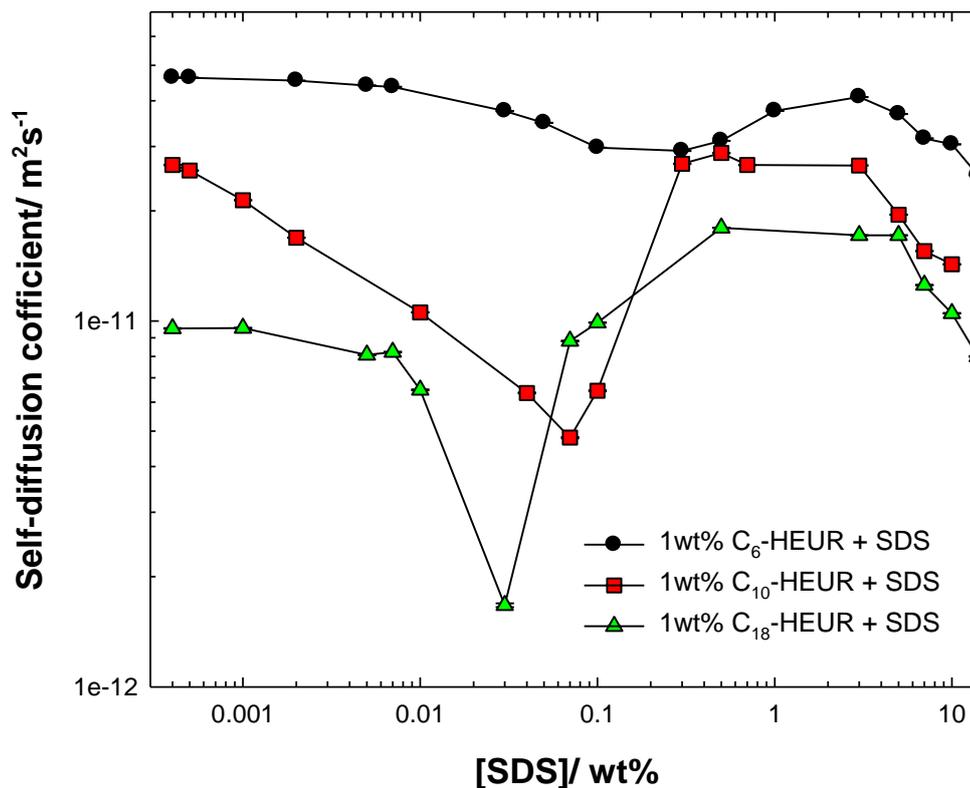
Figure 2.19. Self-diffusion coefficient of 1 wt% C_6-L-$(EO_{100}$-L$)_9$-C_6 (circles), C_{10}-L-$(EO_{200}$-L$)_4$-C_{10} (squares), and C_{18}-L-$(EO_{200}$-L$)_7$-C_{18} (triangles) as a function of SDS concentration. Measurements were carried out at 25 °C, pH 9, and ionic strength 100 mM. The solid lines are guides for the eye. The error bars are the standard deviation of three measurements for the same sample and a second set of the samples.

Similar behaviour in D_s has been observed here for C_{10}-L-$(EO_{200}$-L$)_4$-C_{10}, and C_{18}-L-$(EO_{200}$-L$)_7$-C_{18} as a function of SDS concentration (Figure 2.19). However, the SDS concentration at which the minimum diffusion (D_{min}) of the HEUR/SDS mixture is observed, shifts to lower SDS concentration as molecular weight and C-chain length of the polymer increases. The D_{min} occurred at the lowest SDS concentration for C_{18}-L-$(EO_{200}$-L$)_7$-$C_{18} < C_{10}$-L-$(EO_{200}$-L$)_4$-$C_{10} < C_6$-L-$(EO_{100}$-L$)_9$-C_6. The effect of SDS on D_{min} has not been reported previously, but Hulden reported the shift of the SDS concentration at which a viscosity maximum V_{max} of the HEUR/SDS mixture is observed to lower SDS concentration as the molecular weight or C-chain length of the polymer is increased (14).

The diffusion minimum shift to lower SDS concentration in the three polymers comparison can be understood in terms of the number of hydrophobes available for SDS to interact with at a fixed concentration. C_{18}-L-$(EO_{200}$-L$)_7$-C_{18} has the fewest number of hydrophobes

followed by C_{10}-L-$(EO_{200}$-L$)_4$-C_{10} and C_6-L-$(EO_{100}$-L$)_9$-C_6, therefore, it is expected to note the diffusion increase (network breakage) in C_{18}-L-$(EO_{200}$-L$)_7$-C_{18} before C_{10}-L-$(EO_{200}$-L$)_4$-C_{10} and C_6-L-$(EO_{100}$-L$)_9$-C_6. Hulden varied the concentration of the polymer to get the same viscosity at 0 wt% SDS, but that does not consider the number of hydrophobes available for the SDS to interact with (14). Alami *et al.* reported that at V_{max} for PEOM-22-12/SDS mixture the mixed hydrophobic aggregates have two polymeric end-groups per aggregate and D_{min} has 4 hydrophobes per aggregate. The number of polymer end-groups was extracted from quenching fluorescence experiment (25). Therefore it may be concluded that the number of the polymer hydrophobic end-group available has an influence on the SDS concentration at which the V_{max} or D_{min} is observed.

2.4.2.1.3. Analysis of HEUR/SDS hydrophobic aggregates in polymer dilute regime

Since the surface tension and diffusion/viscosity insights reflect different, but complementary facets of the polymer/surfactant blend, fluorescence was also used to probe the effect of SDS on the hydrophobic domains, formed initially from the polymer end-groups. The fluorescence data show a decrease of ANS intensity as a function of SDS concentration to a minimum (I_{min}), which then rises to a maximum and finally decreases and approaches the ANS intensity of pure SDS at the highest SDS concentration studied (Figure 2.20). The decrease of ANS intensity occurs over the region where SDS anti-cooperative binding occurs. I_{ANS} decreases when the binding is less, or the environment is less polar or more mobile. A combination of all of these factors could be occurring here.
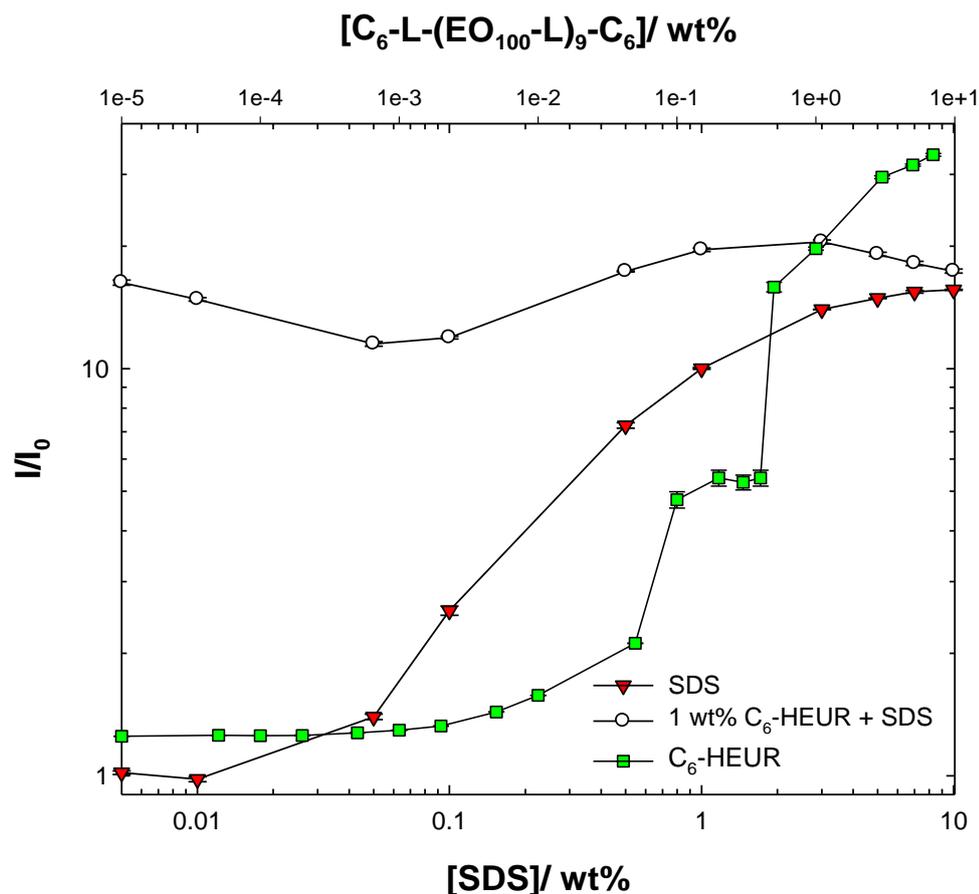
Figure 2.20. ANS fluorescence intensity of C_6-L-(EO100-L)$_9$-C_6 (squares) as a function of polymer concentration, SDS (triangles), and C_6-L-(EO100-L)$_9$-C_6/SDS (circles) at $C_{polymer}$ = 1 wt% as a function of SDS concentration. Measurements were carried out at 25 °C, pH 9, and ionic strength 100 mM. The solid lines are guides for the eye. The error bars are the standard deviation of three measurements for the same sample and a second set of samples.

For the other polymers, similar broad trend is observed with the intensities of the ANS fluorescence decreasing for a given SDS concentration (Figure 2.21). However, the increase of the ANS intensity after I_{min} is less intense than C_6-L-(EO$_{100}$-L)$_9$-C_6 case.
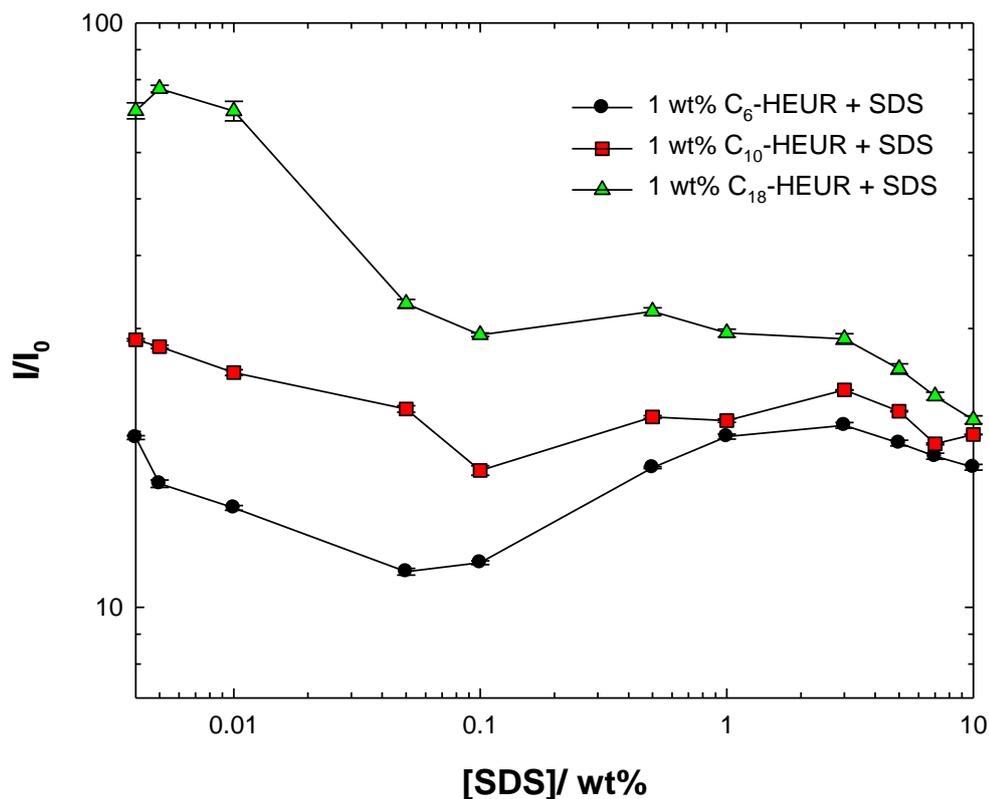
Figure 2.21. ANS intensity of C_6-L-(EO$_{100}$-L)$_9$-C$_6$ (circles), C_{10}-L-(EO$_{200}$-L)$_4$-C_{10} (squares), and C_{18}-L-(EO$_{200}$-L)$_7$-C_{18} (triangles) as a function of SDS concentration. Measurements were carried out at 25 °C, pH 9, and ionic strength 100 mM. The solid lines are guides for the eye. The error bars are the standard deviation of three measurements for the same sample and a second set of samples.
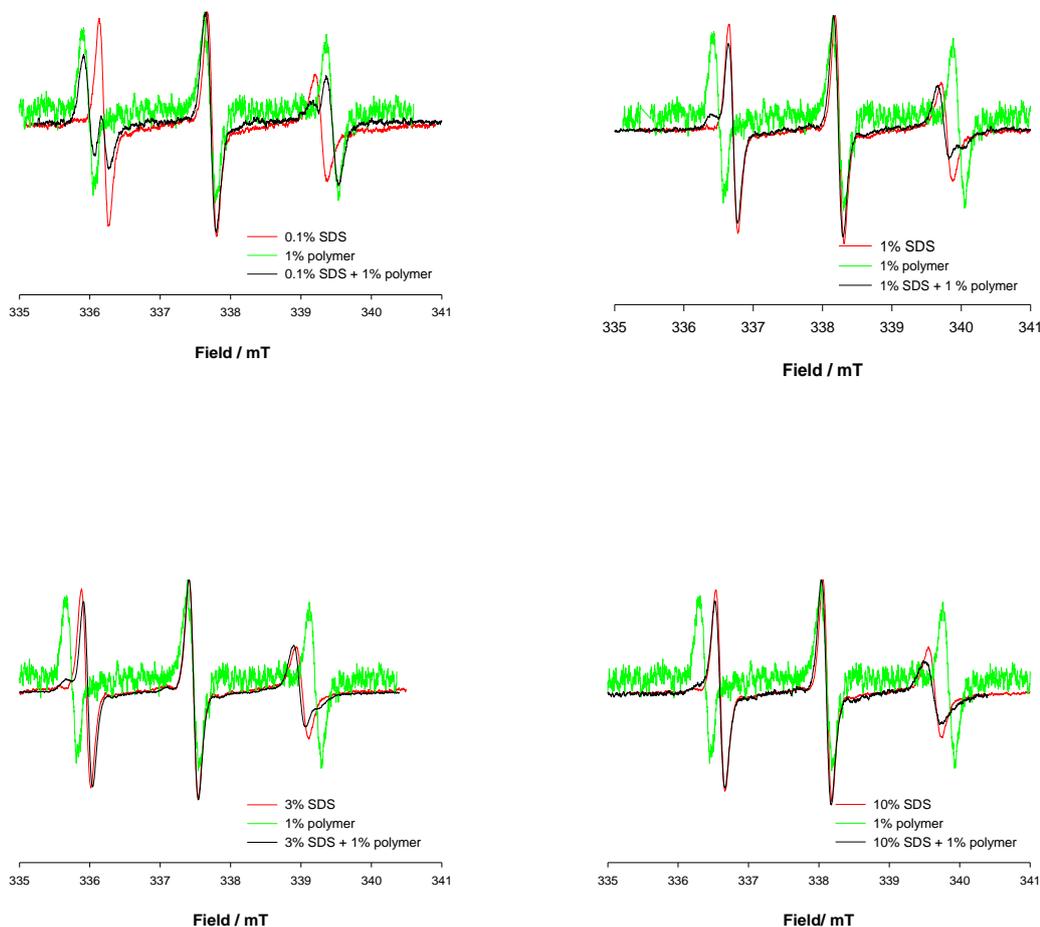
Figure 2.22. EPR spectrum for 16-DSE in the presence of four different concentrations of SDS, 1 wt% C_6-L-(EO_{100}-L)$_9$-C_6, and the polymer/SDS blend. Measurements were carried out at 25 °C, pH 9, and ionic strength 100 mM.

The change in the hydrophobic aggregate structure as the SDS interacts with the polymer is also reflected by changes in 16-DSE signal. The 16-DSE shows a signal for 1 wt% C_6-L-(EO_{100}-L)$_9$-C_6 and the SDS concentrations used in this experiment (0.1, 1, 3, and 10 wt%) indicative of the presence of hydrophobic aggregates (Figure 2.22). The EPR spectrum shows splitting of the 1st (low-field) and 3rd (high-field) peak. The peak splitting is reflective of the presence of two different environments, a polymer, and surfactant-like environment. This may be correlated to the SDS binding mechanism to the polymer. At low SDS concentration where monomeric binding occurs, the signal from the polymer-like environment is more intense. However, at higher SDS concentrations where micellar binding takes place, the surfactant-like signal becomes dominant.

64
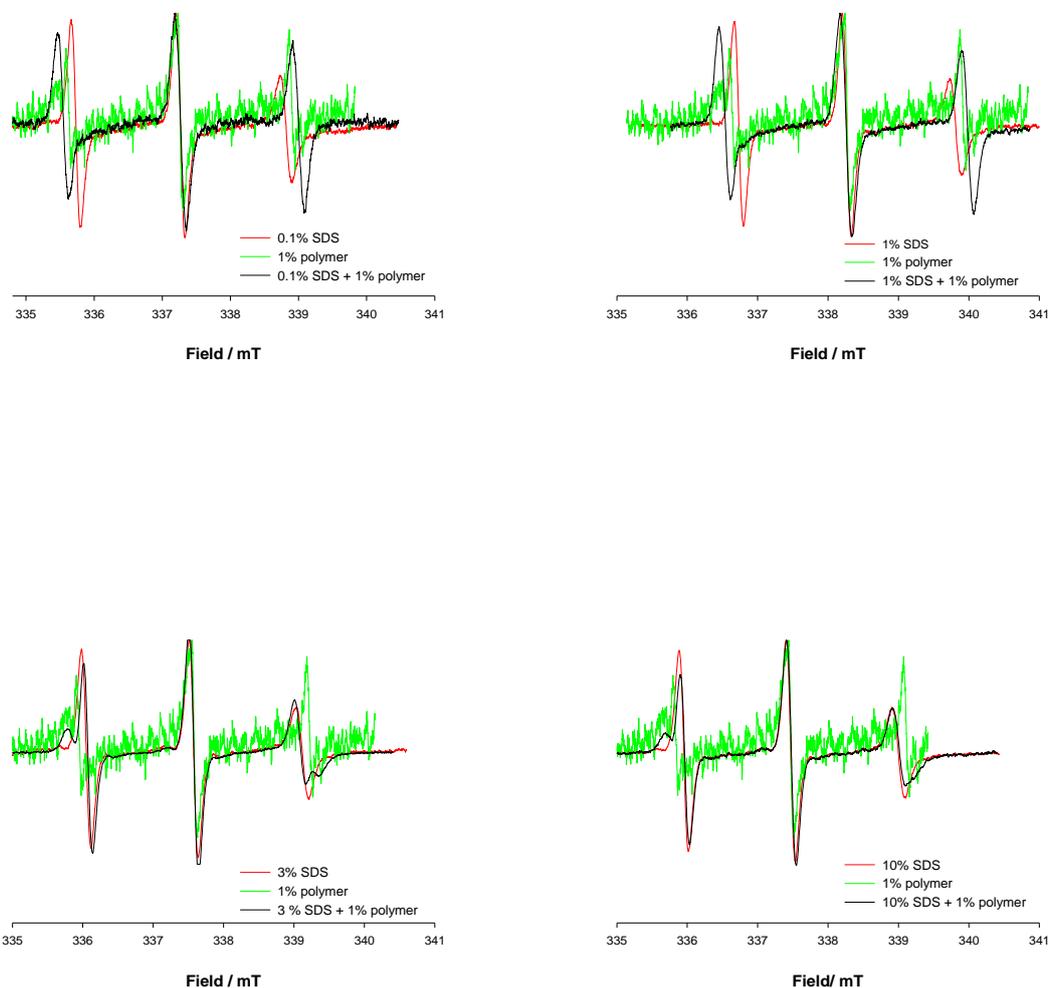
Figure 2.23. EPR spectrum for 16-DSE in the presence of four different concentrations of SDS, 1 wt% C_{18}-L-(EO$_{200}$-L)$_7$-C_{18}, and the polymer/SDS blend. Measurements were carried out at 25 °C, pH 9, and ionic strength 100 mM.
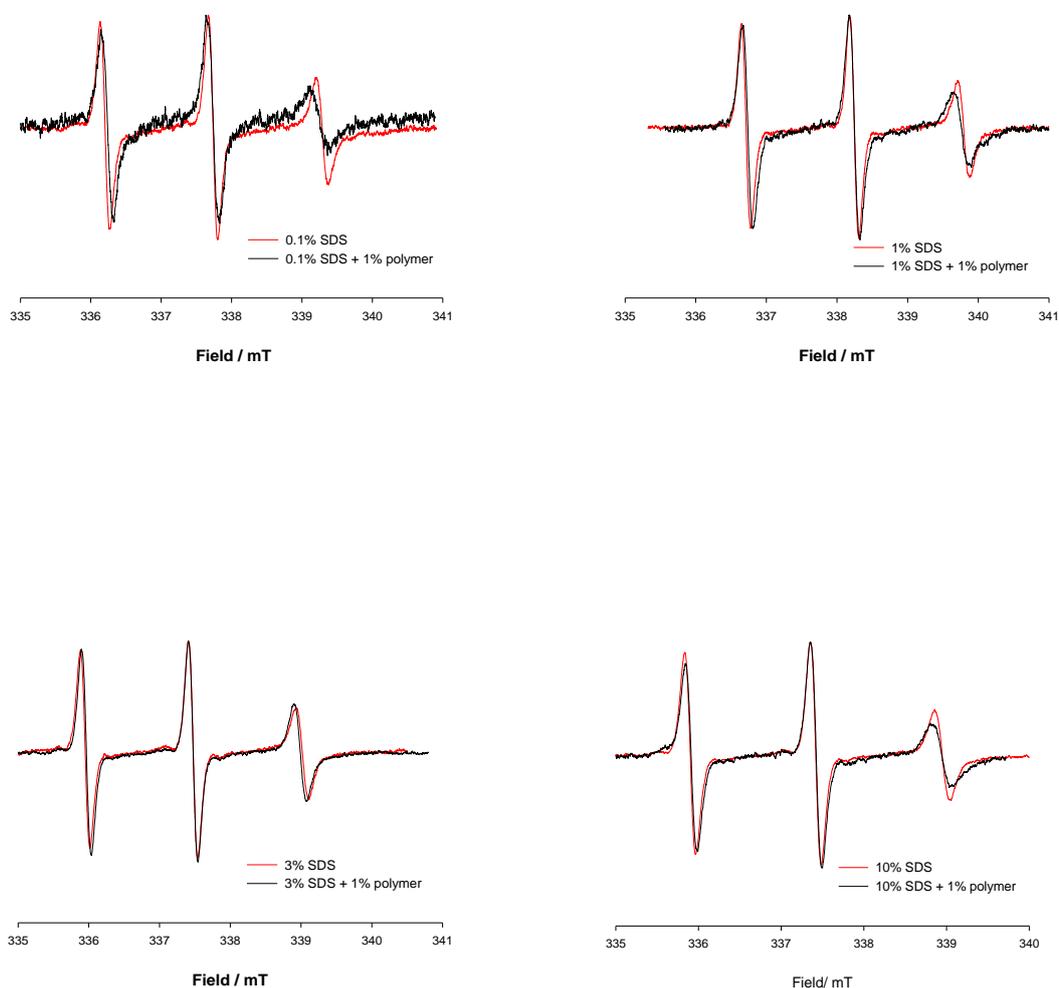
Figure 2.24. EPR spectrum for 16-DSE in the presence of four different concentrations of SDS, 1 wt% C_{10}-L-(EO_{200}-L)$_4$-C_{10}, and the polymer/SDS blend. Measurements were carried out at 25 °C, pH 9, and ionic strength 100 mM.

A similar behaviour is observed for the C_{18}-L-(EO_{200}-L)$_7$-C_{18} (Figure 2.23) but not for the C_{10}-L-(EO_{200}-L)$_4$-C_{10} (Figure 2.24), though these data are much noisier; both facts are indicative of the absence of polymer dominated hydrophobic domains of sufficient size to solubilise the probe. It is interesting that this corresponds to the polymer system with fewest urethane linkers, suggesting that the urethane groups are key component to the aggregate. When SDS is present in the system, the observed behaviour for C_{10}-L-(EO_{200}-L)$_4$-C_{10} is dominated by SDS rich environment, however, for the C_{18}-L-(EO_{200}-L)$_7$-C_{18} the

66

two environments are observed at a higher SDS concentration if compared with the C_6-L-$(EO_{100}$-L$)_9$-C_6.

Persson *et al.* studied the polarity of PEOM-10-12/SDS by EPR using 16-DSE. The polarity sensed by the probe increases as the SDS interacts with the PEOM hydrophobes up to 20-30 mM (7). The polarity decreased at higher SDS concentration due to the increase in the N_{agg} of SDS. Those results agree with the fluorescence data (Figure 2.20), however the ANS I_{min} is observed at lower SDS concentration 1 mM (0.05 wt%) and intensity increased at 17 mM (0.5 wt%) to reach the value of C_6-L-$(EO_{100}$-L$)_9$-C_6 in the absence of SDS. The increase in the ANS intensity after I_{min} is interpreted differently here, where it is hypothesised that the increase in the intensity is due to the cooperative micellar binding of SDS micelles, rather than changes in the SDS N_{agg}. The scattering data presented in Section 2.3.2.1.4 suggests the absence of change in the size of the SDS micelles adsorbed to the polymer as a function of SDS concentration where I_{ANS} increases after I_{min}, hence no change in SDS N_{agg} may occur.

The EPR data reported by Persson *et al.* show the presence of single environment for PEOM-10-20/SDS mixtures. However, two environments are reported in this study due to the difference in the polymers architectures studied here. Persson *et al.* used hydrophobically modified PEO whereas the HEURs used here has hydrophobic segments along the polymer backbone (urethane linkers).

2.4.2.1.4. SANS from HEUR/SDS mixtures in polymer dilute regime

To gain a better understanding of the polymer conformation, and the impact of the surfactant aggregation on the polymer conformation, a series of "contrast-variation" neutron scattering experiments were undertaken. The degree of interaction between the neutrons and a molecule consisting of atoms, *I*, is given by the scattering length density ρ, Equation 2.4:

$$\rho = \sum_i b_i \left(\frac{\delta N_A}{M_W}\right) \qquad\qquad \text{Equation 2.4}$$

where *b* is the scattering length, δ is the bulk density, N_A is Avogadro's number (6.02 x 10^{23} mol^{-1}) and M_W is the molecular weight of the scattering body. The contrast is the difference in ρ value between the molecule of interest ρ_p, and the surrounding medium ρ_m, squared *i.e.* $(\Delta\rho)^2$ so if this equals zero there is little/no scattering and the scattering

bodies are said to be "contrast matched". In such an approach, the scattering from the polymer or surfactant may be highlighted through judicious choice of hydrogenous and deuterated materials *e.g.* the scattering arising from a deuterated surfactant/hydrogenous polymer/hydrogenous solvent blend is dominated by the surfactant, whereas that from a deuterated surfactant/hydrogenous polymer/deuterated solvent blend arises principally from the polymer. The examination of the polymer/SDS with different contrasts highlighted different facets of the system.
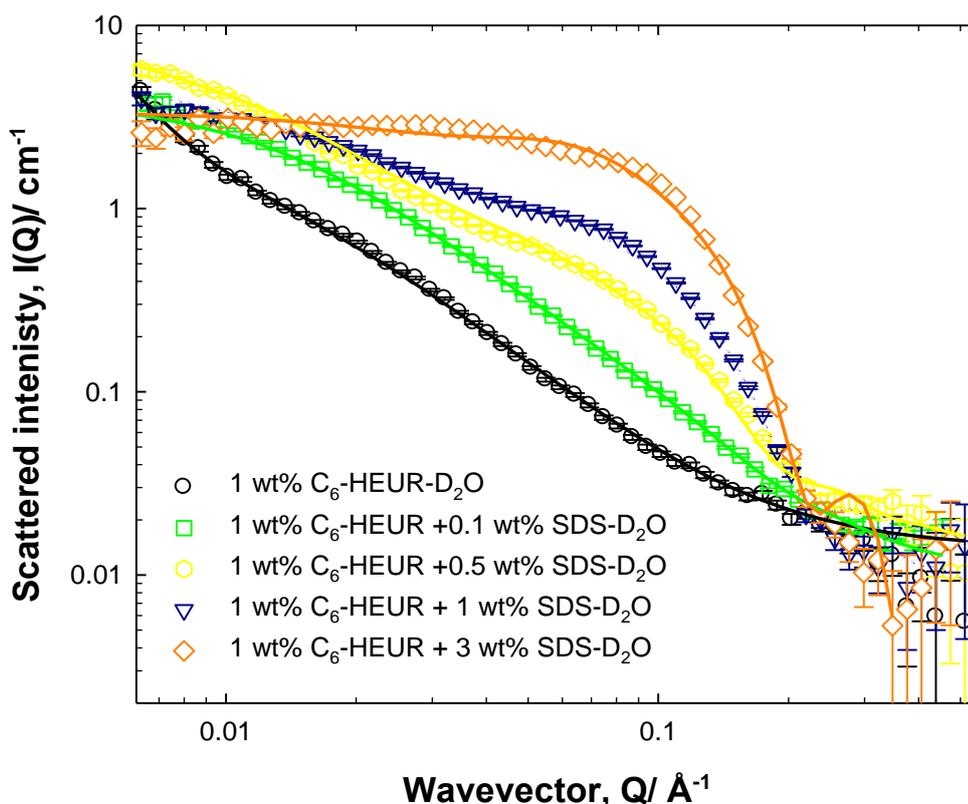
Figure 2.25. Small-angle neutron scattering from h-C_6-L-$(EO_{100}$-L$)_9$-C_6/h-surfactant/D_2O; $C_{polymer}$ = 1 wt% with SDS 0 (circles), 0.1 (squares), 0.5 (hexagons), 1 (triangles) and 3 (diamonds) wt% (last three points have been omitted for clarity). The scattering contribution is from the polymer/SDS in polymer/SDS blend. Measurements were carried out at 25 °C, pH 9, and ionic strength 100 mM. The solid lines are fit for sphere and gel model. Key fitting parameters value are presented in Table 2.3.

Figure 2.25 presents the scattering from h-C_6-L-$(EO_{100}$-L$)_9$-C_6/h-SDS/D_2O, where the overall size and shape of the polymer/surfactant complex is characterised. There is a clear SDS concentration-dependent increase in the scattering intensity with pronounced inflexia evident around mid-Q values. These features are characteristic of micellar-like

scattering, indicative of the formation of more hydrophobic aggregates as a function of SDS concentration. There is a concomitant decrease in intensity at low-Q values, indicative of repulsive interactions between charged structures. Worthy of note, is the presence of surfactant-like scattering around mid-Q (0.02 Å^{-1}), even at very low concentrations of SDS, reflecting the structure of the aggregates of hydrophobic groups present within the polymer. Generally, similar conclusions may be drawn from the data obtained for the other polymers, the only difference being subtle changes in scattering intensity at low-Q due to slightly wider Q range (Figures A.10, and A.11).
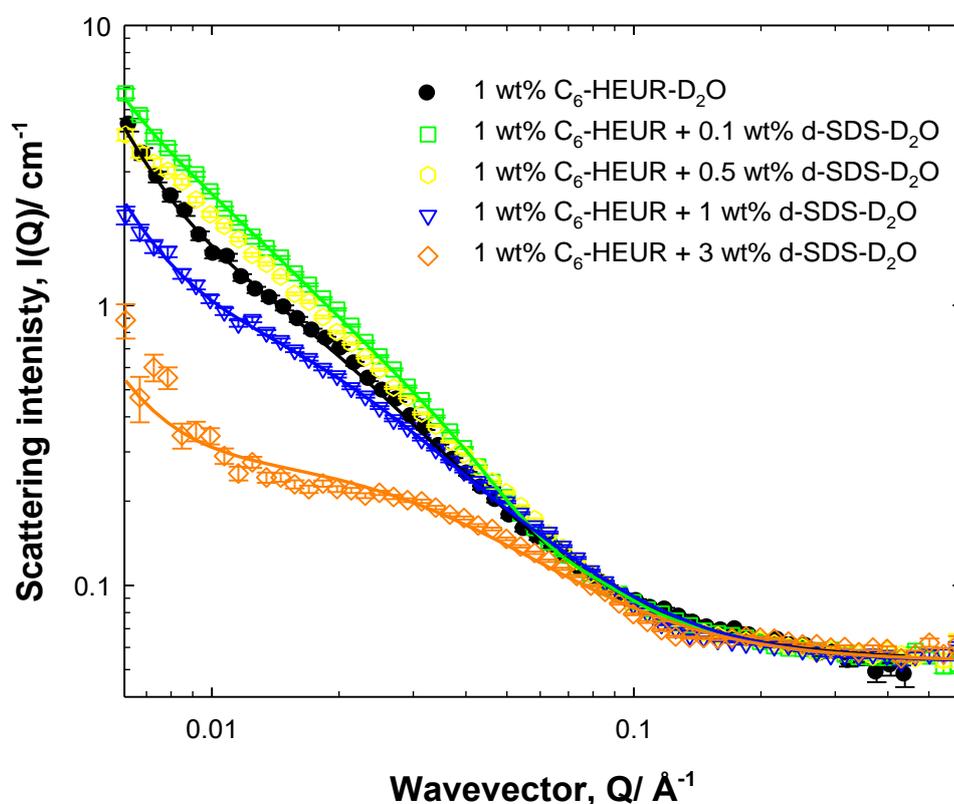
Figure 2.26. Small-angle neutron scattering from h-C$_6$-L-(EO$_{100}$-L)$_9$-C$_6$/d-surfactant/D$_2$O; $C_{polymer}$ = 1 wt% with SDS 0 (circles), 0.1 (squares), 0.5 (hexagons), 1 (triangles) and 3 (diamonds) wt% (last three points have been omitted for clarity). The scattering contribution is from the polymer only in polymer/SDS blend. Measurements were carried out at 25 °C, pH 9, and ionic strength 100 mM. The solid lines are fit for sphere and gel model. Key fitting parameters value are presented in Table 2.4.

Figure 2.26 shows the scattering from h-C$_6$-L-(EO$_{100}$-L)$_9$-C$_6$/d-SDS/D$_2$O, where the scattering is dominated by the polymer. The SLD of d$_{25}$-SDS is 5.9 x 10^{-6} Å^{-2} which is very close to that of the D$_2$O 5.76 x 10^{-6}. The scattering peak (0.02 Å^{-1}) in the 1 wt% HEUR

disappears at low values of surfactant concentration, 0.1 and 0.5 wt% SDS. The disappearance of the features in the data is due to either a loss of intensity at this particular Q value of the scattering intensity is moving to a different value of Q. Both assumptions are consistent with a transition from a smaller structures to bigger *i.e.* conversion of polymer loops to bridges. The peak (0.02 Å^{-1}) reappears at higher SDS concentration, 1 and 3 wt%, where micellar binding of SDS to the PEO backbone occurs, most likely due to the wrapping of the PEO segments around the SDS micelle as expected from the bead and necklace model of PEO/SDS interaction. Once again there are only subtle changes in the gross features of the data with the other polymers (Figures A.12 and A.13).
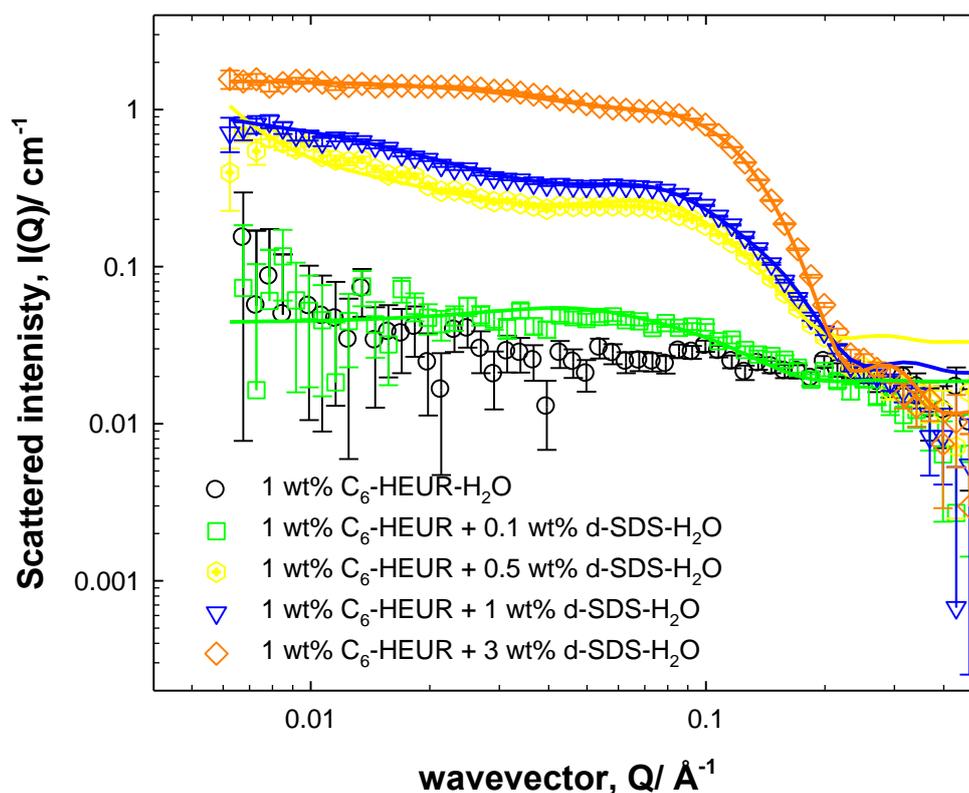
Figure 2.27. Small-angle neutron scattering from h-C_6-L-(EO_{100}-L)$_9$-C_6/d-surfactant/H_2O; $C_{polymer}$ = 1 wt% with SDS 0 (circles), 0.1 (squares), 0.5 (hexagons), 1 (triangles) and 3 (diamonds) wt% (last three points have been omitted for clarity). The scattering contribution is from the SDS only in polymer/SDS blend. Measurements were carried out at 25 °C, pH 9, and ionic strength 100 mM. The solid lines are fits for sphere and gel model. Key fitting parameters value are presented in Table 2.5.

Chapter 2. HEUR/SDS interaction

Figure 2.27 shows the scattering from h-HEUR/d-SDS/H_2O, where the scattering is dominated by the <u>SDS</u>, this was achieved by experimentally finding the match point of the polymer SLD to that of the solvent. In order to checked the absence of polymer contribution to the scattering, polymer scattering was measured in mixture of D_2O/H_2O (SLD = 8.3 x 10^{-7} Å^{-2}), which was used to prepare the samples and flat curve was obtained. The scattered intensity of the peak at mid-Q increases as a function of SDS. There is a move towards more polymer-like scattering emerging in the surfactant-only scattering contrast. It is envisaged that the surfactant interacts first with the hydrophobic domains, illustrative of the micellar-like scattering, and then subsequently interacts with the polymer backbone, giving rise to the polymer-like form to the data in the scattering of SDS only. Once again the scattering across the series of the three polymers is remarkably similar, consistent with the SDS micro-domains being defined by the molecular structure of the SDS (Figures A.14 and A.15). Similar to C_6-L-(EO_{100}-L)$_9$-C_6 the absence scattering contribution of for C_{10}-L-(EO_{200}-L)$_4$-C_{10} and C_{18}-L-(EO_{200}-L)$_7$-C_{18} in the mixtures was confirmed by measuring the polymer scattering in mixture of D_2O/H_2O where the SLD =6.92 x 10^{-7}, and 1.35 x 10^{-7} Å^{-2}, respectively.

The radius of the sphere is not a sensitive parameter in the absence of SDS, however, in the presence of SDS, the sphere radius is 20 ± 2 Å, Table 2.3. The sphere structure factor at low SDS concentrations can be turned off, however, at higher SDS concentration (1 and 3 wt%) the fit becomes sensitive to the charge. The polymer network is described by a short length scale 'ξ' and longer length scale 'A'. As the SDS concentration increases the two length scales decrease.

The length scales extracted from the polymer scattering contrast (Table 2.4) and sphere size extracted from the surfactant scattering contrast (Table 2.5) agrees with the values extracted from the overall scattering fit. The intensity of the shorter length scale is lower in the polymer-only contrast. In addition, at 1 wt% and 3 wt%, the scattering contribution from the longer scale is observed which seemed to disappear from the overall scattering fit. In the surfactant scattering contrast, there are values for the shorter length scale which support the hypothesis of the decoration of the polymer backbone, urethane linkers, by the SDS monomers.

The size of the aggregates in the dilute regime measured in the presence of SDS is equal to the SDS micelle size. The decrease in the polymer length scales at 1 wt% and 3 wt% can be explained by the collapse of the polymer chains as the latter wraps itself around

the SDS micelles. Similar conclusions may be drawn from the other two polymers presented in Appendix A, Tables A.4-A.9.

Fit parameters/ Units	1 % HEUR + 0 % SDS	1 % HEUR + 0.1 % SDS	1 % HEUR + 0.5 % SDS	1 % HEUR + 1 % SDS	1 % HEUR + 3 % SDS
Intensity of radius term	n.d.	n.d.	7.3×10^{-6}	9.4×10^{-5}	4.6×10^{-5}
Radius (Å)	n.d.	n.d.	20 ± 2	20 ± 1	20 ± 1
e	n.d.	n.d.	n.d.	10	10
K^{-1} (Å)	0.3	0.29	0.28	0.27	0.23
φ	0.01	0.011	0.015	0.02	0.04
l_1	1.78	4.4	4.9	3	2.3
ξ (Å)	75 ± 2	79 ± 2	80 ± 2	50 ± 2	40 ± 2
l_2	247	247	247	n.d.	n.d.
A (Å)	455 ± 10	455 ± 10	455 ± 10	n.d.	n.d.

Table 2.3. SANS key parameters from the sphere and network model for C_6-L-(EO_{100}-L)$_9$-C_6/SDS/D_2O $C_{polymer}$ = 1wt%.

Fit parameters/ Units	1 % HEUR + 0 % SDS	1 % HEUR + 0.1 % SDS	1 % HEUR + 0.5 % SDS	1 % HEUR + 1 % SDS	1 % HEUR + 3 % SDS
Intensity of radius term	n.d.	n.d.	n.d.	7.2×10^{-8}	4.5×10^{-7}
Radius (Å)	n.d.	n.d.	n.d.	20 ± 1	30 ± 1
e	n.d.	n.d.	n.d.	n.d.	n.d.
K^{-1} (Å)	0.3	0.29	0.28	0.27	0.23
φ	0.01	0.011	0.015	0.02	0.04
R_g (Å)	n.d.	n.d.	n.d.	n.d.	n.d.
l_1	1.78	2.6	2.6	1	0.5
ξ (Å)	75 ± 2	77 ± 2	80 ± 2	50 ± 2	47 ± 2
l_2	247	247	247	97	97
A (Å)	455 ± 10	455 ± 10	455 ± 10	455 ± 10	455 ± 10

Table 2.4. SANS key parameters from the sphere and network model for C_6-L-(EO_{100}-L)$_9$-C_6/d-SDS/D_2O $C_{polymer}$ = 1 wt%.

Fit parameters/ Units	1 % HEUR + 0.5 % SDS	1 % HEUR + 1 % SDS	1 % HEUR + 3 % SDS
Intensity of radius term	2.5×10^{-6}	4.8×10^{-6}	1.7×10^{-5}
Radius (Å)	20	20	20
e	n.d.	10	10
K^{-1} (Å)	0.28	0.27	0.23
φ	0.015	0.02	0.04
R_g (Å)	n.d.	n.d.	n.d.
l_1	0.7	0.7	1
ξ (Å)	79 ± 2	75 ± 2	25 ± 2
l_2	n.d.	n.d.	n.d.
A (Å)	n.d.	n.d.	n.d.

Table 2.5. SANS key parameters from the sphere and network model for C_6-L-$(EO_{100}$-L$)_9$-C_6/d-SDS/H_2O $C_{polymer}$ = 1wt%.

2.4.2.2. Polymer/surfactant interactions above the polymer overlap concentration (C*)

All the experiments conducted for the dilute regime have been replicated for the concentrated regime.

2.4.2.2.1. Solution behaviour of HEUR/SDS mixtures in polymer dilute regime
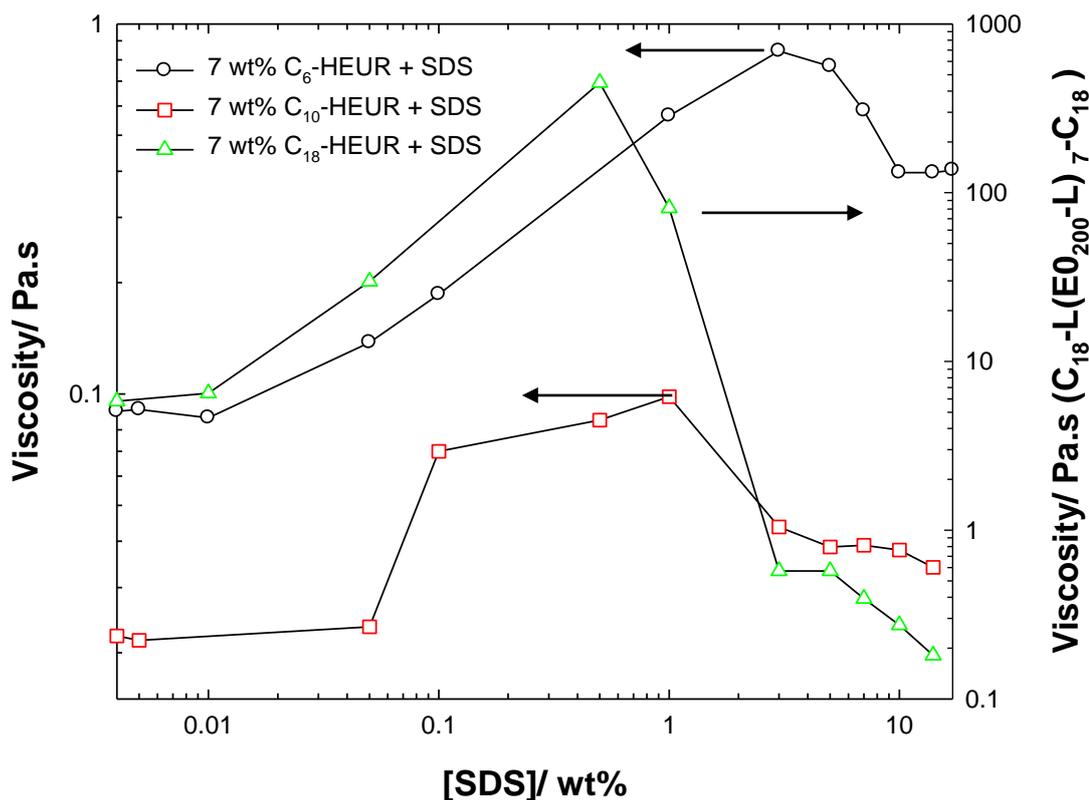
Figure 2.28. Viscosity at shear rate 0.1 s^{-1} of 7 wt% C$_6$-L-(EO$_{100}$-L)$_9$-C$_6$ (circles), C$_{10}$-L-(EO$_{200}$-L)$_4$-C$_{10}$ (squares), and C$_{18}$-L-(EO$_{200}$-L)$_7$-C$_{18}$ (triangles) as a function of SDS concentration. Measurements were carried out at 25 °C, pH 9, and ionic strength 100 mM. The solid lines are guides for the eye. The error bars are the standard deviation of three measurements for the same sample and a second set of samples.

The viscosity and self-diffusion coefficient of C$_6$-L-(EO$_{100}$-L)$_9$-C$_6$ as a function of SDS concentration was measured above C^*. There are fewer studies performed on HEUR in this concentrated regime. Similar features of the viscosity and diffusion curve reported for the HEURs below C^* as a function of SDS concentration (Figure 2.18), are observed for the polymer above C^* (Figure 2.28 and Figure 2.29), respectively. However, the V_{max} and D_{min} are shifted to higher SDS concentration in the concentrated regime (3 wt%) relative

to the dilute regime (0.3 wt%).The peak shifting to higher SDS concentration may be explained by the presence of more polymer hydrophobic end-groups in the concentrated polymer regime. Similar observations are reported for C_{10}-L-$(EO_{200}$-L$)_4$-C_{10} and C_{18}-L-$(EO_{200}$-L$)_7$-C_{18}. Analogous to the dilute regime, the D_{min} in the concentrated regime are shifted to lower SDS concentration for C_{18}-L-$(EO_{200}$-L$)_7$-$C_{18} < C_{10}$-L-$(EO_{200}$-L$)_4$-$C_{10} < C_6$-L-$(EO_{100}$-L$)_9$-C_6 (1 and 0.5 wt% SDS respectively) (see section 2.3.2.1.2).
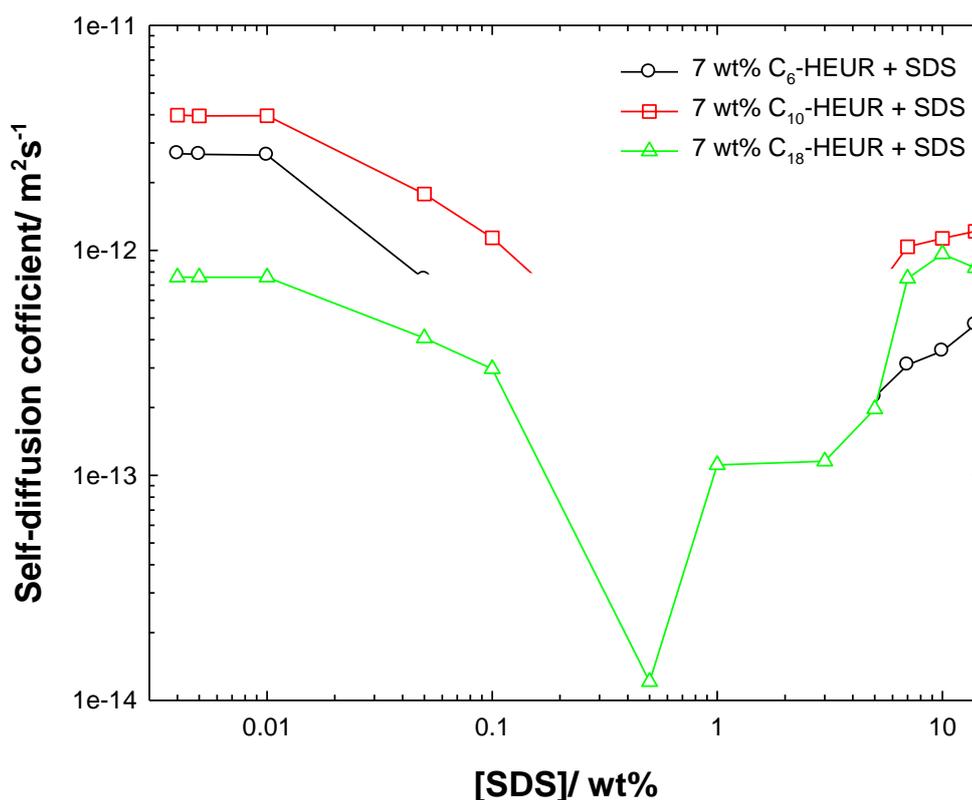
Figure 2.29. Self-diffusion coefficient of 7 wt% C_6-L-$(EO_{100}$-L$)_9$-C_6 (circles), C_{10}-L-$(EO_{200}$-L$)_4$-C_{10} (squares), and C_{18}-L-$(EO_{200}$-L$)_7$-C_{18} (triangles) as a function of SDS concentration. Measurements were carried out at 25 °C, pH 9, and ionic strength 100 mM. The solid lines are guides for the eye. The error bars are the standard deviation of three measurements for the same sample and a second set of samples.

At 7 wt% HEUR a dense network conformation is expected where most of the loop-forming polymer chains in polymer hydrophobic aggregates are converted to bridges. Therefore the adoption of different conformation of polymer chains as a function of SDS is excluded. The viscosity increase and diffusion decrease can be correlated to the strengthening of the network structure due to the formation of more aggregates of smaller size, therefore, the number of cross-links increase, hence the viscosity increases.

Chapter 2. HEUR/SDS interaction

Before V_{max}, the polymer viscosity curve shows a trend where the viscosity of C_{10}-L-$(EO_{200}$-L$)_4$-C_{10} < C_6-L-$(EO_{100}$-L$)_9$-C_6 < C_{18}-L-$(EO_{200}$-L$)_7$-C_{18}, which agrees with the viscosity curves for polymer as a function of its concentration. The viscosity at these concentrations is dependent on the strength and number of cross-links present. The C_{10}-L-$(EO_{200}$-L$)_4$-C_{10} fluorescence data illustrate the formation of more hydrophobic end-group relative to C_6-L-$(EO_{100}$-L$)_9$-C_6 as it has longer hydrophobic end-groups. The EPR data shows no signal for the C_{10}-L-$(EO_{200}$-L$)_4$-C_{10}. Bear in mind that the molecular weight of the two polymers is close, the C_6-L-$(EO_{100}$-L$)_9$-C_6 is 50 kg mol^{-1} and C_{10}-L-$(EO_{200}$-L$)_4$-C_{10} 52 kg mol^{-1}.

Therefore, an indirect conclusion may be drawn the C_6-L-$(EO_{100}$-L$)_9$-C_6 seems to associate through the urethane linkers which enhances the polymer viscosity relative to C_{10}-L-$(EO_{200}$-L$)_4$-C_{10} at the same concentration. After V_{max}, the viscosity curve trends slightly change where the viscosity is lower for C_{18}-L-$(EO_{200}$-L$)_7$-C_{18} < C_{10}-L-$(EO_{200}$-L$)_4$-C_{10} and C_6-L-$(EO_{100}$-L$)_9$-C_6. In addition, the C_{18}-L-$(EO_{200}$-L$)_7$-C_{18} shows the steepest slope for the viscosity decrease.

Similar to viscosity curves, the diffusion data shows the highest diffusion below D_{min} for C_{10}-L-$(EO_{200}$-L$)_4$-C_{10} > C_6-L-$(EO_{100}$-L$)_9$-C_6 > C_{18}-L-$(EO_{200}$-L$)_7$-C_{18}. However, after D_{min}, the trends are different where the highest diffusion is for C_{10}-L-$(EO_{200}$-L$)_4$-C_{10} > C_{18}-L-$(EO_{200}$-L$)_7$-C_{18} > C_6-L-$(EO_{100}$-L$)_9$-C_6.

2.4.2.2.2. Analysis of HEUR/SDS hydrophobic aggregates in polymer concentrated regime
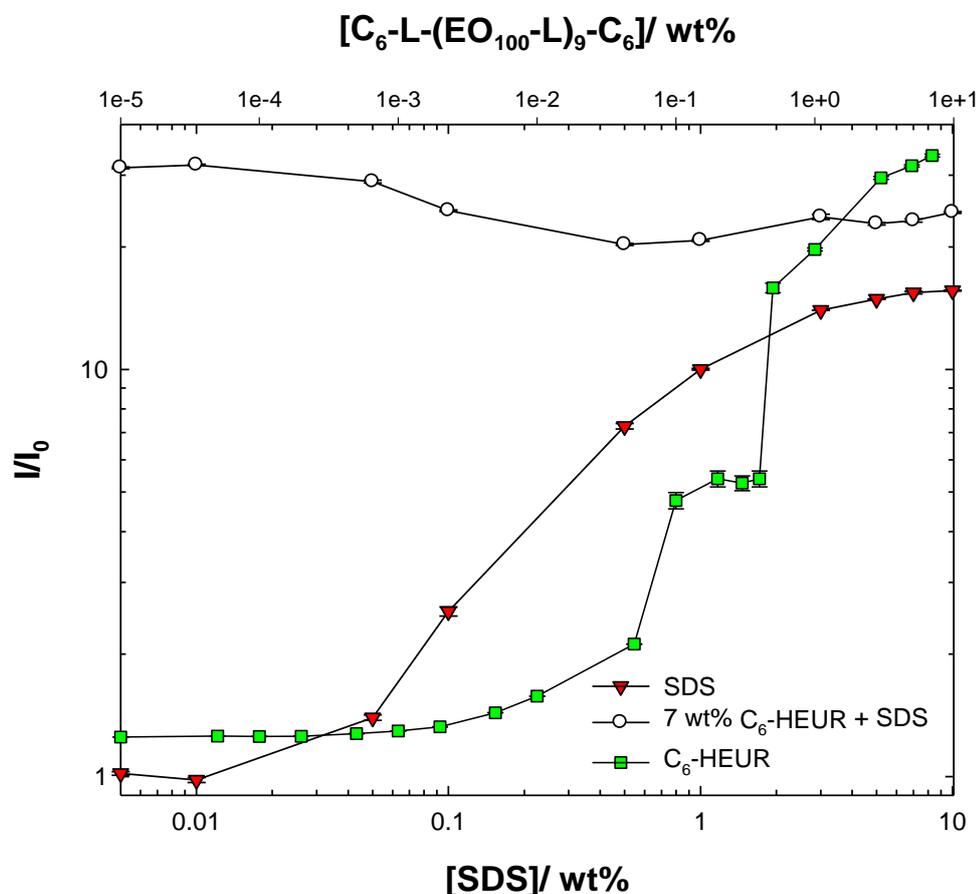
Figure 2.30. ANS fluorescence intensity of C_6-L-(EO100-L)$_9$-C_6 (squares) as a function of polymer concentration, SDS (triangles), and C_6-L-(EO100-L)$_9$-C_6/SDS (circles) at $C_{polymer}$ = 7 wt% as a function of SDS concentration. Measurements were carried out at 25 °C, pH 9, and ionic strength 100 mM. The solid lines are guides for the eye. The error bars are the standard deviation of three measurements for the same sample and a second set of samples.

The gross features of the ANS intensity curves (Figure 2.30) are similar to the polymers in the dilute regime (Figure 2.19). However, the I_{min} is shifted to higher SDS concentrations. The increase in ANS intensity after I_{min} is less than that observed for the dilute system. In the SDS concentration range presented, the intensity does not decrease to overlap with that of pure SDS due to the higher concentration of the HEUR, for C_{18}-L-(EO$_{200}$-L)$_7$-C_{18} the ANS intensity was not measured as the viscosity of the sample was very high in the presence of SDS. There is very subtle difference between the ANS intensity of the C_6-L-(EO$_{100}$-L)$_9$-C_6 and C_{10}-L-(EO$_{200}$-L)$_4$-C_{10} (Figure 2.31).
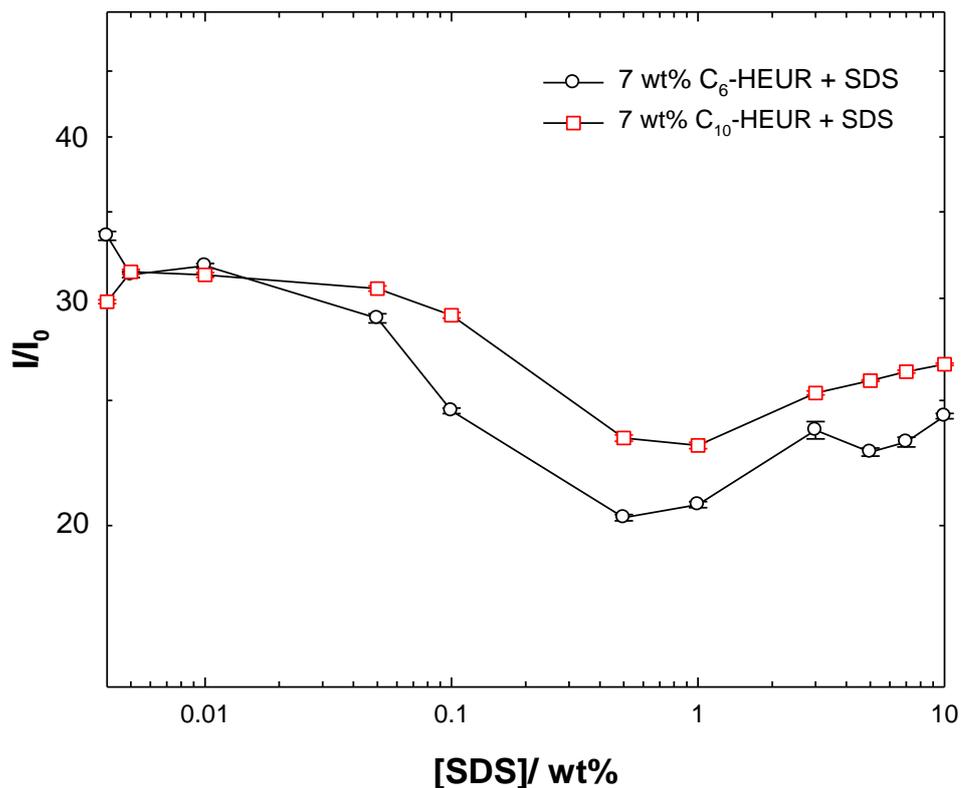
Figure 2.31. ANS fluorescence of 7 wt% C_6-L-$(EO_{100}$-L$)_9$-C_6 (circles), C_{10}-L-$(EO_{200}$-L$)_4$-C_{10} (squares) as a function of SDS concentration. Measurements were carried out at 25 °C, pH 9, and ionic strength 100 mM. The ANS intensity of C_{18}-L-$(EO_{200}$-L$)_7$-C_{18} has not been measured due to very high viscosity. The solid lines are guides for the eye. The error bars are the standard deviation of three measurements for the same sample and a second set of samples.
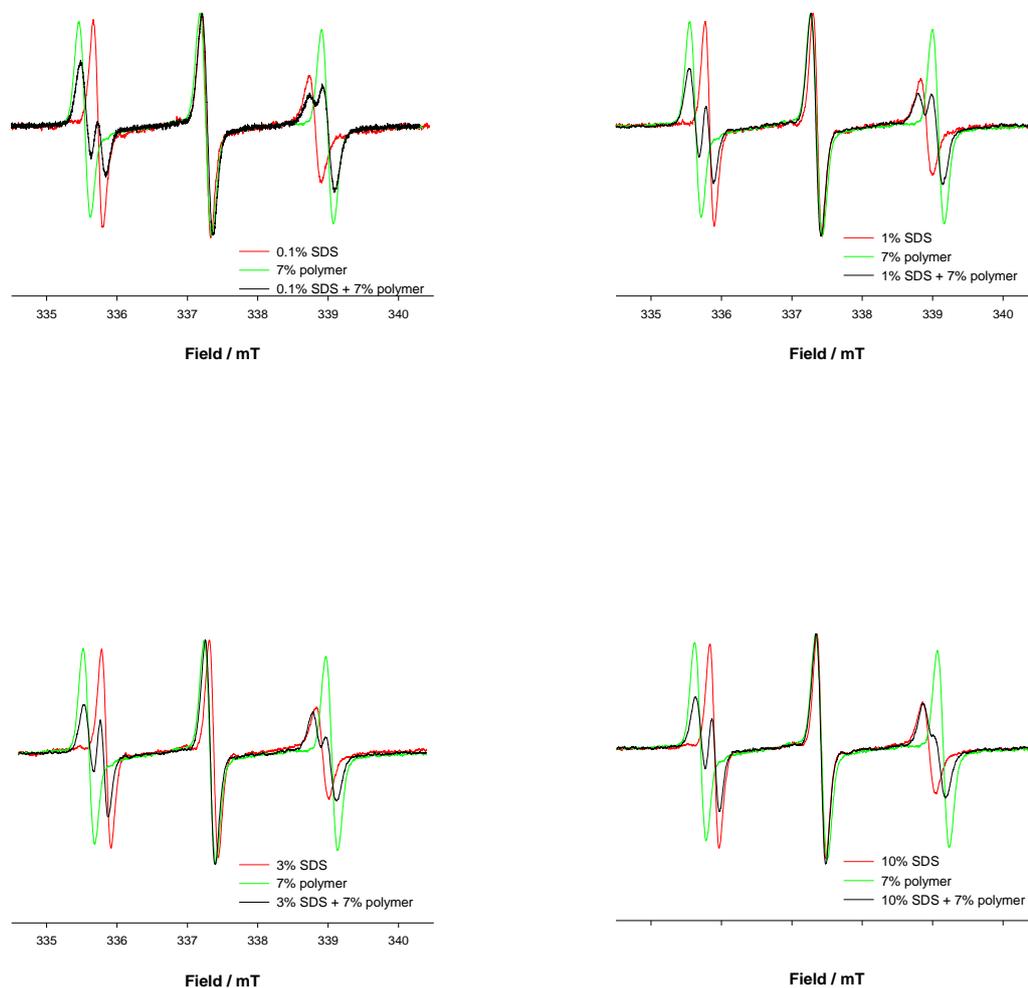
Figure 2.32. EPR spectrum for 16-DSE in the presence of four different concentrations of SDS, 7 wt% C_6-L-(EO_{100}-L)$_9$-C_6, and the polymer/SDS blend. Measurements were carried out at 25 °C, pH 9, and ionic strength 100 mM.

As in the dilute regime, the EPR data for C_6-L-(EO_{100}-L)$_9$-C_6 shows two environments; a polymer and SDS-like environment (Figure 2.32). The polymer-like environment is observed in all the SDS concentration ranges, unlike the dilute regime where the polymer-like environment is not observed at high SDS concentration. The 1st peak (high-field peak) describes the microviscosity, the broader the peak the less the microviscosity of the system. The microviscosity peak in the dilute regime shows one broad peak, whilst in the concentrated regime, a splitting in the signal is noted, reflective of the presence of the

two environments a polymer and SDS-like environment. As the SDS concentration increase the microviscosity shifts towards the SDS-like environment.
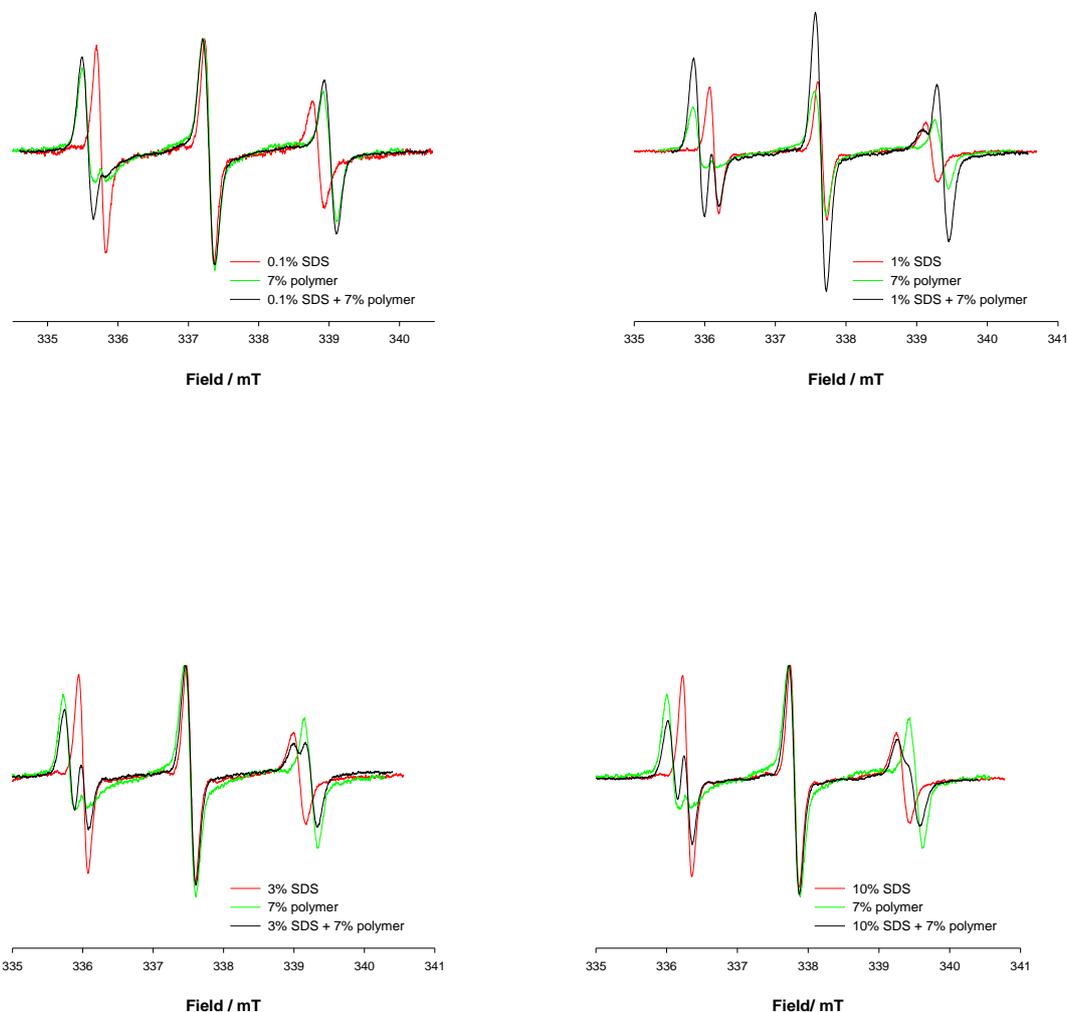
Figure 2.33. EPR spectrum for 16-DSE in the presence of four different concentrations of SDS, 7 wt% C_{18}-L-(EO$_{200}$-L)$_7$-C_{18}, and the polymer/SDS blend. Measurements were carried out at 25 °C, pH 9, and ionic strength 100 mM.
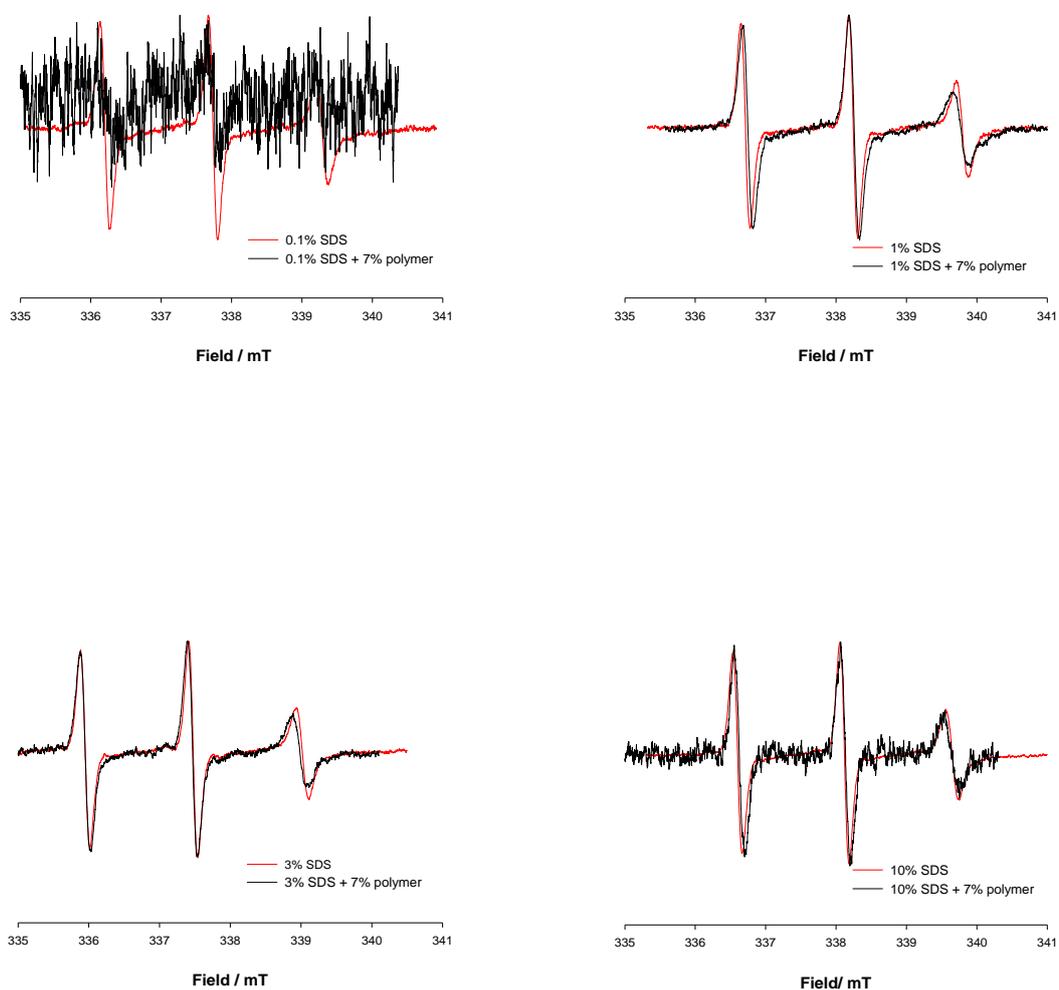
Figure 2.34. EPR spectrum for 16-DSE in the presence of four different concentrations of SDS, 7 wt% C_{10}-L-$(EO_{200}$-L$)_4$-C_{10}, and the polymer/SDS blend. Measurements were carried out at 25 °C, pH 9, and ionic strength 100 mM.

The C_{18}-L-$(EO_{200}$-L$)_7$-C_{18} shows similar features as C_6-L-$(EO_{100}$-L$)_9$-C_6 (Figure 2.33). However, the 16-DSE in the presence of C_{10}-L-$(EO_{200}$-L$)_4$-C_{10} does not give any signal in absence of SDS and noisy signal is observed at 0.1 wt% SDS (Figure 2.34).

2.4.2.2.3. SANS from HEUR/SDS mixtures in polymer concentrated regime
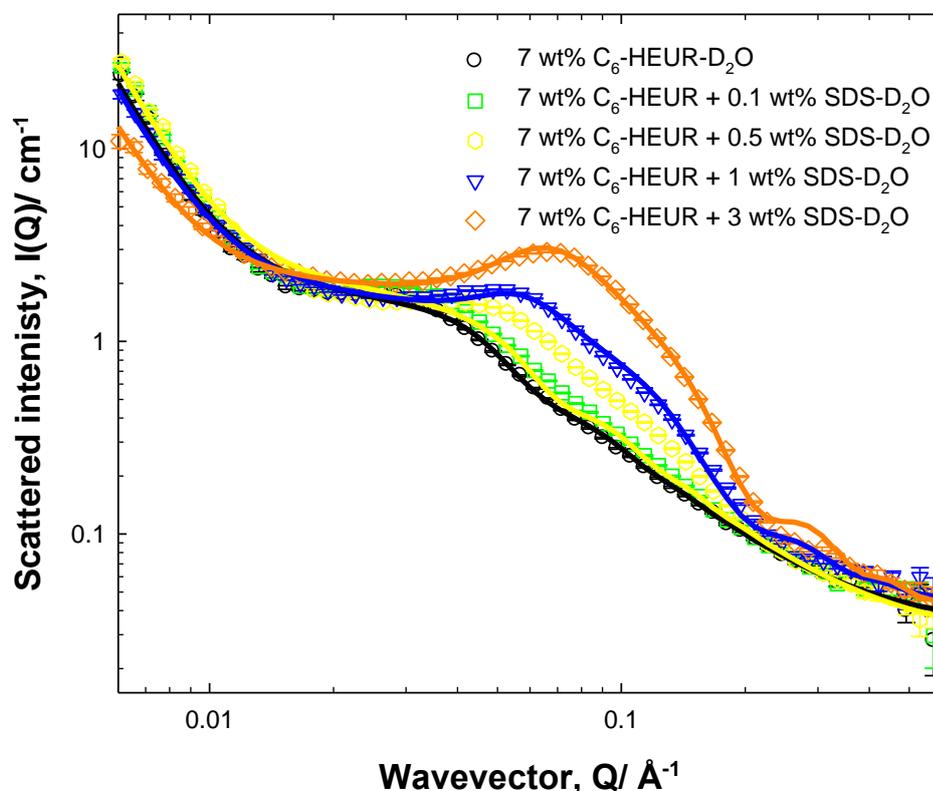
Figure 2.35. Small-angle neutron scattering from h-C$_6$-L-(EO$_{100}$-L)$_9$-C$_6$/h-surfactant/D$_2$O; $C_{polymer}$ = 7 wt% with SDS 0 (circles), 0.1 (squares), 0.5 (hexagons), 1 (triangles) and 3 (diamonds) wt% (last three points have been omitted for clarity). The scattering contribution is from the polymer/SDS in polymer/SDS blend. Measurements were carried out at 25 °C, pH 9, and ionic strength 100 mM. The solid lines are fit for sphere and gel model. Key fitting parameters value are presented in Table 2.6.

The various contrast scattering experiments introduced in Section 2.3.2.1.4 for the polymer in the dilute regime were replicated for the concentrated regime. The overall scattering of the h-C$_6$-L-(EO$_{100}$-L)$_9$-C$_6$/h-surfactant/D$_2$O shows SDS concentration-dependent increase in intensity at mid-Q (Figure 2.35). The scattering peak at mid-Q is shifted to higher Q range as the SDS concentration is increased. The polymer peak shape emerges from a shoulder to a micelle-like scattering peak as the SDS concentration increases. This may be correlated to the decrease of the average size of the aggregates and hence smaller d-spacing is observed. Similar conclusions may be drawn from the overall scattering of the other two polymers (Figure A.16 and A.17).
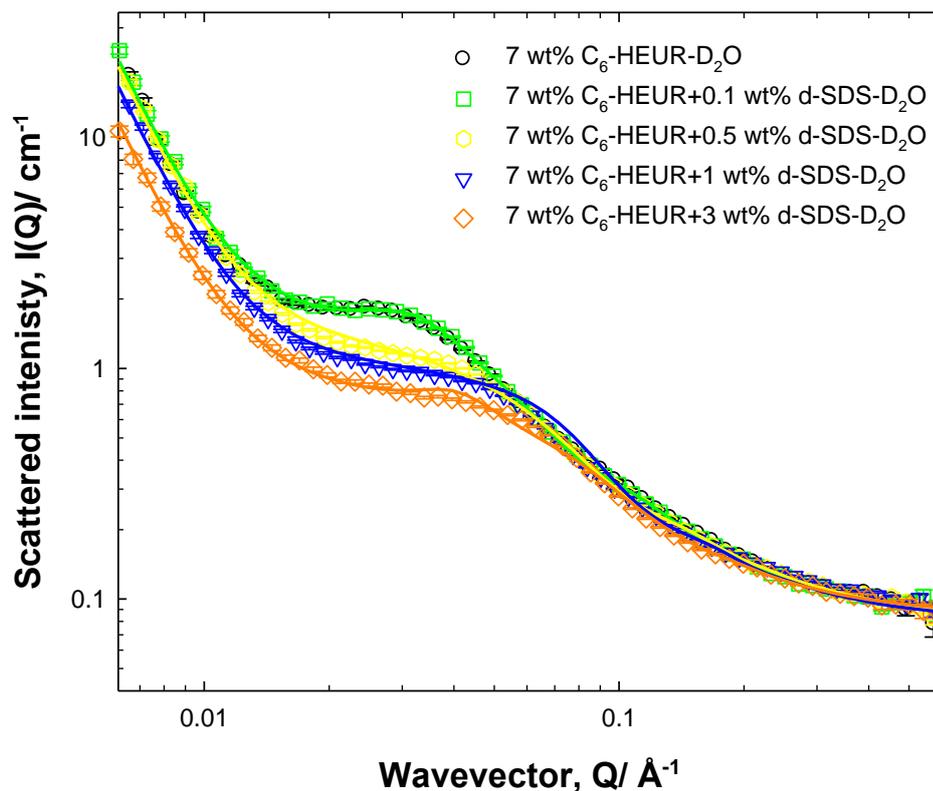
Figure 2.36. Small-angle neutron scattering from h-C₆-L-(EO₁₀₀-L)₉-C₆/d-surfactant/D₂O; $C_{polymer}$ = 7 wt% with SDS 0 (circles), 0.1 (squares), 0.5 (hexagons), 1 (triangles) and 3 (diamonds) wt% (last three points have been omitted for clarity). The scattering contribution is from the polymer only in polymer/SDS blend. Measurements were carried out at 25 °C, pH 9, and ionic strength 100 mM. The solid lines are fit for sphere and gel model. Key fitting parameters value are presented in Table 2.7.

In the h-C₆-L-(EO₁₀₀-L)₉-C₆/d-surfactant/D2O contrast, the intensity of the peak at mid-Q decreases as a function of SDS and moves to higher Q (Figure 2.36). Worthy of note, the peak position of HEUR at 1 and 3 wt% are very close to the 0.5 wt% SDS, therefore the change in peak position after 0.5 wt% SDS becomes subtle. Unlike the dilute regime, the changes in the C₆-L-(EO₁₀₀-L)₉-C₆ scattered intensity at low-Q is very subtle as a function of SDS concentrations. The shift of the peak position to lower Q reflects changes in the size and composition of the HEUR/SDS mixed aggregates, where smaller aggregates are formed, hence the d-spacing decreases. The decrease in the scattered intensity of the polymer peak as a function of SDS concentrations indicates the decrease in the number of polymer hydrophobes in the mixed aggregates. The subtle changes in the scattering at low-Q suggests the presence of subtle changes in the conformation and hence the

84

network structure, this agrees with the viscosity and diffusion data, over this range of SDS concentrations. Similar observations and conclusion may be drawn from the C_{10}-L-$(EO_{200}$-L$)_4$-C_{10} (Figure A.18). However, for C_{18}-L-$(EO_{200}$-L$)_7$-C_{18} the changes in the scattered intensity of the polymer backbone shows more significant decrease at 3 wt% SDS, indicative of the presence of polymer conformation changes in agreement with the viscosity data for this polymer (Figure A.19).
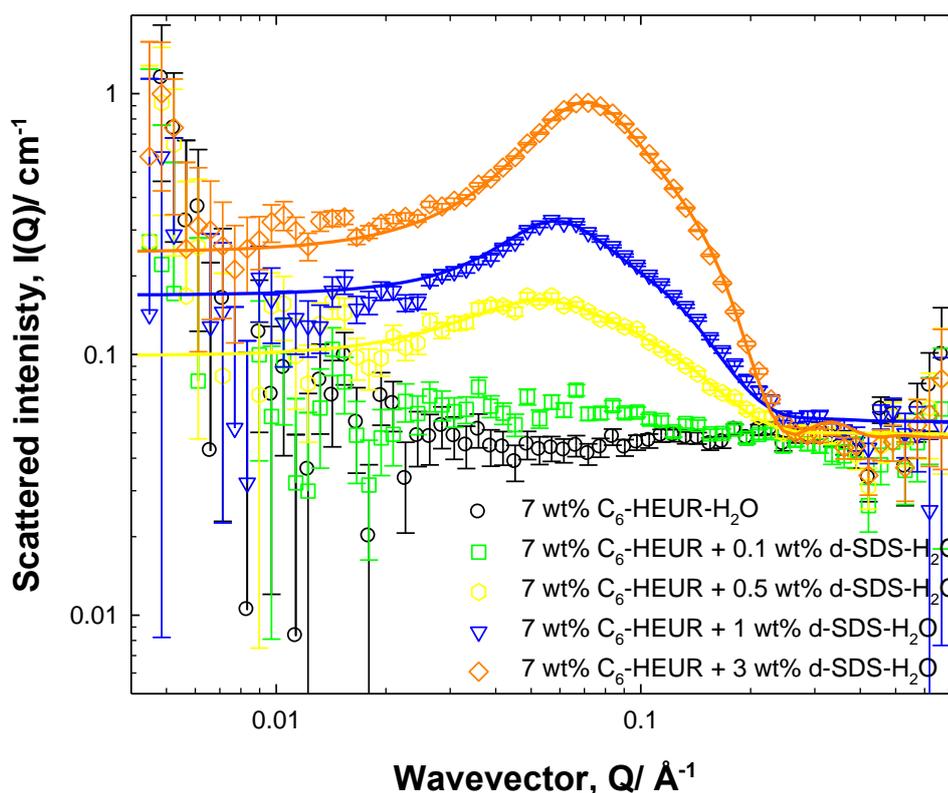
Figure 2.37. Small-angle neutron scattering from h-C_6-L-$(EO_{100}$-L$)_9$-C_6/d-surfactant/H_2O; $C_{polymer}$ = 7 wt% with SDS (circles) 0 (circles), 0.1 (squares), 0.5 (hexagons), 1 (triangles) and 3 (diamonds) wt% (last three points have been omitted for clarity). The scattering contribution is from the SDS only in polymer/SDS blend Measurements were carried out at 25 °C, pH 9, and ionic strength 100 mM. The solid lines are fit for sphere and gel model. Key fitting parameters value are presented in Table 2.8.

In h-C_6-L-$(EO_{100}$-L$)_9$-C_6/d-surfactant/H_2O contrast the 0.1 wt% SDS shows a flat curve as the mixed aggregates are dominated by polymer hydrophobes (Figure 2.37). At higher SDS concentration the peak at mid-Q shows subtle change in position close to that seen the other two contrasts for the polymer in the presence of 0.5, 1 and 3 wt% SDS. The intensity of the peak increases as a function of SDS as the mixed micelles become more

dominated by SDS. Similar conclusions may be drawn for the SDS scattering contrast of the other two polymers (Figures A.20 and A.21). Worth mentioning, the SLD of the C_{10}-L-(EO$_{200}$-L)$_4$-C$_{10}$ and C_{18}-L-(EO$_{200}$-L)$_7$-C$_{18}$ was not perfectly matched and hence there is some scattering from the polymer at low-Q.

In the dense network regime, the size of the aggregates decreases as the SDS concentration increase, where a shift from a large polymer aggregate to a SDS micelle sized aggregate is observed. Similar to the dilute regime (Section 2.3.2.1.4), the fit is sensitive to the charge at 1 and 3 wt% SDS only. The length scales of the polymer show very subtle changes as a function of SDS concentration.

In the polymer scattering contrast, the parameters are in a good agreement with that of the overall scattering contrast. Surprisingly, the surfactant-only contrast show aggregates of SDS micelles size for all the SDS concentrations. Similar conclusions may be drawn from the other two polymers fits is presented in Appendix A, Tables A.10-A.15. In the C_{18}-L-(EO$_{200}$-L)$_7$-C$_{18}$ at 1 and 3 wt% SDS, the network structure is broken reflected by decrease in the scattered intensity at low-Q and decrease in the ξ and A length scales.

In the dense network regime, the only change observed is related to the aggregate size and composition, at least over the range of SDS concentration studied here. The decrease of the sphere radius is reflective of the formation of smaller polymer hydrophobic aggregates. There is a less significant change in the polymer length scale which may be correlated to the maintenance of the polymer network structure in the SDS range studied in this experiment. This agrees with the viscosity data where the decrease in viscosity, which is correlated to the breakage of the network structure, is observed at SDS concentrations higher than 3 wt%.

Fit parameters/ Units	7 % HEUR + 0 % SDS	7 % HEUR + 0.1 % SDS	7 % HEUR + 0.5 % SDS	7 % HEUR + 1 % SDS	7 % HEUR + 3 % SDS
Intensity of radius term	1.8×10^{-6}	2.8×10^{-6}	6.5×10^{-6}	2.0×10^{-6}	7.5×10^{-5}
Radius (Å)	62 ± 5	52 ± 3	42 ± 3	35 ± 1	20
e	n.d.	n.d.	n.d.	10	10
K^{-1} (Å)	0.3	0.29	0.28	0.27	0.23
φ	0.07	0.071	0.075	0.08	0.1
l_1	1.7	1.4	1.4	0.8	0.9
ξ (Å)	20 ± 1	20 ± 1	16 ± 1	17 ± 1	14 ± 1
l_2	7190	7190	7190	6190	6000
A (Å)	672 ± 10	672 ± 10	672 ± 10	672 ± 10	672 ± 10

Table 2.6. SANS key parameters from the sphere and network model for C$_6$-L-(EO$_{100}$-L)$_9$-C$_6$ /SDS/D$_2$O at $C_{polymer}$ = 7 wt%.

Fit parameters/ Units	7 % HEUR + 0 % SDS	7 % HEUR + 0.1 % SDS	7 % HEUR + 0.5 % SDS	7 % HEUR + 1 % SDS	7 % HEUR + 3 % SDS
Intensity of radius term	1.8×10^{-6}	2.0×10^{-6}	2.0×10^{-6}	2.2×10^{-6}	1.9×10^{-6}
Radius (Å)	62 ± 5	54 ± 3	42 ± 3	35 ± 1	30 ± 1
e	n.d.	n.d.	n.d.	10	10
K^{-1} (Å)	0.3	0.29	0.28	0.27	0.23
φ	0.07	0.071	0.075	0.08	0.1
l_1	1.7	1.2	0.8	0.7	0.7
ξ (Å)	20 ± 1	20 ± 1	17 ± 1	17 ± 1	17 ± 1
l_2	7190	7190	7190	5490	3400
A (Å)	672 ± 10	670 ± 10	674 ± 10	674 ± 10	674 ± 10

Table 2.7. SANS key parameters from the sphere and network model for C_6-L-(EO$_{100}$-L)$_9$-C$_6$ /d-SDS/D$_2$O $C_{polymer}$ = 7 wt%.

Fit parameters/ Units	7 % HEUR + 0.5 % SDS	7 % HEUR + 1 % SDS	7 % HEUR + 3 % SDS
Intensity of radius term	4.0×10^{-6}	5.5×10^{-6}	4.8×10^{-5}
Radius (Å)	18	20	17
e	n.d.	10	10
K^{-1} (Å)	0.28	0.27	0.23
φ	0.075	0.08	0.1
l_1	0.065	0.03	0.002
ξ (Å)	7	4	3
l_2	n.d.	n.d.	n.d.
A (Å)	n.d.	n.d.	n.d.

Table 2.8. SANS key parameters from the sphere and network model for C_6-L-$(EO_{100}$-L$)_9$-C_6 /d-SDS/H$_2$O $C_{polymer}$ = 7 wt%.

2.5. Conclusion

HEUR polymers and surfactants are present in many formulations *e.g.* paints and cosmetics. Understanding the behaviour of the HEUR in the presence of surfactants is important for optimizing these formulations. In this chapter, three polymers with general structure C_n-L-$(EO_x$-L$)_y$-C_n have been studied as a function of SDS concentration. Two mechanisms of SDS binding to the HEURs have been observed. The first mechanism is monomeric, anti-cooperative binding of SDS to the already-formed hydrophobic aggregates comprising the polymer end-groups and urethane linkers. The second mechanism is where SDS micelles bind to the PEO backbone of the HEUR in a cooperative manner. Changes in the polymer conformation and characteristics of the hydrophobic aggregates have been detected as a consequence of these two binding mechanisms.

Macroscopic changes, *e.g.* viscosity, are largely due to the monomeric binding of SDS, inducing a redistribution of the end-groups within the (mixed) hydrophobic aggregates. Increasing the polymer concentration resulted in shifts in these characteristic features to higher SDS concentration. On the contrary, the increase in the polymer molecular weight and/or length of hydrophobic end-group shifts the features to lower SDS concentrations. This study should allow a more considered analysis of the rheological profile in terms of the polymer architecture and presence/nature of the surfactant species present in the formulation.

2.6. References

1. Annable T, Buscall R, Ettelaie R, Whittlestone D. The rheology of solutions of associating polymers : Comparison of experimental behavior with transient network theory. *J Rheol.* **1992**;*37*:695-726.

2. Annable T, Buscall R, Ettelaie R. Network formation and its consequences for the physical behaviour of associating polymers in solution. *Colloids Surfaces A Physicochem Eng Asp.* **1996**;*11*:97-116.

3. Paeng KW, Kim B, Kim E, Sohn D. Aggregation processes of hydrophobically modified polethylene oxide. Bull. *Korean Chem. Soc.* **2000**; *21*: 623-627.

4. Yekta A, Xu B, Duhamel J, Adiwidjaja H, Winnik MA. Fluorescence studies of associating polymers in water - determination of the chain-end aggregation number and a model for the association process. *Macromolecules.* **1995**;*28*(4):956–966.

5. Gourier C, Beaudoin E, Duval M, Sarazin D, Maitre S, Francois J. A light scattering study of the association of hydrophobically alpha- and alpha,omega-end-capped poly(ethylene oxide) in water. *J Colloid Interface Sci.* **2000**;*230*(1):41–52. 6. Lafleche F, Durand D, Nicolai T. Association of adhesive spheres formed by hydrophobically end-capped PEO. 1. Influence of the presence of single end-capped PEO. *Macromolecules.* **2003**;*36*(4):1331–40.

7. Persson K, Bales BL. EPR study of an associative polymer in solution: determination of aggregation number and interactions with surfactants. *J Chem Soc Faraday Trans.* **1995**;*91*(17):2863-2870.

8. Abrahmsen-Alami S, Alami E, Francois J. The lyotropic cubic phase of model associative polymers : small- angle X-Ray scattering (SAXS), differential scanning calorimetry (DSC), and turbidity measurements. *J Colloid Interface Sci.* **2000**;*179*(179):20–33.

9. Francois J, Maitre S, Rawiso M, Sarazin D, Beinert G, Isel F. Neutron and X-ray scattering studies of model hydrophobically end-capped poly(ethylene oxide) Aqueous solutions at rest and under shear. *Colloids Surfaces A Physicochem Eng Asp.* **1996**;*112*(1-2)251-265.

10. Beaudoin E, Lapp A, Hiorns RC, Grassl B, François J. Neutron scattering of

hydrophobically modified poly(ethylene oxide) in aqueous solutions in the presence of latex particles. *Polymer*. **2002**;*43*(9):2677–2689.

11. Raspaud E, Lairez D, Adam M, Carton JP. Triblock copolymers in a selective solvent. 1. Aggregation process in dilute solution. *Macromolecules*. **1994**;*27*(11):2956–2964.

12. Xu B, Yekta A, Li L, Masoumi Z, Winnik MA. The functionality of associative polymer networks: the association behavior of hydrophobically modified urethane-ethoxylate (HEUR) associative polymers in aqueous solution. *Colloids Surfaces A Physicochem Eng Asp.* **1996**;112(2-3):239–250.

13. Richey B, Kirk AB, Eisenhart EK, Fitzwater S, Hook J. Interactions of associative thickeners with paint components as studied by the use of a fluorescently labeled model thickener. *J Coatings Thechnology*. **1991**;*63*(798):31–40.

14. Huldun, M. Hydrophobically modified urethane-ethoxylate (HEUR) associative thickeners 1. Rheology of aqueous solutions and interactions with surfactants. *Colloids Surfaces A Physicochem*. **1994**;*82*:263–277.

15. Zhang K, Xu B, Winnik MA, Macdonald PM. Surfactant interactions with HEUR associating polymers. *J Phys Chem*. **1996**;*100*(23):9834–9841.

16. Brown W, Fundin J, Graca Miguel M. Poly(ethylene oxide)-sodium dodecyl sulfate interactions studied using static and dynamic light scattering. *Macromolecules*. **1992**;*25*(26):7192–7198.

17. Smitter LM, Guedez JF, Muller AJ, Saez AE. Interactions between poly(ethylene oxide) and sodium dodecyl sulfate in elongational flows. *J Colloid Interface Sci*. **2001**;*236*(2):343–353.

18. Jones MN. The interaction of sodium dodecyl sulfate with polyethylene oxide. *J Colloid Interface Sci*. **1967**;*23*(1):36–42.

19. Francois J, Dayantis J, Sabbadin J. Hydrodynamical behaviour of the poly(ethylene oxide) -sodium dodecylsulphate complex. *Eur Polym J*. **1985**;*21*(2):165–174.

20. Kaczmarski JP, Glass JE. Synthesis and solution properties of hydrophobically-modified ethoxylated urethanes with variable oxyethylene spacer lengthst. *Macromolecules*. **1993**;*26*(19):5149–5156.

21. Lundberg DJ, Brown RG, Glass JE, Eley RR. Synthesis, characterization, and solution rheology of model hydrophobically-modified, water-soluble ethoxylated urethanes. *Langmuir*. **1994**;*10*(9):3027–3034.

22. Regalado EJJ, Vallejo CCR, Textle HM, Guerrero R, Munoz JFE. Influence of hydrophobe, surfactant and salt concentrations in hydrophobically modified alkali-soluble polymers obtained by solution polymerization. *J Mex Chem Soc*. **2012**;*56*(2):1387-1396.

23. Volpert E, Selb J, Candau F. Associating behaviour of polyacrylamides hydrophobically modified with dihexylacrylamide. *Polyme*r. **1998**;*39*(5):1025–1033.

24. Thuresson K, So O, Hansson P, Wang G. Binding of SDS to ethyl(hydroxyethyl)cellulose. Effect of hydrophobic modification of the polymer. *J Phys Chem*. **1996**:*100*(12):4909–4918.

25. Alami E, Almgren M, Brown W. Interaction of hydrophobically end-capped poly(ethylene oxide) with nonionic surfactants in aqueous solution. Fluorescence and light scattering studies. *Macromolecules*. **1996**;*29*(14):5026–5035.

26. Persson K, Griffiths PC, Stilbs P. Self-diffusion coefficient distributions in solutions containing hydrophobically modified water-soluble polymers and surfactants. *Polymer*. **1996**;*37*(2):253–261.

27. Najafi F, Pishvaei M. Synthesis and characterization of nonionic urethane based linker. *Prog Color Color Coat*. **2011**;*4*:71–77.

28. Barmar M, Barikani M, Kaffashi B. Synthesis of ethoxylated urethane and modification with cetyl alcohol as thickener. *Iran Polym J*. **2001**;*10*(5):331–335.

29. Abrahmsen-Alami S, Stilbs P. NMR self-diffusion of associative polymers in aqueous solution : The influence of the hydrocarbon end-chain length on the polymer transport dynamics in single- and two-component mixtures. *J Colloid Interface Sci*. **1997**;*189*(1):137–143.

30. Claridge TDW. High-Resolution NMR Techniques in Organic Chemistry. Second Edition. Oxford, UK:*Elsvier*, **2009**.

31. Hawe A, Sutter M, Jiskoot W. Extrinsic fluorescent dyes as tools for protein characterization. *Pharm Res*. **2008**;*25*(7):1487–1499.

32. Heenan RK, King SM, Turner DS, Treadgold JR. SANS2d at the ISIS second target station. *17th Meet Int Collab Adv Neutron Sources*. **2005**;1–6. Available from: http://www.isis.stfc.ac.uk/instruments/sans2d/publications/sans2d-at-isis10323.pdf (accessed January 2017).

33. SigmaPlot. Available from: https://sigmaplot.en.softonic.com/ (accessed February 2018).

34. Inkscape. Available from: https://inkscape.org/en/release/0.92.2/ (accessed February 2018).

35. STFC. Beam line soft condensed matter. Available from: http://www.diamond.ac.uk/Beamlines/Soft-Condensed-Matter/small-angle/SAXS-Software/CCP13/FISH.html (accessed February 2018).

36. Bales BL, Peric M. EPR Line Shifts and Line Shape Changes Due to Spin Exchange of Nitroxide Free Radicals in Liquids. *J. Phys. Chem. B*. **1997**;*101*(43):8707–8716.

37. Karlson L. Hydrophobically Modified Polymers Rheology and Molecular Associations. Ph.D. Thesis, *University of Lund*. **2002**.

38. Suzuki S, Uneyama T, Watanabe H. Concentration dependence of nonlinear rheological properties of hydrophobically modified ethoxylated urethane aqueous solutions. *Macromolecules*. **2013;***46*(9):3497–3504.

39. Griffiths PC, Cheung AYF. Interaction between surfactants and gelatin in aqueous solutions. *Mater Sci Technol*. **2002**;*18*(6):591–599.

40. Griffiths PC, Paul A, Fallis IA, Wellappili C, Murphy DM, Jenkins R, et al. Derivatizing weak polyelectrolytes-Solution properties, self-aggregation, and association with anionic surfaces of hydrophobically modified poly(ethylene imine). *J Colloid Interface Sci*. **2007**;*314*(2):460–469.

41. Griffiths PC, Rowlands CC, Goyffon P, Howe AM, Bales BL. EPR insights into aqueous solutions of gelatin and sodium dodecyl sulfate. *J Chem Soc Perkin Trans. 2*, **1997**;*0*(12): 2473-2478.

42. Saffer EM, Lackey MA, Griffin DM, Kishore S, Tew GN, Bhatia SR. SANS study of highly resilient poly(ethylene glycol) hydrogels. *Soft Matter*. **2014**;*10*(12):1905-

1916.

43.   Trefalt G, Borkovec M. Overview of DLVO Theory. *Lab Colloid Surf Chem Univ Genebra*.   .   **2014**;1–10.   Available   from: http://www.colloid.ch/grouppage/pdfs/Overview_DLVO_Theory1.pdf%0Awww.coll oid.ch/dlvo (accessed February 2018).

44.   Rosen M. Surfactants and interfacial phenomena. Second edition. New York, *Wiley*: USA; **1989**.

45.   Guzmán E, Llamas S, Maestro A, Fernández-peña L, Akanno A, Miller R, Ortega F, Rubio RG. Polymer–surfactant systems in bulk and at fluid interfaces.*Adv Colloid Interface Sci*. **2016**;*233*:38–64.

46.   Dai S, Tam KC, Wyn-Jones E, Jenkins RD. Isothermal titration calorimetric and electromotive force studies on binding interactions of hydrophobic ethoxylated urethane and sodium dodecyl sulfate of different molecular masses. *J Phys Chem B*. **2004**;*108*(16):4979–4988.

3. HEUR/latex interaction

3.1. Abstract

HEUR polymers are widely used to control the rheological profile of formulated particulate dispersions. However, HEURs interact with other components in the formulation, in particular latex particles, leading to substantial perturbations in behaviour. In this chapter, the interaction of C_6-L-$(EO_{100}$-L$)_9$-C_6 HEUR with polystyrene-butylacrylate latex (PS-BAL) and acrylic acid-stabilised polystyrene-butylacrylate latex (AA-PS-BAL) are studied to validate the previously postulated models for HEUR/latex interaction. A range of techniques, UV spectroscopy, nuclear magnetic resonance (NMR), small-angle neutron scattering (SANS) and rheology, have been used to quantify the amount of HEUR adsorbed to the latex surface and investigate the conformation of the C_6-L-$(EO_{100}$-L$)_9$-C_6 in the presence of latex. There is a very weak adsorption of C_6-L-$(EO_{100}$-L$)_9$-C_6 to the latex surface, which becomes even weaker in the presence of less hydrophobic latex AA-PS-BAL. The HEUR adsorption to PS-BAL is evidenced by bridging flocculation observed at low polymer concentration and increase in viscosity.

Chapter 3. HEUR/latex interaction

3.2. Introduction

Water-based latex dispersions are used as film formers in a range of formulations (*e.g.* paints, pharmaceutical application) (1,2). Hydrophobically modified ethoxylated urethane (HEURs) are ethylene oxide-urethane block copolymers, widely used to control the rheological profile of latex dispersions. However, polymers with such complex architectures interact with the other formulation components, including surfactants and particulate materials, *e.g.* pigments, latex particles. Most of the studies on HEUR/latex systems suggested the adsorption of HEUR on latices with different surface chemistry (3,4). The nature of the adsorption between the HEUR and the latex is sensitive to the hydrophobicity of the latex surface as both the HEUR hydrophobic end-groups and urethane linkers can adsorb on the surface of hydrophobic latex. However, with decreasing hydrophobicity (*e.g.* incorporation of acrylic and methacrylic acid or 2-hydroxyethyl methacrylate (HEMA) monomers), only the polymer hydrophobes adsorb to the surface (5), and ultimately fewer end-groups adsorb as the percentage of the hydrophilic monomer incorporation in particle synthesis increases as shown by *e.g.* Quadrat *et al.* (6). Ou-Yang *et al.* studied the change in conformation of the adsorbed HEUR-51-12 (the first number is the molecular weight of the polymer in kg mol^{-1} and the second number is the length of the hydrophobic end-group) to the hydrophobic latex (polystyrene latex, diameter = 91 nm) as a function of HEUR concentration by dynamic light scattering (DLS) (7). At low concentration, the end-groups and urethane linkers adsorb to the latex surface forming a pancake-like structure. However, at higher concentrations the urethane linkers desorb and only hydrophobic end groups at both ends remain adsorbed and formed a brush structure.

Generally, the viscosity builds up in these particulate formulations due to the polymer network. One element of the network comes from the inherent viscosity of the polymer bridging between the particles, hence a dynamic space-filling network is formed. Finally, the dispersion viscosity comes from increasing the effective volume of the particle due to HEUR adsorption. The architecture of the polymer affects the viscosity and performance of the HEUR/particle dispersion. Increasing the polymer hydrophobic end-group length strengthens the adsorption and hence the viscosity increases (8). The molecular weight of the polymer affects the shear thinning behaviour of the polymer dispersion at high shear, the higher the molecular weight the more shear thinning the samples become upon mixing the HEUR with the latex (9). The lower molecular weight HEURs decrease this

shear thinning behaviour at high shear, however, they induce bridging flocculation. Jenkins *et al.* studied the relationship between HEUR molecular weight and bridging flocculation, where the bridging flocculation peaks for C_{16} HEURs with molecular weights between 50,000-80,000 g mol^{-1} for a range of polymer concentrations (0-2 wt%) and polystyrene latex (PSL) (10 wt%, 190 nm) (10).

Flocculation in HEUR/latex dispersions is observed at low polymer concentration: Kostansek studied the phase diagram of HEUR/latex system using a model HEUR-50-12 with butylacrylate-methylmethacrylic acid (BA-MMAL), and butylacrylate-styrene (BA-PSL) latices, all contain 1% methacrylic acid and 0.05-0.1 wt% sodium dodecyl benzene sulphonate (11). The latex concentration was held constant at 25 wt%. The resulting phase diagram described the correlation between flocculation, particle size, and surface chemistry. The region of bridging flocculation increases with the hydrophobic character and size of the latex particles. Where increasing the diameter of BA-MMAL from 300 to 600 nm or using a more hydrophobic latex, such as 300 nm BA-PSL resulted in doubling the flocculation region. Below saturation of the latex surface, the HEUR end-groups preferentially adsorb to the latex surface, but at higher polymer concentrations or in the presence of the surfactant, the polymer end-groups are preferentially solubilised into hydrophobic aggregates in solution, and stability is regained.

Pham *et al.* considered HEUR/latex interactions as a number of idealised configurations assuming that one hydrophobic end-group adsorbs on the latex surface, the other end-group is adsorbed to: (a) the same latex particle ("loop"), (b) another latex particle ("bridge"), or (c) the end-group hydrophobic aggregate of another HEUR polymer ("micelle" or "network") (12). There are two models for the possible arrangement of HEURs and particles in paint formulation. The new model proposed by Beshah, there is a greater association of the hydrophobic moieties with the particle surface (5), whereas the old model postulated by Pham *et al.* a greater self-association of the hydrophobic groups in solution (12) (Figure 3.1). The new model polymer configuration may have the same configuration as the old model in presence of surfactant or higher HEUR concentration (5).
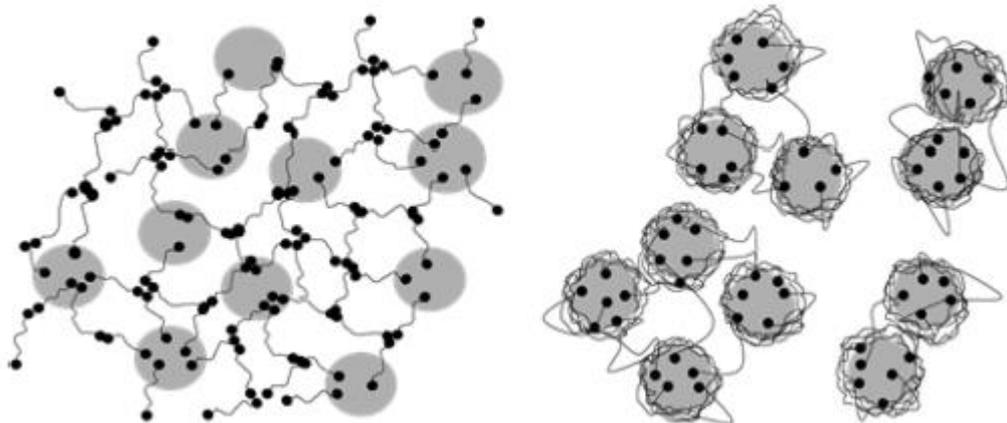
Figure 3.1. Cartoon illustrating (a) old and (b) new model conformation of the HEUR in the presence of latex in paint formulation (5).

In terms of the rheology, as the shear rate increases, there is an increase in the re-distribution of bridges and loops, thus the network structure is disrupted. This leads to shear thinning behaviour of the HEUR/latex blends as proposed by Beshah *et al.* (5) or the desorption of the polymer molecules from the latex surface, as proposed by Santos *et al.* (13). A rheo-small-angle neutron scattering (rheo-SANS) experiment was conducted on HEUR/latex system, where the scattering of the sample was recorded as a function of shear. The rheo-SANS results suggest the thinning of the polymer adsorbed layer on the latex particles as a function of shear due to expelling of solvent molecules from the polymer adsorbed layer (14).

A further SANS experiment has been conducted by Beaudoin *et al.* on PSL of two different radii PSL1 95 ± 5 nm, and PSL2 80 ± 5 nm, at latex concentration 1 and 10 wt% (15). The latex samples were mixed with a range of end-capped hydrophobically modified poly (ethylene-oxide) (PEOM-20-16) concentrations (1-20 %). In these experiments, the PEOM/latex mixtures have been measured at different contrasts to get the scattering from one component in the mixture. In the first contrast, the scattering contribution was recorded only from the PEOM in PEOM/latex mixtures. At low polymer concentration, adsorption of PEOM on the PSL is observed, however, at higher polymer concentration a polymer scattering peak arising from the polymer end-hydrophobes was observed, originated from the presence of excess polymer associating forming micelles in solution. The second contrast, where the scattering contribution is only from the latex in PEOM/latex mixture, could only be understood in terms of latex aggregation. The

absence of polymer adsorption on the latex surface and particle aggregation is postulated in presence of sodium dodecylsulphate (SDS), used to stabilise the latex (1 % w/w).

Clearly, HEUR/latex interactions are dependent on many factors (*e.g.* latex surface chemistry, size, polymer architecture, concentration). Previous papers identified two models of HEUR/latex interaction, old and new model presented in Figure 3.1, where in presence of surfactant or the increase of HEUR concentrations, the configuration of the HEUR adsorbed to the latex changes from the new to the old model. In this chapter, the binary mixtures of the HEUR/latex have been studied with two latices of different surface chemistry, hence hydrophobicity, in an attempt to differentiate the two models.

3.3. Material and methods

3.3.1. Materials

Sodium persulphate (>99%, Aldrich), d_8-styrene (>98%, Fischer Scientific), h-butylacrylate (>99%, Aldrich), polystyrene-butylacrylate latex (diameter = 173 nm, PDI 0.03) (AkzoNobel), acrylic acid stabilised polystyrene-butylacrylate latex (diameter = 154 nm, PDI 0.03, acid level 3 %) (AkzoNobel), sodium dodecylsulphate (SDS) (Aldrich, no impurity observed, (Figure D.9)), deuterated sodium dodecylsulphate (d_{25}-SDS) (ISIS deuteration facility), Hydroin buffer pH 9 (Aldrich), deionized water (Purite Select deionizer) and deuterium oxide (99.9%, Aldrich) were used as received. Acrysol® RM2020E C_6-L-$(EO_{100}$-L$)_9$-C_6 (Dow) was purified from cyclodextrin before use as described in the Appendix D, Section D.1.

Synthesis of deuterated latex particles

The polymerization was carried out in a sealed, stirred, thermostatted 5-port round bottom flask. The polymerisation reaction was initiated by adding 0.08 g sodium persulphate to 6 g d_8-styrene, 5 g butylacrylate, and 0.7 g of 20% (w/w) sodium dodecylsulphate (SDS). The initiator, monomers, and SDS were slowly injected into water kept under nitrogen gas at 70 °C. The reaction was terminated by cooling the reaction vessel to room temperature. The sample was filtered using glass wool. The unreacted monomers and SDS (adsorbed on the surface) were removed by spinning down the particles twice using high-speed centrifuge (Hitachi CR22N) at 20,000 rpm and resuspending them in D_2O/H_2O mixture. The particle concentration was calculated from dry weight analysis to be 20 wt%. The diameter of the particles was measured by dynamic light scattering (zetasizer Nano-ZS,

Malvern) as 160 nm and PDI 0.067. The detailed synthesis procedure was held for intellectual property rights.
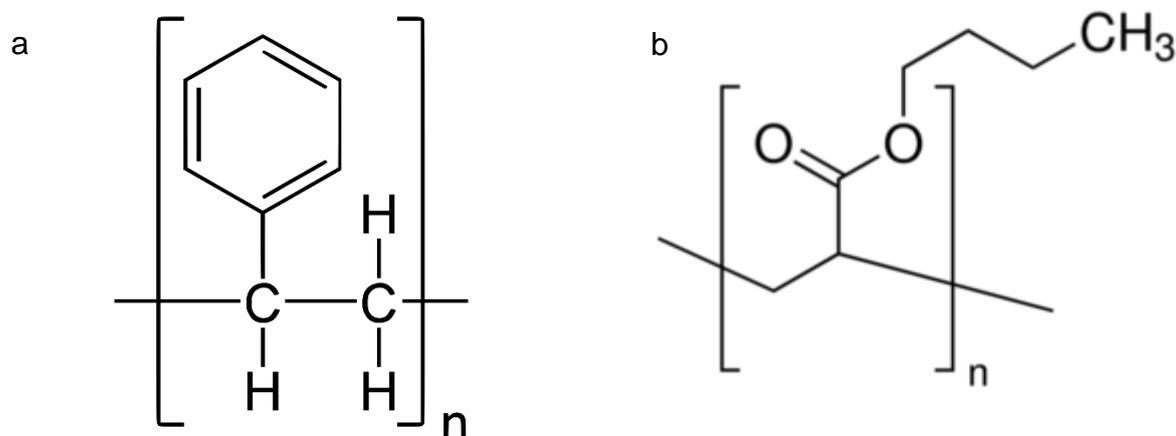
Figure 3.2. The structure of (a) polystyrene and (b) poly(butylacrylate) polymers.

3.3.2. Methods

The unreacted monomers and SDS were removed from the supplied AkzoNobel latices by spinning down the particles twice using a bench-top Eppendorf 5430R centrifuge at 14,200 rpm and resuspending them in the suitable solvent. The size and PDI of the latices were checked after resuspending them in the solvent to check the presence of aggregates; however each time the size and PDI were within experimental error relative to the samples supplied. All the HEUR/latex samples were prepared in the appropriate solvent according to the experiment and mixed using a hula-mixer for 24 hours before measurement.

3.3.2.1. *Adsorption isotherm determination by ultra-violet (UV) spectroscopy*

Adsorption isotherm of PS-BAL was studied as a function of C_6-L-$(EO_{100}$-L$)_9$-C_6 concentration. The HEURs do not possess a UV chromophore, all solutions were mixed with an I_2/KI mixture, where I_2 interacts with the PEO backbone of the polymer. I_2/KI mixture was prepared by mixing 1 g of I_2 with 2 g of KI in 250 mL of water (16,17). A range of HEUR concentrations (0-0.001 wt% were prepared) and 10 mL of each concentration was mixed with 0.25 mL of I_2/KI, The absorbance of the samples was measured after 30 min (18) at wavelength 500 nm in a quartz cuvette of 1 cm path length using a Cary 100 UV-Vis spectrometer. A linear calibration curve was obtained for the polymer solutions.

Chapter 3. HEUR/latex interaction

A range of C_6-L-$(EO_{100}$-L$)_9$-C_6 concentrations were mixed with 5 wt% PS-BAL in Hydroin buffered water, pH 9 for 24 hrs. A second set of polymer solutions were prepared as controls. HEUR/PS-BAL mixtures and control samples were centrifuged using a desktop Eppendorf 5430R centrifuge at 14,200 rpm and the supernatant was used to determine the concentration of unbound HEUR. The supernatant of the HEUR/PS-BAL mixtures, and control samples were diluted to a suitable concentration, mixed with I_2/KI, and the absorbance was measured in the same manner as the calibration curve samples.

The adsorbed amount of the HEUR in mg per surface area of PS-BAL in m^2 was plotted as a function of initial polymer concentration. The concentration of the control samples was calculated from the absorbance using a calibration curve equation. The concentration was invariant after centrifugation.

3.3.2.2. Nuclear Magnetic resonance techniques

3.3.2.2.1. Solvent relaxation NMR

HEUR/latex mixtures were dissolved in Hydroin buffered H_2O at pH 9, experiments were carried out at 25 °C on a bench-top Acorn XIGO nanotools spectrometer. A Carr−Purcell−Meiboom−Gill CPMG sequence was used with a spacing of 0.5 ms, between the 90° and 180° pulse, and a recycle delay of at least 5 times the spin−lattice relaxation time between consecutive scans was necessary to ensure full recovery of the magnetisation. Typically, 2118 data points were collected for each scan, and the signal was averaged over four scans for each sample. Data were phase corrected and fitted to a single exponential on the instrument software.

3.3.2.2.2. Pulsed-Gradient Spin-Echo Nuclear Magnetic Resonance (PGSE-NMR)

HEUR/latex mixtures were dissolved in Hydroin buffered D_2O at pH 9. Experiments were carried out at 25 °C on a 400 MHz Bruker FT NMR spectrometer. A stimulated echo sequence was used, in which the diffusion time (Δ) was set to 800 ms, the duration (δ) of the gradient pulses was held constant at 1 ms and their intensity (G) varied from 5 - 800 G cm^{-1}. Typically, 16 scans were accumulated over 32 gradient steps. Self-diffusion coefficients were extracted by fitting the peak intensities (I) to Equation 3.1 for the peaks at 3.75 ppm (EO) where I_0 is signal intensity in the absence of gradient pulses, D_s the diffusion coefficient, γ the gyromagnetic ratio of protons (19,20).

$$I = I_0 \, e^{-D_S \gamma^2 G^2 \delta^2 \left(\Delta - \frac{\delta}{3}\right)}$$

<div align="right">Equation 3.1</div>

3.3.2.3. Neutron Scattering

SANS measurements were carried out at 25 °C on the SANS 2D instrument (ISIS spallation Neutron Source, Oxfordshire, UK). Neutrons wavelengths spanning 2-14 Å were used to access a Q range of 0.002 to 3 Å^{-1} (Q=4π sin(θ/2)/λ) (21) with a fixed sample-detector distance of 4 and 2.4 m for the rear and front detector respectively. Temperature control was achieved through the use of a thermostatted circulating bath pumping fluids through the base of the sample changer, which allowed the experiment to be run at 25 ± 0.5 °C. Samples were contained in UV-spectrophotometer grade 1 mm path length quartz cuvettes (Hellma). The scattering data were normalized for the sample transmission and the incident wavelength distribution, corrected for instrumental and sample backgrounds using a quartz cell filled with D_2O (this also removes the incoherent instrumental background arising from vacuum windows), and corrected for the linearity and efficiency of the detector response using the instrument specific software package. The data were put onto an absolute scale using a well characterised, partially deuterated PSL blend standard sample. The intensity of the scattered radiation, I(Q), as a function of the wave vector, Q, is given by Equation 3.2:

$$I(Q) = N_p V_P^2 \Delta\rho^2 P(Q)S(Q) + B_{inc}$$

<div align="right">Equation 3.2</div>

where N_p is the number and V_p the volume of the scattering species, $\Delta\rho$ is the difference between the neutron scattering length density of the scattering species and the solvent, $P(Q)$ describes the morphology of the scattering species, and $S(Q)$ describes the spatial arrangement of the scatterers in solution, B_{inc} incoherent background.

In the contrast-match experiment, d-styrene and h-butylacrylate monomers were used to synthesize partially deuterated latex particles, referred to as d-PS-h-BAL. The d-PS-h-BAL was diluted to 3 wt% in the scattering experiment with the appropriate solvent (D_2O or H_2O) to make different ratios of H_2O: D_2O to find experimentally the match point of the latex (Figure 3.3) *i.e.* where $\Delta\rho^2$ in Equation 3.2 is equal to zero. After detecting the match point, conventionally found where the $\sqrt{I(Q)} = 0$, and hence $\Delta\rho$=0, the HEUR and latex mixtures were prepared in the correct ratio of D_2O: H_2O and the scattered intensity was recorded. In this contrast, only the C_6-L-(EO_{100}-L)$_9$-C_6 is contributing to the scattering intensity. Contrast-match experiments were conducted on similar systems such as

particles consist of polystyrene solid core with network of poly(*N*-isopropylacrylamide) grafted to the surface (22), and polystyrene particles with PEG polymer chemically grafted to the surface (23).
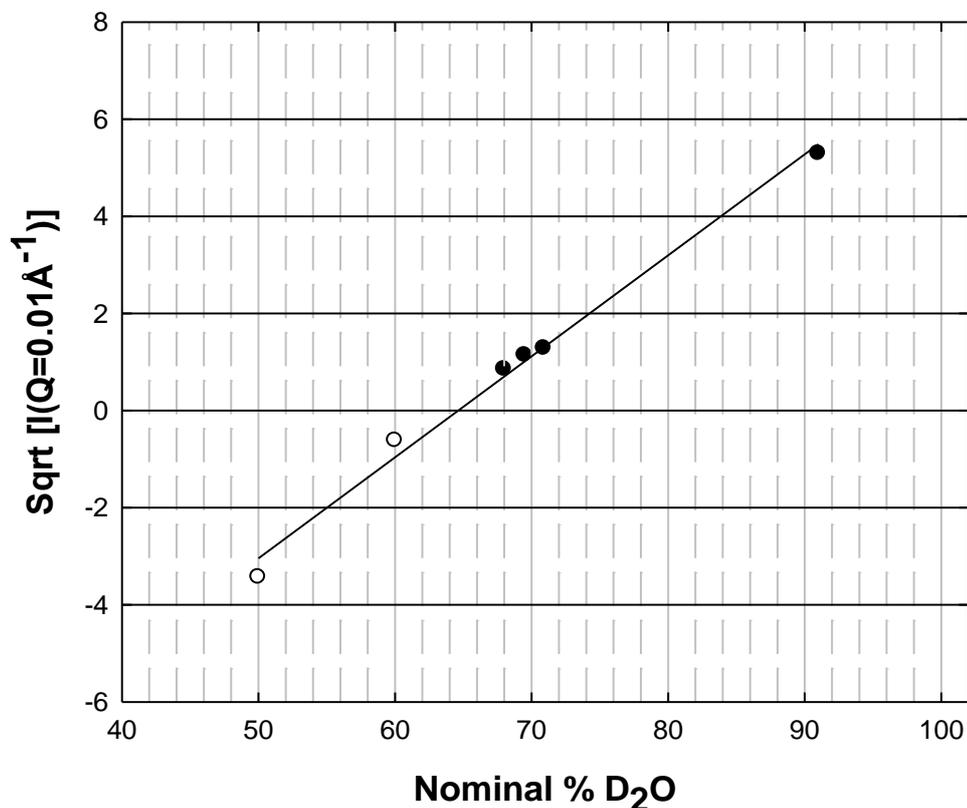
Figure 3.3. Contrast variation experiment from 3 wt% d-PS-h-BAL synthesised from d-styrene monomers and h-butyl-acrylate. Samples were prepared in different ratios of Hydroin buffered D_2O: H_2O, pH 9. Measurements were carried out at 25 °C. The solid line is a guide for the eye.

3.3.2.4. Rheology

The rheology of mixtures of C_6-L-$(EO_{100}$-L$)_9$-C_6 HEUR/PS-BAL have been examined where HEUR concentration was held constant at 5 wt% and latex concentration was varied (0.5, 3, and 5 wt%) in Hydroin buffered water, pH 9. The samples were measured using TA instrument rheometer AR-2000ex, with a 2°/40 mm cone and plate geometry at 25°C. Shear profiles were recorded at 25 °C for a shear range of 1-1000 s^{-1}, with an integration time of 5 s, and delay time of 5 s.

3.3.3. Programs

The Insanity VS 21L program is developed by T. Cosgrove, the program predicts the scattering pattern of a sample based on some knowledge of the sample properties. For example here, the adsorbed polymer layer is predicted based on the polymer molecular weight, R_g, density, volume fraction, SLD and background. SasView program is a small-angle neutron scattering program which has various fitting models for the samples (24).

3.4. Results and discussion

The interaction of HEUR denoted as C_6-L-$(EO_{100}$-L$)_9$-C_6 was studied with two latices polystyrene-butylacrylate (PS-BAL) and 3 wt% acrylic acid stabilised polystyrene-butylacrylate latex (AA-PS-BAL). First, the adsorption isotherm of C_6-L-$(EO_{100}$-L$)_9$-C_6 to PS-BAL was studied to determine the amount of polymer adsorbed to the particle (mg per m^2). The solvent relaxation NMR was then studied to track the changes of the particle surface area for PS-BAL as a function of C_6-L-$(EO_{100}$-L$)_9$-C_6 concentration, reflected by changes of R_{2sp} of the mixtures. Changes of the polymer self-diffusion coefficient were studied in the presence and absence of latex by diffusion NMR to track changes of the unadsorbed polymer aggregates. A scattering contrast-match experiments are presented where the scattering contribution is from the polymer only in presence of d-latex. The scattering curves of the polymer in the absence and presence of a range of d-PS-h-BAL concentrations are then compared. Finally, the shear profile and polymer viscosity changes as a function of PS-BAL concentration are noted. All these measurements attempt to quantify the amount of polymer adsorbed to PS-BAL and track the changes in latex and polymer properties in the presence of each another. After establishing a good understanding of C_6-L-$(EO_{100}$-L$)_9$-C_6/PS-BAL interactions, some selected experiments are repeated in the presence of the less hydrophobic latex AA-PS-BAL to study the effect of latex surface chemistry on polymer adsorption.

3.4.1. Interaction of HEUR/PS-BAL mixtures

3.4.1.1. Determination of C_6-L-$(EO_{100}$-L$)_9$-C_6 adsorption to PS-BAL
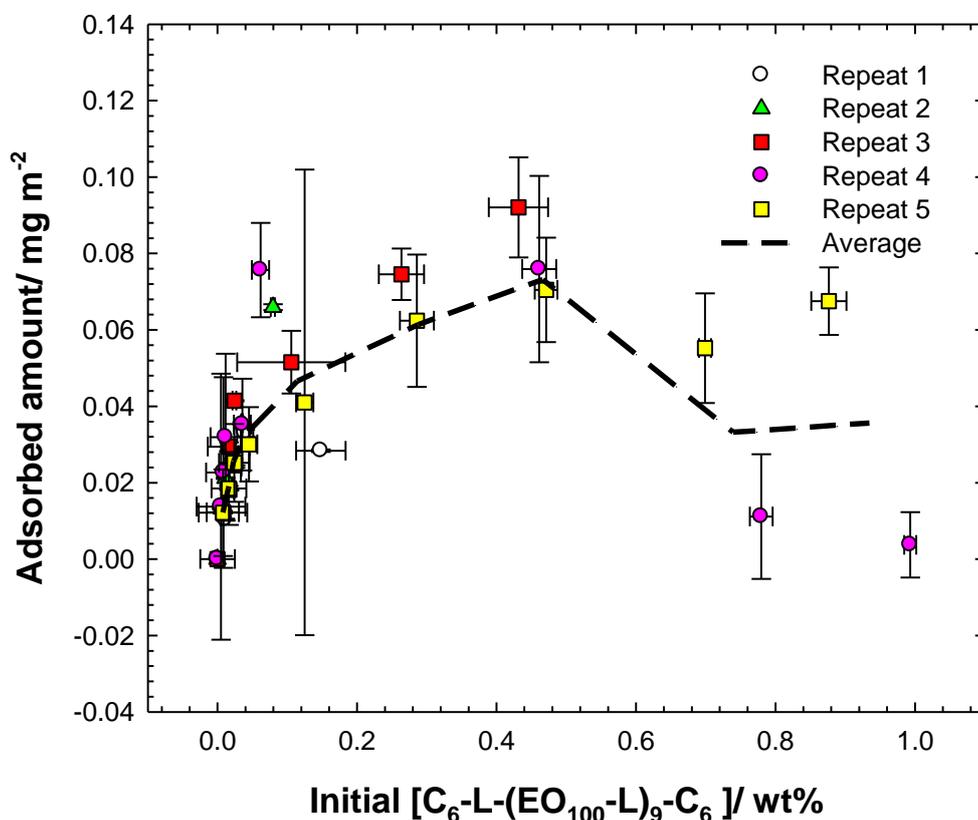
Figure 3.4. Adsorption of (50,100 g mol^{-1}) C_6-L-$(EO_{100}$-L$)_9$-C_6 HEUR onto 5 wt% PS-BAL at 25°C in Hydroin buffered water, pH 9. The horizontal error bars are for three measurements for the same sample (polymer/latex mixtures), and the vertical error bars are for the control samples of polymer in absence of latex.

The adsorption isotherm of C_6-L-$(EO_{100}$-L$)_9$-C_6 to PS-BAL was determined as set out in Section 3.3.3.1. Several attempts were made, having validated the methodology. The raw data of supernatant polymer concentrations as a function of initial polymer concentration have been recast into the adsorbed amount from a knowledge of the particle concentration and particle size (surface area). The derived data are presented in Figure 3.4, as a "classical" adsorption isotherm.

Clearly, the HEUR adsorption to PS-BAL is very weak, 0.051 ± 0.019 mg m^{-2} (equivalent to 0.095 ± 0.035 wt% HEUR for 5 wt% PS-BAL). For comparison, the adsorbed amount of poly(ethylene oxide) (PEO) of the same molecular weight is 0.7 mg m^{-2} (13.7 times)

(25). In a typical paint formulation, the HEUR and latex concentrations are 1 and 30 %, respectively. By calculating the amount of polymer adsorbed that would be $\approx 0.57 \pm 0.2$ wt% of C_6-L-$(EO_{100}$-L$)_9$-C_6 adsorbed to the PS-BAL. The adsorption isotherm shows a decrease in the adsorbed polymer at 0.6 wt%, at this concentration it was difficult to spin down all the particles.

3.4.1.2. Surface area determination for PS-BAL

Solvent relaxation NMR technique is sensitive to surface area. In this approach, as particles are suspended in water, the protons of the water molecules bind to the surface of the particles and show a restricted motion if compared with the atoms in the bulk, hence the efficiency of relaxation is improved. As the concentration of discrete particles increases the surface area available for water molecules to bind to also increases, hence more relaxation enhancement is observed.

The enhancement of relaxation is indicated by a decrease in the measured relaxation time T_2. Therefore the average relaxation rate (R) of the protons can be calculated, ($R = \frac{1}{T_2}$). A more convenient way of presenting the data is to calculate the specific relaxation rate (R_{2sp}) by normalizing the relaxation rate of the sample to the solvent, ($R_{2sp} = \frac{R_2}{R_2^\circ} - 1$). For example, for PS-BAL suspended in water R_2 of PS-BAL in water is normalized to R_2° of water on its own. The R_{2sp} can be plotted as a function of sample concentration or surface area. The surface area of the particles can be calculated from the particle density, size and concentration.
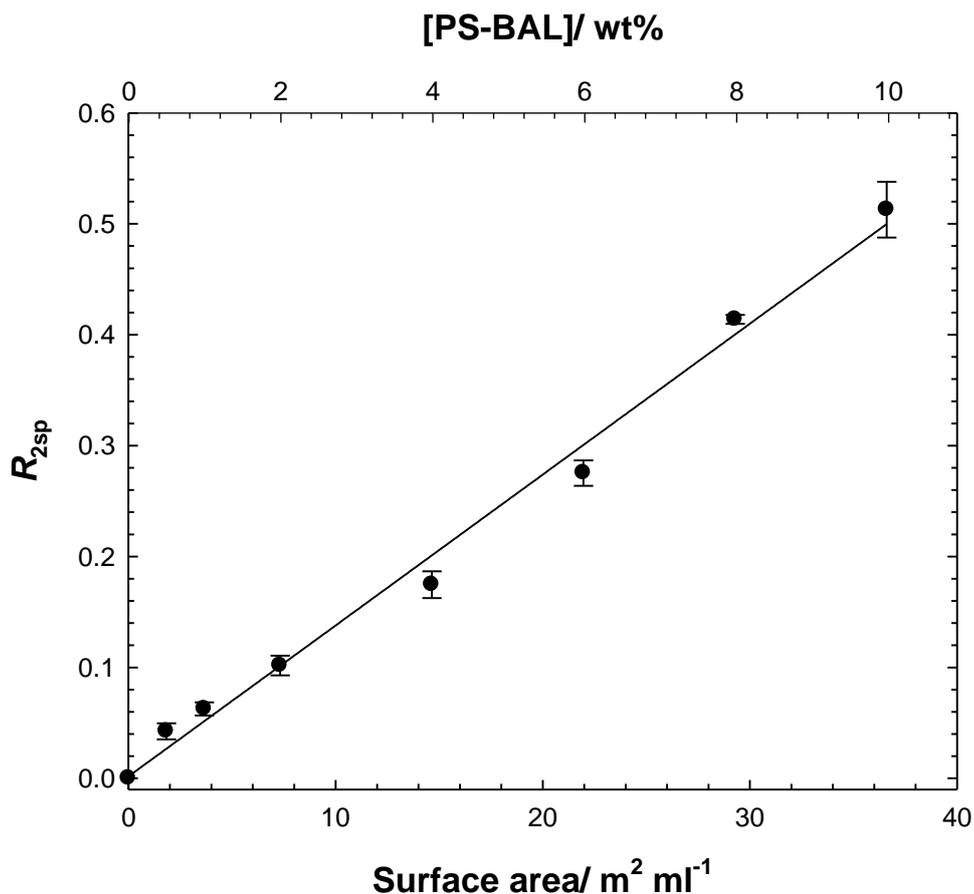
Figure 3.5. R_{2sp} **of PS-BAL as a function of its surface area which is correlated to the concentration of the particles. Samples were prepared in Hydroin buffered water, pH 9.** R_{2sp} **of latex is corrected relative to Hydroin buffered water. Measurements were carried out at 25 °C. The solid line is a linear fit. The error bars are the standard deviation of three measurements for the same sample and a second set of samples.**

The R_{2sp} shows a linear dependence on surface area (which is correlated to the particles concentration) (Figure 3.5). Therefore, any change in R_{2sp} of a suspension at fixed particle concentration reflects a change in dispersion of the particles *i.e.* if R_{2sp} decreases then the particles are aggregating, if increases the particles are becoming well dispersed.
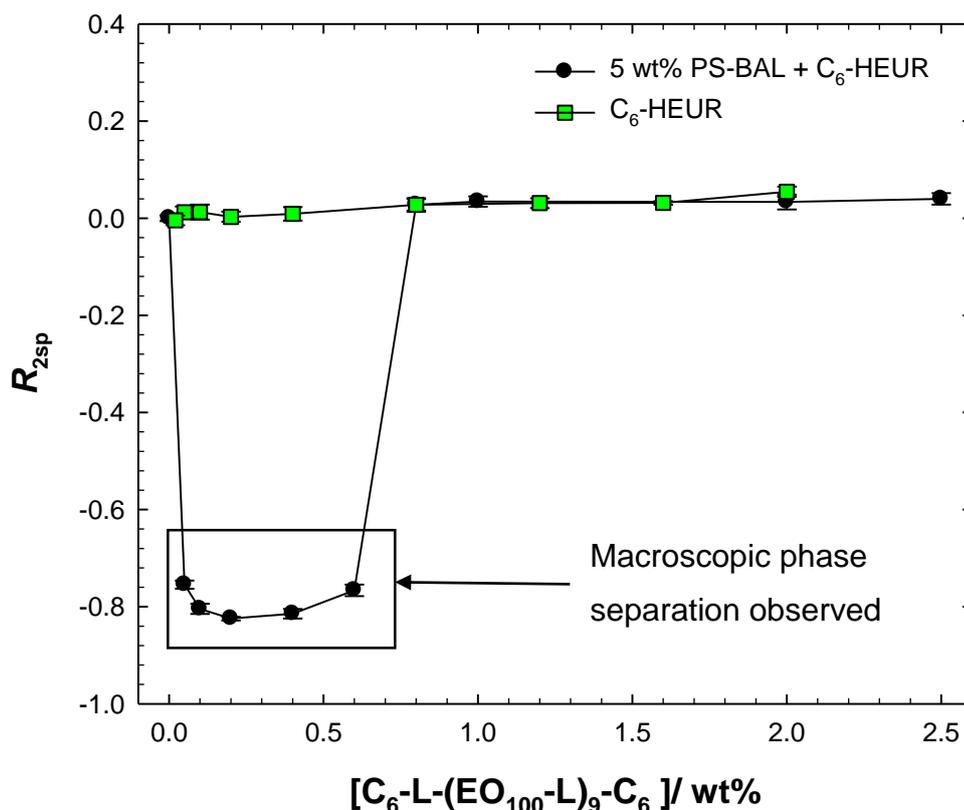
Figure 3.6. R_{2sp} of C_6-L-$(EO_{100}$-L$)_9$-C_6 as a function of its concentration in the absence (green squares) and presence of 5 wt% PS-BAL (black circles) in Hydroin buffered water, pH 9. R_{2sp} of HEUR/PS-BAL mixtures is corrected relative to the bare particle, and HEUR as a function of its concentration relative to water. Measurements were carried out at 25 °C. The solid lines are guides for the eye. The error bars are the standard deviation of three measurements for the same sample and a second set of the samples.

The dependence of R_{2sp} on C_6-L-$(EO_{100}$-L$)_9$-C_6 concentration is illustrated in Figure 3.6. The R_{2sp} = 0 for most of the polymer range. Only at highest polymer concentrations the R_{2sp}>0. The increase in R_{2sp} values at high polymer concentrations is due to the increase in solution viscosity which restricts the motion of the solvent molecules and enhances the relaxation of the protons within the water molecule (26).

For all the data sets, the R_2 of the polymer/latex mixtures are normalized to the R_2 of the latex, hence R_{2sp} of the mixture is sensitive to changes due to polymer adsorption to latex. Therefore, the R_{2sp} of PS-BAL equals zero (first data point). Upon addition of polymer, the R_{2sp} of the polymer/latex mixture goes negative as the $R_{2\ mixture}$ < $R_{2\ particles}$ and then returns back to zero as the $R_{2\ mixture}$ ≥ $R_{2\ particles}$.

Chapter 3. HEUR/latex interaction

The dip in the HEUR/latex curve at low HEUR concentration is reflective of the loss of surface, *i.e.* aggregation of particles, as the R_2 value of the mixture is lower than that of the particles on their own (Figure 3.6). At high HEUR concentrations, the R_{2sp} returns to zero at $C_{polymer} > 0.5$ wt%, therefore the surface coverage is at 0.5 wt% polymer, which does not agree with the adsorption isotherm. Once the surface is saturated, stability of the HEUR/latex was observed may be due to the ability of the polymer to associate in solution at those concentrations, where one hydrophobic end-end group is adsorbed to the latex surface and the other end is in a polymer hydrophobic aggregate. The phase behaviour of C_6-L-$(EO_{100}$-L$)_9$-C_6 /PS-BAL agrees with observations of Kostansek (11), Reuvers (9), and Jenkins (10), where the phase separation was correlated to bridging flocculation, the dispersion re-stabilised when the adsorbed HEUR hydrophobes associate with the HEUR aggregates in the aqueous phase.

The shape of the R_{2sp} curve for the C_6-L-$(EO_{100}$-L$)_9$-C_6 /PS-BAL mixtures suggests the absence of classical adsorption of the HEUR in the form of loops, trains and tails on PS-BAL surface, as the enhancement of relaxation is attributed to trains rather than loops or tails (27).

A typical adsorption isotherm of a polymer/particle mixture shows an increase of the R_{2sp} as a function of polymer concentration until the particle surface is saturated, above saturation concentration the polymer is present in the bulk in an unbound state where the R_{2sp} plateaus (26,27). The solvent relaxation NMR magnetisation decay of C_6-L-$(EO_{100}$-L$)_9$-C_6/PS-BAL mixtures as a function of time fits to single exponential decay curve, suggesting the presence of only one population of the polymer, which may be explained the adsorption of a small number of polymer hydrophobic end-group to the particle surface (Figure B.1).

To date, few T_2 measurements have been done on these systems, Uemura *et al.* reported studied the adsorption of a HEUR-51-16 (recall the first number is the molecular weight of the polymer in kg mol^{-1} and the second number is the length of the hydrophobic end-group) in presence of PSL of diameter 168 nm, which showed a strong adsorption, where at 1 wt% HEUR more than 50% of the polymer was adsorbed to the 4 wt% PSL (29). A shorter T_2 has been reported for the PSL particles as a function of C_{16}-HEUR concentration. The magnetisation decay as a function of time showed the presence of two populations, representing the free and bound HEUR.

3.4.1.3.   *Solution polymer aggregates in presence of PS-BAL*
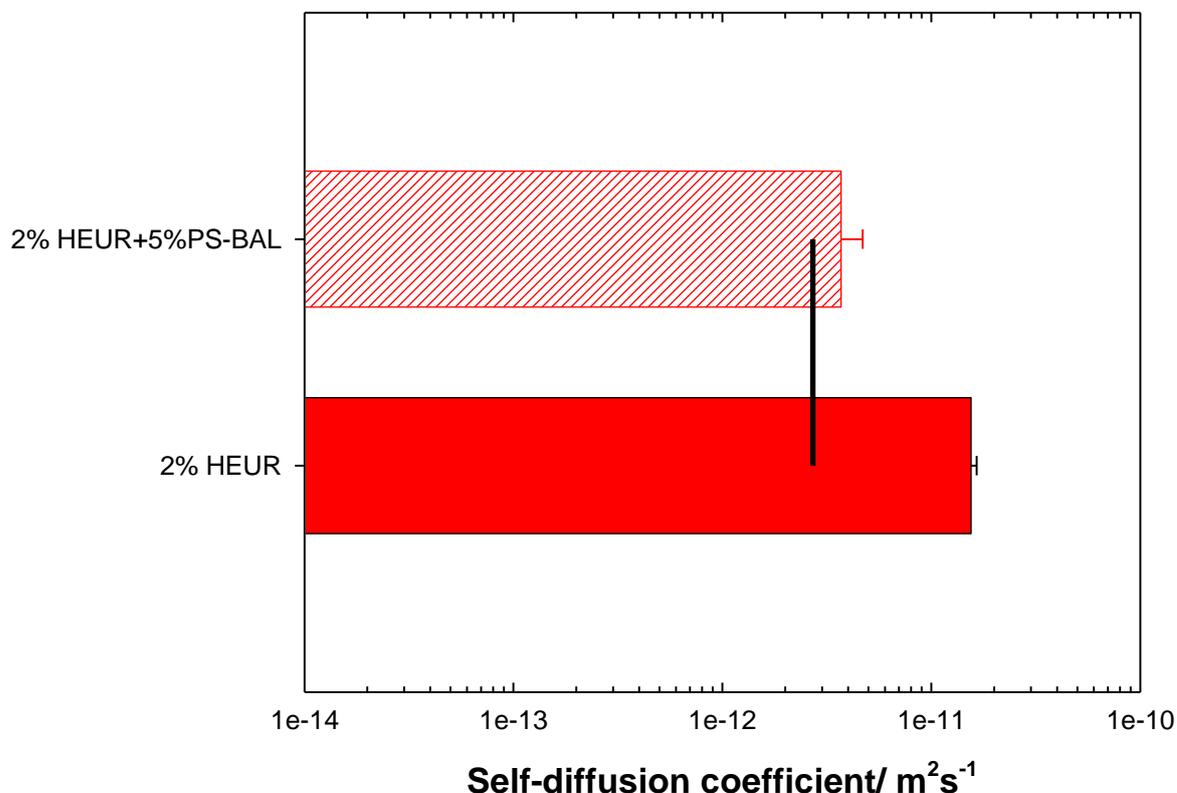
Figure 3.7. Self-diffusion coefficient of C_6-L-$(EO_{100}$-L$)_9$-C_6 in the absence and presence of PS-BAL. Samples were prepared in Hydroin buffered D_2O, pH 9. Measurements were carried out at 25 °C. The solid black line is the calculated diffusion of PS-BAL. The error bars are the standard deviation of three measurements for the same sample and a second set of samples.

The choice of the polymer concentration (2 wt%) was dependent on the HEUR/PS-BAL mixture stability from the solvent relaxation graph. It is hypothesised that if there is a considerable level of bridging occurring (Figure 3.1-a), the diffusion of the polymer should be reflective of the state of aggregation, at least to a crude comparison of the simple polymer case. Therefore, measurements of diffusion were conducted in the presence and absence of the latex and the values of the polymer diffusion explored.

The decay of the signal as a function of gradient parameter was plotted for C_6-L-$(EO_{100}$-L$)_9$-C_6 in the presence and absence of PS-BAL, the data were fitted to single stretched model reflective of the presence of one population (Figure B.2). In addition, the beta parameter (β) was extracted for the polymer in the presence and absence of latex. The β is reflective of polydispersity of the polymer where if $\beta = 1$, therefore the sample is

monodisperse, whereas if *β* < 1 the sample is polydisperse. The beta parameter is in-sensitive to adsorption, the samples showed a very subtle change in β value where the pure polymer shows a value of 0.92, whilst in presence of latex is 0.892.

Figure 3.7 shows the self-diffusion coefficient of HEUR in the presence and absence of PS-BAL. The diffusion of the PS-BAL particles, and thus the expected value for the polymer if completely adsorbed, has been calculated from Stokes-Einstein equation using the particle size measured by DLS ($D = \frac{k_B T}{6\pi r \eta}$), where D is the diffusion of the particles, k_B Boltzmann constant, T absolute temperature, r radius of the particle, η viscosity. As may be seen, the HEUR diffusion is slightly slower in presence of latex particles relative to HEUR on its own.

Ukerma *et al.* studied the diffusion of HEUR-51-16 in presence of PSL (diameter = 168 nm), where the HEUR concentration was varied (0.2, 0.6, 1 wt%) and the latex concentration was held constant to 4 wt% PSL latex (29). Similar to the experiment presented here, no signal from PSL was detected due to very short spin-spin relaxation (T_2) for a large solid particle with minimal internal molecular decay. The signal from HEUR PEO backbone was detected, the hydrophobes were not detected due to either short T_2 or relatively low abundance. The adsorption of HEUR to PSL was indicated by extraction of two diffusion coefficients, the faster one was assigned to the free HEUR and the slower to the adsorbed polymer. At 1 wt% HEUR and 4 wt% PSL the unbound HEUR showed a faster diffusion relative to HEUR in the absence of PSL as the unbound HEUR is nearly half the original concentration (0.53 wt%), where the bound HEUR diffused at the same speed as the calculated latex diffusion. Uemura *et al.* results are different from the results presented here in terms of polymer populations observed in presence of latex, here only one population is identified whereas in the HEUR-51-16/PSL system two populations were detected (30). The presence of two populations may be explained by the presence of stronger adsorption of HEUR-51-16 to PSL.

Beshah *et al.* conducted a PFG-NMR experiment to filter the signals of low molecular weight species. In this study, HEUR-90-10 was used which possess a hexamethylene diisocyanate (HDI) linkers, the HEUR concentration was 1 wt% mixed with 30 wt% butylacrylate-methacrylic acid latex (BA-MMAL, 130 nm) (5). Beshah *et al.* detected signals from the HEUR hydrophobic end-group where the absence of signal coming from

the HEUR hydrophobes reflects adsorption of end-group to BA-MMAL. Here, neither the signal from the hydrophobes nor from the urethane linker was observed.

3.4.1.4.   SANS from HEUR in the presence and absence of PS-BAL

To gain a better understanding of the HEUR conformation in the presence of latex, a partially deuterated PS-BAL was synthesised and the particles scattering length density (SLD) were matched with the solvent (Figure 3.3). Hence, the only scattering observed is from the polymer, which allows direct comparison with the polymer-only case.

The scattering experiments were conducted only on the d-PS-h-BAL due to the high cost of deuterated monomers and that it has been shown that even weaker adsorption is observed in presence of the more hydrophilic latices.
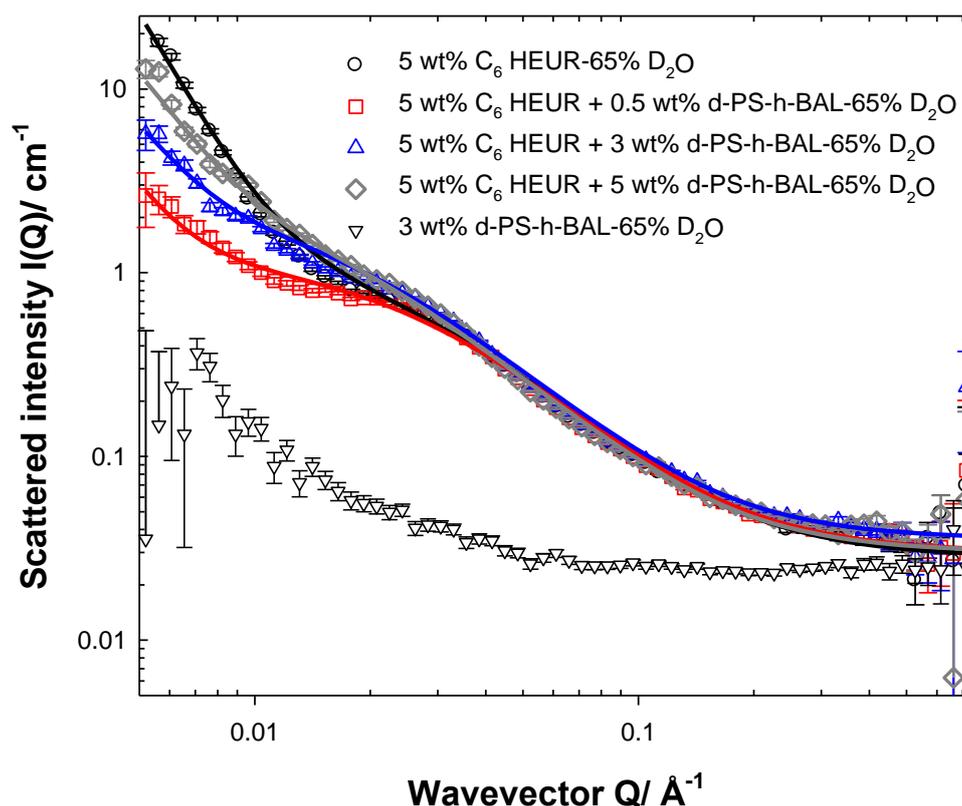
Figure 3.8. Small-angle neutron scattering from a series of polymer/particle blends; 5 wt% polymer in presence of 0.5 (squares), 3 (blue triangle), and 5 (diamonds) wt% d-PS-h-BAL, plus controls; 3 wt% d-PS-BAL on match (white triangle), and 5 wt% C_6-L-$(EO_{100}$-L$)_9$-C_6 (circles) in 65% D_2O/H_2O mixture. The scattering contribution arises from the polymer only in the polymer/latex blend. Samples were prepared in Hydroin buffered solvents, pH 9. The solid lines are sphere and network model fits. The model is presented later in this section. Key fitting parameters value are presented in Table 3.1.

Figure 3.8**Error! Reference source not found.** presents the observed scattering from a series of samples at a H_2O/D_2O ratio that renders the particles "invisible". Evidence of this is the weak/negligible scattering from the 3 wt% particle-only dispersion (triangles). Also shown, is the scattering from the simple 5 wt% polymer (C_6-L-(EO_{100}-L)$_9$-C_6) structure (circles). The remaining data set are mixtures of 5 wt% polymer mixes with 0.5 wt% (squares), 3 wt% (blue triangles), and 5 wt% (diamonds) d-PS-h-BAL.

New points are striking in these data. Firstly, at mid-Q where smaller length scales contributes to the scattering, the HEUR scattering peak (this feature might be more aptly described as a shoulder but the term "peak" will be used to highlight the comparison with surfactant scattering in Chapter 4 (Figures 4.7 and 4.8)) is invariant as a function of latex concentration. Secondly, at higher-Q there is a significant decrease in the scattered intensity in the 0.5 wt% d-PS-h-BAL sample, but which returns to a value close to the original with increasing latex concentration, *i.e.* at higher latex concentration (3 and 5 wt% latex) the low-Q scattered intensity increases to be very close to the HEUR on its own.

The scattering peak present in HEUR scattering curve Q = 0.02 Å^{-1} represents the presence of an order in the sample coming from the hydrophobic end-group. The absence of changes in the intensity of HEUR scattering peak as a function of latex particles at mid-Q indicates that only a few hydrophobic end-groups adsorb to the PS-BAL surface, which do not disrupt the polymer hydrophobic aggregates arrangement in solution. The change in scattered intensity at low-Q reflect changes in the larger length scale of the polymer (the bridging HEUR molecules).

The decrease in the scattered intensity at low-Q suggests the formation of bigger structures that can be observed at lower Q ranges than that studied here. At higher concentration of particles, the increase of the intensity at low-Q may be due to particle aggregating and microscopic phase separation; however, this can be excluded as R_{2sp} of the particles as a function of its concentration in the presence and absence of 5 wt% HEUR is barely changing (Figure 3.9).
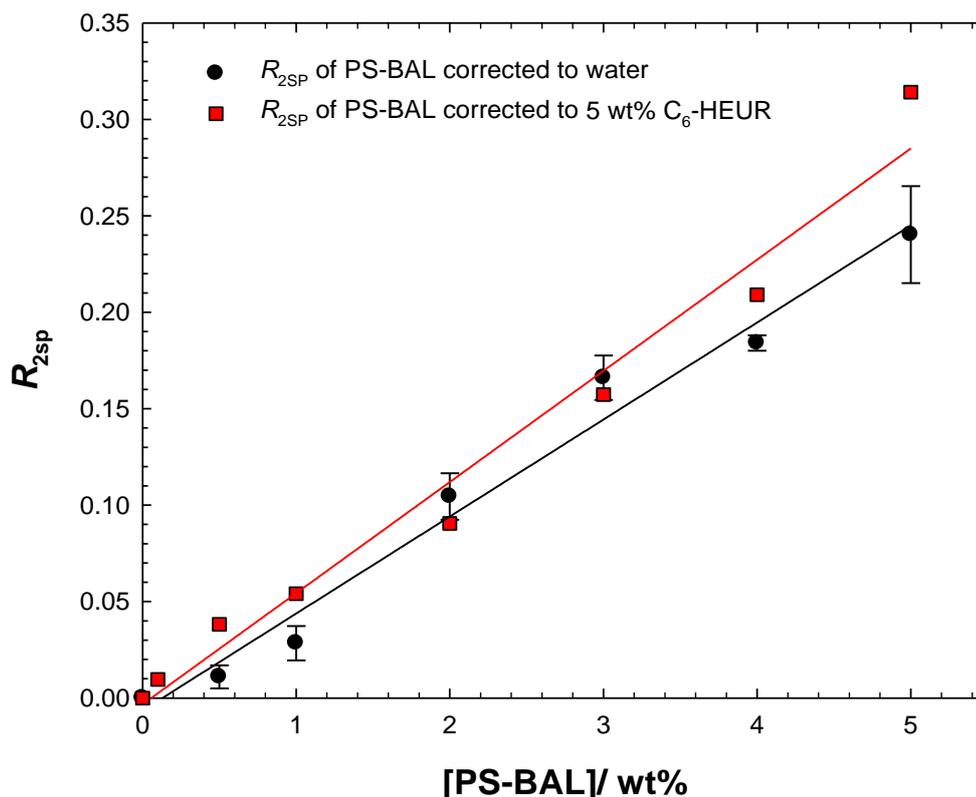
Figure 3.9. R_{2sp} **of PS-BAL as a function of its concentration in the absence (black circles) and presence of 5 wt% C$_6$-L-(EO$_{100}$-L)$_9$-C$_6$. Samples prepared in the absence of 5 wt% HEUR were corrected relative to Hydroin buffered water and samples prepared in the presence of 5 wt% HEUR corrected relative to 5 wt% HEUR. Samples were prepared in Hydroin buffer, pH 9. Measurements were carried out at 25 °C. The solid lines are linear fits. The error bars are the standard deviation of three measurements for the same sample and a second set of samples.**

Increasing concentration of latex
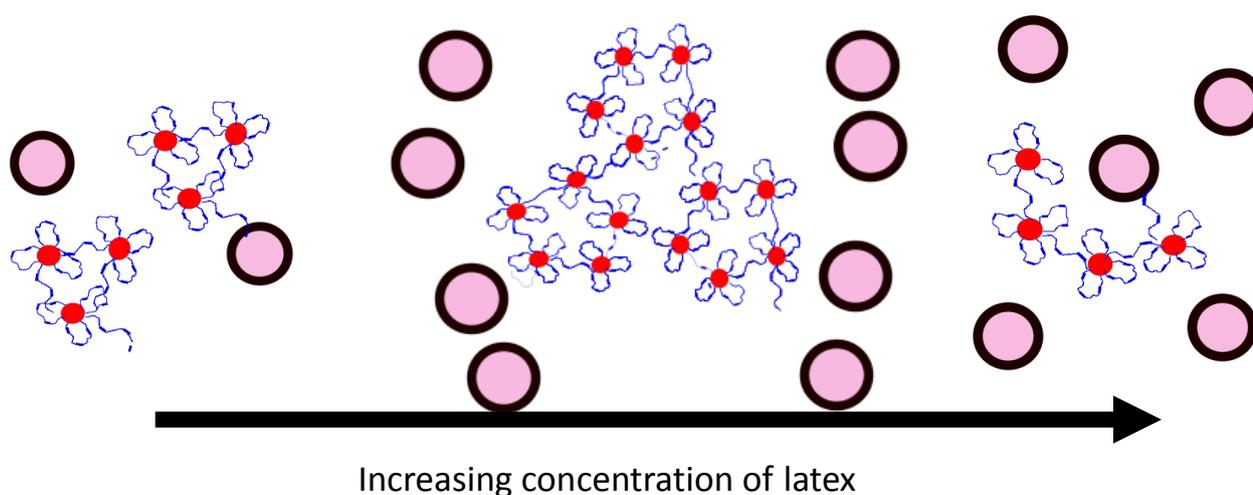
Figure 3.10. Possiblities of HEUR configuration in solution as a function of latex concentration.

Figure 3.10 is an attempt to capture the different probabilities of the polymer arrangement in solution as a function of d-PS-h-BAL concentration. Clusters of hydrophobic aggregates of the polymer joined together in a dense network structure are expected at these HEUR concentrations. There are three scenarios postulated for the HEUR/latex scattering changes. The first scenario, at low concentration of the latex, postulates the loss of the larger length scale or shift of the particle and adsorbed polymer to low-Q range. The second scenario, in the presence of higher latex concentrations, a microscopic phase separation is hypothesised with polymer clusters joining up in a manner similar to polymer in the absence of latex. However, the second scenario can be excluded as the solvent relaxation data indicates the absence of particles aggregation at this polymer concentration (Figure 3.9). In the third scenario, the polymer rearranges in a manner similar to higher polymer concentrations due to volume restriction induced by latex addition. At high latex concentration, scenarios one and three may occur.

The data has been fitted to a two-component complex model. The first component of the fit is a sphere model to determine the size of the latex particles and/or polymer hydrophobic aggregates ®; however, the latex size is too big to be detected in the experimental window. The structure factor of the sphere is represented by the charge density (e) present in SDS micelle or the HEUR/SDS mixed micelle and inverse the Debye screening length (K^{-1}). The network model considers polymer two correlation length scales; a Lorentzian length (ξ), which is hypothesised to be fluctuation in the polymer network structure, a Debye-Bueche length (A) which is postulated to be length scale coming from large network of the polymer and the intensities of the two terms I_1 and I_2, respectively. The volume fraction (φ) of the sample and Debye screening length (K^{-1}) were calculated from the sample concentration and ionic strength, respectively. The values of the size of the polymer aggregates (R), and two correlation lengths; (ξ) and (A) of the polymer were extracted from the fit. The sensitivity of the fit to the parameters changes are presented in Appendix A (Figures A.5-A.8). The fitting key parameters of the sphere and network model are presented in Table 3.1.

The sphere model captures the changes in the hydrophobic aggregates size whilst the network model describes the changes of polymer shorter and longer length scales. From the fitting parameters, the sphere radius, intensity of the Lorentzian term, and the Lorentzian term have not changed as a function of latex concentration. The Debye-

Bueche intensity and term 'A' decreases as a function of latex concentration. This may be explained by changes in the polymer network in the presence of latex.

Fit parameters/ Units	5 % HEUR	5 % HEUR + 0.5 % latex	5 % HEUR + 3 % latex	5 % HEUR + 5 % latex
Intensity of radius term	7.2×10^{-7}	7.2×10^{-7}	7.2×10^{-7}	7.2×10^{-7}
Radius (Å)	65 ± 5	65 ± 5	65 ± 5	65 ± 5
e	n.d.	n.d.	n.d.	n.d.
K^{-1} (Å)	0.3	0.3	0.3	0.3
φ	0.05	0.055	0.08	0.1
l_1	0.44	0.44	0.44	0.44
ξ (Å)	25 ± 1	25 ± 1	25 ± 1	25 ± 1
l_2	325	325	325	305
A (Å)	650 ± 10	600 ± 10	450 ± 10	80 ± 10

Table 3.1. SANS key parameters from the sphere and network model for the polymer and polymer/latex mixtures.
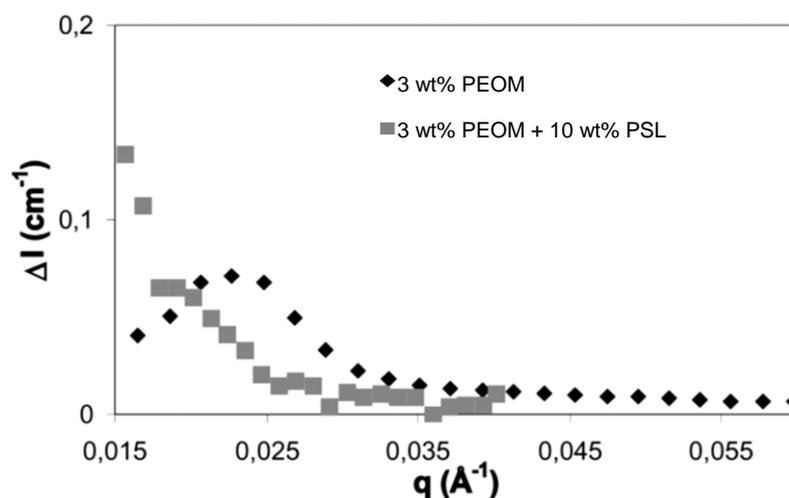
Figure 3.11: SANS from 3 wt% PEOM and 3 wt% PEOM + 10 wt% PSL1 mixture in D_2O/H_2O mixture, where the latex SLD was matched to the solvent, graph was obtained from Beaudoin *et al.* (15).
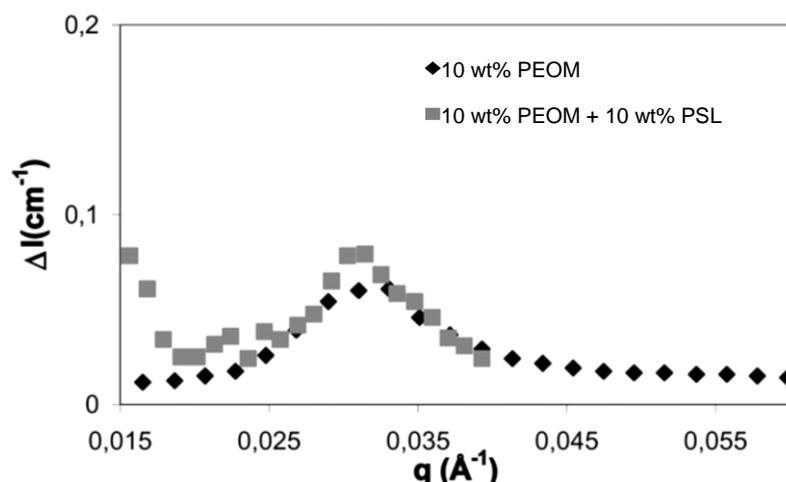
Figure 3.12: SANS from 10 wt% PEOM and 10 wt% PEOM + 10 wt% PSL1 mixture in D_2O/H_2O mixture, where the latex SLD was matched to the solvent, graph was obtained from Beaudoin *et al.* (15).

Beaudoin *et al.* conducted a series of contrast variation experiments for a 20,000 g mol^{-1} PEOM-20-16 and PSL with radius 90 ± 5 nm mixtures (15). In the first contrast, the SLD of the latex particles was matched to the solvent; so that the scattering contribution is from the PEOM only in PEOM/latex mixture. The PEOM only scattering shows a scattering peak at mid-Q which upon mixing with 10 wt% PSL, at $C_{polymer}$ = 3 wt%, is replaced by a shoulder and shifted to lower Q, indicative of polymer adsorption to the latex particles (Figure 3.11). However, at higher polymer concentration (10 wt%) with 10 wt% PS-BAL the scattering peak position and intensity of the polymer in the absence and presence of particles is unchanged; as the adsorbed fraction is negligible relative to total polymer concentration (Figure 3.12). These results agree with C_6-L-(EO_{100}-L)$_9$-C_6/PS-BAL the difference between the two studies would be the polymer architecture and the Q range of the experiment. Beaudoin *et al.* Q range is from 0.015-0.055 Å^{-1}, however, here the changes in scattered intensity are observed round 0.01Å^{-1}. In addition, Beaudoin *et al.* scattering data were merely presented and not analysed, however in this chapter attempts to fit and analyse the data are presented.

In the second contrast variation experiment, Beaudoin *et al.* matched the SLD of the polymer to the solvent where the PSL concentration was held constant at 10 wt% and polymer concentration was varied from 0-20 wt%, the scattering contribution is only from the latex (15). The particles form factor scattering peak was used to calculate the distance between the centres of the scattering species. It was postulated that the particles are aggregating based on the d-spacing calculations. A decrease in the scattered intensity at

low-Q was observed as a function of polymer concentration which has not been considered in the discussion of the results. It was recommended in the paper the use of d-latex for better contrast and accuracy of the measurements, which has been considered in the experimental design here.

Chatterjee *et al.* conducted a rheo-SANS experiment for a C_{10-12} HEUR and a 46 butylacrylate/52 ethylmethacrylate/1.0 ureido monomer /1.0 methacrylic acid (%mass) latex, 120 nm, at concentrations 1 %(w/w) and $\varphi = 0.28$, respectively; where the scattered intensity *vs.* wavevector was recorded at different shear rates (14). An increase in the scattered intensity at low-Q as a function of shear was observed, which was correlated to the breakage of larger aggregates that falls out of the instrument scale upon shearing the samples. The scattering data were fitted to a spherical core-shell form factor with polydisperse core-radius and hard sphere structure factor for *inter*-particle repulsion. The fit captured the peaks at mid-Q, however, the changes at low-Q were not captured. The inability of the model to capture the low-Q features is due to the presence of polymer network as shown in Figure 3.1. Here, the experimental design is different where no shear is applied to the sample, in addition, a different trend of the scattered intensity change is observed at low-Q as a function of latex concentration. The model used to analyse the SANS data in this chapter captured all the scattering curves features as the polymer network is described by two length scales in addition to the sphere term.

3.4.1.5.   Rheology of HEUR in the absence and presence of PS-BAL
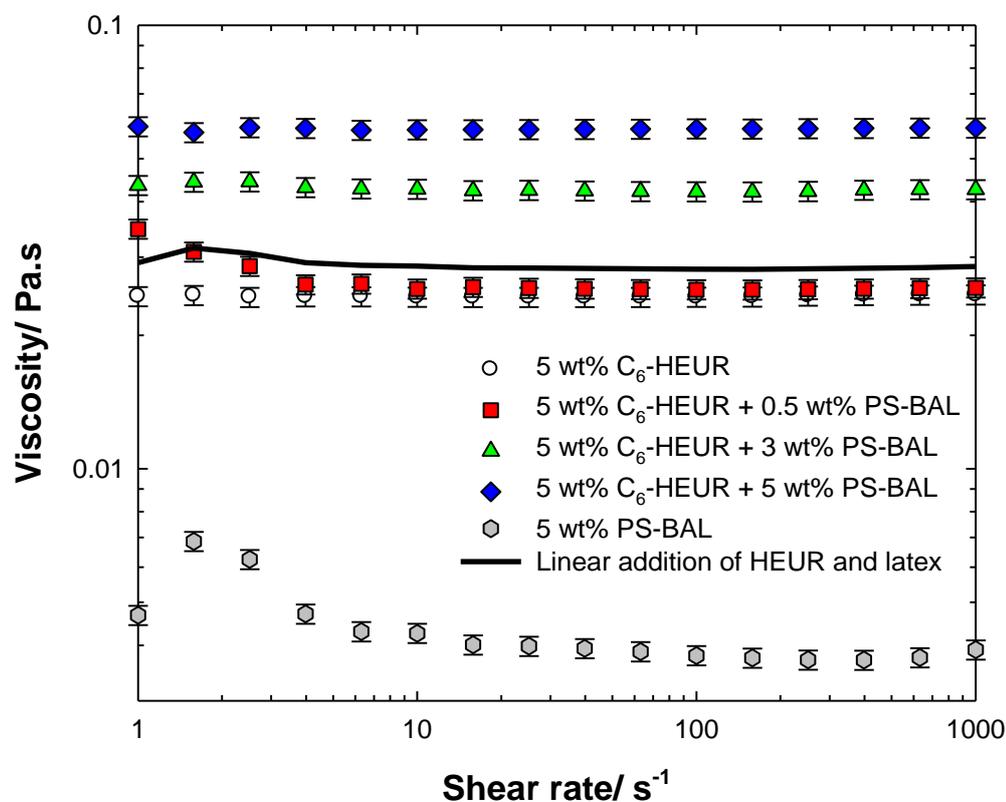
Figure 3.13. Shear profile of 5 wt% PS-BAL (grey hexagon), 5 wt% HEUR in the absence (white circles) and presence of 0.5 (red squares), 3 (green triangles), 5 (blue diamonds) wt% PS-BAL; linear addition of 5 wt% HEUR and 5 wt% PS-BAL (black line). Samples were prepared in Hydroin buffer, pH 9. Measurements were carried out at 25 °C. The error bars are the standard deviation of two measurements for two sets of sample.

In these experiments, the shear profile of the polymer at 5 wt% is measured as a function of latex concentration, where a shear-independent viscosity is observed. The shear profiles of the C_6-L-$(EO_{100}$-L$)_9$-C_6/PS-BAL mixtures are Newtonian (Figure 3.13).
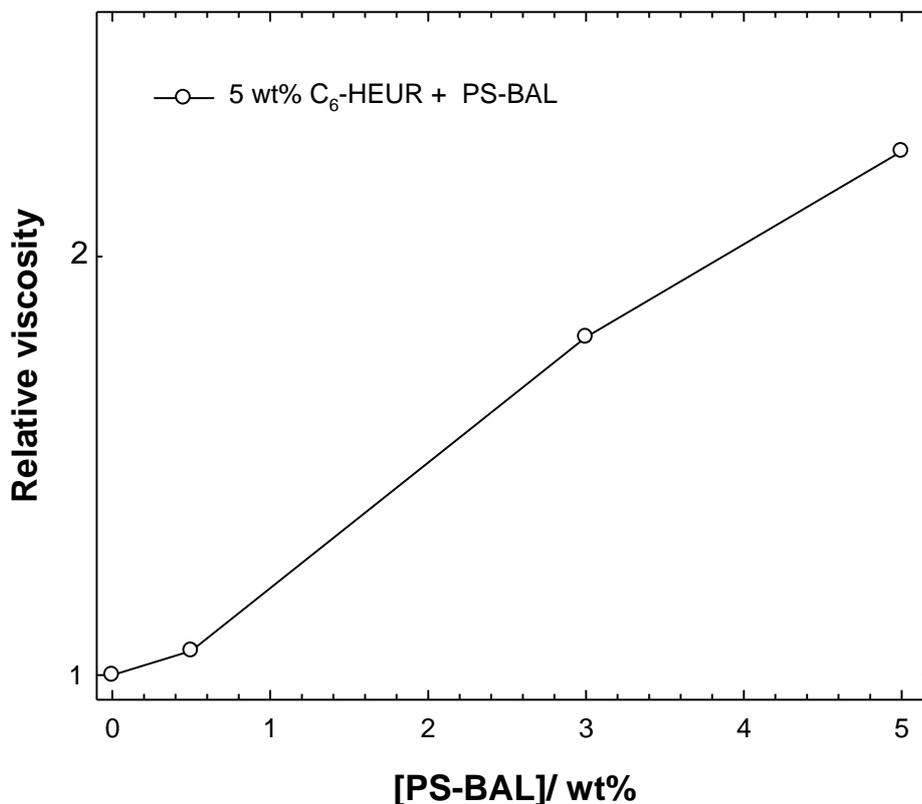
Figure 3.14. Relative viscosity at shear rate 4 s^{-1} of C$_6$-L-(EO$_{100}$-L)$_9$-C$_6$/PS-BAL to HEUR. Samples were prepared in Hydroin buffered water, pH 9. Measurements were carried out at 25 °C. The solid line is a guide for the eye.

The relative viscosity (η_r) of the mixture to the polymer ($\eta_r = \frac{\eta_{mixture}}{\eta_{polymer}}$) at shear rate 4 s^{-1} was then plotted as a function of latex concentration, to study the effect of varying latex concentration on the polymer viscosity (Figure 3.14). The viscosity of the mixture increases as a function of latex concentration. The increase in HEUR/PS-BAL viscosity is not additive (*i.e.* $\eta_{mixture} \neq \eta_{polymer} + \eta_{dispersion}$), reflective of synergistic increase of viscosity due C$_6$-L-(EO$_{100}$-L)$_9$-C$_6$ adsorption.

some published papers presented a shear thinning profile for HEUR and latex mixtures (5,13,14). Santos *et al.* presented a shear thinning profile for a commercial HEUR of molecular weight 22,800 g mol^{-1} with acrylic acid latex of 149 nm at 1 and 25 wt%, respectively. The shear-thinning behaviour was correlated to the desorption of the HEUR from the latex surface at high shear rates (13). Chatterjee *et al.* noted similar behaviour for a mixture of C$_{10-12}$ HEUR of molecular weight 28-32 kg mol^{-1} with 46 butylacrylate/52 ethylmethacrylate/1.0 ureido monomer /1.0 methacrylic acid (%mass) latex, 120 nm, at

121

concentrations 1% (w/w) and φ = 0.28, respectively (14). Shearing the polymer/latex mixture expelled the solvent from the polymer adsorbed layer, which decreased the adsorbed polymer layer thickness and consequently a shear thinning behaviour was observed. Beshah *et al.* correlated the shear thinning behaviour to the conversion of the HEUR bridging molecules between the latex particles to loops for HEUR-90-10/BA-MMAL mixtures (5). However, the comparison between the data presented here and the published work might not be informative as in the former the polymer behaviour is dominating the system, considering the concentrations used.

3.4.2. Interaction of HEUR/AA-PS-BAL mixtures

3.4.2.1. Surface area determination of AA-PS-BAL
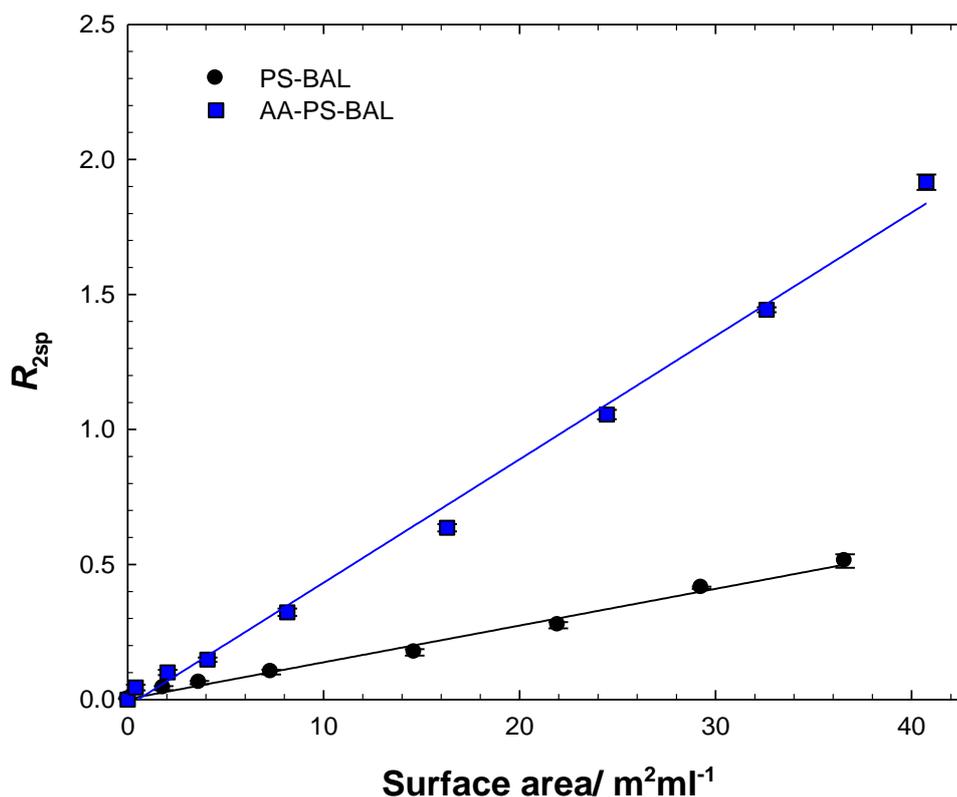
Figure 3.15. Comparison of R_{2sp} of AA-PS-BAL (blue squares) and PS-BAL (black circles) as a function of its surface area. Samples were prepared in Hydroin buffered water, pH 9. Measurements were carried out at 25 °C. R_{2sp} is corrected relative to Hydroin buffered water. The solid lines are linear fits. The error bars are the standard deviation of three measurements for the same sample and a second set of samples.

The R_{2sp} of AA-PS-BAL shows a linear increase as a function of latex concentration. The AA-PS-BAL shows a higher R_{2sp} as a function of surface area when compared to PS-BAL (Figure 3.15). This may be correlated to the hydrophilicity of the particles where the binding of water molecules to the AA-PS-BAL surface is more favourable, hence the enhancement of relaxation significantly increases as the surface area increase. The R_{2sp} is plotted as a function of surface area so the difference in the particles size is removed. The surface area of the AA-PS-BAL is larger than that of PS-BAL owing to the smaller size of the particles.
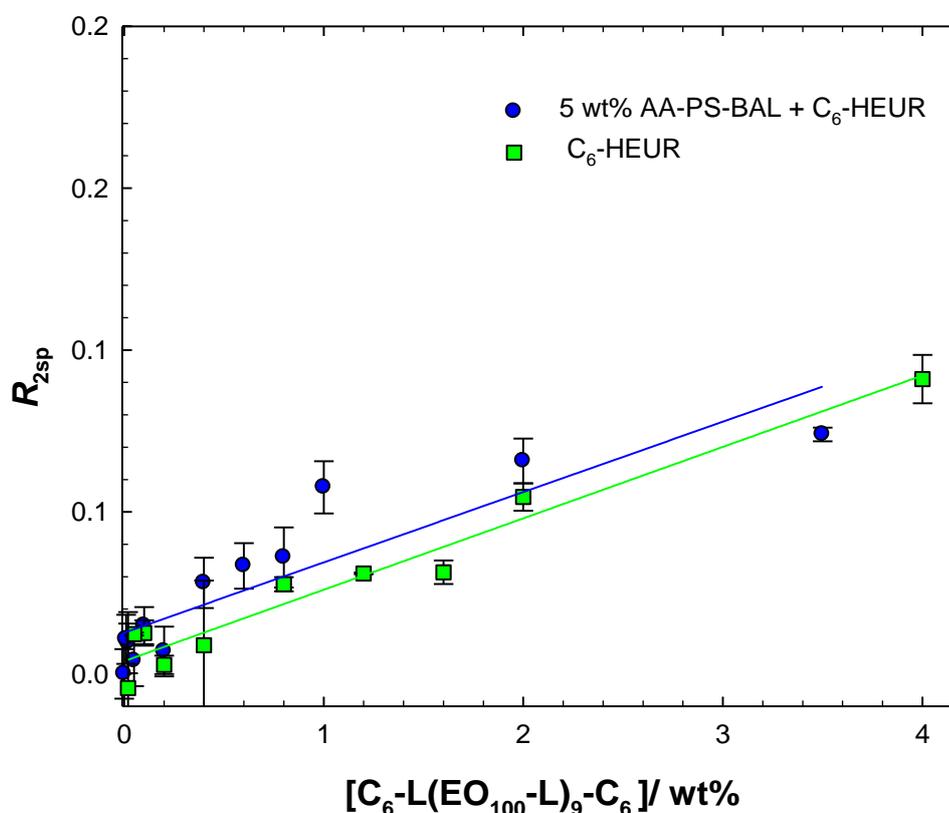
Figure 3.16. R_{2sp} **of** C_6-L-$(EO_{100}$-L$)_9$-C_6 **(squares) 5 wt% AA-PS-BAL (circles) as a function of HEUR concentration.** R_{2sp} **of HEUR/AA-PS-BAL mixtures is corrected relative to bare particle, and HEUR as a function of its concentration relative to water. Samples were prepared in Hydroin buffered water, pH 9. Measurements were carried out at 25 °C. The solid lines are linear fits. The error bars are the standard deviation of three measurements for the same sample and a second set of samples.**

The more hydrophilic particles AA-PS-BAL show no phase separation as a function of C_6-L-$(EO_{100}$-L$)_9$-C_6, unlike the PS-BAL particles that show phase separation at low HEUR

concentration which was shown to be correlated to the adsorption of HEUR on the latex surface (Figure 3.16).

The R_{2sp} of the HEUR/AA-PS-BAL mixtures at low polymer concentration equals zero, though at higher concentrations there is a subtle increase in the R_{2sp}, the HEUR/AA-PS-BAL curve is overlapping with the simple HEUR. The absence of phase separation and the overlapping of the polymer/latex curve with the simple polymer curve suggest the absence of polymer adsorption to the latex particles. These results are in agreement with Quadrat *et al.* where decreasing the latex hydrophobicity was shown to decrease the HEUR adsorption to the surface (6).

3.4.2.2. Size distribution of the AA-PS-BAL in the presence of polymer
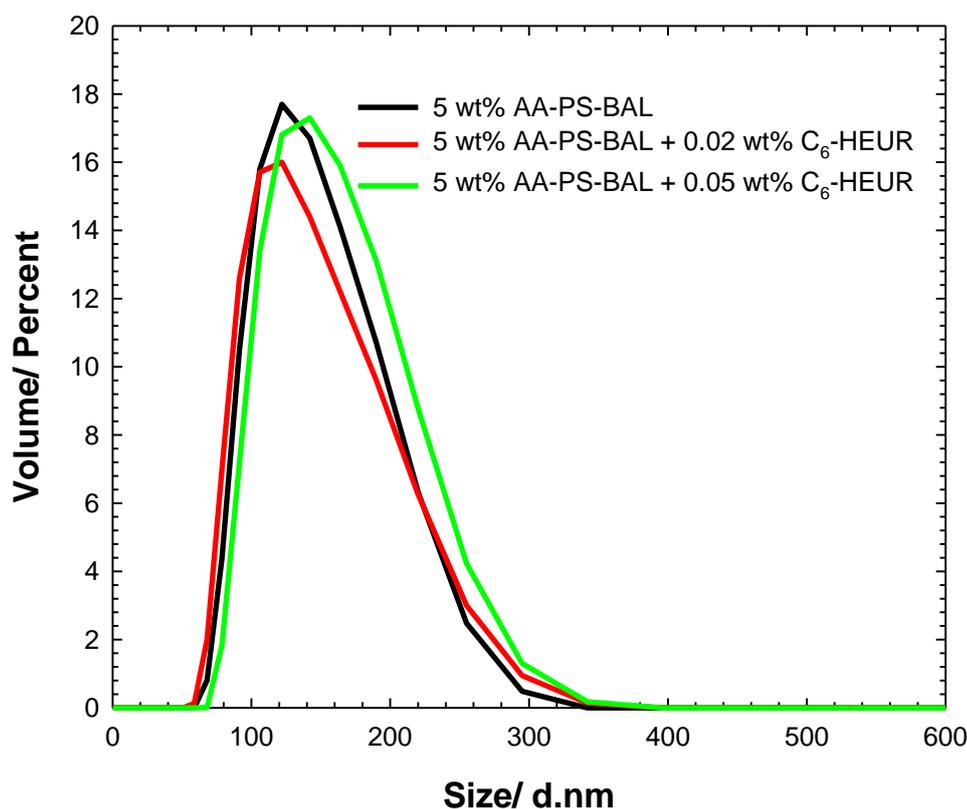
Figure 3.17. Size of 5 wt% acrylic acid/polystyrene latex in the absence (red line) and presence of 0.02 (black line), and 0.05 (green line) wt% C$_6$-L-(EO$_{100}$-L)$_9$-C$_6$.

The absence of phase separation at low polymer concentrations in the presence of AA-PS-BAL allowed the use of DLS to study the mixtures. C$_6$-L-(EO$_{100}$-L)$_9$-C$_6$/AA-PS-BAL mixtures were studied at a low HEUR concentration where the increase of the viscosity

of the mixtures is expected to be relatively negligible, to avoid the false size increase due to viscosity changes. The particles distribution is very sensitive to adsorption, where if the polymer adsorbs to the latex, increase in distribution is expected. The DLS showed no change in particle distribution upon mixing C_6-L-$(EO_{100}$-L$)_9$-C_6 with the AA-PS-BAL (Figure 3.17).

3.4.2.3. *Solution polymer aggregates in the presence of AA-PS-BAL*

Similar to Section 3.4.1.3, diffusion NMR experiments have been conducted with the more hydrophilic particles to compare the results of the two latices. The AA-PS-BAL particles did not show a signal in NMR spectrum so the diffusion of the particles was calculated from Stokes-Einstein equation from the particle size measured by DLS.
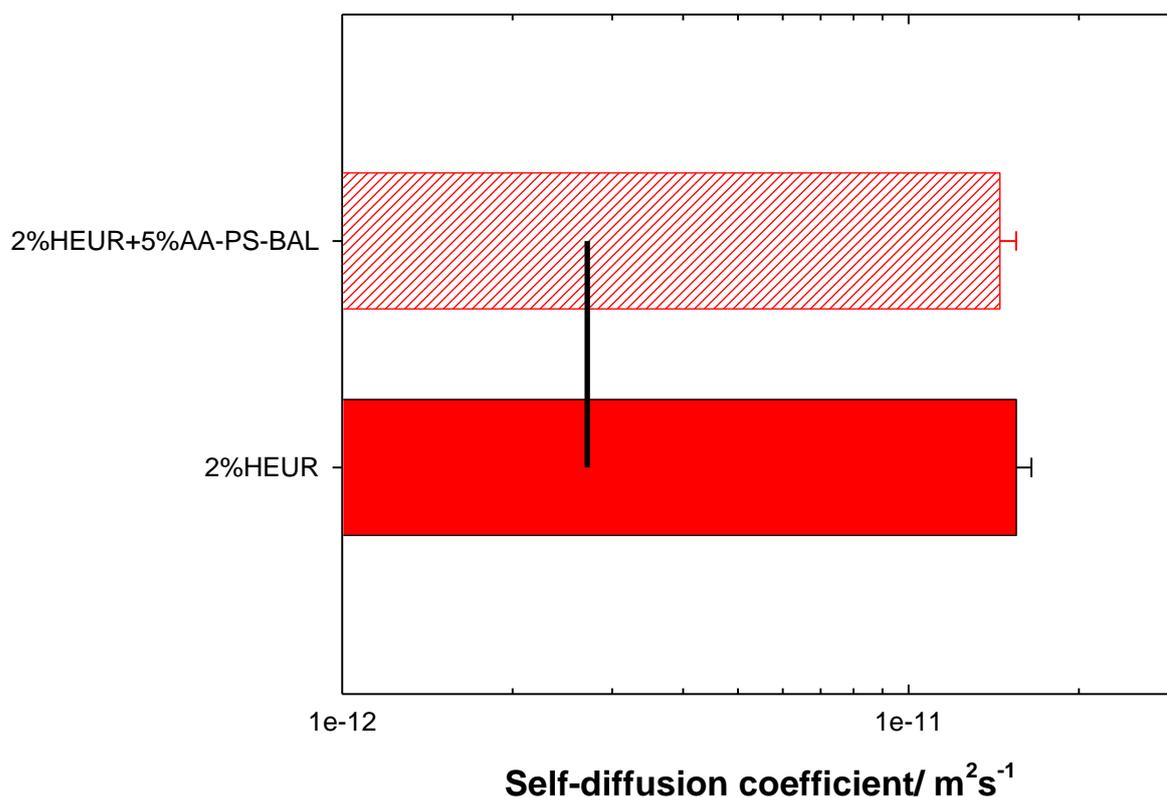
Figure 3.18: Self-diffusion coefficient of C_6-L-$(EO_{100}$-L$)_9$-C_6 in the absence and presence of 5 wt% AA-PS-BAL. Samples were prepared in Hydroin buffered D_2O pH 9. Measurements were carried out at 25 °C. The solid black line is the calculated diffusion of AA-PS-BAL. The error bars are the standard deviation of three measurements for the same sample and a second set of samples.

Chapter 3. HEUR/latex interaction

The HEUR diffusion in the HEUR/AA-PS-BAL mixtures is barely changing in the presence and absence of the latex particles (Figure 3.18).

3.5. Conclusion

The interaction of HEUR and latex is complex and dependent on many factors (*e.g.* latex surface chemistry, size, polymer architecture, and concentration). In this chapter, a HEUR and latices used in commercial formulations have been studied. The use of more hydrophilic AA-PS-BAL shows no evidence of HEUR adsorption to the latex surface. This is evidenced by the absence of enhancement of T_2 (spin-spin relaxation) of HEUR/AA-PS-BAL mixtures, no change in the distribution of the particles in the presence of the polymer and diffusion of the HEUR is not changed in presence of latex. On the contrary, there is a weak interaction between the HEUR and PS-BAL evidenced by the changes in surface area of the particles attributed to bridging flocculation at low polymer concentrations. The increase of the HEUR solution viscosity as a function of latex concentration and a decrease of polymer diffusion upon addition of latex supports the presence of interaction. In addition, some changes in the polymer larger scale length (bridging polymer chains) has been observed in the SANS data. The presence of weak adsorption of C_6-L-(EO$_{100}$-L)$_9$-C$_6$ HEUR may be due to aggregation in solution or a diffusive conformation at the particle surface because of the short hydrophobic end-group of the polymer. In the C_6-L-(EO$_{100}$-L)$_9$-C$_6$ /AA-PS-BAL mixtures the old model presented by Pham *et al.* (12) better describes the system. The model suggested in literature considered the concentration of HEUR and the presence of surfactants in the systems to change HEUR configuration from the new model proposed by Beshah *et al.* (5) to the old model (12); however, the affinity of the HEUR to the latex is an important factor that should be considered *i.e.* in the presence of weakly-interacting HEUR/latex or non-interacting HEUR/latex system would be better described by the old model where there is a greater association of the polymer hydrophobes in solution.

3.6. References

1. Holmberg K. Handbook of Surface and Colloid Chemistry. Fourth Edition. Florida, USA:*CPR Press*; **2015**.

2. Aulton ME. Pharmaceutics–The Science of Dosage from Design. Second Edition. New York, USA:*Churchill Livingstone*; **2002**.

3. Richey B, Kirk AB, Eisenhart EK, Fitzwater S, Hook J. Interactions of associative thickeners with paint components as studied by the use of a fluorescently labeled model thickener. *J Coatings Thechnol.* **1991**;*63*(798):31–40.

4. Glass JE. Adsorption of hydrophobically-modified, ethoxylated urethane thickeners on latex and titanium dioxide disperse phases. *Adv Colloid Interface Sci.* **1999**;*79*(2):123–148.

5. Beshah K, Izmitli A, Van Dyk AK, Rabasco JJ, Bohling J, Fitzwater SJ. Diffusion-weighted PFGNMR study of molecular level interactions of loops and direct bridges of HEURs on latex particles. *Macromolecules.* **2013**;*46*(6):2216–2227.

6. Quadrat O, Horsky J, Snuparek J. Thickening effect of commercial associative thickeners on the latices of copolymers of acrylic monomers carrying hydrophilic reactive groups. *J Dispersion Sci Technol.* **2003**;*24*(2)179-184.

7. Ou-yang HD, Gao Z. A pancake-to-brush transition in polymer adsorption. *J Phys II.* **1991**;*1*(11):1375–1385.

8. Hulden M. Hydrophobically modified urethane-ethoxylate (HEUR) associative thickeners 2. Interaction with latex. C*olloids Surfaces A Physicochem Eng Asp.* **1994**;*88*(2–3):207–221.

9. Reuvers AJ. Control of rheology of water-borne paints using associative thickeners. *Prog Org Coatings.* **1999**;*35*:171–181.

10. Jenkins RD, Durali M, Silebi CA, El-Aasser MS. Adsorption of model associative polymers on monodisperse polystyrene latex. *J Colloid Interface Sci.* **1992**;*154*(2):502–521.

11. Kostansek E. Using Dispersion/fiocculation phase diagrams to visualize interactions of associative polymers, latexes, and surfactants. *J Coat Technol.* **2003**;*75*(940)1-8.

12. Pham QT, Russel WB, Lau W. The effects of adsorbed layers and solution polymer on the viscosity of dispersions containing associative polymers. *J Rheol*. **1998**;*42*(1)159-176.

13. Santos FA, Bell TJ, Stevenson AR, Christensen DJ, Pfau MR, Nghiem BQ, Kasprzak CR, Smith TB, Fernando RH. Syneresis and rheology mechanisms of a latex-HEUR associative thickener system. *J Coatings Technol Res*. **2017**;*14*(1):57-67.

14. Chatterjee T, Nakatani AI, Dyk AKV. Shear-dependent interactions in hydrophobically modified ethylene oxide urethane (HEUR) based rheology modifier−latex suspensions: Part 1. Molecular microstructure. *Macromolecules*. **2014**;*47*(3):1155–1174.

15. Beaudoin E, Lapp A, Hiorns RC, Grassl B, François J. Neutron scattering of hydrophobically modified poly(ethylene oxide) in aqueous solutions in the presence of latex particles. *Polymer*. **2002**;*43*(9):2677–2689.

16. Tadros TF, Vincent B. Influence of temperature and electrolytes on the adsorption of poly(ethylene oxide)-poly(propylene oxide) block copolymer on polystyrene latex and on the stability of the polymer-coated particles. *J Phys Chem*. **1980**;*84*(12):1575–1580.

17. Khalak KY, Gilbert TW. Determination of polyethylene glycols by thermometric titration. *Analyst*. **1978**;*103*:623-627.

18. Brown W, Zhao J. Adsorption of sodium dodecyl sulfate on polystyrene latex particles using dynamic light scattering and zeta potential measurements. *Macromolecules*. **1993**;*26*(11):2711–2715.

19. Abrahmsen-Alami S, Stilbs P. NMR self-diffusion of associative polymers in aqueous solution: the influence of the hydrocarbon end-chain length on the polymer transport dynamics in single-and two-component mixtures. *J Colloid Interface Sci*. **1997**;*189*(1):137–143.

20. Claridge TDW. High-Resolution NMR Techniques in Organic Chemistry. Second edition. Oxford, UK: *Elsvier*, **2009**.

21. Heenan RK, King SM, Turner DS, Treadgold JR. SANS2d at the ISIS Second Target Station. *17th Meet Int Collab Adv Neutron Sources*. **2005**;1–6. Available

from: http://www.isis.stfc.ac.uk/instruments/sans2d/publications/sans2d-at-isis10323.pdf, (accessed January 2016).

22. Ballauff M. SAXS and SANS studies of polymer colloids. *Curr Opin Colloid Interface Sci.* **2001**;*6*(2):132–139.

23. Zackrisson M, Stradner A, Schurtenberger P, Bergenholtz J. Small-angle neutron scattering on a core-shell colloidal system: A contrast-variation study. *Langmuir.* **2005**;*21*(23):10835–10845.

24. SasView. Available from: http://www.sasview.org/, (accessed February 2018).

25. Cosgrove T, Mears SJ, Obey T, Thompson L, Wesley RD. Polymer, particle, surfactant interactions. C*olloids Surfaces A Physicochem Eng Asp.* **1999**;*149*(1-3):329–338.

26. Cooper CL, Cosgrove T, Duijneveldt JS van, Murray M, Prescott SW. The use of solvent relaxation NMR to study colloidal suspensions. *Soft Matter.* **2013**;*9*(30):7211–7228.

27. Van der Beek GP, Stuart MAC, Cosgrove T. Polymer adsorption and desorption studies via ^{1}H NMR relaxation of the solvent. *Langmuir.* **1991**;*7*;327-334.

28. Cosgrove T, Grifiths PC, Lloyd PM. Polymer Adsorption . The Effect of the Relative Sizes of Polymer and Particle. **1995**;*11*(5):1457–63.

29. Uemura Y, Macdonald PM. Associating polymer binding to polystyrene latex. *Macromolecules.* **1996**;*29*(1):63–69. .

30. Zhang K, Xu B, Winnik MA, Macdonald PM. Surfactant Interactions with HEUR Associating Polymers. *J Phys Chem.* **1996**;*100*(23):9834–9841.

---

4. HEUR/SDS/latex

4.1. Abstract

A model formulation made of C_6-L-$(EO_{100}$-L$)_9$-C_6/SDS/polystyrene-butylacrylate (PS-BAL) was studied by solvent relaxation nuclear magnetic resonance, pulsed-gradient spin-echo nuclear magnetic resonance (PGSE-NMR), rheology and small-angle neutron scattering (SANS) to elucidate the key interaction(s) in the system. The results suggest a stronger interaction between the SDS and polymer relative to polymer and latex in the three-component formulation. The results revealed a weakened adsorption of the HEUR on the latex particles in the presence of the SDS, with the observed behaviour highly reminiscent of the polymer/surfactant system. The weakened adsorption of the polymer to the latex particles was evidenced by less significant changes of the polymer/SDS mixture viscosity, self-diffusion coefficient and scattering curves in the presence and absence of PS-BAL relative to the changes observed for HEUR in the presence of PS-BAL. This study should allow a more considered analysis of the rheological profile in terms of the presence and concentration of the surfactant (present in) the formulation.

4.2. Introduction

4.2.1. SDS/latex interaction

Surfactants are used as dispersing agents in complex multi-component formulations *e.g.* cosmetics, paints, *etc.* The interaction of the surfactants with other components in the formulation may affect the end-product performance, which highlights the importance of understanding the various interactions within the formulation. Various studies investigated two-component mixtures of sodium dodecylsulphate (SDS) and latex particles. The adsorption of SDS to the polystyrene latex (PSL) has been studied by dynamic light scattering (DLS), and zeta-potential by Brown *et al.* (1). At low SDS concentration, an increase in the latex hydrodynamic diameter (R_H) and zeta-potential is observed due to non-cooperative binding of SDS monomers. As the SDS concentration increases, cooperative binding takes place with a strong increase in R_H which may be correlated to more than a single layer involved in the adsorption. After surface saturation, free SDS micelles are formed in the bulk, increasing the counter-ion (Na^+) concentration. The counter-ion reduces the surface potential and a more compact structure of SDS/PSL is formed. Nodehi *et al.* used conductometric titration techniques to study the SDS/PSL system where a breakpoint is observed upon surface saturation (2). Bloze *et al.* suggested a core-shell structure for the SDS adsorbed on PSL (61 nm) surface, studied by small-angle X-ray scattering (SAXS) (3). The saturation concentration was calculated to be 65 mg SDS/g PS. Above this concentration scattering from free micelles was observed.

4.2.2. Polymer/Surfactant/latex interactions

In a three-component model system comprising polymer/latex/surfactant, various interactions can occur in the system. The affinity of the surfactant for the polymer or latex particles is likely to determine whether the polymer is desorbed or not from the latex surface and the mechanism of desorption. Polymer desorption from latex surface in the presence of surfactant can be due to direct competition for adsorption site (4) or due to polymer/surfactant solution complexation (5).

Cosgrove *et al.* studied the adsorption of an unmodified poly(ethylene oxide) (PEO) (molecular weight, 200,000 g mol^{-1}) to PSL (180 nm) in the presence of sodium dodecylsulphate (SDS) by photon correlation spectroscopy (PCS), small-angle neutron

scattering (SANS), and diffusion nuclear magnetic resonance (diff-NMR) (6). From the adsorption isotherm experiments, the affinity of PEO to (adsorb on) PSL surface is high (0.82 ± 0.1 mg m^{-2}). The addition of a range of SDS concentrations (200-14000 ppm) increases the thickness of the PEO adsorbed layer measured by the SANS and PCS. The size of the adsorbed layer increases to a maximum and then the curve plateaus. The self-diffusion coefficient data shows the same, but inverted features as the PCS data where the increase of the thickness of the PEO adsorbed layer is reflected by a decrease in the self-diffusion coefficient of the polymer. The SDS interacts with the PEO, and the PEO/SDS complex can adsorb on the PSL surface to increase the thickness of the adsorbed layer. The PEO desorbs from the surface of the latex at higher SDS concentration due to solution complexation rather than competition of PEO and SDS for the surface site. The SANS data reflect the reduction of PEO adsorption on PSL surface from 0.91(in the absence of SDS) to 0.21 mg m^{-2} (in the presence of SDS).

Pisarcik *et al.* measured the viscosity of 1 wt% hydrophobically modified hydroxyethyl cellulose (HM-HEC) with a range of SDS concentrations at a fixed concentration of PSL of different sizes (84, 216 d.nm) (7). The viscosity increases upon the addition of latex at $C_{SDS} <$ CMC. The latex provides linking points in the polymer network, hence the viscosity increase. At $C_{SDS} >$ CMC, the viscosity drops as the HM-HEC is desorbed from the PSL surface as a result of the solubilisation of the polymer hydrophobic segments in the SDS micelles, hence the cross-linking effect of the latex becomes negligible. The diffusion coefficient measured by DLS of PSL in HM-HEC/PSL mixture increases as a function of SDS, indicative of the formation of smaller species due to polymer desorption from the latex surface.

Lauten *et al.* used DLS to study the change of the R_H measured by DLS of 0.01 % hydrophobically modified ethylhydroxyethyl cellulose (HM-EHEC, molecular weight 100,000) and 0.001 wt% PSL (174 d.nm) mixtures in the presence of a range of SDS concentrations (5-50 mmolal) (8,9). The R_H of HM-EHEC/PSL mixture decreases, reflective of HM-EHEC desorption. This has been explained by the binding of SDS to HM-EHEC which increases the hydrophilicity of the complex, hence the complex favours the presence in the bulk than adsorption to the PSL.

Mahli *et al.* studied the effect of 0.25 and 0.6 wt% SDS on the adsorption of HEUR-31-16 (the first number is the molecular weight of the polymer in kg mol^{-1} and the second number is the length of the hydrophobic end-group, the linkers are two isophorone diisocyanate

Chapter 4. HEUR/SDS/latex interaction

(IPDI) molecules at the ends only) on methylmethacrylic acid-methacrylic acid latex (MMA-MAAL, 600 d.nm) (10). The concentration of the desorbed HEUR was determined by ultraviolet spectroscopy (UV) as a function of SDS. The SDS displaces all the adsorbed HEUR on the latex surface at 0.35 wt%. The same experiment was conducted in the presence of the non-ionic surfactant nonylphenol ethoxylate-12 NPE12. The non-ionic surfactant partially desorbs the HEUR from the latex surface, where from 0.25-1.25 wt% NPE12 the concentration of the desorbed HEUR is constant (0.39 wt%). Worthy of note, is that the affinity of SDS to HEUR is higher than non-ionic surfactants as the former interacts with hydrophobes and PEO backbone, whereas the latter interacts with the hydrophobic end-groups only (11–14). Therefore, the SDS is more capable of solubilising the polymer in the bulk, hence polymer desorption from the latex surface occurs.

Glass *et al.* studied the viscosity of HEUR-35-12 (hexamethylene diisocyanate (HDI) linkers are present at the ends of the polymer only) at 2.5 and 0.5 with 25 wt% MAA-MMAL (120 d.nm) (15).The addition of SDS at 0.3 wt% shows a drop in the viscosity of the polymer/latex mixture. This was correlated to the desorption of the HEUR from the latex particle surface due to direct site competition with SDS. The absence of evidence of HEUR/SDS interaction is postulated.

In contrary to the conclusions drawn by Glass *et al.*, Hulden suggested that the thickener does not adsorb to latex in the presence of SDS due to thickener/surfactant interaction (16). A HEUR-19-18 adsorbs to methylacrylate-butyl acrylate latex (MA-BAL, 536 d.nm) in the presence of non-ionic surfactant (nonylphenol ethoxylate-10, NPE-10) but not in the presence of SDS. Since NPE10 can displace the SDS from the MA-BAL surface, the lack of HEUR adsorption can be explained by solution complexation of HEUR and SDS. Chatterjee *et al.* postulated that the SDS does not competitively desorb the HEUR from the latex surface in agreement with Hulden (5). However, the SDS micelles provide additional surface for the HEUR end-hydrophobe adsorption, hence the HEUR hydrophobes desorb from the latex surface.

Ma *et al.* used UV spectroscopy to determine the amount of non-ionic surfactant NPE12 adsorbed to the latex after removal of the particles from the mixture by centrifugation and measuring the unadsorbed surfactant concentration in the supernatant (4). The competitive adsorption of the HEUR and surfactant has been studied by measuring the amount of surfactant liberated in solution as a function of HEUR concentration. A HEUR-24-12 (the linkers are 4,4'-methylene diphenyl diisocyanate (MDI) linkers) could not

desorb the NPE12 from the latex surface; however, a HEUR-24-18 desorbed the surfactant.

The inhomogeneity of HM-HEC/SDS/PSL mixture was reported by Lauten *et al.* at $C_{polymer}$ 0.16 % and C_{SDS} below CMC (8). Pisarcik *et al.* noted the phase separation of HM-EHEC/ PSL mixture at 0.01 and 0.001 wt%, respectively in the presence of 2-4 mmolal SDS (7).

Kostansek studied the phase diagram of HEUR/surfactant/latex system using a model HEUR-50-12, butylacrylate/methylmethacrylic acid (BA-MMAL), and butylacrylate/styrene (BA-PSL) latices with various sizes 140-600 nm (17). All latices contained 1 % methacrylic acid and 0.05-0.1 wt% sodium dodecyl benzene sulphonate. The latex concentration was held constant at 25 wt%, whilst the HEUR and surfactant concentrations are varied. The addition of small SDS concentration reverses the bridging flocculation observed in HEUR/latex mixtures at low HEUR concentrations. At higher HEUR concentration where HEUR/latex mixtures show a good dispersion behaviour, further addition of SDS induces depletion flocculation. The SDS concentration that reverses the bridging flocculation or induces depletion flocculation is dependent on the size, and surface chemistry of the latex. The reversal of bridging flocculation induced by C_{12} HEUR for BA-MMAL with bigger size occurred at lower SDS concentration relative to smaller particles, as well as the depletion flocculation. The BA-PSL (more hydrophobic latex) has a larger bridging flocculation regions and good dispersion region relative to the BA-MAAL(less hydrophilic) latex.

The phase diagram of the three-component system was studied as a function of non-ionic surfactant, Triton X-100 (t-Oct-C_6H_4-$(OCH_2CH_2)_x$OH, x = 9-10). The addition of Triton X-100 reverses the bridging flocculation at higher surfactant concentration relative to SDS, and at high Triton X-100 concentration, the depletion flocculation of the HEUR/latex mixture was not observed (17).

In summary, there is still some debate on the mechanism of HEUR desorption from latex surface between direct site competition presented by Glass *et al.* (15) and formation of a HEUR/surfactant complex in the bulk suggested by Hulden (16). To differentiate between the two cases the HEUR/latex mixtures were studied here in the presence of two SDS concentration 0.1 and 1 wt%, where latex surface area changes and polymer solution behaviour are explored in the mixtures.

Chapter 4. HEUR/SDS/latex interaction

4.3. Materials and methods

4.3.1. Materials

Deuterated PS-h-BAL (160 d.nm, PDI 0.06, synthesised in house, detailed description is presented in Chapter 3, Section 3.3.1), polystyrene-butylacrylate latex (173 d.nm, PDI 0.03, AkzoNobel), acrylic acid stabilised polystyrene-butylacrylate latex (154 d.nm, PDI 0.03, acid level 3, AkzoNobel), sodium dodecylsulphate (SDS) (Aldrich, no impurity observed), deuterated sodium dodecylsulphate (d_{25}-SDS, ISIS deuteration facility), Hydroin buffer pH 9 (Aldrich), deionized water (Purite Select deionizer) and deuterium oxide (purity 99.9 %, Aldrich) were used as received. Acrysol® RM2020E C_6-L-(EO$_{100}$-L)$_9$-C_6 (Dow) was purified to remove any cyclodextrin before use, as described in Appendix D, Section D.1.

4.3.2. Methods

All the HEUR/SDS/PS-BAL samples were prepared in the appropriate solvent according to the experiment and mixed using a hula-mixer for 24 hours before measurements.

4.3.2.1. Nuclear Magnetic Resonance techniques

4.3.2.1.1. Solvent relaxation NMR

SDS/PS-BAL, HEUR/SDS/PS-BAL mixtures were prepared in Hydroin buffered water pH 9, the NMR experiments were carried out at 25 °C on a bench-top Acorn XIGO nanotools spectrometer. A Carr−Purcell−Meiboom−Gill (CPMG) sequence was used with a spacing of 0.5 ms, between the 90° and 180° pulses, and a recycle delay of at least 5 times the spin−lattice relaxation time between consecutive scans was necessary to ensure full recovery of the magnetisation. Typically, 2118 data points were collected for each scan, and the signal was averaged over four scans for each sample. Data were phase corrected and fitted to a single exponential decay on the instrument software.

4.3.2.1.2. Pulsed-Gradient Spin-Echo Nuclear Magnetic Resonance (PGSE-NMR)

HEUR/SDS/latex mixtures were dissolved in Hydroin buffered deuterium oxide (D_2O), pH 9. Experiments were carried out at 25 °C on a 400 MHz Bruker FT NMR spectrometer.

Chapter 4. HEUR/SDS/latex interaction

A stimulated echo sequence was used, in which the diffusion time (Δ) was set to 800 ms, the duration of the gradient pulses (δ) was held constant at 1 ms and their intensity (G) varied from 5 - 800 G cm^{-1}. Typically, 16 scans were accumulated over 32 gradient steps. Self-diffusion coefficients were extracted by fitting the peak intensities (I) to Equation 4.1 for the peaks at 3.75 ppm (ethylene oxide peak) where I_0 is signal intensity in the absence of gradient pulses, D_s the diffusion coefficient, γ the gyromagnetic ratio of protons (18,19).

$$I = I_0\, e^{-D_s \gamma^2 G^2 \delta^2 \left(\Delta - \frac{\delta}{3}\right)}$$
<div align="right">Equation 4.1</div>

4.3.2.2. Neutron Scattering

SANS measurements were carried out at 25 °C on the SANS 2D instrument (ISIS spallation Neutron Source, Oxfordshire, UK). Neutrons wavelengths spanning 2-14 Å were used to access a Q range of 0.002 to 3 Å^{-1} ($Q=4\pi \sin(\theta/2)/\lambda$) (20) with a fixed sample-detector distance of 4 and 2.4 m for the rear and front detector, respectively. Temperature control was achieved through the use of a thermostatted circulating bath pumping fluids through the base of the sample changer, which allowed the experiment to be run at 25 ± 0.5 °C. Samples were contained in UV-spectrophotometer grade 1 mm path length quartz cuvettes (Hellma). The scattering data were normalized for the sample transmission and the incident wavelength distribution, corrected for instrumental and sample backgrounds using a quartz cell filled with D_2O (this also removes the incoherent instrumental background arising from vacuum windows), and corrected for the linearity and efficiency of the detector response using the instrument specific software package. The data were put onto an absolute scale using a well characterised, partially deuterated PSL blend standard sample.

The contrast-match experiment for HEUR/d-PS-h-BAL presented in Chapter 3 (Figures 3.3 and 3.8) has been replicated in the presence of SDS at two concentrations: 0.1 and 1 wt%. A mixture of h/d-SDS (SLD = 3.9 x 10^{-6} Å^{-2}) was used to match the scattering length density of the surfactant to the solvent, hence the scattering contribution would be only from the C_6-L-(EO$_{100}$-L)$_9$-C_6. The model used to fit the polymer scattering in polymer/surfactant/ latex blend is sphere and network model presented in chapter three section 3.4.1.4. Recall, the fit parameters are size of the sphere (polymer aggregates) (R), number of electrons per sphere (e), Debye screening length (K^{-1}), volume fraction (φ), and two network correlation lengths; shorter (ξ), and longer length scale (A). The

_____

model was used to get values for the size of the polymer aggregates (R), and two correlation lengths; (ξ) and (A) of the polymer. The volume fraction (φ) of the sample and Debye screening length (K^{-1}) were calculated from the sample concentration and ionic strength, respectively.

4.3.2.3.   Rheology

The shear profiles of C_6-L-$(EO_{100}$-L$)_9$-C_6/PS-BAL mixtures have been measured in the presence of SDS at two concentrations: 0.1 and 1 wt%. The HEUR concentration was held constant at 5 wt%, whereas the latex concentration was varied (0.5, 3, and 5 wt%) in Hydroin buffered water, pH 9. The samples were measured using TA instrument rheometer AR-2000ex, with a 2°/40 mm cone and plate geometry at 25 °C. Shear profiles were recorded at 25 °C for a shear range of 1-1000 s^{-1}, with an integration time of 5 s, and delay time of 5 s.

4.4. Results and discussion

This chapter builds on the work from Chapter 3 which studied the behaviour of HEUR solutions in the presence and absence of latex. The effect of the addition of sodium dodecylsulphate (SDS) on C_6-L-$(EO_{100}$-L$)_9$-C_6 polymer solution behaviour in the presence of polystyrene-butylacrylate latex (PS-BAL) latex is presented here. Therefore the same methodology used in the previous chapters are used here. In this chapter, the changes in the PS-BAL surface area, hence aggregation behaviour is studied by solvent relaxation NMR in the ternary mixture (HEUR/SDS/latex). The solution behaviour of the polymer is studied by PGSE-NMR, rheology, and scattering in the ternary mixture.

4.4.1. Surface area of PS-BAL in the presence of HEUR and SDS

The change of the latex surface area in the presence of HEUR and SDS was studied by tracking the changes in the particle in the presence of 0.1 wt% SDS as a function of HEUR concentration. At 0.1 wt% the SDS in Hydroin buffer forms micelles, this concentration is double the concentration used to stabilise the latex as per the manufacturer.
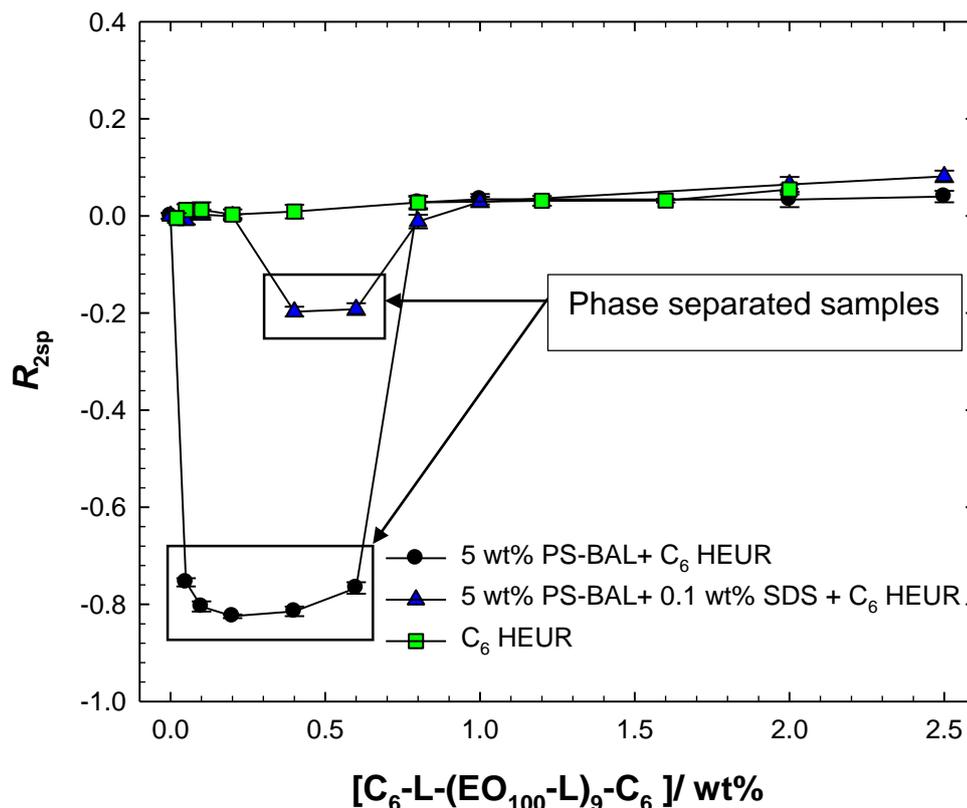
Figure 4.1. R_{2sp} **of** C_6-L-$(EO_{100}$-L$)_9$-C_6 **as a function of its concentration in the absence (green squares) and the presence of 5 wt% PS-BAL (black circles), and 0.1 wt% SDS/5 wt% PS-BAL (blue triangles) in Hydroin buffered water, pH 9.** R_{2sp} **of HEUR/PS-BAL mixtures are corrected relative to bare particle, and HEUR as a function of its concentration relative to water. Measurements were carried out at 25 °C. The solid lines are guides for the eye. The error bars are the standard deviation of three measurements for the same sample and a second set of the samples.**

The behaviour of the latex/polymer mixtures in the presence and absence of SDS are compared (Figure 4.1). The R_{2sp} for all ternary mixtures are corrected relative to the particle, hence the change in R_{2sp} is sensitive to changes due to the interaction of the polymer and/or surfactant with the particles. At low HEUR concentration, $R_{2sp} = 0$ for ternary mixture of HEUR/SDS/latex, then the R_{2sp} values go negative and returns back to zero. As it has been demonstrated in Chapter 3, a negative R_{2sp} value indicates the aggregation of the particles, however, the ternary mixture shows a less decrease in the R_{2sp} values and a narrower aggregation window relative to the binary mixture of C_6-L-$(EO_{100}$-L$)_9$-C_6/PS-BAL. This may be explained by the interaction of HEUR with SDS as demonstrated in Chapter 2; the HEUR chains interact with the available SDS micelles, hence the bridging flocculation is reversed. As all the available HEUR hydrophobes are

solubilized in the SDS micelle, the addition of more polymer chains induces bridging. Similar to the binary mixture, the ternary mixtures re-stabilise as the polymer hydrophobes start to associate in solution, where one hydrophobic end is adsorbed to the latex and the other end is in polymer hydrophobic aggregates. Jenkins *et al.* (21), and Kostansek (17) reported the reversing of the bridging flocculation induced by the HEUR in latex suspension in the presence of SDS, however, the mechanism behind this effect has not been discussed.
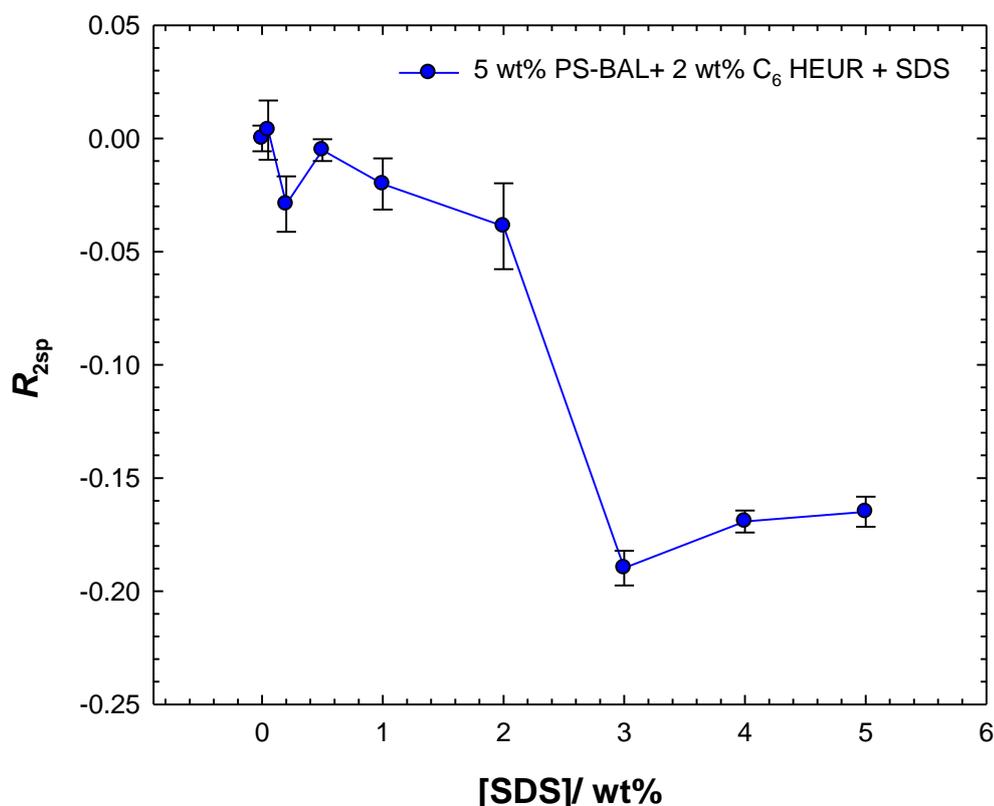
Figure 4.2. R_{2sp} **of 5 wt% PS-BAL/2 wt% C_6-L-(EO$_{100}$-L)$_9$-C_6 as a function of SDS concentration in Hydroin buffered water, pH 9. R_{2sp} of SDS/PS-BAL mixtures are corrected relative to bare particle. Measurements were carried out at 25 °C. The solid line is a guide for the eye. The error bars are the standard deviation of three measurements for the same sample and a second set of the samples.**

The changes in the surface area of 5 wt% particles were then studied at fixed polymer concentration (2 wt%) as a function of SDS concentration (Figure 4.2). At low SDS concentration, the R_{2sp} of the latex and 2 wt% HEUR mixtures show very subtle changes. The R_{2sp} has negative values at 3 wt% SDS and higher concentrations, where macroscopic phase separation is observed as well.

Chapter 4. HEUR/SDS/latex interaction

The phase separation of the ternary mixture has been observed by Kostansek, where a phase diagram for 25 wt% BA-PSL and BA-MMAL with HEUR-50-12 as a function of SDS was studied (17). The ternary mixture in Kostansek's studies showed phase separation from 0.5-1 wt% SDS depending on the concentration of the HEUR, surface chemistry and size of the latex. Increasing the HEUR concentration and decreasing the size of the latex shifts the depletion flocculation region to higher SDS concentration. Here, the structure of the HEUR, and concentration of latex are different, therefore a comparison of the concentrations of SDS at which the phase separation occurs might not be very informative. The phase separation was correlated to depletion flocculation due to the interaction of HEUR with SDS. Hulden illustrated the absence of HEUR-19-18 adsorption on acrylic acid (373 nm) latex in the presence of SDS at concentrations above the CMC due to the interaction of the SDS with the HEUR in solution (16). Therefore, the depletion flocculation is due to the presence of a non-adsorbing polymer/surfactant complex. However, depletion flocculation could occur due to the presence of free SDS micelles at high concentrations.

Furusawa *et al.* studied the viscosity of aqueous dispersions of 10 wt%, 230 nm polystyrene particles as a function of SDS concentration (22). A viscosity maximum was observed at 3 wt% SDS, the magnitude of which was correlated to the strength of interaction forces, hence depletion flocculation was concluded to occur due to the volume restriction effect of free micelles.
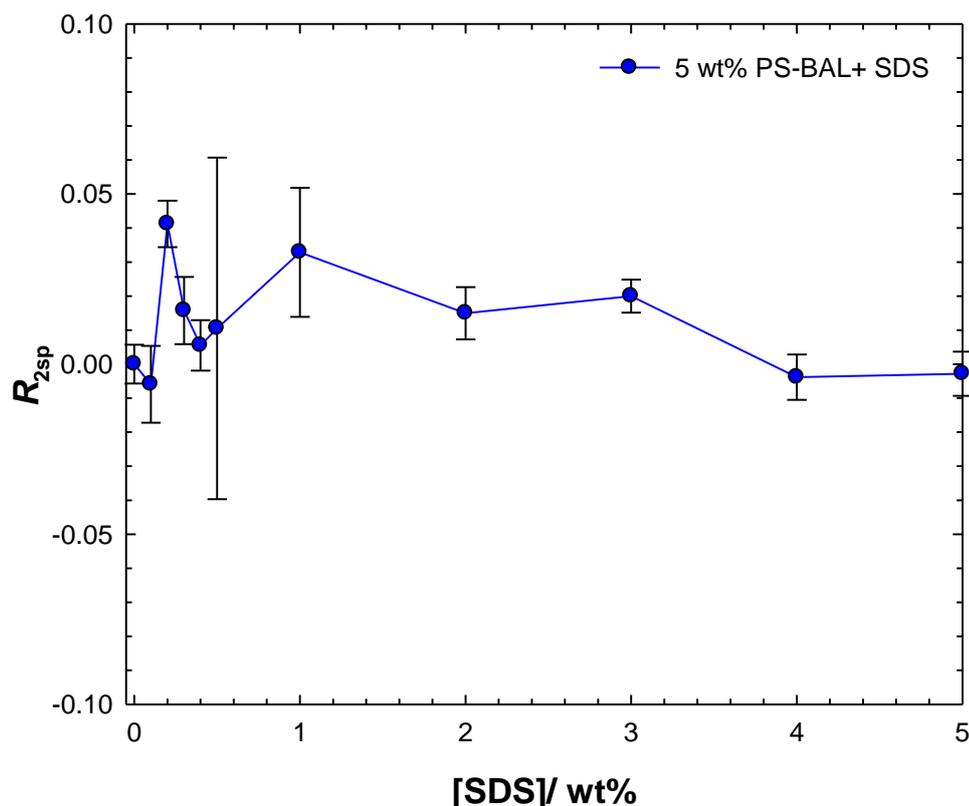
Figure 4.3: R_{2sp} **of 5 wt% PS-BAL as a function of SDS concentration in Hydroin buffered water, pH 9.** R_{2sp} **of SDS/PS-BAL mixtures are corrected relative to the bare particles. Measurements were carried out at 25 °C. The solid line is a guide for the eye. The error bars are the standard deviation of three measurements for the same sample and a second set of the samples.**

In this study, to differentiate the two potential mechanisms of depletion flocculation, it was decided to study changes in R_{2sp}, and hence surface area of the particles, as a function of SDS, in the absence of polymer. The R_{2sp} of 5 wt% latex shows no significant changes as a function of SDS (Figure 4.3), hence the surface area of the latex changes within experimental error. Therefore, the observed depletion flocculation for the ternary system here is due to the presence of non-adsorbing HEUR/SDS complex. Typically adsorption of surfactant on particles is indicated by increases of R_{2sp} due to the increase of bound water molecules, associated with surfactant head-group, to the particles (23), however, the sensitivity of the techniques is system-dependent.

4.4.2. Solution polymer aggregates in the presence of SDS and latex

Relative diffusion of HEUR/SDS/PS-BAL mixtures
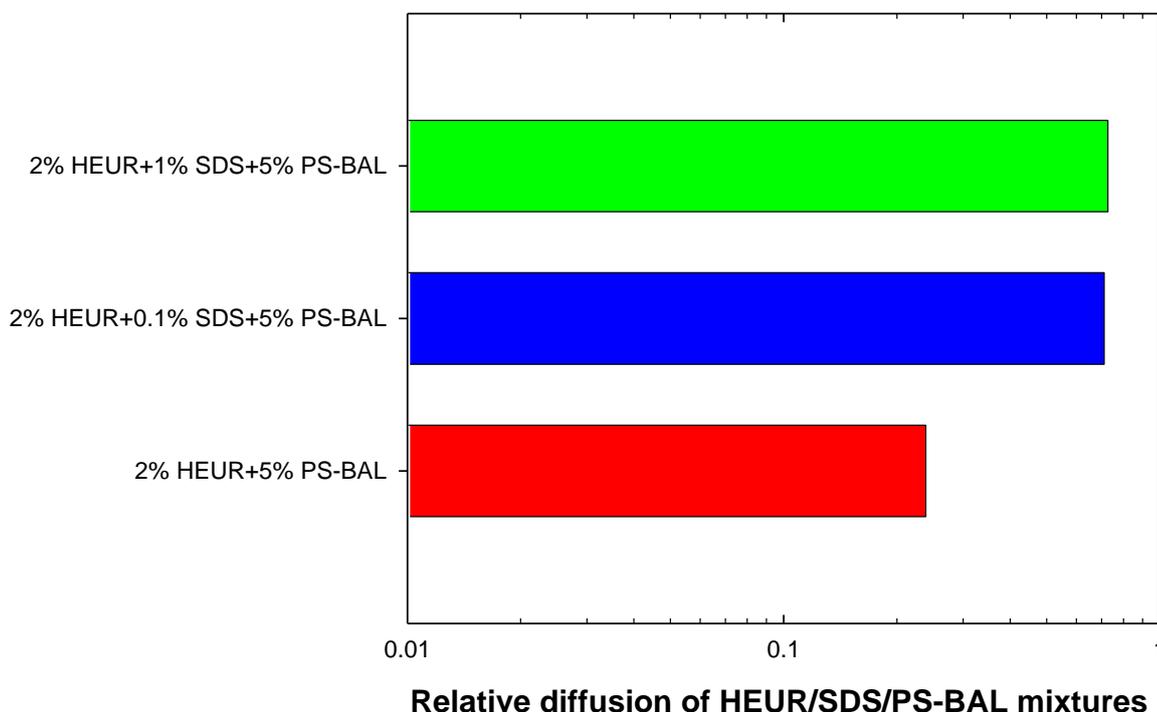
Figure 4.4. Relative diffusion coefficient of C_6-L-$(EO_{100}$-L$)_9$-C_6 in the ternary mixture (HEUR/SDS/PS-BAL) and binary mixtures (HEUR/PS-BAL) in Hydroin buffered D_2O, pH 9. Measurements were carried out at 25 °C.

Since very subtle changes in surface area of the ternary mixture are observed in the stable regions (Figure 4.2), the solution behaviour of the polymer in the ternary mixture was studied by diffusion NMR and compared to the polymer/SDS behaviour studied in Chapter 2 (Figures 2.18 and 2.29). Two concentrations of SDS were selected, 0.1 and 1 wt%, to study the polymer behaviour at 2 wt% in the presence of 5 wt% PS-BAL.

The diffusion coefficients of the polymer in C_6-L-$(EO_{100}$-L$)_9$-C_6/SDS/PS-BAL mixtures were divided by the C_6-L-$(EO_{100}$-L$)_9$-C_6/PS-BAL diffusion coefficient to yield a relative diffusion (D_r) coefficient of the polymer in the ternary mixtures. If D_r =1, the diffusion of the polymer/surfactant complex is comparable in the absence and presence of latex, whereas if D_r < 1, the polymer/surfactant complex in the presence of latex diffuses more slowly.

The D_r values for all the samples are less than one, reflective of the presence of polymer adsorption to the latex. However, in the presence of SDS the values of the D_r approach unity (Figure 4.4).

4.4.3. Rheology and viscosity of the ternary mixture
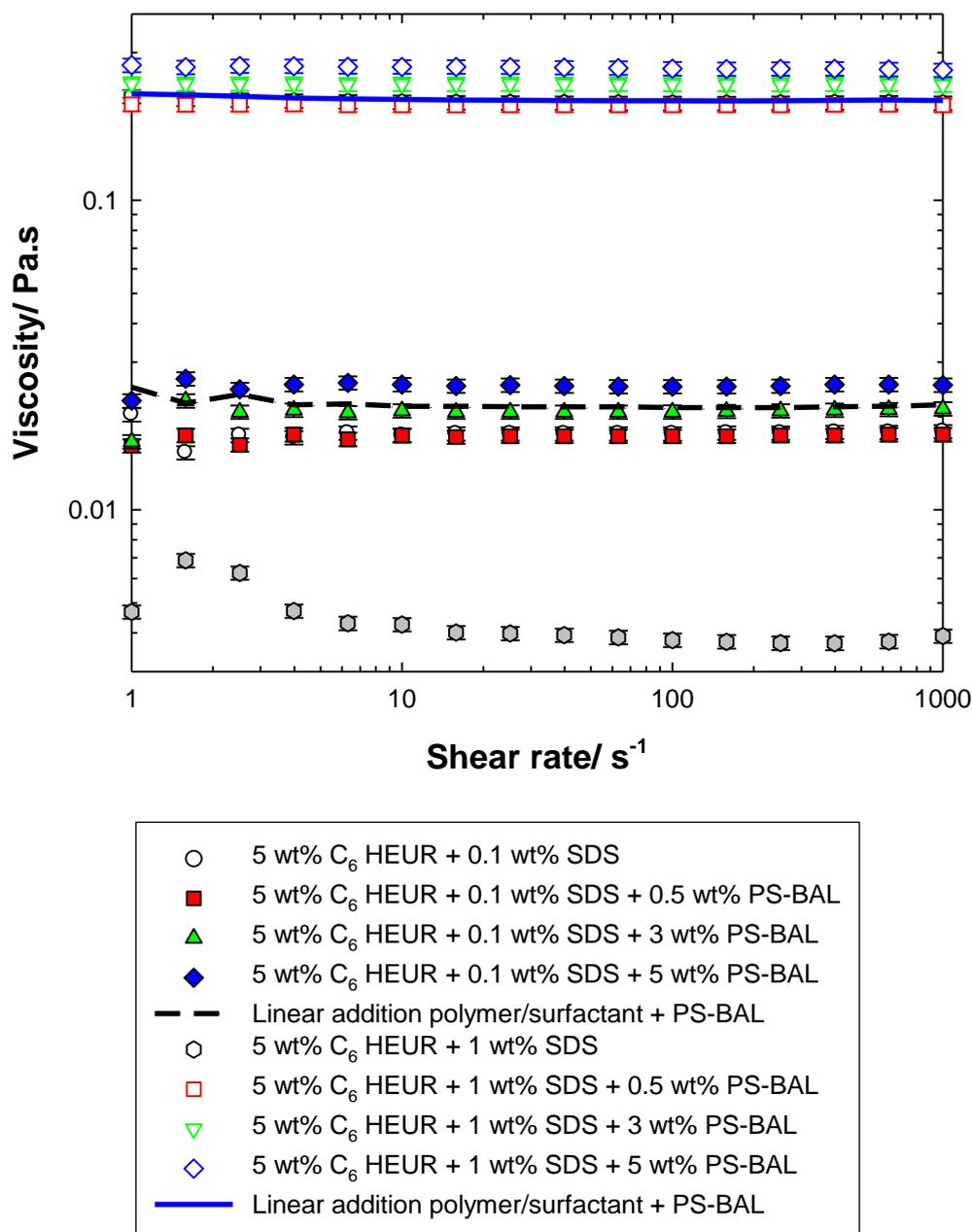
Figure 4.5. Shear profile of 5 wt% PS-BAL (hexagon), 5 wt% HEUR in the absence (white circles) and the presence of 0.5 (squares), 3 (triangles), and 5 (diamonds) wt% PS-BAL at 0.1 wt% SDS (closed symbols) and 1 wt% SDS (open symbols). Linear addition 5 wt% C_6-L-$(EO_{100}$-L$)_9$-C_6/0.1 wt% SDS/5 wt% PS-BAL (black dashed line), and 5 wt% C_6-L-$(EO_{100}$-L$)_9$-C_6/1 wt% SDS/5 wt% PS-BAL (blue solid line). Samples were prepared in Hydroin buffered water, pH 9. Measurements were carried out at 25 °C. The error bars are the standard deviation of three measurements for the same sample and a second set of samples.

Chapter 4. HEUR/SDS/latex interaction

Shear profiles of the C_6-L-$(EO_{100}$-L$)_9$-C_6/PS-BAL mixtures in the presence of 0.1 and 1 wt% SDS are Newtonian (Figure 4.5). Recall that the viscosity of the polymer solution increases as a function of SDS concentration, as has been discussed in details in Chapter 2 (Figures 2.18 and 2.28). The viscosity of the polymer/SDS mixture increases as a function of PS-BAL concentration, and the viscosity increase is not additive across the binary systems.
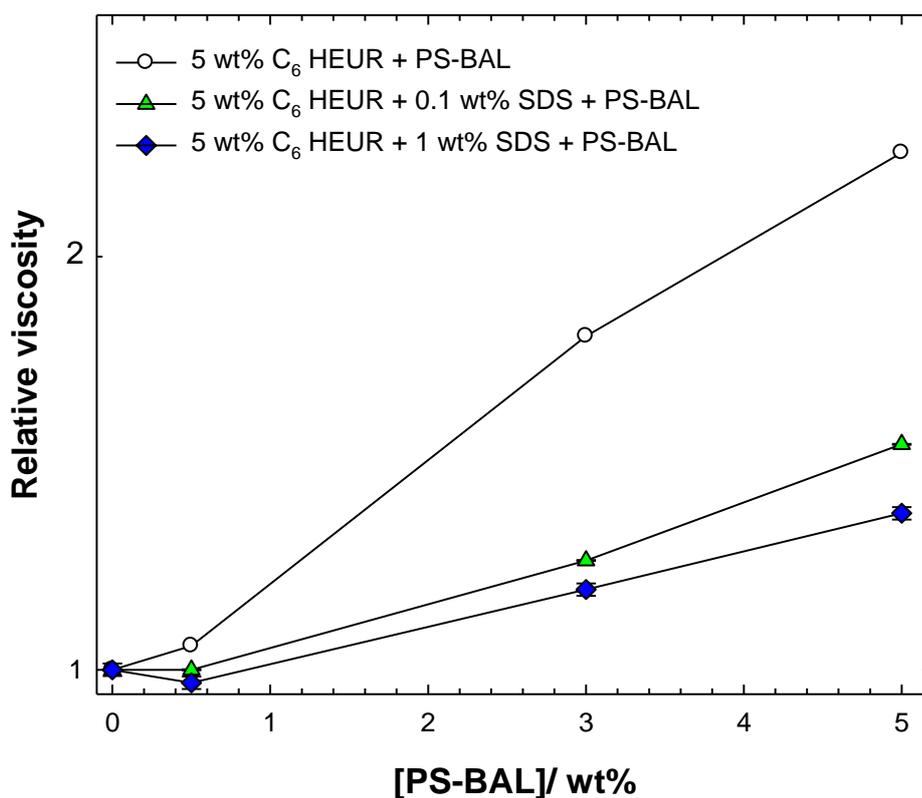
Figure 4.6. Relative viscosity at shear rate 4 s^{-1} of C_6-L-$(EO_{100}$-L$)_9$-C_6/PS-BAL mixtures in the absence (white circles), and the presence of 0.1 (triangles), and 1 (diamonds) wt% SDS. Samples were prepared in Hydroin buffered water, pH 9. Measurements were carried out at 25 °C. The solid lines are guides for the eye.

To discuss the viscosity changes in the polymer/latex mixtures in the presence of SDS more easily, the relative viscosity (η_r) of the ternary mixture is plotted in Error! Reference source not found. as a function of latex concentration, $\eta_r = \frac{\eta_{ternary\,mixture}}{\eta_{polymer}}$. As the SDS concentration increases, there is a weaker increase in the viscosity of the ternary mixture as a function of latex concentration, illustrated by a steeper slope of the η_r latex concentration plot.

Chapter 4. HEUR/SDS/latex interaction

The non-additive increase in the viscosity indicates the presence of polymer adsorption to the latex particles at the two SDS concentrations studied here. However, the steeper slope of the relative viscosity as a function of SDS suggests the weakening of the interaction between the polymer and latex in the presence of SDS.

Glass *et al.* measured the viscosity of 120 nm MAA-MMAL at 25 wt% and HEUR-35-12 at two concentrations, 0.5 and 2.5 wt%, in the presence of 0.3 wt% SDS (15). A drop in the HEUR/latex mixture viscosity was observed and explained by desorption of the polymer from the latex surface. Glass *et al.* mentioned the absence of HEUR/SDS interaction at the studied concentration without supporting the statement. It has been illustrated in Chapter 2 (Figures 2.18, 2.26) that there is a strong interaction between the HEUR and SDS at concentrations below the CMC of SDS. The experiment here shows an increase in the viscosity of HEUR as a function of latex concentration in the presence of low and high SDS concentration. However, the experiment here is designed differently where the effect of viscosity increase due to adsorption of the HEUR to the latex is highlighted by holding the polymer and surfactant concentration constant and varying the latex concentration.

4.4.4. SANS from the ternary mixture

These experiments are designed to gain a better understanding of the changes in the polymer conformation in the presence of SDS and latex. The contrast-match experiment described in Chapter 3, Section 3.4.1.4, is replicated with the addition of two concentrations of d/h SDS mixture to match the SLD of the SDS to the solvent, hence the scattering contribution is from the polymer only. The scattering behaviour of the polymer in the ternary mixture is compared to the HEUR in HEUR/SDS complex and pure HEUR solutions.
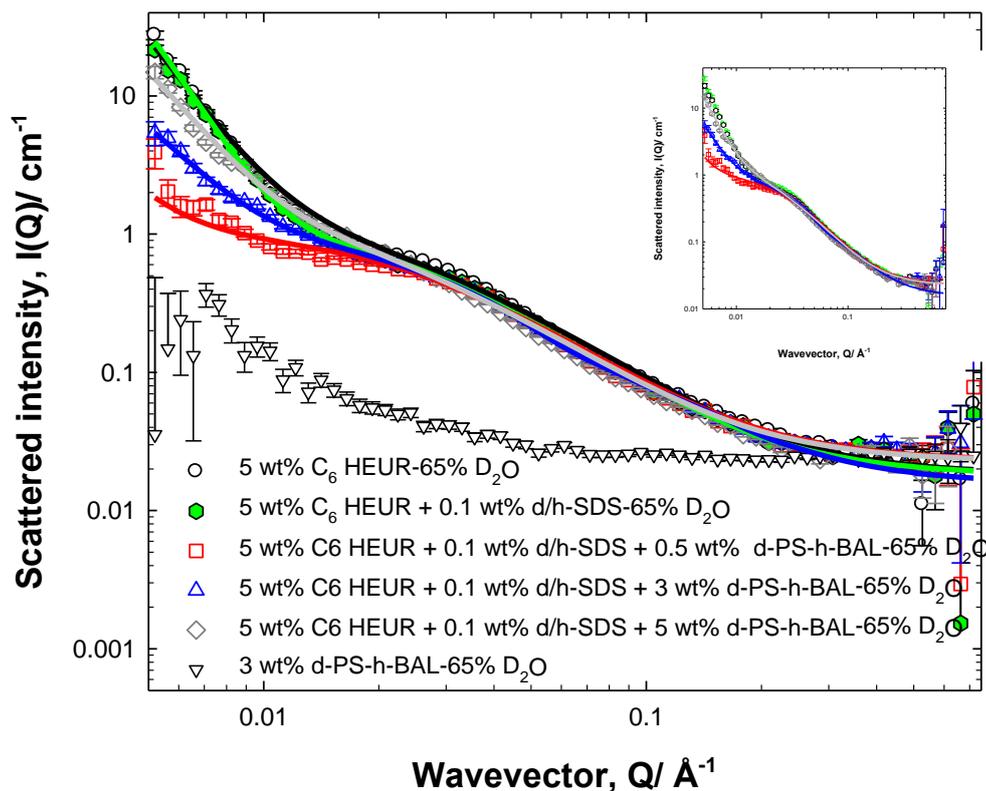
Figure 4.7. Small-angle neutron scattering from a series of polymer/SDS/particle blends: 5 wt% polymer/0.1 wt% SDS in the presence of 0.5 (squares), 3 (blue triangles), and 5 (diamonds) wt% d-PS-h-BAL, plus controls; 3 wt% d-PS-h-BAL on match (white triangles), 5 wt% C_6-L-$(EO_{100}$-L$)_9$-C_6 (circles), and 5 wt% C_6-L-$(EO_{100}$-L$)_9$-C_6/0.1 wt% SDS (green hexagons) in 65% D_2O/H_2O mixture. The scattering contribution is from the polymer only in polymer/surfactant/latex blend. Samples were prepared in Hydroin buffered solvents, pH 9. The solid lines are sphere and network model fit presented in Chapter 3 section 3.4.1.4. Key fitting parameters value are presented in Table 4.1.

The peak position (Q = 0.03 Å^{-1}) of the polymer in the presence and absence of 0.1 wt% d/h SDS does not show significant changes relative to the pure polymer solution (Figure 4.7). The addition of PS-BAL to polymer/SDS does not significantly change the intensity or position of the peak at mid-Q. However, a significant change in C_6-L-$(EO_{100}$-L$)_9$-C_6/SDS scattering is observed at low-Q, similar to those observed in polymer/latex mixture in Chapter 3, where the same trend of intensity changes are observed.
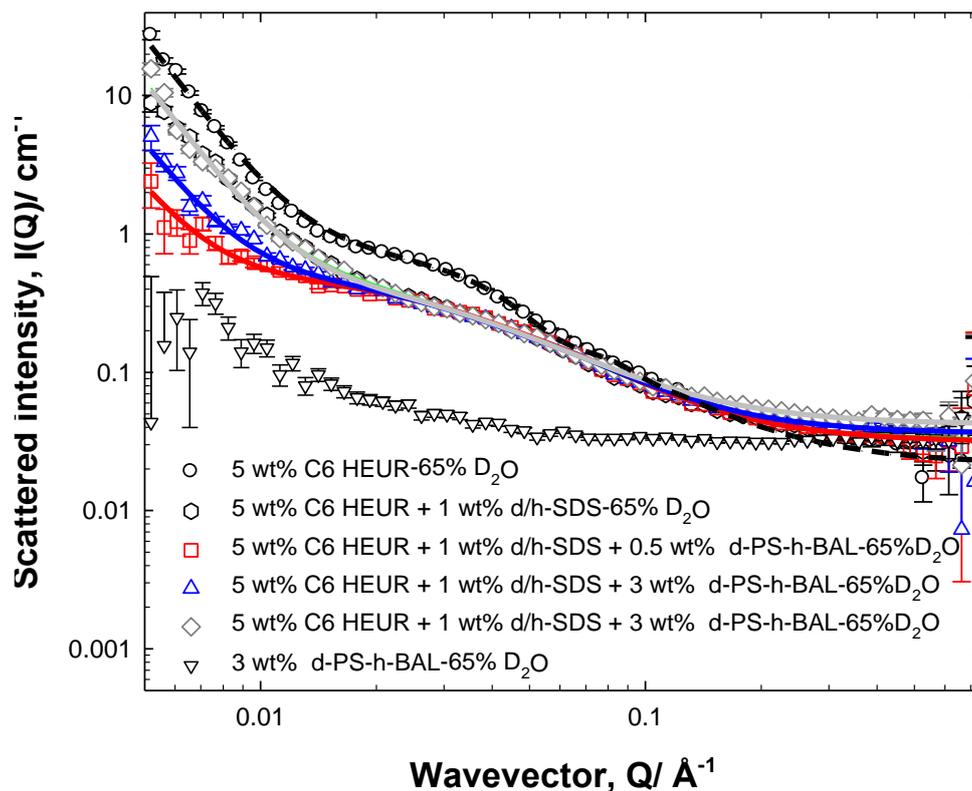
Figure 4.8. Small-angle neutron scattering from a series of polymer/SDS/particle blends: 5 wt% polymer/1 wt% SDS in the presence of 0.5 (squares), 3 (blue triangles), and 5 (diamonds) wt% d-PS-h-BAL, plus controls; 3 wt% d-PS-h-BAL on match (white triangles), 5 wt% C_6-L-$(EO_{100}$-L$)_9$-C_6 (circles), and 5 wt% C_6-L-$(EO_{100}$-L$)_9$-C_6/1 wt% SDS (green hexagons) in 65% D_2O/H_2O mixture. The scattering contribution is from the polymer only in polymer/surfactant/latex blend. Samples were prepared in Hydroin buffered solvents, pH 9. The solid lines are sphere and network model fit presented in Chapter 3 section 3.4.1.4. Key fitting parameters value are presented in Table 4.2.

In the presence of 1 wt% d/h SDS, the polymer peak position is shifted to higher Q range (Figure 4.8). The position of the polymer peak in the ternary mixture overlaps with the polymer/SDS complex rather than pure polymer. The same trend of scattering changes at low-Q as a function of latex concentration noted for the binary mixture (HEUR/PS-BAL) and ternary mixture (HEUR/SDS/PS-BAL) in the presence of 0.1 wt% SDS is observed in the presence of 1 wt% SDS. The main fitting parameters of the sphere and network model described in Chapter 3, Section 3.4.1.4 are presented for the 0.1 and 1 wt% SDS datasets in Table 4.1, and Table 4.2, respectively. Similar trends observed for polymer/latex mixtures are noted here. From the fitting parameters, the sphere radius, Lorentzian length intensity, and Lorentzian length do not change as a function of latex

concentration. However, similar to the HEUR/latex mixture, the Debye-Bueche intensity, and length 'A' decreases as a function of latex concentration. The decrease in the 'A' term and its intensity in the presence of 1 wt% SDS < 0.1 wt% SDS < 0 wt% SDS. These results suggest the weakening of the HEUR adsorption.

The overlapping of the polymer peak in the presence of 1 wt% SDS and latex suggests that the SDS favourably interacts with the HEUR, these results are consistent with the conclusions of Hulden (16), who noted the absence of HEUR-19-18 adsorption to latex in the presence of SDS due to solution complexation. This has been concluded based on the measurement of free polymer concentration by UV spectroscopy after spinning the latex down by centrifugation. Though the methodology and system (MA-BAL 536 d.nm, and HEUR-19-18) are different from those presented in this chapter, however, the results are in a good agreement. Attempts to fit the scattering data to the theory proposed by *Cosgrove et al.* in the Insanity program for adsorbed polymer layer were unsuccessful and the scattering curve looks different from the presented here, where an increase in the scattering intensity at low-Q is expected. This suggests that the polymer adsorbed layer is probably shifted to low-Q.

Fit parameters/ Units	0.1 % SDS+ 0 % latex	0.1 % SDS+ 0.5 % latex	0.1 % SDS+ 3 % latex	0.1 % SDS+ 5 % latex
Intensity of radius term	6.1×10^{-7}	6.1×10^{-7}	6.1×10^{-7}	6.1×10^{-7}
Radius (Å)	65 ± 5	65 ± 5	65 ± 5	65 ± 5
e	10	10	10	10
K^{-1} (Å)	0.29	0.29	0.29	0.29
φ	0.051	0.056	0.081	0.101
l_1	0.4	0.4	0.4	0.4
ξ (Å)	25 ± 1	25 ± 1	25 ± 1	25 ± 1
l_2	3000	350	60	80
A (Å)	650 ± 10	600 ± 10	300 ± 3	250 ± 3

Table 4.1. SANS key parameters from the sphere and network model for 5 wt% HEUR and HEUR/latex in the presence of 0.1 wt% SDS.

Fit parameters/ Units	1 % SDS+ 0 % latex	1 % SDS+ 0.5 % latex	1 % SDS+ 3 % latex	1 % SDS+ 5 % latex
Intensity of radius term	1.0×10^{-7}	1.0×10^{-7}	1.0×10^{-7}	1.0×10^{-7}
Radius (Å)	50 ± 3	50 ± 3	50 ± 3	50 ± 3
e	10	10	10	10
K^{-1} (Å)	0.27	0.27	0.27	0.27
φ	0.06	0.065	0.09	0.11
l_1	0.4	0.4	0.4	0.4
ξ (Å)	30 ± 1	30 ± 1	30 ± 1	30 ± 1
l_2	3000	450	450	40
A (Å)	700 ± 10	700 ± 10	600 ± 10	450 ± 3

Table 4.2. SANS key parameters from the sphere and network model for 5 wt% HEUR and HEUR/latex in the presence of 1 wt% SDS.

4.5. Conclusion

HEUR/latex showed a weak interaction, evidenced by changes in latex surface area in the presence of polymer, as has been shown in Chapter 3. The polymer solution viscosity increases and a decrease in self-diffusion coefficient of the polymer in the presence of latex are observed, indicative of polymer adsorption to the latex. The addition of SDS to polymer/surfactant seemed to weaken the polymer adsorption to the latex evidenced by the close values of the polymer self-diffusion coefficient in HEUR/SDS and HEUR/SDS/latex mixtures. The increase of the HEUR viscosity as a function of latex concentration is weakened in the presence of SDS. The polymer appears to strongly interact with the SDS evidenced by depletion flocculation observed at high SDS concentration. Finally, the contrast-match experiment where scattering contribution is from the polymer in the ternary mixture, the polymer peak at mid-Q in the presence of 1 wt% SDS overlapped with HEUR/SDS complex peak rather than the pure HEUR.

Chapter 4. HEUR/SDS/latex interaction

4.6. References

1.   Brown W, Zhao J. Adsorption of sodium dodecyl sulfate on polystyrene latex particles using dynamic light scattering and zeta potential measurements. *Macromolecules*. **1993**;*26*(11):2711–2715.

2.   Nodehi A, Moosavian MA, Haghighi MN, Sadr A. A new method for determination of the adsorption isotherm of SDS on polystyrene latex particles using conductometric titrations. *Chem Eng Technol*. **2007**;*30*(12):1732–1738.

3.   Bloze D, Horner KD. Competitive adsorption of an anionic and a nonionic surfactant on polystyrene latex particles as monitored by small X-ray scattering. *Colloid Poly Sci*. **1996**;*274*(12):1099–1108.

4.   Ma Z, Chen M, Glass JE. Adsorption of nonionic surfactants and model HEUR associative thickeners on oligomeric acid-stabilized poly(methyl methacrylate) lattices. *Colloids Surf, A Physicochem Eng Asp*. **1996**;*112*(2):163-184.

5.   Chatterjee T, Nakatani AI, Dyk AKV. Shear-dependent interactions in hydrophobically modified ethylene oxide urethane (HEUR) based rheology modifier−latex suspensions: Part 1. Molecular microstructure. *Macromolecules*. **2014**;*47*(3):1155–1174.

6.   Cosgrove T, Mears SJ, Obey T, Thompson L, Wesley RD. Polymer, particle, surfactant interactions. *Colloids Surf, A Physicochem Eng Asp*. **1999**;*149*(1-3):329–338.

7.   Pisarcik M, Bakos D, Ceppan M. Interactions of latex spheres and anionic surfactant in hydrophobically modified polymer aqueous solution. *Colloids Surf, A Physicochem Eng Asp*. **1993**;*81*:161–166.

8.   Lauten RA, Kjoniksen A, Nystrom B. Adsorption and desorption of unmodified and hydrophobically modified ethyl(hydroxyethyl)cellulose on polystyrene latex particles in the presence of ionic surfactants using dynamic light scattering. *Langmuir*. **2000**;*16*(10):4478–4484.

9.   Lauten RA, Kjoniksen A, Nystro B. Colloid polymer interactions and aggregation in aqueous mixtures of polystyrene latex, sodium dodecyl sulfate, and a hydrophobically modified polymer : A dynamic light scattering study. *Langmuir*.

Chapter 4. HEUR/SDS/latex interaction

2001;*17*(3):924–930. 2001;(3):924–30.

10. Mahli DM, Steffenhagen MJ, Xing L, Glass JE. Surfactant behavior and its influence on the viscosity of associative thickeners solutions, thickened latex dispersions, and waterborne latex coatings. *J Coat Technol.* **2003**;*75*(938):39–51.

11. Winnik MA, Yekta A. Associative polymers in aqueous solution. *Curr Opin Colloid Interface Sci.* **1997**;*2*(4):4234–4236.

12. Alami E, Almgren M, Brown W. Interaction of hydrophobically end-capped poly(ethylene oxide) with nonionic surfactants in aqueous solution. Fluorescence and light scattering studies. *Macromolecules.* **1996**;*29*(14):5026–5035.

13. Zhang K, Xu B, Winnik MA, Macdonald PM. Surfactant Interactions with HEUR Associating Polymers. *J Phys Chem.* **1996**;*100*(23):9834–9841.

14. Hulden M. Hydrophobically modified urethane-ethoxylate (HEUR) associative thickeners 1. Rheology of aqueous solutions and interactions with surfactants. *Colloids Surf, A Physicochem Eng Asp.* **1994**;*82*(3):263–277.

15. Glass JE. Adsorption of hydrophobically-modified, ethoxylated urethane thickeners on latex and titanium dioxide disperse phases. *Adv Colloid Interface Sci.* **1999**;*79*(2):123–148.

16. Hulden M. Hydrophobically modified urethane-ethoxylate (HEUR) associative thickeners 2. Interaction with latex. *Colloids Surfaces A Physicochem Eng Asp.* **1994**;*88*(2–3):207–221.

17. Kostansek E. Using Dispersion/flocculation phase diagrams to visualize interactions of associative polymers, latexes, and surfactants. *J Coat Technol.* **2003**;*75*(940):1-8.

18. Abrahmsen-Alami S, Stilbs P. NMR self-diffusion of associative polymers in aqueous solution: the influence of the hydrocarbon end-chain length on the polymer transport dynamics in single-and two-component mixtures. *J Colloid Interface Sci.* **1997**;*189*(1):137–143.

19. Claridge TDW. High-Resolution NMR Techniques in Organic Chemistry. Second edition. Oxford, UK: *Elsevier*; **2009**.

20. Heenan RK, King SM, Turner DS, Treadgold JR. SANS2d at the ISIS Second

Target Station. *17th Meet Int Collab Adv Neutron Sources.* **2005**;1–6. Available from: http://www.isis.stfc.ac.uk/instruments/sans2d/publications/sans2d-at-isis10323.pdf, (accessed November 2016).

21.   Jenkins RD, Durali M, Silebi CA, El-Aasser MS. Adsorption of model associative polymers on monodisperse polystyrene latex. *J Colloid Interface Sci.* **1992**;*154*(2):502–521.

22.   Furusawa K, Sato A, Shirai J, Nashima T. Depletion flocculation of latex dispersion in ionic micellar systems. *J Colloid Interface Sci.* **2002**;*253*:273–2788.

23.   Cooper CL, Cosgrove T, Duijneveldt JS, Murray M, Prescott SW. The use of solvent relaxation NMR to study colloidal suspensions. *Soft Matter.* **2013**;*9*(30):7211–7228.

---

5. Stabilisation of an oil in water emulsion by HEUR and HEUR/SDS mixtures

5.1. Abstract

In this study, three different HEURs have been used as a model emulsifier, C_6-L-(EO_{100}-L)$_9$-C_6, C_{10}-L-(EO_{200}-L)$_4$-C_{10}, and C_{18}-L-(EO_{200}-L)$_7$-C_{18} to stabilise dodecane/water emulsions in absence and presence of SDS. These systems have been studied by nuclear magnetic resonance (NMR), and small-angle neutron scattering (SANS). The diffusion NMR data showed the ability of the three polymers to stabilise the dodecane in water forming oil droplets of diameter 450 nm. The scattering curves do not fit to an adsorbed layer model but are better described by a model that depicts the polymer as a network. The network model better describes the data due to the adsorption mechanism of the HEUR where its hydrophobic moieties reside in the oil phase whilst the hydrophilic moieties extend into the aqueous phase, thereby lowering interfacial tension as well as preventing coalescence through steric stabilisation. The emulsions were left for a week where phase separation occurred. The partitioning of the polymers in the phase separated samples was studied by ^{1}H NMR where the C_{18}-L-(EO_{200}-L)$_7$-C_{18} showed higher partitioning in the oil phase relative to C_6-L-(EO_{100}-L)$_9$-C_6 and C_{10}-L-(EO_{200}-L)$_4$-C_{10} which may be correlated to the architecture of the HEURs. The SDS showed a positive correlation between its partitioning in the two layers and the polymer partitioning, in agreement with the scattering data results, where the SDS showed evidence of interaction with the polymer. The balance between the length of the hydrophobic end-group, and hydrophilic backbone, as well as the number of urethane likers, is shown to affect the hydrophobicity of the polymer. This work should help formulators make more informed choices regarding the HEUR structure in commercial formulations.

Chapter 5. HEUR and HEUR/SDS stabilised dodecane emulsion

5.2. Introduction

Emulsions are commonly used in the personal care industry to minimise the undesirable "greasy feel" of actives and emollients (oils), which can be a negative attribute for the consumer. By dispersing such oils in an aqueous environment, the sensory perception can be altered to make it more favourable to consumers. Emulsions usually contain surfactants in conjunction with thickeners to provide stability of the two phases with the appropriate viscosity. Although there are a variety of rheological modifiers available in the personal care industry, there is a desire for shorter formulation lists, which in turn drives the need for multifunctional additives, such as the hydrophobically modified ethoxylated urethane polymers (HEURs).

Emulsions are commonly stabilised by surfactants (1–3), proteins (4,5), hydrocolloids (6) and particles (7–9), which have been extensively studied. To date, few studies have attempted to stabilise emulsions with hydrophobically modified polyethylene oxide (PEOM). Filali *et al.* studied the network structure of PEOM-10-12 (the first number is the molecular weight of the polymer in kg mol^{-1} and the second number is the hydrophobic end-group C-chain length) in decane/water emulsion by small-angle neutron scattering (SANS) (10). The decane emulsion is pre-stabilised by cetylpyridinum chloride (CPCl) and octanol (co-surfactant), before the addition of the PEOM. The amount of PEOM added was calculated so that the volume fraction (φ) of the hydrophobes is constant, therefore as the PEOM is added to the emulsion, the concentration of the CPCl and octanol decreases. Surprisingly, it is proposed that the radius of the oil droplet is fixed (62 ± 2 Å) at the various concentrations of decane (7 - 26 %), therefore the solutions are characterised by the number of chains adsorbed per droplet (r) and the hydrophobic content (φ) of the emulsion. The scattering curves show a sphere form factor, from which the radius of the oil droplet is calculated. The structure factor is typically observed at low-Q where the scattered intensity is reflective of repulsive or attractive interactions between the oil droplets. It is postulated that the hydrophobic end-groups of the polymer tend to adsorb to the oil, as the φ of the oil increases the distance (d) between the droplets is comparable to the polymer R_g hence the polymer tends to bridge between the droplets (Figure 5.1). This is evidenced by the increase in the scattered intensity at low-Q reflective of attractive interaction. At higher φ, $d < R_g$, therefore, the bridging of the polymer chain between two oil droplets is not reflected by any changes in the scattered intensity at low-Q.
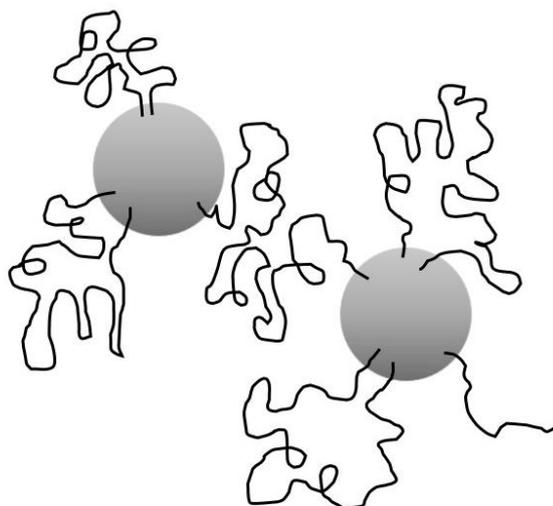
Figure 5.1. Cartoon illustrating the adsorption of PEOM on oil droplet reproduced from Filali *et al.* (10).

Bagger-Jorgensen *et al.* studied the diffusion of PEOM-11-18 in decane emulsion pre-stabilised by penta(ethylene glycol) monododecyl ether ($C_{12}E_5$) (11). In this study, the oil concentration was held constant to 0.2 weight fraction whereas the polymer concentration was varied from 0.002-0.02 weight fraction. The self-diffusion coefficient of the polymer measured by NMR decreases in the presence of the oil droplet, suggesting the adsorption of the polymer hydrophobic end-groups to the oil droplets. The parent PEO was added to the decane emulsion, no change in the diffusion coefficient of the polymer in the emulsion is noted, and therefore the polymer does not adsorb to the droplets. The scattering from the emulsion as a function of PEOM concentration showed a sphere form factor of radius 72 ± 2 Å. The variation of the polymer concentration does not affect the size of the oil droplet whereas a change in the *inter*-droplet distance is observed. The increase in the polymer concentration leads to increase in the attractive force, hence the distance between the droplets decreases. Bagger-Jorgensen, in agreement with Filali *et al.* (10), postulates that the PEOM hydrophobes adsorb to the oil droplets, where some polymer chains bridge between two droplets with the PEO backbone extended in water.

Pluronic L64 (poly(ethylene oxide)–poly(propylene oxide)–poly(ethylene oxide)), (EO)n–(PO)m–(EO)n, where n = 13, m = 30 was used to stabilise tributylphosphate (TBP)/water emulsions that were studied by SANS, and the scattering curves were fitted to a core-shell model (12). The concentration of the Pluronic was held constant at 10 wt% and the oil concentration was varied from 0, 25, 50, and 150 (the concentration of the TBP added

is presented as $\frac{C}{C_{sat}}$ where C_{sat} is the solubility of TBP in deionized water). Increasing the oil content increases the hydrophobic core radius whereas the shell thickness is constant to (35 Å).

Stieber *et al.* studied water/octane polymer stabilised emulsion by static and dynamic light scattering. The polymer is triblock copolymers of the ABA type, where A is a hydrophilic (poly(ethylene oxide) = PEO) and B a hydrophobic (polyisoprene = PI) moiety (13). Two diffusion coefficients were observed for the polymer stabilised emulsion, a fast diffusion coefficient of 3×10^{-11} m^2 s^{-1}, and a slow diffusion (1×10^{-12} to 1×10^{-14} m^2 s^{-1}). Increasing the polymer concentration doesn't show any change in the fast diffusing component, whereas the slow diffusion gets slower as the polymer concentration increases. The fast diffusion might be explained by the collective droplet diffusion. The slow diffusion is correlated to the adsorbed polymer chain on the oil droplet where the polymer chains tend to bridge between two droplets and larger aggregates are formed. The diffusion coefficient of the same system was measured by diffusion NMR and similar conclusions are reported by Struis *et al.* (14).

The effect of SDS on PEOM stabilised emulsions has not been reported, however, the effect of SDS presence on homopolymer stabilised emulsions was reported. A mixture of polymer and surfactant has proved to provide a better stabilizing effect than polymer or surfactant on its own where PVP (neutral polymer) and SDS were used to stabilize xylene (30 %) in water; the SDS concentration was held constant at 5 mM and the PVP concentration was varied (0.01-0.2 wt%). This may be explained by adsorption of the polymer/surfactant complex on oil droplet which provides two stabilising mechanisms steric and electrostatic. The stability of the emulsion was assessed by counting the droplets concentration by a manual technique using hemocytometer cell. Increasing the number of droplets reflects better stability of the particles, where the emulsion stabilised by PVP/SDS mixture showed larger number of droplets relative to that stabilised by PVP or SDS only (15).

In summary, the research done in this area explored model PEOM polymers in a pre-stabilised emulsions. In this chapter, the ability of three HEURs with different architecture to stabilise oil-in-water emulsions were explored in absence and presence of SDS.

Chapter 5. HEUR and HEUR/SDS stabilised dodecane emulsion

5.3. Materials and methods

5.3.1. Materials

Sodium dodecylsulfate (SDS) (Aldrich, no impurity observed (Figure D.9), deuterated sodium dodecylsulfate (d_{25}-SDS) (ISIS deuteration facility), dodecane (Aldrich, ≥ 99 %), d_{26}-dodecane (Aldrich, ≥ 98% D), deionized water (Purite Select deionizer) and deuterium oxide (Aldrich, purity 99.9%) were used as received. RM2020E C_6-L-$(EO_{100}$-L$)_9$-C_6 (Dow), RM8W C_{10}-L-$(EO_{200}$-L$)_4$-C_{10} (Dow), and RM12W C_{18}-L-$(EO_{200}$-L$)_7$-C_{18} (Dow) were purified from cyclodextrin before use as described in the Appendix D, Section D.1.

5.3.2. Methods

The emulsions were prepared by probe sonicating (Hielscher UP 40 st ultrasonic processor) the polymer at a range of concentrations with 5 or 20 wt% dodecane in presence and absence of SDS for 5 min.

5.3.2.1. Nuclear Magnetic Resonance techniques

5.3.2.1.1. High-resolution ^{1}H Nuclear magnetic resonance

The emulsions were prepared in D_2O. These experiments were designed to detect the concentration of polymer, dodecane and SDS in the phase separated emulsion of polymer/dodecane and polymer/SDS/dodecane mixtures. The intensity of the peak was integrated relative to an external probe (chloroform), the probe was loaded in a coaxial inset and inserted in the samples. The same coaxial inset was used in the sets of samples to be compared to ensure the same concentration of chloroform was used each time. Experiments were carried out at 25 °C on a 400 MHz Bruker FT NMR spectrometer. A 90° pulse was used, averaging 4 scans with a recycle delay of at least 5 times the spin−lattice relaxation time between consecutive scans.

5.3.2.1.2. Pulsed-Gradient Spin-Echo Nuclear Magnetic Resonance (PGSE-NMR)

Polymers/dodecane and polymer/dodecane/SDS mixtures were prepared in deuterium oxide (D_2O), Experiments were carried out at 25 °C on a 400 MHz Bruker FT NMR spectrometer.

Chapter 5. HEUR and HEUR/SDS stabilised dodecane emulsion

A stimulated echo sequence was used, in which the diffusion time (Δ) was set to 800ms, the duration (δ) of the gradient pulses was held constant to 1 ms and their intensity (G) varied from 5 - 800 G cm^{-1}. Typically, 16 scans were accumulated over 32 gradient steps. Self-diffusion coefficients were extracted by fitting the peak intensities (I) to Equation 5.1 for the peaks at 3.75 ppm (EO), 4 ppm (SDS) and 1 ppm (dodecane) where I_0 is signal intensity in the absence of gradient pulses, D_s the diffusion coefficient, γ the gyromagnetic ratio of protons (16,17).

$$\mathrm{I} = \mathrm{I}_0 \, e^{-D_s \gamma^2 G^2 \delta^2 \left(\Delta - \frac{\delta}{3}\right)}$$
<div align="right">Equation 5.1</div>

5.3.2.2.   Neutron Scattering

SANS measurements were carried out at 25 °C on the LOQ diffractometer (ISIS spallation Neutron Source, Oxfordshire, UK). Neutrons wavelengths spanning 2.2-10 Å were used to access a Q range of 0.0008 to 0.25 Å^{-1} ($Q = 4\pi \sin(\theta/2)/\lambda$) (18) with a fixed sample-detector distance of 4.1 m. Temperature control was achieved through the use of a thermostatted circulating bath pumping fluids through the base of the sample changer, which allowed the experiment to run at 25 ± 0.5 °C. Samples were contained in UV-spectrophotometer grade 1 mm path length quartz cuvettes (Hellma). The scattering data were normalized for the sample transmission and the incident wavelength distribution, corrected for instrumental and sample backgrounds using a quartz cell filled with D_2O (this also removes the incoherent instrumental background arising from vacuum windows), and corrected for the linearity and efficiency of the detector response using the instrument specific software package. The data were put onto an absolute scale using a well characterised, partially deuterated polystyrene blend standard sample. The intensity of the scattered radiation, $I(Q)$, as a function of the wave vector, Q, is given by Equation 5.2.

$$I(Q) = N_p V_P^2 \Delta\rho^2 P(Q) S(Q) + B_{inc}$$
<div align="right">Equation 5.2</div>

where N_p is the number and V_p the volume of the scattering species, $\Delta\rho$ the difference between the neutron scattering length density (SLD) of the scattering species and the solvent, $P(Q)$ describes the morphology of the scattering species and, $S(Q)$ describes the spatial arrangement of the scatterers in solution, B_{inc} incoherent background.

Chapter 5. HEUR and HEUR/SDS stabilised dodecane emulsion

In this chapter, various contrast-match experiments were performed where the SLD of the d-dodecane was matched to the solvent (92 % D_2O). Therefore, the scattering contribution is from the polymers only in the emulsions. In presence of SDS, two contrasts were performed, in the first contrast the scattering contribution is from the polymer/SDS in the polymer/SDS/dodecane mixtures. The second contrast the scattering contribution is from the polymer only in polymer/d-SDS/dodecane mixtures, where the SLD of SDS was matched to the solvent.

5.4. Results and discussion

Emulsions stabilised by three HEUR polymers of different architecture (hydrophobicity) are studied. The diffusion of the polymers and dodecane droplets are studied in presence and absence of SDS. The scattering from the polymer in HEUR/dodecane, and HEUR/SDS/dodecane mixtures is presented. The phase separated emulsions are studied to track the partitioning of the polymers, SDS, and dodecane in the oil and aqueous phase.

5.4.1. Diffusion NMR analysis of the emulsion
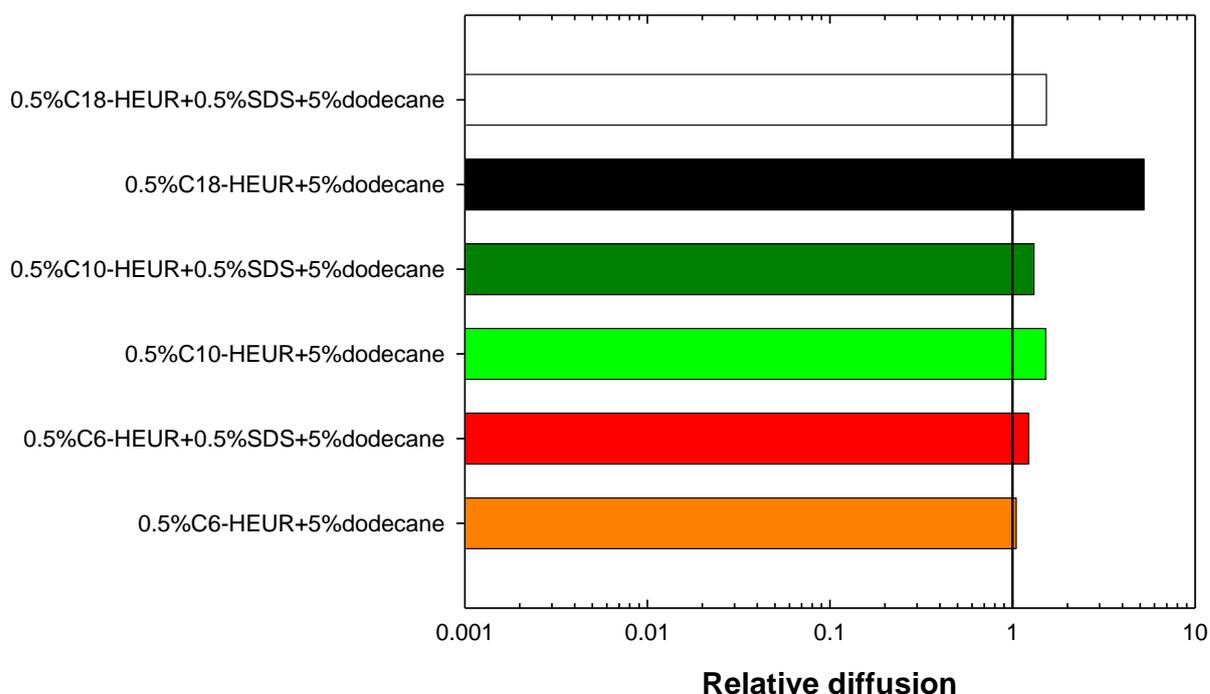
Figure 5.2. Relative diffusion of C_6-L-(EO$_{100}$-L)$_9$-C$_6$ (C$_6$-HEUR) , C_{10}-L-(EO$_{200}$-L)$_4$-C$_{10}$ (C$_{10}$-HEUR), and C_{18}-L-(EO$_{200}$-L)$_7$-C$_{18}$ (C$_{18}$-HEUR) in polymer/dodecane and polymer/SDS/dodecane mixtures. The solid line is to bench mark D_r = 1.

160
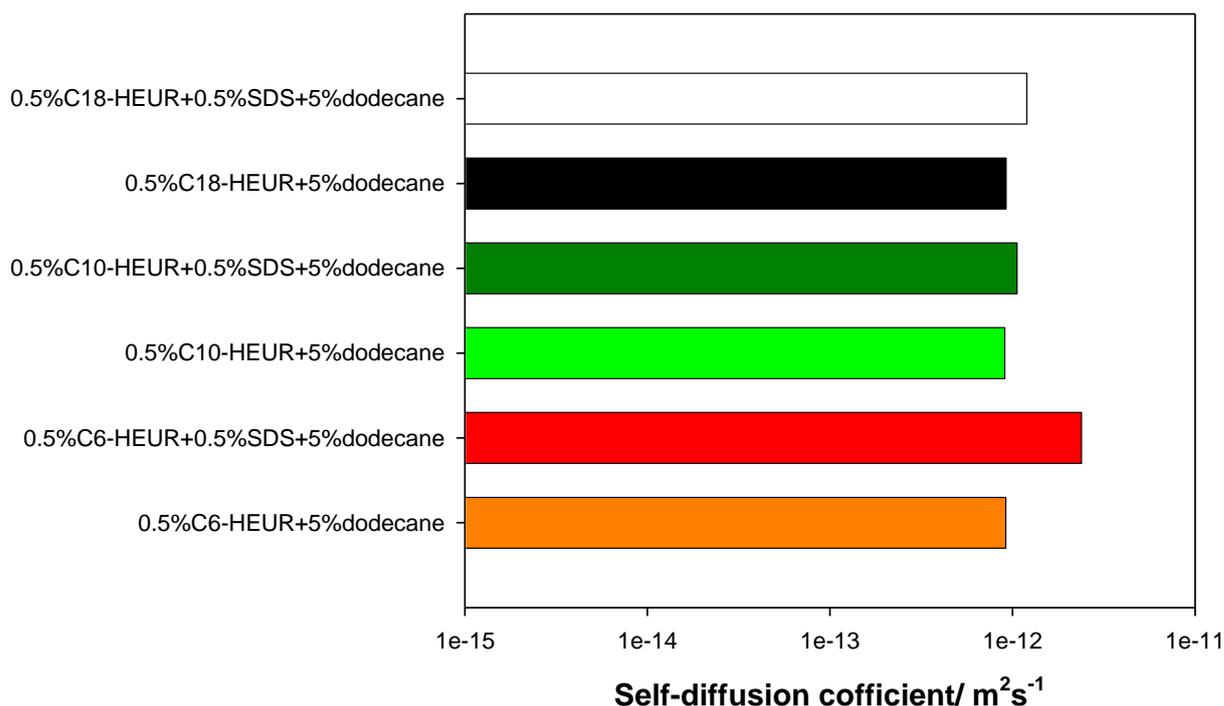
Figure 5.3. Self-diffusion coefficient of dodecane in polymer/dodecane and polymer/SDS/dodecane mixtures, where three polymers were studied C_6-L-(EO_{100}-L)$_9$-C_6 (C_6-HEUR), C_{10}-L-(EO_{200}-L)$_4$-C_{10} (C_{10}-HEUR) , and C_{18}-L-(EO_{200}-L)$_7$-C_{18} (C_{18}-HEUR).

For easier analysis of the polymers diffusion behaviour in the emulsions, the relative diffusion (D_r) of the polymer is presented, where $D_r = \frac{D_{polymer\ in\ emulsion}}{D_{pure\ polymer}}$. If D_r = 1, the diffusion of the polymers is comparable in absence and presence of dodecane, whereas if D_r < 1, the polymer diffuses faster in presence of dodecane. The D_r values for all the polymers are greater than one (Figure 5.2). Therefore the diffusion of the polymer extracted from the EO peak at 3.75 ppm in the emulsion is for the unadsorbed polymer, hence it diffuses faster than the pure polymer at the same concentration. The C_{18}-L-(EO_{200}-L)$_7$-C_{18} show the highest diffusion. This may be explained by the presence of lower concentration of the free polymer in solution. In presence of SDS, the $D_r = \frac{D_{polymer\ in\ emulsion}}{D_{polymer/SDS\ comlex}}$, where the D_r values for the polymer in the emulsion approach unity, except for the C_6-L-(EO_{100}-L)$_9$-C_6. The dodecane droplet has the same diffusion in the presence of the three polymers and in absence and presence of SDS (Figure 5.3), except for the C_6-L-(EO_{100}-L)$_9$-C_6/SDS complex.

161

Chapter 5. HEUR and HEUR/SDS stabilised dodecane emulsion

The dodecane droplets have a diameter of 450 nm calculated from the diffusion coefficients using Stokes-Einstein equation. The presence of the SDS has subtle effect on the droplet size except in the C_6-L-$(EO_{100}$-L$)_9$-C_6 case where the droplet size decreased to half the size 200 nm. This may explain the higher D_f value of the C_6-L-$(EO_{100}$-L$)_9$-C_6/SDS mixture relative to C_6-L-$(EO_{100}$-L$)_9$-C_6 where smaller droplets are formed and hence more surface area is available for the polymer to adsorb.

Bragger-Jorgensen *et al.* studied the diffusion of PEOM-11-18 in pre-stabilised decane/$C_{12}E_6$/water emulsion. The polymer diffusion decreased in the presence of oil droplets (11). Here, the diffusion of the polymer increased in the presence of dodecane. The difference between the results of the two studies may be related to the difference in the two systems. Here, only HEUR is used to stabilise the oil emulsion, it is expected that at concentration of 5 wt% dodecane some polymer chains are adsorbed and some free polymers chains are present in solution. Therefore, the diffusion extracted from the polymer peak represents the diffusion of the free polymer chain, whereas the polymer adsorbed to the oil droplet diffuses at the same speed as the droplet.

5.4.2. SANS analysis of the polymers in the emulsion

Three different contrasts have been carried out to study the emulsion systems, Table 5.1. In the first contrast the SLD of the deuterated dodecane was calculated and matched to the solvent using a mixture of D_2O and H_2O (92 % D_2O), hence the scattering contribution is from the polymer only (polymer/d-dodecane/92% D_2O). The second set of experiments were carried out in presence of d-dodecane, h-polymers and h-SDS in 92 % D_2O, therefore the scattering contribution is from the polymer/SDS complex. Finally, in the third contrast, the scattering from d-dodecane, h/d-SDS, and h-polymer in 92 % D_2O was measured, where only the polymer contributes to the scattered intensity in the mixture. In the three cases the contrast-matching was based on calculating the SLD of the components (d-dodecane and SDS) and mixing the appropriate volumes of deuterated and hydrogenous material (surfactant, solvent) to get the required SLD.

Sample	Components contributing to the scattering and SLD values	Components contrast-matched to the solvent
Polymer/d-dodecane/92% D$_2$O (Figure 5.4 andFigure 5.5)	Polymer C$_6$-L-(EO$_{100}$-L)$_9$-C$_6$, (SLD = 8.3 x 10^{-7} Å^{-2}) C$_{10}$-L-(EO$_{200}$-L)$_4$-C$_{10}$, (SLD = 6.92 x 10^{-7} Å^{-2}) C$_{18}$-L-(EO$_{200}$-L)$_7$-C$_{18}$, (SLD = 1.35 x 10^{-7} Å^{-2})	Dodecane, (SLD = 5.84 x 10^{-6} Å^{-2}) Solvent 92% D$_2$O and 8% H$_2$O mixture, (SLD = 5.84 x 10^{-6} Å^{-2})
Polymer/h-SDS/d-dodecane/92% D$_2$O (Figure 5.6)	Polymer SDS, (SLD = 3.37 x 10^{-7} Å^{-2})	Dodecane, (SLD = 5.84 x 10^{-6} Å^{-2}) Solvent 92% D$_2$O and 8% H$_2$O mixture, (SLD = 5.84 x 10^{-6} Å^{-2})
Polymer/h/d-SDS/d-dodecane/92% D$_2$O (Figure 5.7)	Polymer	Dodecane, (SLD = 5.84 x 10^{-6} Å^{-2}) Solvent 92% D$_2$O and 8% H$_2$O mixture, (SLD = 5.84 x 10^{-6} Å^{-2}) h/d-SDS mixture, (SLD = 5.84 x 10^{-6} Å^{-2})

Table 5.1. Summary of the different contrasts experiments performed on the polymer/dodecane and polymer/SDS/dodecane mixtures.
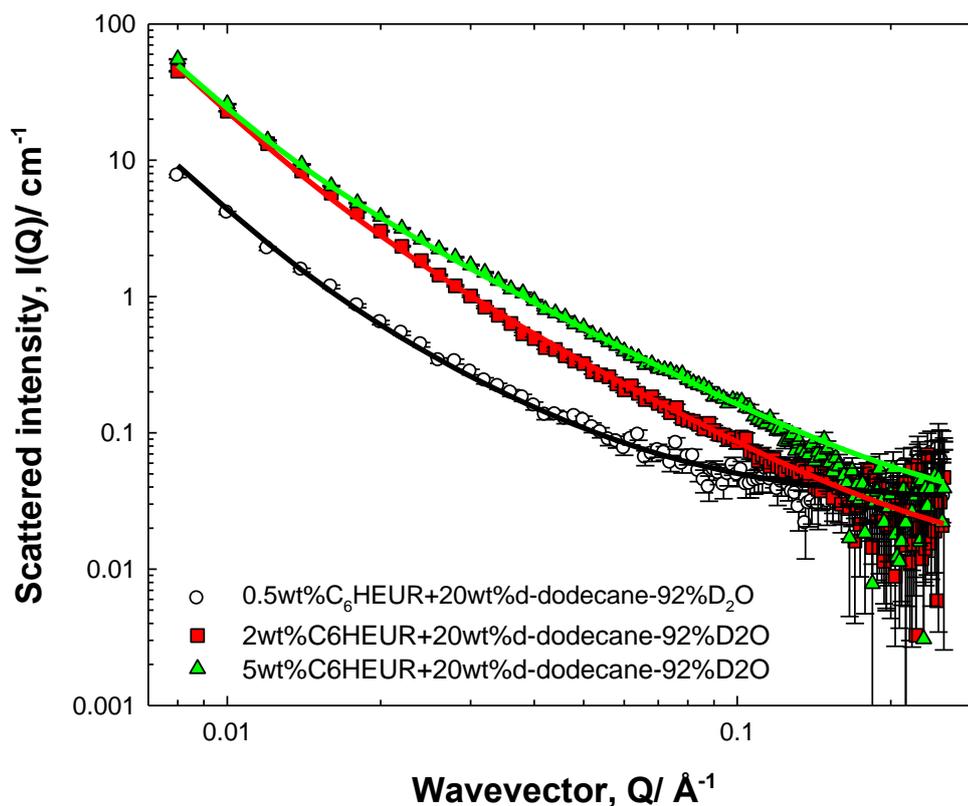
Figure 5.4. Small-angle neutron scattering from 20 wt% d-dodecane in presence of 0.5 (white circles), 2 (red squares), and 5 (green triangles) wt% h-C_6-L-(EO$_{100}$-L)$_9$-C_6 in 92 %(v/v) D$_2$O. Measurements were carried out at 25 °C. The solid lines are fit for sphere and network model. Key fitting parameters value are presented in Table C.1.

In the polymer-only scattering contrast in C_6-L-(EO$_{100}$-L)$_9$-C_6/dodecane mixtures, the intensity of the polymer scattering increases as a function of polymer concentration (Figure 5.4). The scattering of the polymer in absence of dodecane shows a shoulder at Q = 0.02 and 0.03 Å at 2 and 5 wt%, respectively (Figure C.1), the shoulder is lost in presence of dodecane droplet. This indicates the adsorption of the polymer hydrophobes on the oil droplet. This system possess a structure similar to a sphere or a core-shell, however, these models failed to capture the scattering curve features as the oil droplets are very large as detected by the diffusion NMR, 450 nm. Attempts to fit the data sets to polymer adsorbed layer in SasView program (this model describes adsorbed polymer layer on a large sphere where the sphere SLD of the sphere is matched to hat of the solvent) failed. Trials to fit the data sets to a network and sphere model introduced in Chapter 3 Section 3.4.1.4 were more successful, where the latex particles are substituted by the oil droplets. The sphere model is turned off in the polymer only stabilised emulsion.

Chapter 5. HEUR and HEUR/SDS stabilised dodecane emulsion

The key fitting parameters of the sphere and network model are presented in Table C.1. The Lorentzian length intensity increases whereas the Debye-Bueche intensity shows insignificant variation as a function of polymer concentration. The Lorentzian length and Debye-Bueche length are constant as a function of polymer concentration. The increase in the intensity of the Lorentzian length is due to the increased of the polymer concentration. Similar conclusions may be drawn from the C_{10}-L-$(EO_{200}$-L$)_4$-C_{10} and C_{18}-L-$(EO_{200}$-L$)_7$-C_{18} in presence of 20 wt% dodecane (Figure C.2 and C.3), respectively.

Bagger-Jorgensen *et al.* presented the scattering of the PEOM in pre-stabilised emulsions as a function of polymer concentration (11). The scattering data showed evidence of scattering from sphere structure and changes in the scattered intensity at low-Q is observed due to the attractive interaction between the oil droplets. Here, the increase in the scattered intensity at low-Q could be correlated to the formation of bigger structure as the polymer concentration increases.
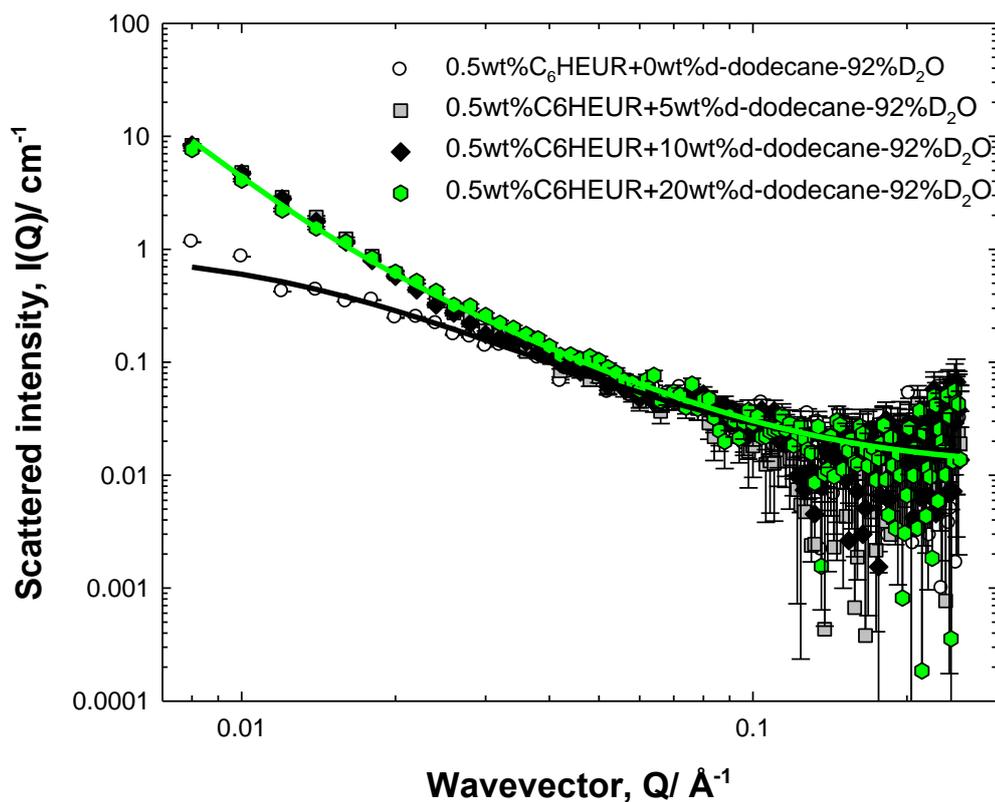
Figure 5.5. Small-angle neutron scattering from 0.5 wt% h-C_6-L-(EO_{100}-L)$_9$-C_6 in absence (white circles) and presence of 5 (grey squares), 10 (black diamonds), and 20 (hexagons) wt% d-dodecane in 92 %(v/v) D_2O. Measurements were carried out at 25 °C. The solid lines are fit for sphere and network model. Key fitting parameters value are presented in Table C.2.

Varying the dodecane concentration induces very subtle changes in the polymer scattering at 0.5 wt% C_6-L-(EO_{100}-L)$_9$-C_6 (Figure 5.5). However, there is a change in the polymer intensity at low-Q in the presence and absence of dodecane, the presence of dodecane increases the scattered intensity at low-Q. The increase in the scattered intensity is reflective of the formation of bigger aggregates. In terms of the fitting, the parameters are presented in Table C.2 where in absence of dodecane only the Lorentzian length is determined whereas the presence of dodecane leads to the introduction of the Debye-Bueche length scale. Similar conclusions may be drawn from the C_{18}-L-(EO_{200}-L)$_7$-C_{18} (Figure C.4), however, in the C_{10}-L-(EO_{200}-L)$_4$-C_{10} the scattered intensity increases at low-Q as a function of dodecane concentration, reflective of the formation of bigger structures (Figure C.5).

Chapter 5. HEUR and HEUR/SDS stabilised dodecane emulsion

The scattering data for the PEOM adsorbed to pre-stabilised decane emulsions as a function of oil concentration is presented by Filali *et al.*, where changes in the scattered intensity are observed at low-Q, reflective of an attractive interaction (10). Varying the oil percentage in the emulsions here had very subtle changes. This might support the hypothesis of the presence of free polymer from the diffusion data at 5 wt% dodecane, where the 0.5 wt% polymer is able to stabilise the dodecane in water up to 20 wt%.
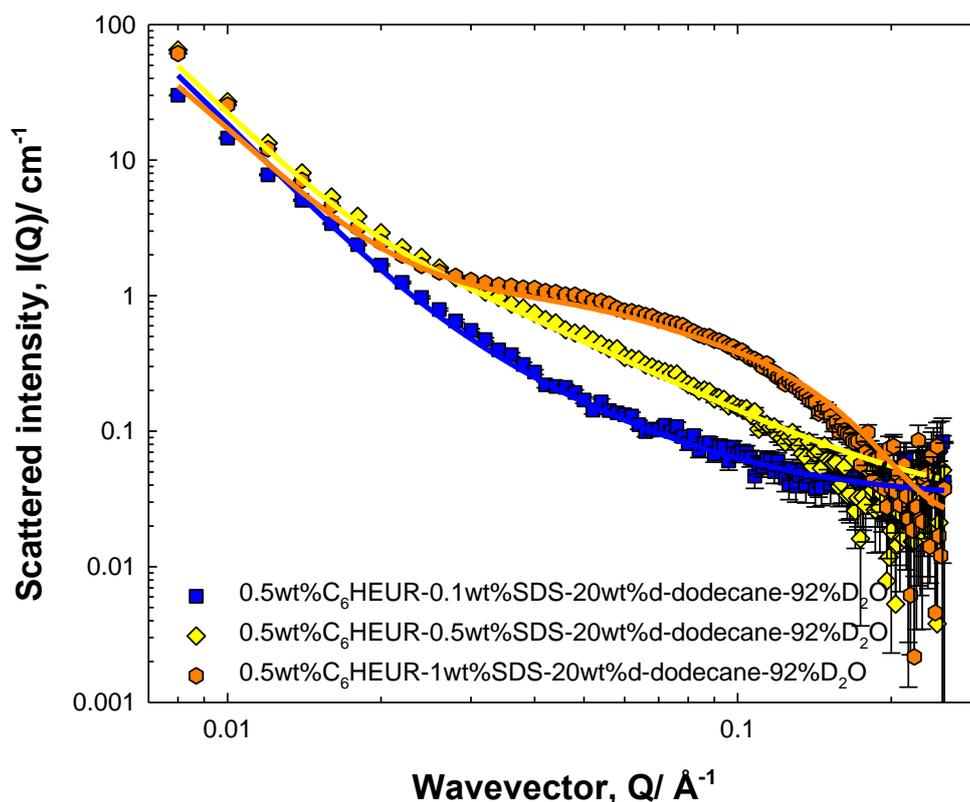
Figure 5.6. Small-angle neutron scattering from 0.5 wt% h-C$_6$-L-(EO$_{100}$-L)$_9$-C$_6$/20 wt% d-dodecane in presence of presence 0.1 (blue squares), 0.5 (yellow diamonds), and 1 (orange hexagons) wt% d-SDS in 92 %(v/v) D$_2$O. Measurements were carried out at 25 °C. The solid lines are fit for sphere and network model. Key fitting parameters value are presented in Table C.3.

The scattering of the polymer/SDS in presence of 20 wt% dodecane is presented in Figure 5.6. The scattered intensity at low-Q increases and micelle-like scattering is observed at Q = 0.07 Å. The data sets were fitted to the sphere and network model, the key parameters are presented in Table C.3. The sphere term is important only at high SDS concentration, where a micelle of 18 Å is formed, this may be explained by the interaction of the SDS micelles with the polymer rather than stabilising the oil droplet as

the oil droplet is 450 nm (from the diffusion data). The Lorentzian length and its intensity decrease as a function of SDS concentration whereas the Debye-Bueche length and its intensity increase. The increase in the Debye-Bueche length scale may reflect larger distances between the oil droplets in presence of SDS, which may be correlated to the electrostatic stabilisation imparted by the presence of SDS in addition to the steric stabilisation of the polymer. Similar conclusions may be drawn from the C_{10}-L-$(EO_{200}$-L$)_4$-C_{10} and C_{18}-L-$(EO_{200}$-L$)_7$-C_{18} in presence of 20 wt% dodecane (Figures C.6 and C.7), respectively.
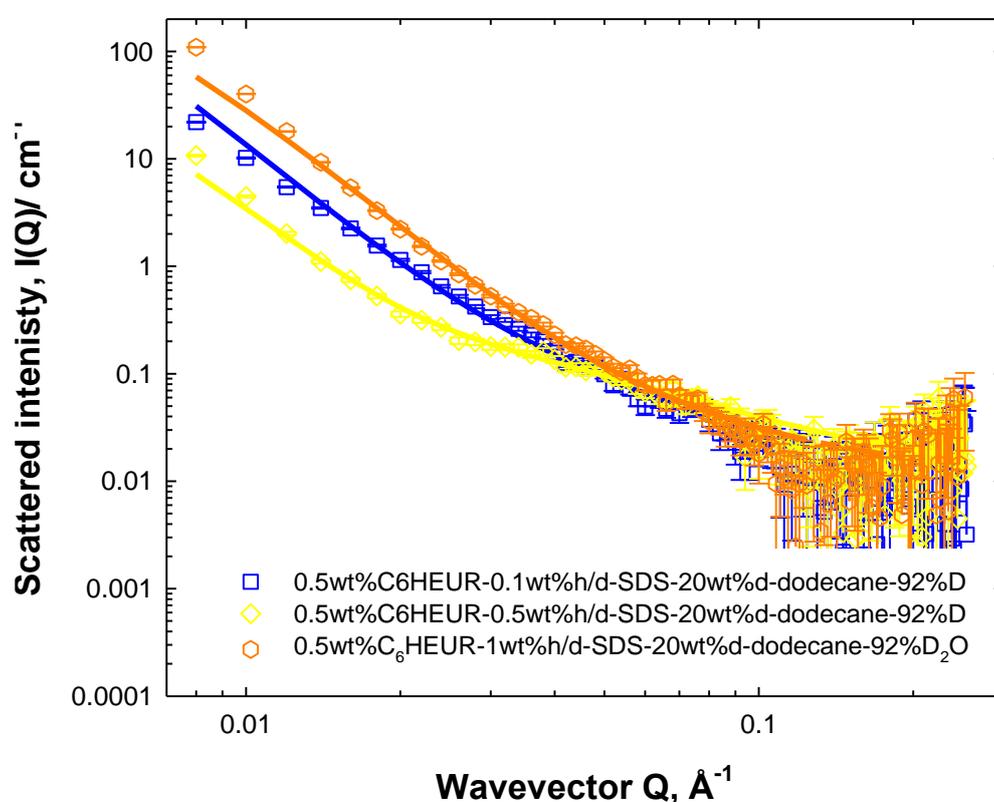
Figure 5.7. Small-angle neutron scattering from 0.5 wt% h-C_6-L-$(EO_{100}$-L$)_9$-C_6/20 wt% d-dodecane in presence of presence 0.1 (blue squares), 0.5 (yellow diamonds), and 1 (orange hexagons) wt% d-SDS in 92 %(v/v) D_2O. Measurements were carried out at 25 °C. The solid lines are fit for sphere and network model. Key fitting parameters value are presented in Table C.4.

In this contrast, the scattering is from the polymer-only in polymer/SDS/dodecane mixture (Figure 5.7). There are changes in the polymer scattering at low-Q as a function of SDS concentration, which is not surprising given there is interaction between the polymer and SDS. The fitting parameters are presented in Table C.4. Here, the parameters show

similar changes in the network length scales as the polymer/SDS contrast, however, the intensities of the length scales are slightly lower. Similar conclusions may be drawn from the C_{10}-L-$(EO_{200}$-L$)_4$-C_{10} and C_{18}-L-$(EO_{200}$-L$)_7$-C_{18} in presence of 20 wt% dodecane (Figures C.8 and C.9), respectively.

5.4.3. ^{1}H NMR studied for the phase separated emulsions

The emulsions stabilised by 0.5 wt% HEURs/SDS/20 wt% dodecane were left for a week where the emulsions phase separated into oil top layer and aqueous bottom layer (Figure 5.8). Samples from the two layers were transferred to NMR tube and the integration of the polymer, SDS, and dodecane peaks detected by ^{1}H NMR was determined relative to chloroform (Figure C.10). The integration values are presented in Table 5.2 for the aqueous phase and Table 5.3 for the oil phase. The values of the polymer, SDS, and dodecane integrals relative to the chloroform peak give information on the partitioning of the polymer, SDS, and dodecane in the two layers of the phase separated emulsion. The integration of the C_{10}-L-$(EO_{200}$-L$)_4$-C_{10} and C_{18}-L-$(EO_{200}$-L$)_7$-C_{18} polymers in presence of SDS are presented in Tables C.5 and C.6 for the aqueous layer and Tables C.7 and C.8 for the oil layer.
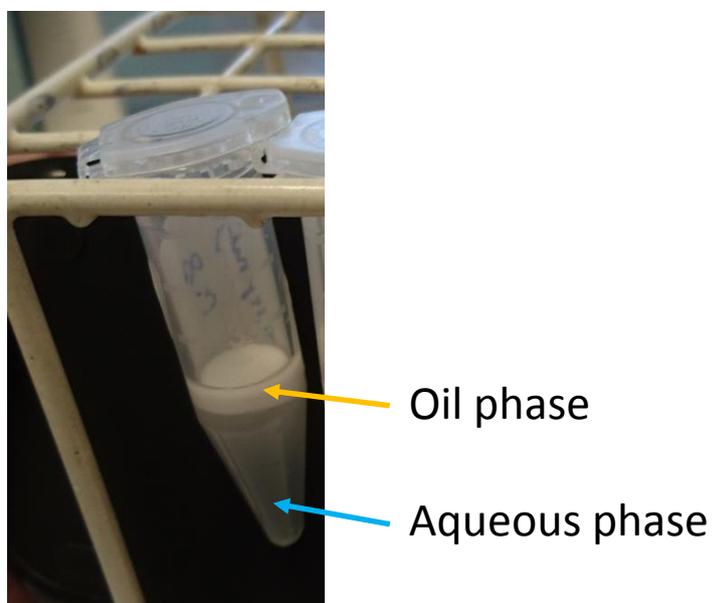
Figure 5.8. Phase separates emulsion into two layers, oil top layer, and aqueous bottom layer.

Sample	Chloroform	SDS ± 0.2	Polymer ± 0.2	Dodecane ± 0.2
5 % SDS/0.5 % polymer	1	6.3	7.3	121
3 % SDS/0.5 % polymer	1	2.8	5	41.4
1 % SDS/0.5 % polymer	1	1	5	14.2
0.1 % SDS/0.5 % polymer	1	n.d.	3	8.1

Table 5.2. Integration of C_6-L-$(EO_{100}$-L$)_9$-C_6, SDS and dodecane peaks relative to the chloroform (external probe) peak in aqueous layer of phase separated emulsions.

Sample	Chloroform	SDS ± 0.2	Polymer ± 0.2	Dodecane ± 0.2
5 % SDS/0.5 % polymer	1	4.5	4.5	251
3 % SDS/0.5 % polymer	1	3	5.5	59
0.5 % SDS/0.5 % polymer	1	n.d.	5.3	322
0.1 % SDS/0.5 % polymer	1	n.d.	6	6814

Table 5.3. Integration of C_6-L-$(EO_{100}$-L$)_9$-C_6, SDS and dodecane peaks relative to the chloroform (external probe) peak in oil layer of phase separated emulsions.

The polymer partitioning in the three-component mixture polymer/SDS/dodecane is higher in the aqueous phase for the C_6-L-$(EO_{100}$-L$)_9$-C_6, C_{10}-L-$(EO_{200}$-L$)_4$-C_{10}, whereas C_{18}-L-$(EO_{200}$-L$)_7$-C_{18} shows higher partitioning in the oil layer, which may be correlated to

the architecture of the polymers. The SDS partitioning is higher in the aqueous phase in presence of C_6-L-$(EO_{100}$-L$)_9$-C_6 and C_{10}-L-$(EO_{200}$-L$)_4$-C_{10} whilst in presence of C_{18}-L-$(EO_{200}$-L$)_7$-C_{18} the SDS partitioning is higher in the oil phase. The dodecane concentration in the aqueous phase is very low, increasing the SDS concentration enhances the solubilisation of dodecane in the aqueous phase. Therefore, the SDS has a synergistic solubilising effect to the polymer. The SDS/polymer interaction is present evidenced by the direct correlation between polymer and SDS partitioning in the aqueous and oil phase.

5.5. Conclusion

Three different HEURs denoted as C_6-L-$(EO_{100}$-L$)_9$-C_6, C_{10}-L-$(EO_{200}$-L$)_4$-C_{10}, and C_{18}-L-$(EO_{200}$-L$)_7$-C_{18} were used to stabilised dodecane/water emulsion in the absence and presence of SDS. The architecture of the polymers and the addition of SDS had very subtle effects on the size of the formed oil droplet. The scattering data showed evidence of stabilisation of the oil droplet in the polymer network structure, where the scattering curves fit to network model in absence of SDS. Consider first the polymer/SDS scattering in polymer/SDS/dodecane mixture, sphere and network model better describes the data where the sphere comes from the SDS micelles adsorbed on the polymer backbone at 1 wt% SDS. The interaction between SDS/polymer is evidenced by changes in the polymer scattering where the scattering of the polymer goes through a minimum as a function of SDS concentration in the polymer only scattering in the polymer/SDS/dodecane mixture. In addition, the phase separated emulsion studies showed a direct correlation between the polymer and SDS partitioning in the aqueous and oil layers, where as the polymer concentration increases in a layer the SDS concentration increases as well. The architecture of the polymers affected the polymer partitioning in the two layers of the phase separated emulsion where the C_{18}-L-$(EO_{200}$-L$)_7$-C_{18} showed higher portioning in the oil layer whereas the C_6-L-$(EO_{100}$-L$)_9$-C_6, and C_{10}-L-$(EO_{200}$-L$)_4$-C_{10} favoured the aqueous layer.

5.6. References

1. Mancuso JR, McClements DJ, Decker EA. The effects of surfactant type, pH, and chelators on the oxidation of salmon oil-in-water emulsions. *J Agric Food Chem.* **1999**;*47*(10):4112–4116.

2. Zaki NN. Surfactant stabilized crude oil-in-water emulsions for pipeline transportation of viscous crude oils. *Colloids Surfaces A Physicochem Eng Asp.* **1997**;*125*(1):19–25.

3. Church J, Paynter DM, Lee WH. In Situ Characterization of oil-in-water emulsions stabilized by surfactant and salt using microsensors. *Langmuir.* **2017**;*33*(38):9731–9739.

4. Qian C, McClements DJ. Formation of nanoemulsions stabilized by model food-grade emulsifiers using high-pressure homogenization: Factors affecting particle size. *Food Hydrocoll.* **2011**;*25*(5):1000–1008.

5. Cheetangdee N, Fukada K. Protein stabilized oil-in-water emulsions modified by uniformity of size by premix membrane extrusion and their colloidal stability. *Colloids Surfaces A Physicochem Eng Asp.* **2012**;*403*:54–61.

6. Dickinson E. Hydrocolloids as emulsifiers and emulsion stabilizers. *Food Hydrocoll.* **2009**;*23*(6):1473–1482.

7. Ashby NP, Binks BP. Pickering emulsions stabilised by Laponite clay particles. *Phys Chem Chem Phys.* **2000**;*2*(24):5640–5646.

8. Binks BP, Lumsdon SO. Pickering emulsions stabilized by monodisperse latex particles: Effects of particle size. *Langmuir.* **2001**;*17*(15):4540–4547.

9. Chevalier Y, Bolzinger MA. Emulsions stabilized with solid nanoparticles: Pickering emulsions. *Colloids Surfaces A Physicochem Eng Asp.* **2013**;*439*:23–34.

10. Filali M, Aznar R, Svenson M, Porte G, Appell J. Swollen Micelles Plus Hydrophobically Modified Hydrosoluble Polymers in Aqueous Solutions: Decoration versus Bridging. A Small Angle Neutron Scattering Study. *J Phys Chem B.* **1999**;*103*(34):7293–7301.

11. Bagger-Jorgensen H, Coppola L, Thuresson K, Olsson U, Mortensen K. Phase

behavior, microstructure, and dynamics in a nonionic microemulsion on addition of hydrophobically end-capped poly(ethylene oxide). *Langmuir.* **1997**;*13*(16):4204–4218.

12.   Causse J, Oberdisse J, Jestin J, Lagerge S. Small-angle neutron scattering study of solubilization of tributyl phosphate in aqueous solutions of L64 pluronic triblock copolymers. *Langmuir.* **2010**;*26*(20):15745–15753.

13.   Stieber F, Eicke HF. Solution of telechelic ionomers in water/AOT/oil (w/o) microemulsions: a static and dynamic light scattering study. *Colloid & Polym Sci.* **1996**;*274*(9):826–835.

14.   Struis RPWJ, Eicke HF. Polymers in complex fluids: Dynamic and equilibrium properties of nanodroplet-ABA block copolymer structures. *J Phys Chem.* **1991**;*95*(15):5989–5996.

15.   Parihar SK, Goswami AK, Raina AM. Stabilization of o/w emulsions by polymer surfactant mixture. *Int J Chem Sci.* **2008**;*6*(1):205–211.

16.   Abrahmsen-Alami S, Stilbs P. NMR Self-Diffusion of associative polymers in aqueous solution: The influence of the hydrocarbon end-chain length on the polymer transport dynamics in single-and two-component mixtures. *J Colloid Interface Sci.* **1997**;*189*(1):137–143.

17.   Claridge TDW. High-Resolution NMR Techniques in Organic Chemistry. Second Edition. Oxford,UK: *Elsevier*; **2009**.

18.   Heenan RK, King SM, Turner DS, Treadgold JR. SANS2d at the ISIS second target station. 17th Meet Int Collab Adv Neutron Sources. **2005**;1–6. Available from: http://www.isis.stfc.ac.uk/instruments/sans2d/publications/sans2d-at-isis10323.pdf (accessed January 2016).

Chapter 6. Summary and recommendation for future work

6. Summary and recommendations for future work

6.1. Summary

In this thesis, the characterisation of the ternary mixture (HEUR/SDS/latex) is built upon an understanding of the different binary interactions (HEUR/SDS and HEUR/latex). Chapter 2, therefore, focused on HEURs/surfactant mixtures where HEURs with different architectures were studied in dilute and concentrated regimes as a function of sodium dodecylsulphate (SDS) concentration. A range of techniques were used to study these systems: surface tension was used to detect the CAC_1 and CAC_2 of the mixture, diffusion NMR data and viscosity tracked the changes in the HEUR solution properties (hydrophobic aggregates, and network structure) as a function of SDS, fluorescence and electron paramagnetic resonance (EPR) spectra were used to assess the hydrophobicity of the HEUR/SDS mixed hydrophobic aggregates, in each technique a different probe is used, thus different information is provided. Finally, a series of SANS contrast variation experiments have been conducted to study the conformation of the HEUR and surfactant in the HEUR/SDS mixture. The dilute regime was studied to validate the experiments and techniques; the work has was then expanded to the more concentrated systems, which has been less studied in literature. Three main conclusions were drawn from this chapter: (a) two binding mechanisms of SDS to HEUR have been detected; (b) polymer conformation changes especially in the dilute regime; and (c) the major viscosity change occurs in the anticooperative binding region of SDS to the HEURs.

Chapter 3 elaborates the behaviour of HEUR in the presence and absence of lattices with different surface chemistries. In this chapter, a classical adsorption isotherm of HEUR/polystyrene-butylacrylate latex (PS-BAL) was studied to quantify the amount of HEUR adsorbed. Solvent relaxation NMR was deployed to study the changes in the surface area of the latex dispersions in the presence of HEUR. Diffusion NMR was used to compare the polymer diffusion in the presence and absence of the latex particles. A series of SANS contrast match experiments were conducted to study the changes in the polymer scattering in the presence of a range of latex concentrations, where deuterated latex (d-PS-h-BAL) was used to enhance the contrast, hence the data quality. Lastly, the rheology of the HEUR/latex systems were measured to study the changes in the viscosity and shear profile as a function of latex concentration. The effect of the latex surface chemistry on HEUR/particle interaction was studied using acrylic acid stabilised

Chapter 6. Summary and recommendation for future work

polystyrene-butylacrylate latex (AA-PS-BAL) which gives more hydrophilic particles. The more hydrophilic latex shows the absence of HEUR adsorption evidenced by the absence of changes in the surface area and particle size distribution of the latex dispersions in the presence of polymer measured by solvent relaxation NMR and DLS, respectively. The absence of changes in polymer diffusion in the absence and presence of latex particles also confirmed that no significant adsorption was present. In the presence of more hydrophobic particles, the HEUR shows very weak adsorption evidenced by changes in the polymer viscosity, diffusion and scattering intensity in the presence of PS-BAL. The more hydrophobic latex particles show changes in the surface area in the presence of polymer.

In Chapter 4, solvent relaxation was used to study the effect of HEUR/SDS on the surface area of the latex dispersion. The diffusion NMR, rheology and SANS data provided information on the changes in the HEUR/SDS solution behaviour in the presence of latex particles. The presence of SDS weakened the adsorption of the HEUR to the latex. This conclusion is supported by the subtle changes in the diffusion coefficient, viscosity, and scattering curves of the polymer/SDS mixture in the presence of latex, relative to their absence. Therefore the interaction between the HEUR/SDS is stronger than that of the HEUR/latex.

Chapter 5 studied the adsorption of HEURs with different architectures and hence hydrophobicity at liquid/liquid interface in presence and absence of SDS. The HEURs are used as model systems for stabilising oil (dodecane) in cosmetic and transdermal formulations. Diffusion NMR was used to calculate the size of oil droplets and change in polymer diffusion in the presence and absence of oil and SDS. SANS contrast experiments were designed so that the scattering contribution is from the polymer only. The oil droplets are stabilised in the polymer network evidenced by the scattering data were the data sets fits to network model. The phase-separated systems were employed to study the affinity of the polymer and SDS to the water and oil layer using ^{1}H NMR. From the studies of the phase-separated emulsion stabilised by C_{18}-L-(EO_{200}-L)$_7$-$C_{18,}$ the polymer favours the oil phase, whilst C_{10}-L-(EO_{200}-L)$_4$-C_{10} and C_6-L-(EO_{100}-L)$_9$-C_6 polymers favour the aqueous phase. In the presence of SDS, the concentration of SDS in the phase-separated samples is higher in the polymer rich layer, which may be correlated to the preferential interaction of the SDS with the HEUR. Evidence of SDS

interaction with the polymer was observed in the scattering data, where the polymer scattering pattern vary as a function of SDS concentration.

6.2. Recommendations for future work

The main focus of this thesis was to study and elucidate the key interactions in a model formulation. The systems studied here are mainly two or three component ones. However, actual formulations are more complex and contain more components than the systems studied here. To gain better understanding for these complex formulations the interactions of the components in simpler model formulations were studied.

In Chapter 2, though it was pointed out that the urethane linkers affect the behaviour and interaction of the HEUR with SDS, more defintive conclusions would be drawn if the PEO molecular weight and hydrophobic end-group length are kept constant. The number and distribution of the urethane linkers can be varied to study their effect on the polymer behaviour and interactions with the surfactant and latex, relative to parent unmodified PEO, PEOM, and PEO modified with urethane linkers only without the terminal hydrophobic end-group. In addition, usually a mixture of surfactants are used in formulations. It would be useful to study the interaction of two surfactants in solution and their ability to form a mixed micelle, then HEUR interaction with surfactants mixtures can be investigated.

In Chapter 3, it has been demonstrated that the size of the deuterated polystyrene-butylacrylated latex (PS-BAL) particles used in the experiment are large. Therefore the scattering from the particle plus the polymer adsorbed layer cannot be observed in the SANS2D instrument window. It is recommended to replicate the experiment at lower Q ranges where the larger structure can be observed *e.g.* SESANS experiment on the Lamour instrument at the ISIS scattering facility.

Of course this study is still inherently simple as a typical paint formulations contain different particle types and a range of surfactants.

Appendix A.

A. Supplemental figures and tables for Chapter 2
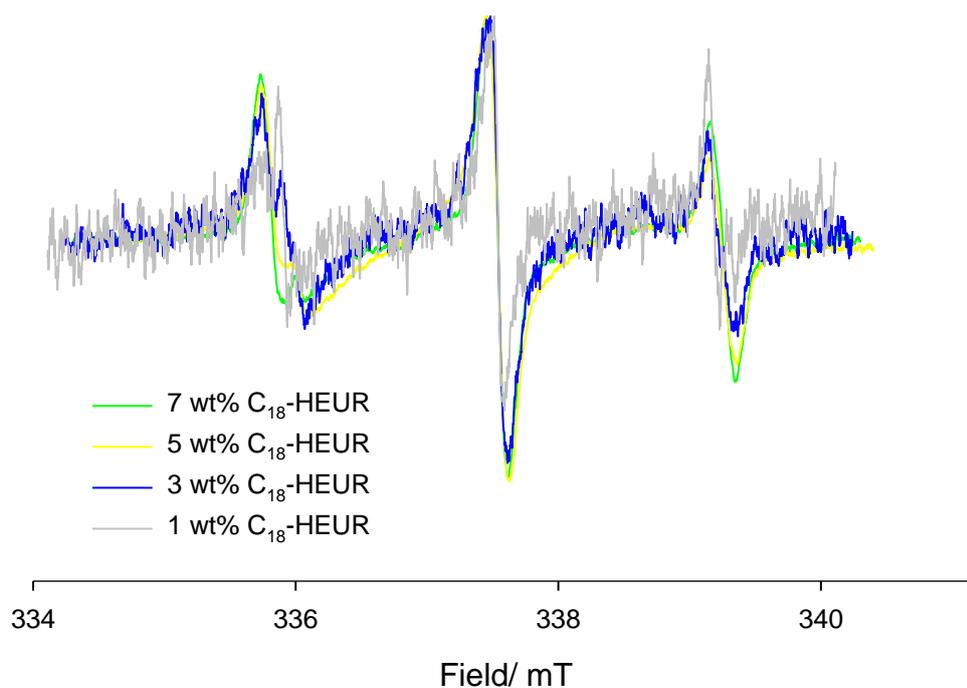
Figure A.1. EPR spectrum for 16-DSE in the presence of 1 (grey line), 3 (blue line), 5 (yellow line), and 7 (green line) wt% C_{18}-L-(EO$_{200}$-L)$_7$-C_{18}. Measurements were carried out at 25 °C, pH 9, and ionic strength 100 mM.
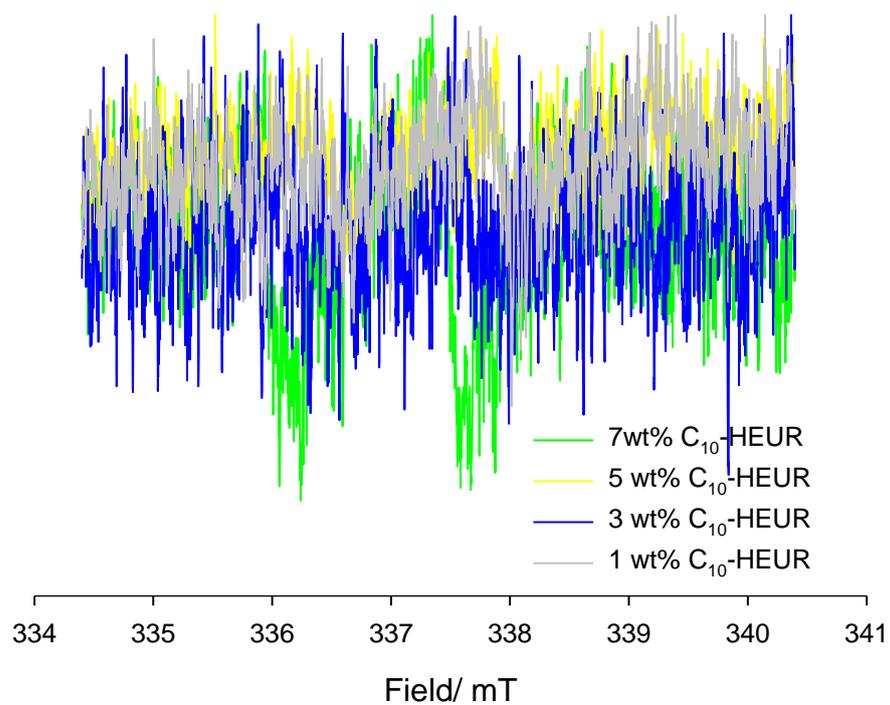
Figure A.2. EPR spectrum for 16-DSE in the presence of 1 (grey line), 3 (blue line), 5 (yellow line), and 7 (green line) wt% C_{10}-L-(EO$_{200}$-L)$_4$-C$_{10}$. Measurements were carried out at 25 °C, pH 9, and ionic strength 100 mM.
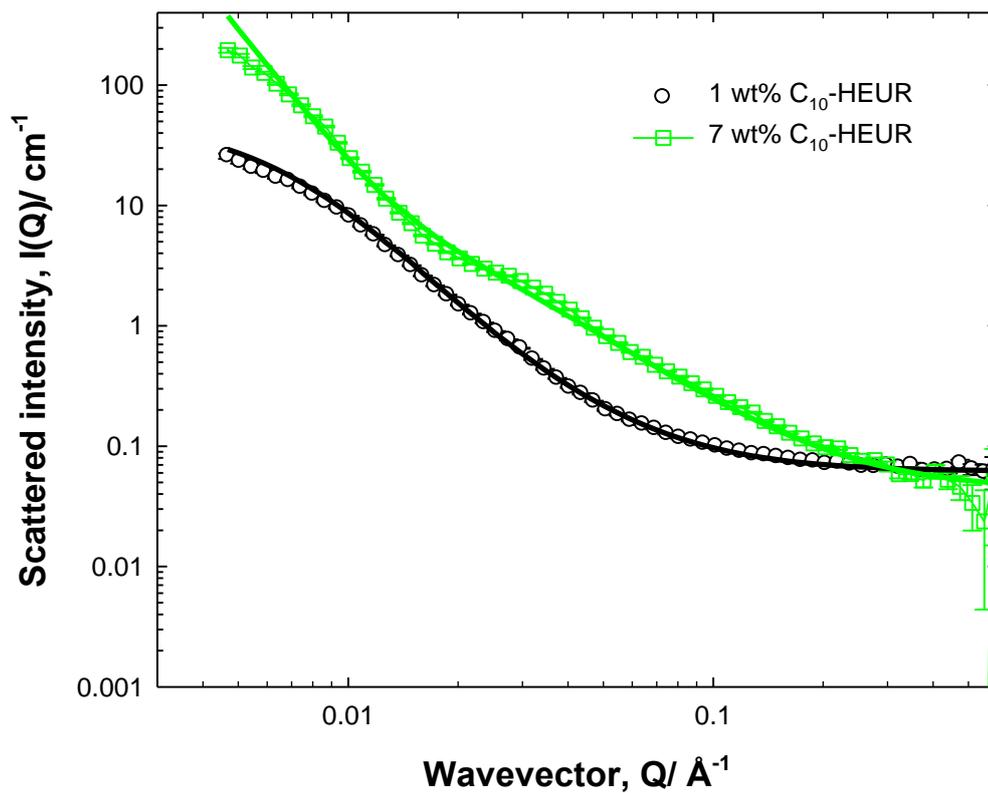
Figure A.3. Small-angle neutron scattering from h-C_{10}-L-(EO_{100}-L)$_4$-C_{10}/D_2O at 1 (circles) and 7 (rectangles) wt% polymer. Measurements were carried out at 25 °C, pH 9, and ionic strength 100 mM. The solid lines are fit for sphere and gel model.
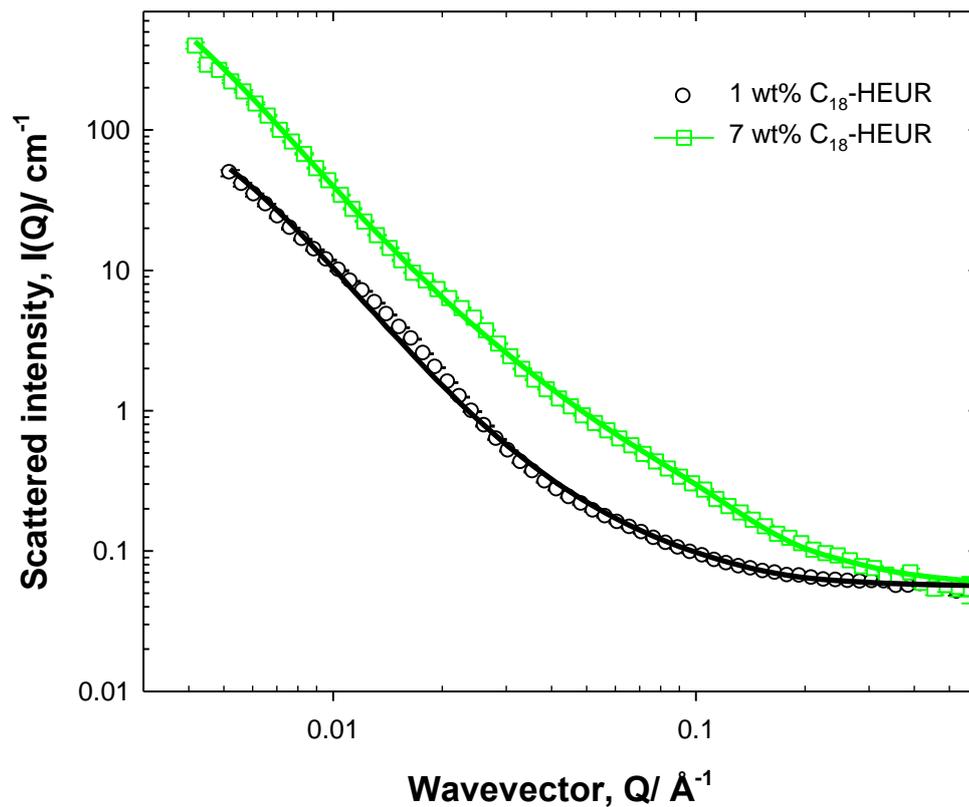
Figure A.4. Small-angle neutron scattering from h-C_{18}-L-(EO$_{100}$-L)$_7$-C_{100}/D$_2$O at 1 (circles) and 7 (rectangles) wt% polymer. Measurements were carried out at 25 °C, pH 9, and ionic strength 100 mM. The solid lines are fit for sphere and gel model.

Appendix A.

Fit parameters/ Units	1 % HEUR + 0 % SDS	1 % HEUR + 0.1 % SDS
Intensity of radius term	7.9×10^{-8}	3.4×10^{-6}
Radius (Å)	20 ± 2	74 ± 4
e	n.d.	n.d.
K^{-1} (Å)	n.d.	n.d.
φ	0.01	0.07
l_1	1.7	2.6
ξ (Å)	73 ± 3	33 ± 2
l_2	34	2680
A (Å)	120 ± 2	320 ± 5

Table A.1. SANS key parameters from the sphere and network model for C_{10}-L-$(EO_{200}$-L$)_4$-C_{10} at $C_{polymer}$ = 1 and 7 wt%.

Fit parameters/ Units	1 % HEUR + 0 % SDS	7 % HEUR + 0 % SDS
Intensity of radius term	9.3×10^{-7}	1.2×10^{-6}
Radius (Å)	20 ± 2	70 ± 5
e	n.d.	n.d.
K^{-1} (Å)	n.d.	n.d.
φ	0.01	0.07
l_1	0.6	8.9
ξ (Å)	53 ± 3	66 ± 3
l_2	153	1106
A (Å)	160 ± 2	217 ± 5

Table A.2. SANS key parameters from the sphere and network model for for C_{18}-L-$(EO_{200}$-L$)_7$-C_{18} at $C_{polymer}$ = 1 and 7 wt%.
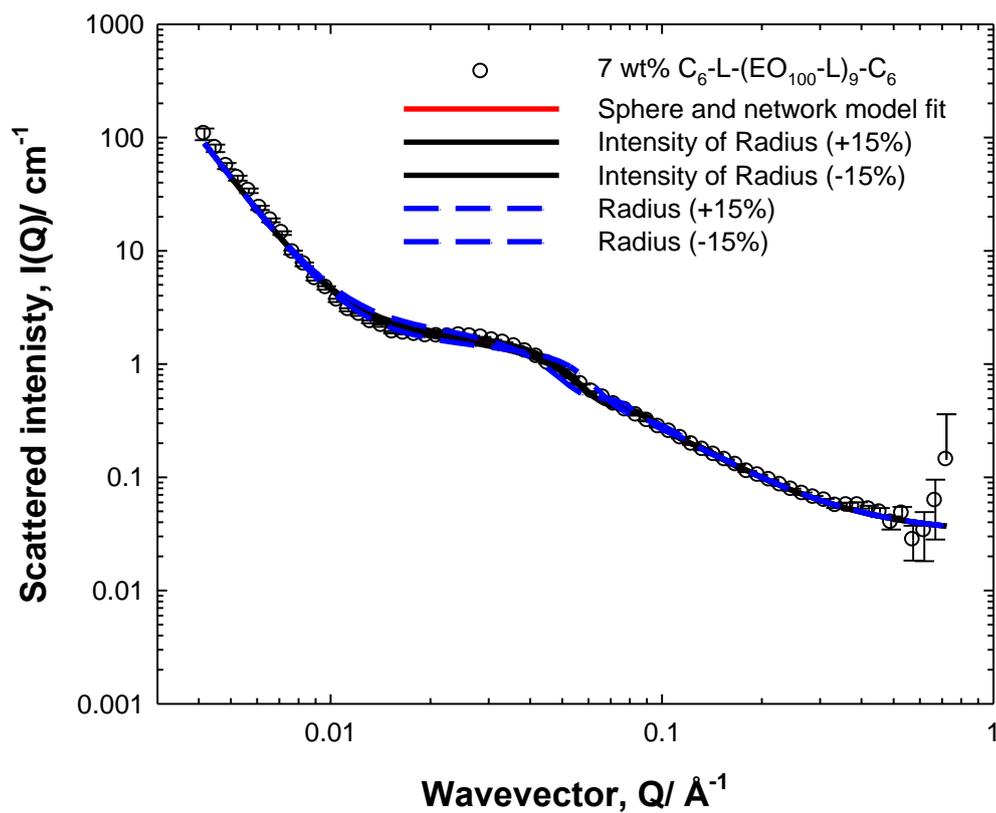
Figure A.5. Sensitivity of the sphere and network model fit to changing the sphere form factor parameters.
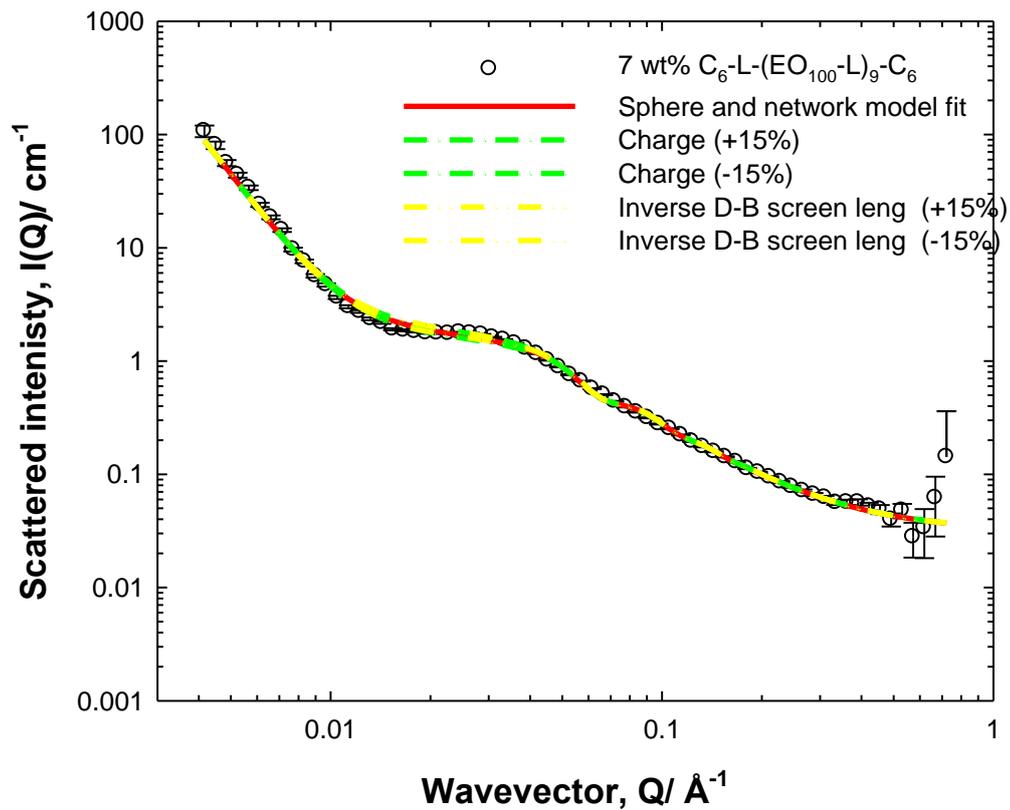
Figure A.6. Sensitivity of the sphere and network model fit to changing the sphere structure factor parameters.
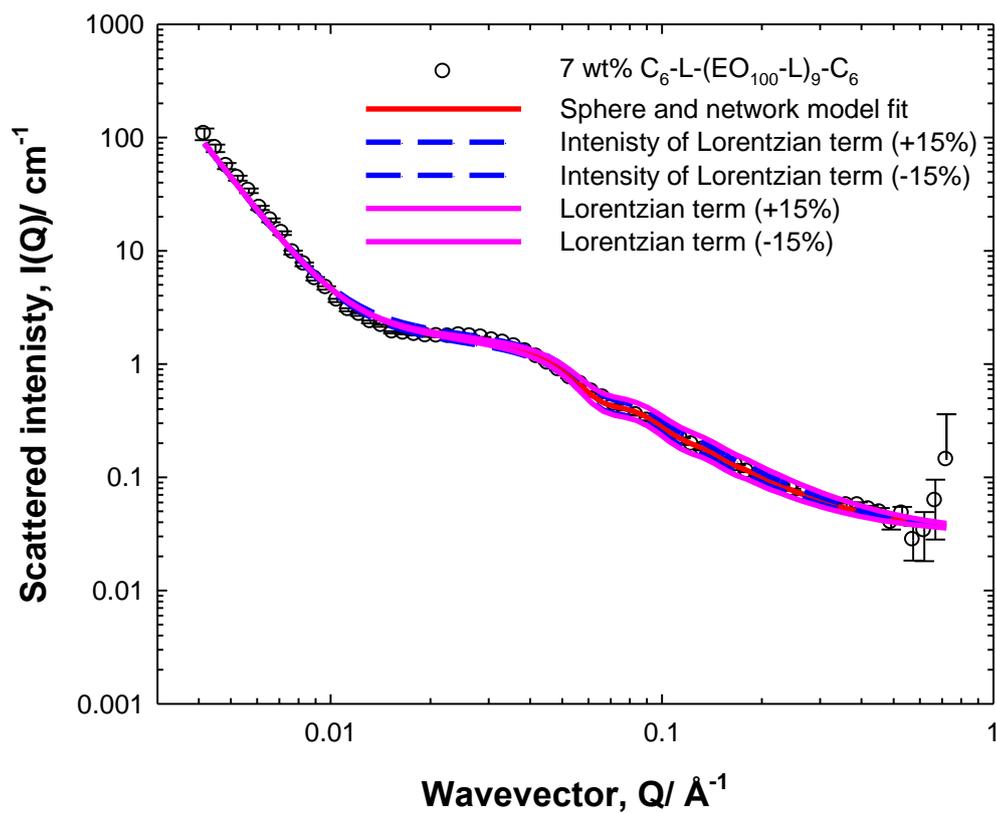
Figure A.7. Sensitivity of the sphere and network model fit to changing the network form factor parameters, Lorentzian term.
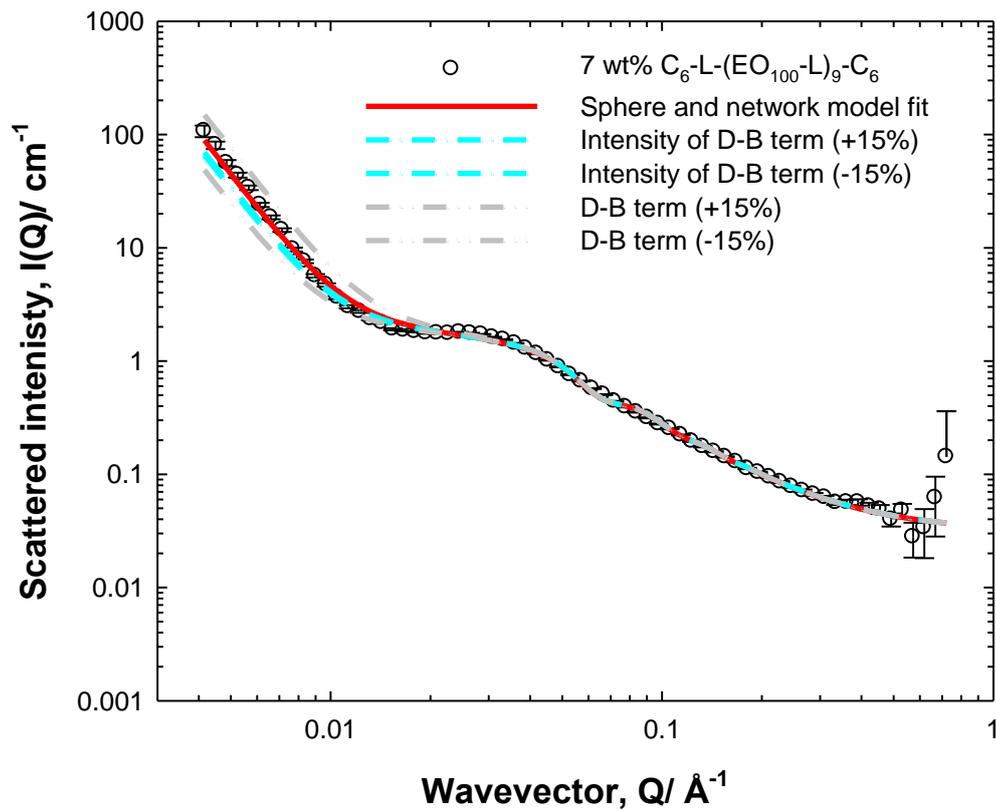
Figure A.8. Sensitivity of the sphere and network model fit to changing the network form factor parameters, Debye-Bueche term.
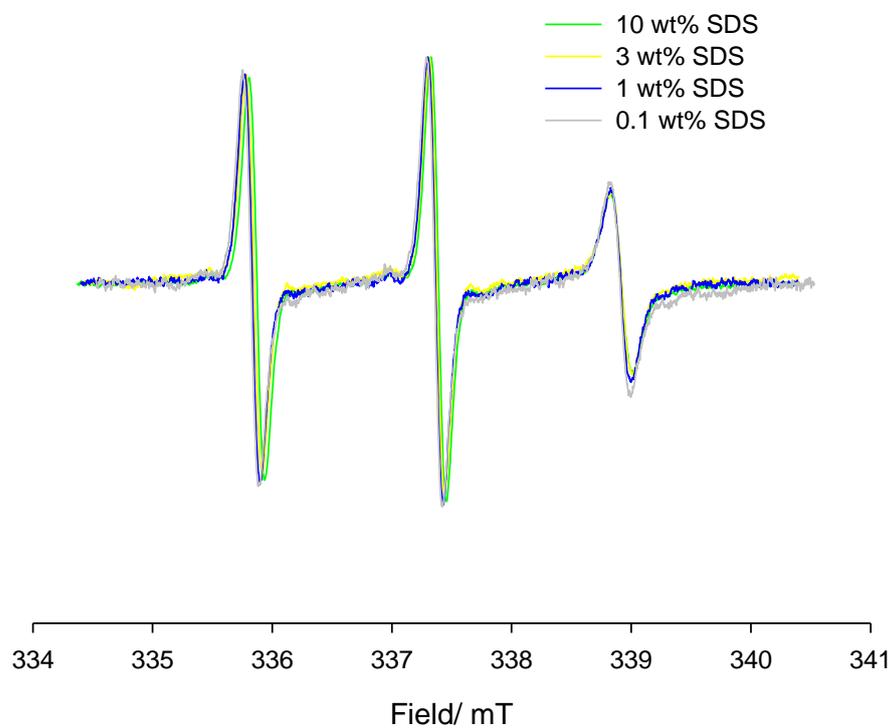
Figure A.9. EPR spectrum for 16-DSE in the presence 0.1 (grey line), 1 (blue line), 3 (yellow line), and 10 (green line) wt% SDS. Measurements were carried out at 25 °C, pH 9, and ionic strength 100 mM.

Fit parameters/ Units	1 % SDS	3 % SDS
Intensity of radius term	2.4×10^{-5}	7.8×10^{-5}
Radius (Å)	21 ± 2	21 ± 2
e	0.5	10
K^{-1} (Å)	0.27	0.23
φ	0.01	0.03

Table A.3. SANS key parameters from the charged sphere model for SDS.
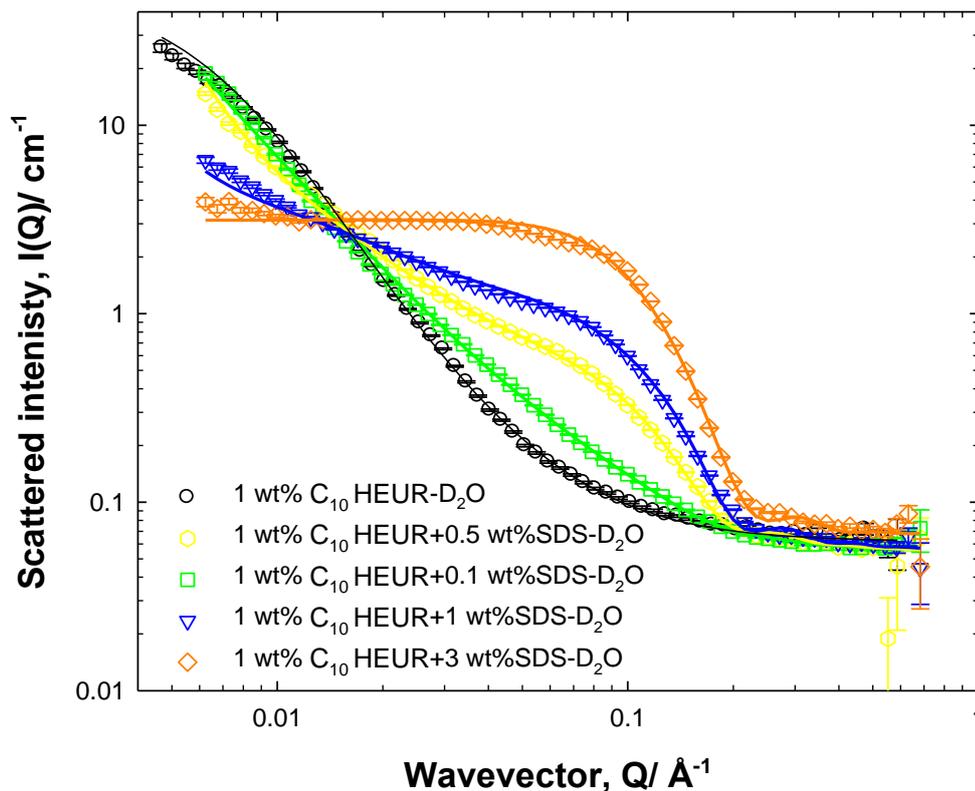
Figure A.10. Small-angle neutron scattering from h-C$_{10}$-L-(EO$_{200}$-L)$_4$-C$_{10}$/h-surfactant/D$_2$O; $C_{polymer}$ = 1 wt% with SDS 0 (circles), 0.1 (squares), 0.5 (hexagons), 1 (triangles) and 3 (diamonds) wt% (last three points have been omitted for clarity). The scattering contribution is from the polymer/SDS in polymer/SDS blend. Measurements were carried out at 25 °C, pH 9, and ionic strength 100 mM. The solid lines are fits for sphere and gel model. Key fitting parameters value are presented in Table A.4.
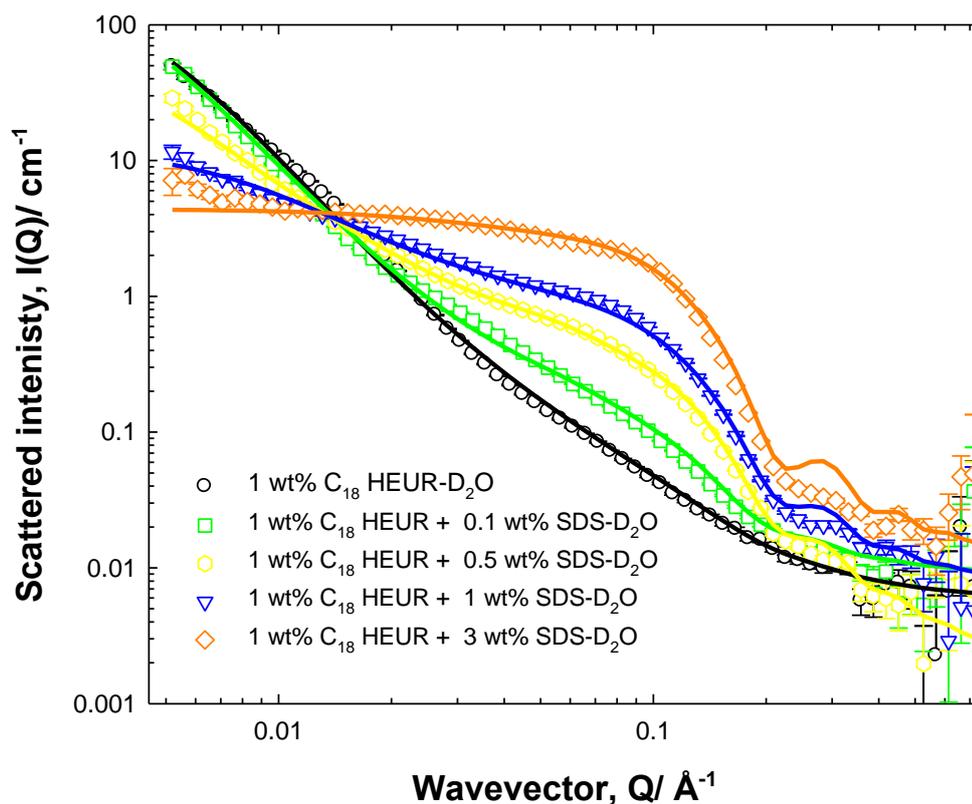
Figure A.11. Small-angle neutron scattering from h-C$_{18}$-L-(EO$_{200}$-L)$_7$-C$_{18}$/h-surfactant/D$_2$O; $C_{polymer}$ = 1 wt% with SDS 0 (circles), 0.1 (squares), 0.5 (hexagons), 1 (triangles) and 3 (diamonds) wt% (last three points have been omitted for clarity). The scattering contribution is from the polymer/SDS in polymer/SDS blend. Measurements were carried out at 25 °C, pH 9, and ionic strength 100 mM. The solid lines are fits for sphere and gel model. Key fitting parameters value are presented in Table A.7.
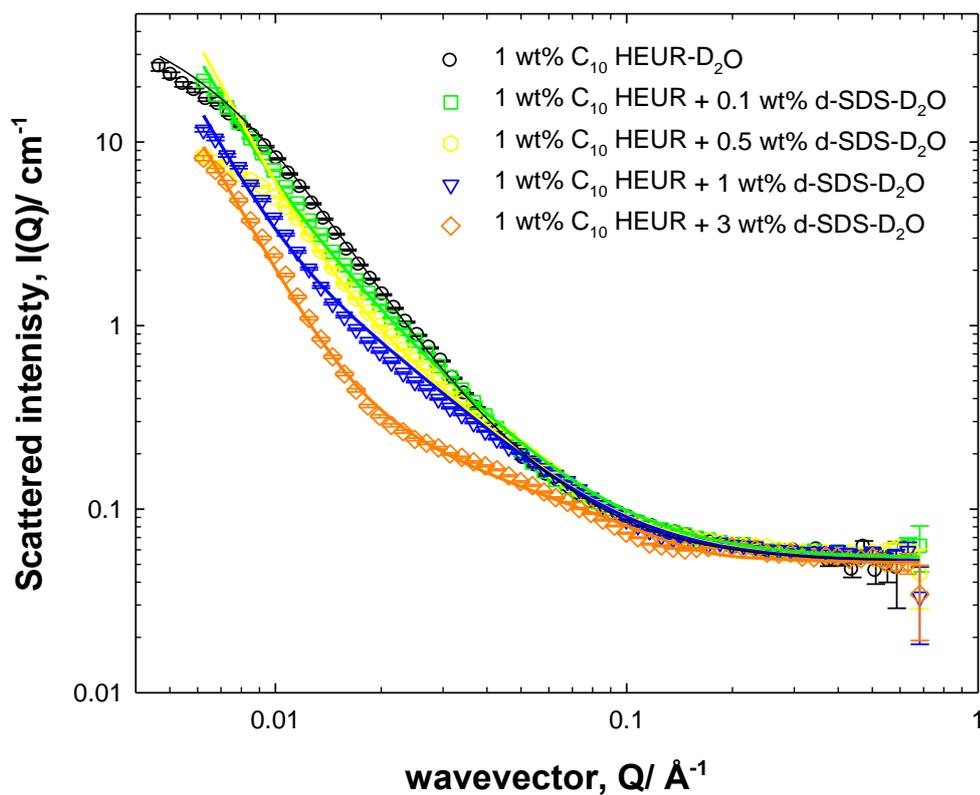
Figure A.12. Small-angle neutron scattering from h-C$_{10}$-L-(EO$_{200}$-L)$_4$-C$_{10}$/d-surfactant/D$_2$O; $C_{polymer}$ = 1 wt% with SDS 0 (circles), 0.1 (squares), 0.5 (hexagons), 1 (triangles) and 3 (diamonds) wt% (last three points have been omitted for clarity). The scattering contribution is from the polymer only in polymer/SDS blend. Measurements were carried out at 25 °C, pH 9, and ionic strength 100 mM. The solid lines are fits for sphere and gel model. Key fitting parameters value are presented in Table A.5.
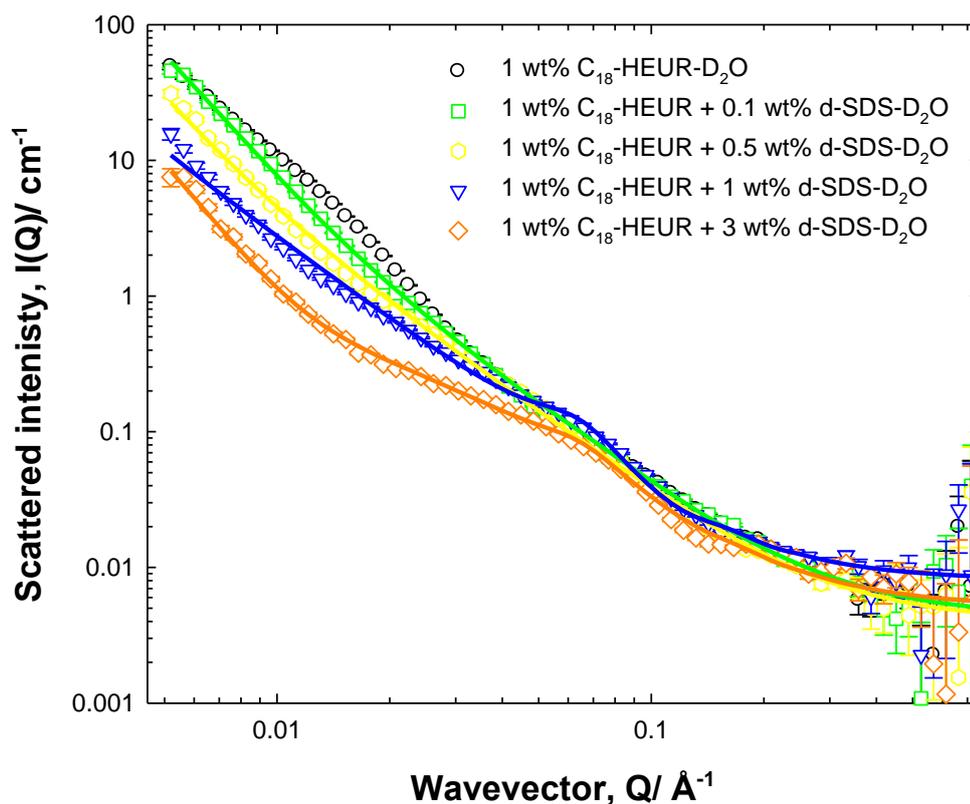
Figure A.13. Small-angle neutron scattering from h-C$_{18}$-L-(EO$_{200}$-L)$_7$-C$_{18}$/d-surfactant/D$_2$O; $C_{polymer}$ = 1 wt% with SDS 0 (circles), 0.1 (squares), 0.5 (hexagons), 1 (triangles) and 3 (diamonds) wt% (last three points have been omitted for clarity). The scattering contribution is from the polymer only in polymer/SDS blend. Measurements were carried out at 25 °C, pH 9, and ionic strength 100 mM. The solid lines are fits for sphere and gel model. Key fitting parameters value are presented in Table A.8.
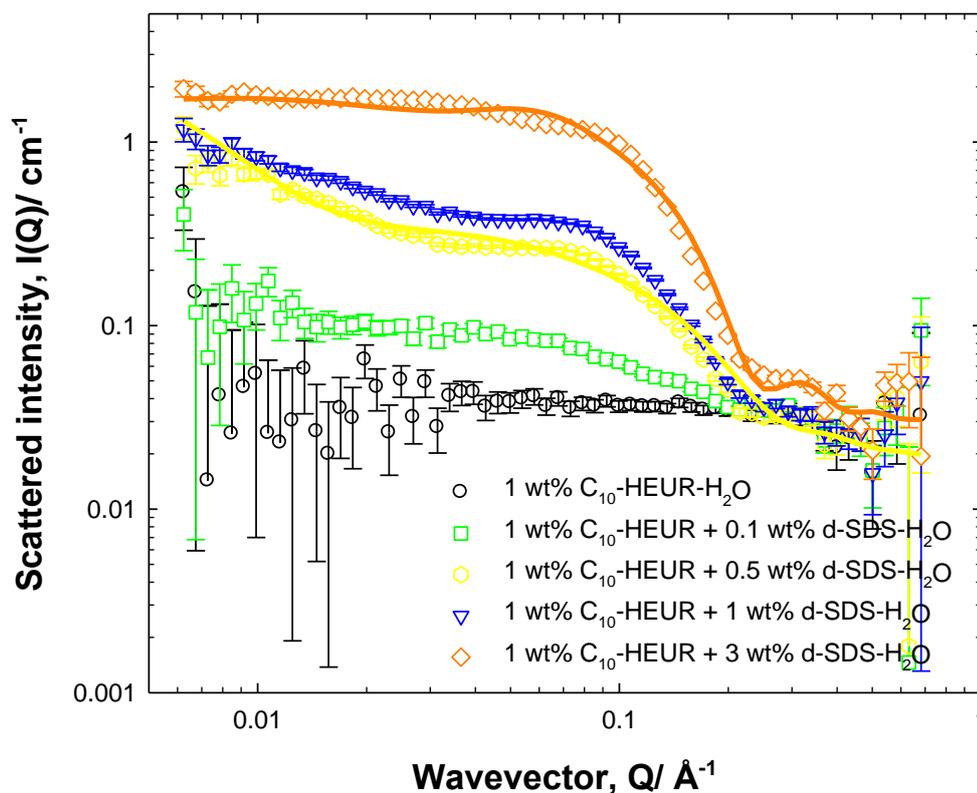
Figure A.14. Small-angle neutron scattering from h-C₁₀-L-(EO₂₀₀-L)₄-C₁₀ /d-surfactant/H₂O; $C_{polymer}$ = 1 wt% with 0 (circles), 0.1 (squares), 0.5 (hexagons), 1 (triangles) and 3 (diamonds) wt% (last three points have been omitted for clarity0. The scattering contribution is from the SDS only in polymer/SDS blend. Measurements were carried out at 25 °C, pH 9, and ionic strength 100 mM. The solid lines are fits for sphere and gel model. Key fitting parameters value are presented in Table A.6.
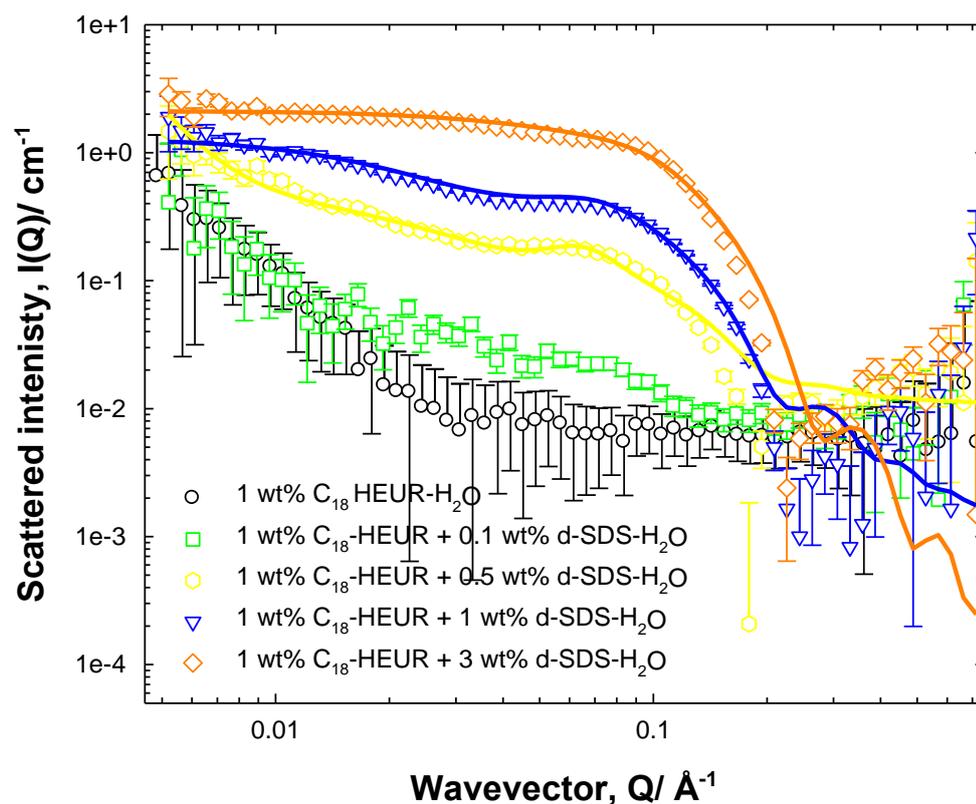
Figure A.15. Small-angle neutron scattering from h-C_{18}-L-$(EO_{200}$-L$)_7$-C_{18}/d-surfactant/H_2O; $C_{polymer}$ = 1 wt% with SDS 0 (circles), 0.1 (squares), 0.5 (hexagons), 1 (triangles) and 3 (diamonds) wt% (last three points have been omitted for clarity). The scattering contribution is from the SDS only in polymer/SDS blend. Measurements were carried out at 25 °C, pH 9, and ionic strength 100 mM. The solid lines are fits for sphere and gel model. Key fitting parameters value are presented in Table A.9.

Appendix A.

Fit parameters/ Units	1 % HEUR + 0 % SDS	1 % HEUR + 0.1 % SDS	1 % HEUR + 0.5 % SDS	1 % HEUR + 1 % SDS	1 % HEUR + 3 % SDS
Intensity of radius term	7.9×10^{-8}	9.9×10^{-7}	8.5×10^{-6}	2.7×10^{-5}	5.3×10^{-5}
Radius (Å)	20 ± 2	20 ± 2	20 ± 2	20 ± 1	20 ± 1
e	n.d.	n.d.	n.d.	10	10
K^{-1} (Å)	0.3	0.29	0.28	0.27	0.23
φ	0.01	0.011	0.015	0.02	0.04
l_1	1.7	1.7	1.7	1.7	2.5
ξ (Å)	73 ± 2	50 ± 2	50 ± 2	40 ± 2	38 ± 2
l_2	34	34	20	5.72	n.d.
A (Å)	120 ± 2	120 ± 2	100 ± 2	100 ± 2	n.d.

Table A.4. SANS key parameters from the sphere and network model for h-C_{10}-L-(EO_{200}-L)$_4$-C_{10}/h-SDS/D_2O $C_{polymer}$ = 1 wt%.

Appendix A.

Fit parameters/ Units	1 % HEUR + 0 % SDS	1 % HEUR + 0.1 % SDS	1 % HEUR + 0.5% SDS	1 % HEUR + 1 % SDS	1 % HEUR + 3 % SDS
Intensity of radius term	7.9×10^{-8}	n.d.	n.d.	n.d.	n.d.
Radius (Å)	20 ± 2	n.d.	n.d.	n.d.	n.d.
e	n.d.	n.d.	n.d.	10	10
K^{-1} (Å)	0.3	0.29	0.28	0.27	0.23
φ	0.01	0.011	0.015	0.02	0.04
l_1	1.7	1.0	1.7	0.5	0.5
ξ (Å)	73 ± 2	50 ± 2	50 ± 2	36 ± 2	30 ± 2
l_2	34	34	20	5	186
A (Å)	120 ± 2	120 ± 2	100 ± 2	165 ± 2	300 ± 2

Table A.5. SANS key parameters from the sphere and network model for h-C_{10}-L-(EO$_{200}$-L)$_4$-C$_{10}$/d-SDS/D$_2$O $C_{polymer}$ = 1 wt%.

Appendix A.

Fit parameters/ Units	1 % HEUR + 0.5 % SDS	1 % HEUR + 1 % SDS	1 % HEUR + 3 % SDS
Intensity of radius term	1.09×10^{-6}	1.6×10^{-6}	6.0×10^{-6}
Radius (Å)	18	17	18
e	0	10	10
K^{-1} (Å)	0.28	0.27	0.23
φ	0.015	0.02	0.04
l_1	0.6	0.6	1.38
ξ (Å)	50 ± 2	38 ± 2	35 ± 2
l_2	1.2	0.9	n.d.
A (Å)	100 ± 5	100 ± 5	n.d.

Table A.6. SANS key parameters from the sphere and network model for h-C_{10}-L-(EO$_{200}$-L)$_4$-C$_{10}$/d-SDS/H$_2$O $C_{polymer}$ = 1 wt%.

it parameters/ Units	1 % HEUR + 0 % SDS	1 % HEUR + 0.1 % SDS	1 % HEUR + 0.5 % SDS	1 % HEUR + 1 % SDS	1 % HEUR + 3 % SDS
Intensity of radius term	9.3×10^{-6}	2.0×10^{-6}	1.3×10^{-5}	1.9×10^{-5}	5.9×10^{-5}
Radius (Å)	20 ± 1	20 ± 1	21 ± 1	20 ± 1	20 ± 1
e	n.d.	n.d.	n.d.	10	10
K-1 (Å)	0.3	0.29	0.28	0.27	0.23
φ	0.01	0.011	0.015	0.02	0.04
l_1	0.6	1.3	1.5	1.5	1.5
ξ (Å)	53 ± 2	42 ± 2	42 ± 2	35 ± 2	30 ± 2
l_2	153	93	24	9.7	n.d.
A (Å)	160 ± 2	160 ± 2	120 ± 2	87 ± 2	n.d.

Table A.7. SANS key parameters from the sphere and network model for h-C_{18}-L-(EO$_{200}$-L)$_7$-C$_{18}$/h-SDS/D$_2$O $C_{polymer}$ = 1 wt%.

Appendix A.

Fit parameters/ Units	1 % HEUR + 0 % SDS	1 % HEUR + 0.1 % SDS	1 % HEUR + 0.5 % SDS	1 % HEUR + 1 % SDS	1 % HEUR + 3 % SDS
Intensity of radius term	9.3×10^{-7}	2.6×10^{-8}	2.6×10^{-8}	8.3×10^{-7}	4.6×10^{-6}
Radius (Å)	20 ± 1	20 ± 1	20 ± 1	30 ± 1	30 ± 1
e	0	0	0	10	10
K^{-1} (Å)	0.3	0.29	0.28	0.27	0.23
φ	0.01	0.011	0.015	0.02	0.04
l_1	0.6	0.6	0.64	0.17	0.34
ξ (Å)	53 ± 2	44 ± 2	40 ± 2	26 ± 2	34 ± 2
l_2	93	70	21	3.4	39
A (Å)	123 ± 2	123 ± 2	120 ± 2	58 ± 2	230 ± 2

Table A.8. SANS key parameters from the sphere and network model for h-C_{18}-L-(EO$_{200}$-L)$_7$-C$_{18}$/d-SDS/D$_2$O $C_{polymer}$ = 1 wt%.

Fit parameters/ Units	1 % HEUR + 0.5 % SDS	1 % HEUR + 1 % SDS	1 % HEUR + 3 % SDS
Intensity of radius term	1.9×10^{-6}	2.6×10^{-6}	6.6×10^{-5}
Radius (Å)	20 ± 1	20 ± 1	18
e	n.d.	10	10
K^{-1} (Å)	0.28	0.27	0.23
φ	0.015	0.02	0.04
l_1	n.d.	n.d.	2.1
ξ (Å)	n.d.	n.d.	39 ± 2
l_2	2.7	1.3	n.d.
A (Å)	120 ± 2	55 ± 2	n.d.

Table A.9. SANS key parameters from the sphere and network model for h-C$_{18}$-L-(EO$_{200}$-L)$_7$-C$_{18}$ /d-SDS/H$_2$O $C_{polymer}$ = 1 wt%.
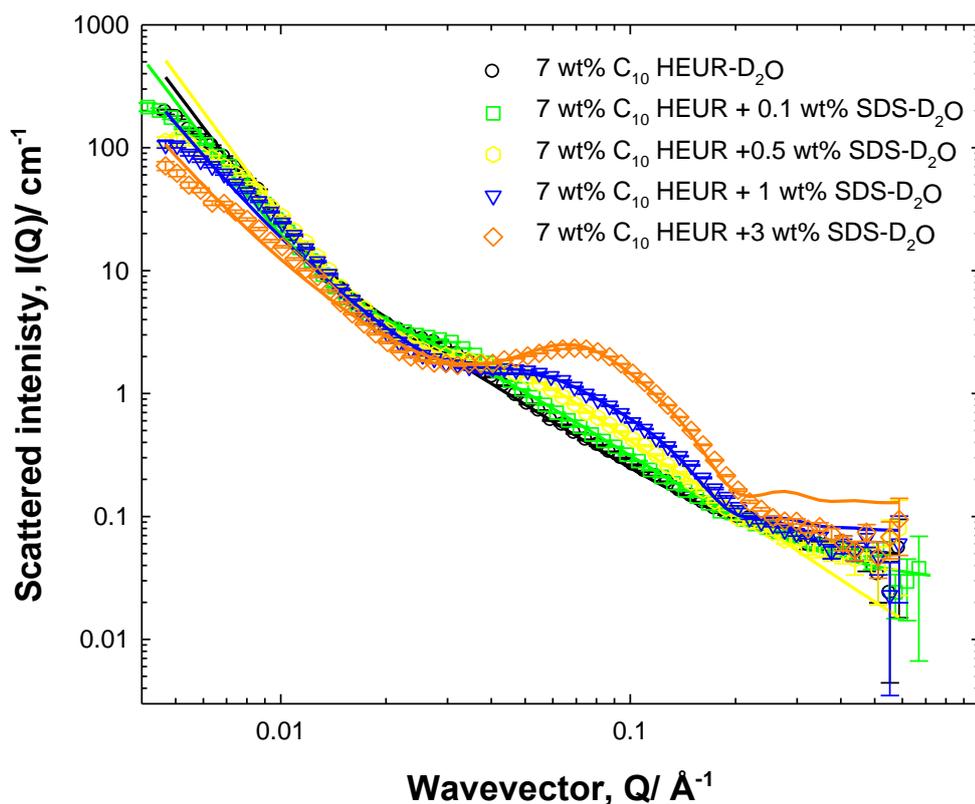
Figure A.16. Small-angle neutron scattering from h-C$_{10}$-L-(EO$_{200}$-L)$_4$-C$_{10}$/h-surfactant/D$_2$O; $C_{polymer}$ = 7 wt% with SDS 0 (circles), 0.1 (squares), 0.5 (hexagons), 1 (triangles) and 3 (diamonds) wt% (last three points have been omitted for clarity). The scattering contribution is from the polymer/SDS in polymer/SDS blend. Measurements were carried out at 25 °C, pH 9, and ionic strength 100 mM. The solid lines are fits for sphere and gel model. Key fitting parameters value are presented in Table A.10.
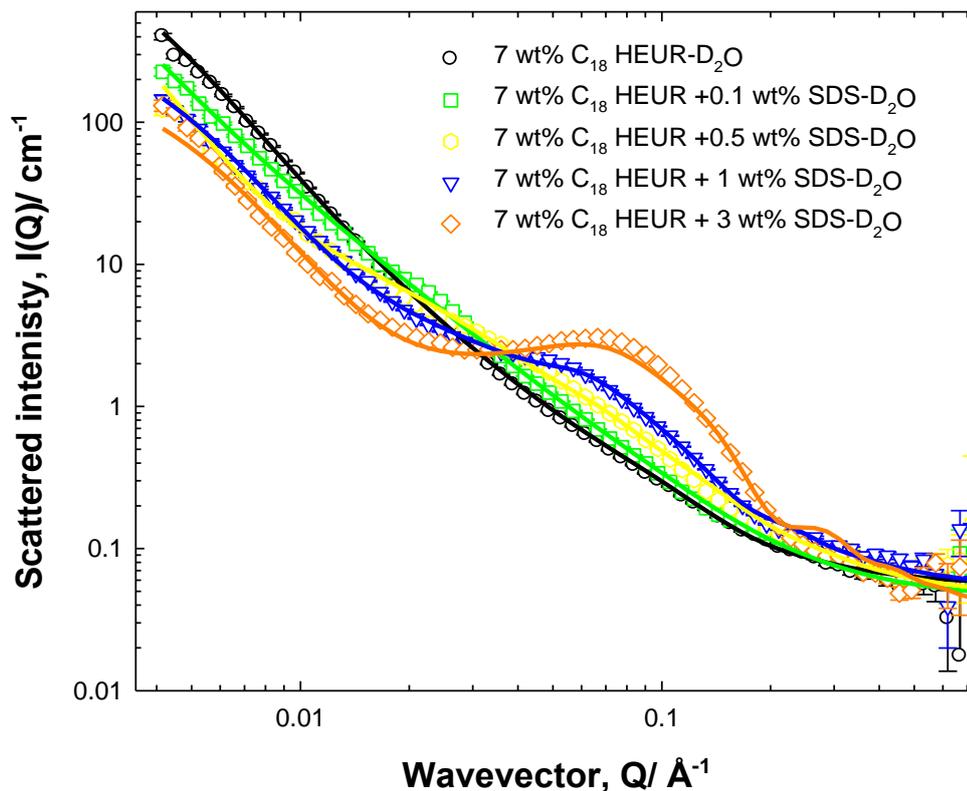
Figure A.17. Small-angle neutron scattering from h-C_{18}-L-(EO_{200}-L)$_7$-C_{18}/h-surfactant/D_2O; $C_{polymer}$ = 7 wt% with SDS 0 (circles), 0.1 (squares), 0.5 (hexagons), 1 (triangles) and 3 (diamonds) wt% (last three points have been omitted for clarity). The scattering contribution is from the polymer/SDS in polymer/SDS blend. Measurements were carried out at 25 °C, pH 9, and ionic strength 100 mM. The solid lines are fits for sphere and gel model. Key fitting parameters value are presented in Table A.13.
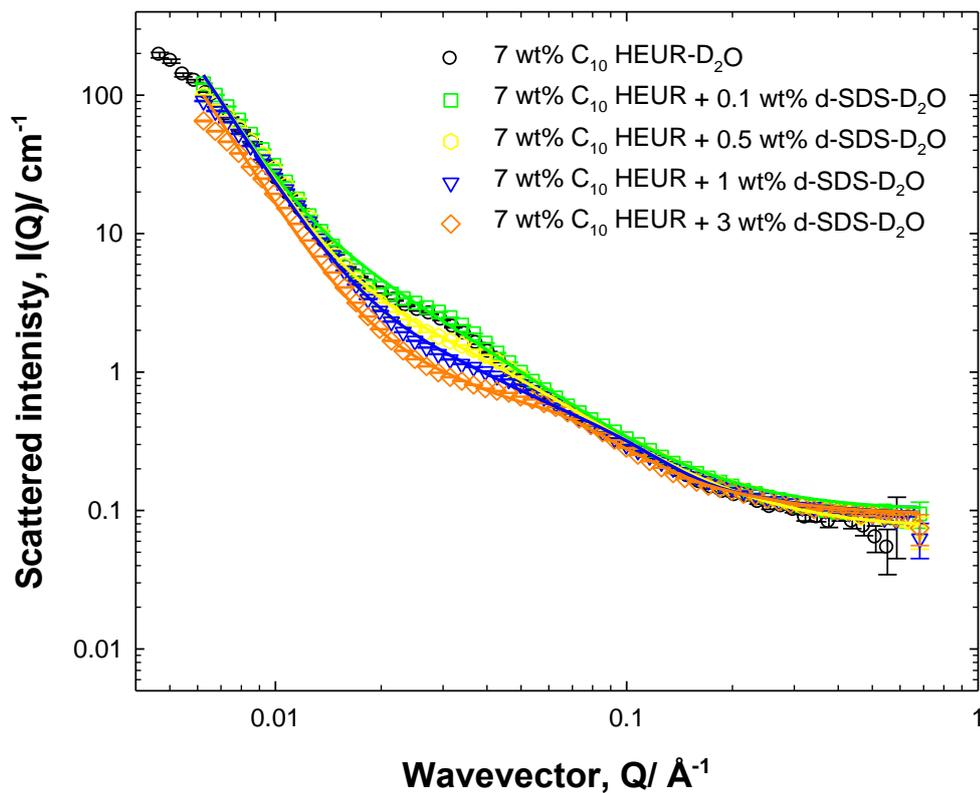
Figure A.18. Small-angle neutron scattering from h-C$_{10}$-L-(EO$_{200}$-L)$_4$-C$_{10}$/d-surfactant/D$_2$O; $C_{polymer}$ = 7 wt% with SDS 0 (circles), 0.1 (squares), 0.5 (hexagons), 1 (triangles) and 3 (diamonds) wt% (last three points have been omitted for clarity). The scattering contribution is from the polymer only in polymer/SDS blend. Measurements were carried out at 25 °C, pH 9, and ionic strength 100 mM. The solid lines are fits for sphere and gel model. Key fitting parameters value are presented in Table A.11.
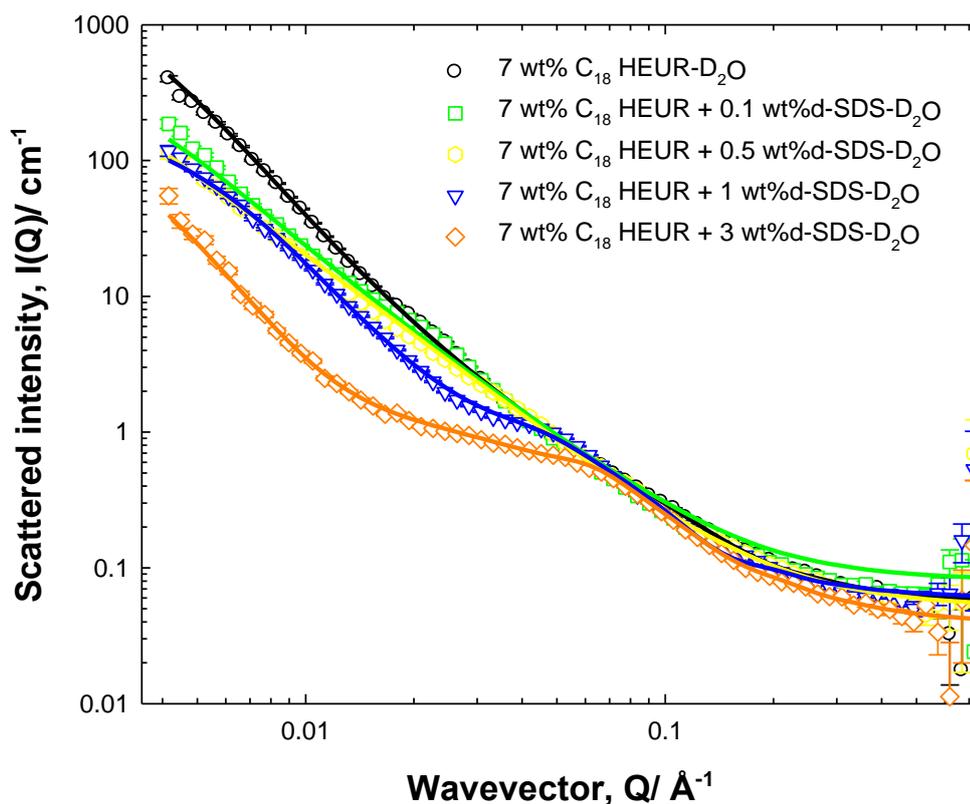
Figure A.19. Small-angle neutron scattering from h-C$_{18}$-L-(EO$_{200}$-L)$_7$-C$_{18}$/d-surfactant/D$_2$O; $C_{polymer}$ = 7 wt% with SDS 0 (circles), 0.1 (squares), 0.5 (hexagons), 1 (triangles) and 3 (diamonds) wt% (last three points have been omitted for clarity). The scattering contribution is from the polymer only in polymer/SDS blend. Measurements were carried out at 25 °C, pH 9, and ionic strength 100 mM. The solid lines are fits for sphere and gel model. Key fitting parameters value are presented in Table A.14.
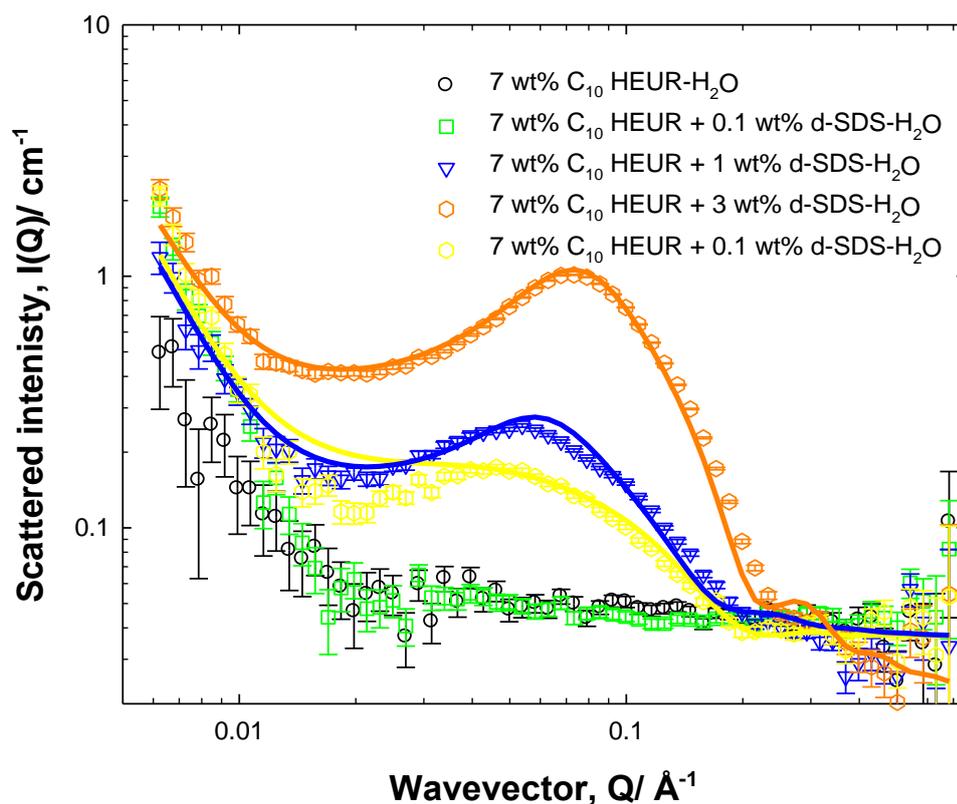
Figure A.20. Small-angle neutron scattering from h-C$_{10}$-L-(EO$_{200}$-L)$_4$-C$_{10}$/d-surfactant/H$_2$O; $C_{polymer}$ = 7 wt% with SDS 0 (circles), 0.1 (squares), 0.5 (hexagons), 1 (triangles) and 3 (diamonds) wt% (last three points have been omitted for clarity). The scattering contribution is from the SDS only in polymer/SDS blend. Measurements were carried out at 25 °C, pH 9, and ionic strength 10 0mM. The solid lines are fits for sphere and gel model. Key fitting parameters value are presented in Table A.12.
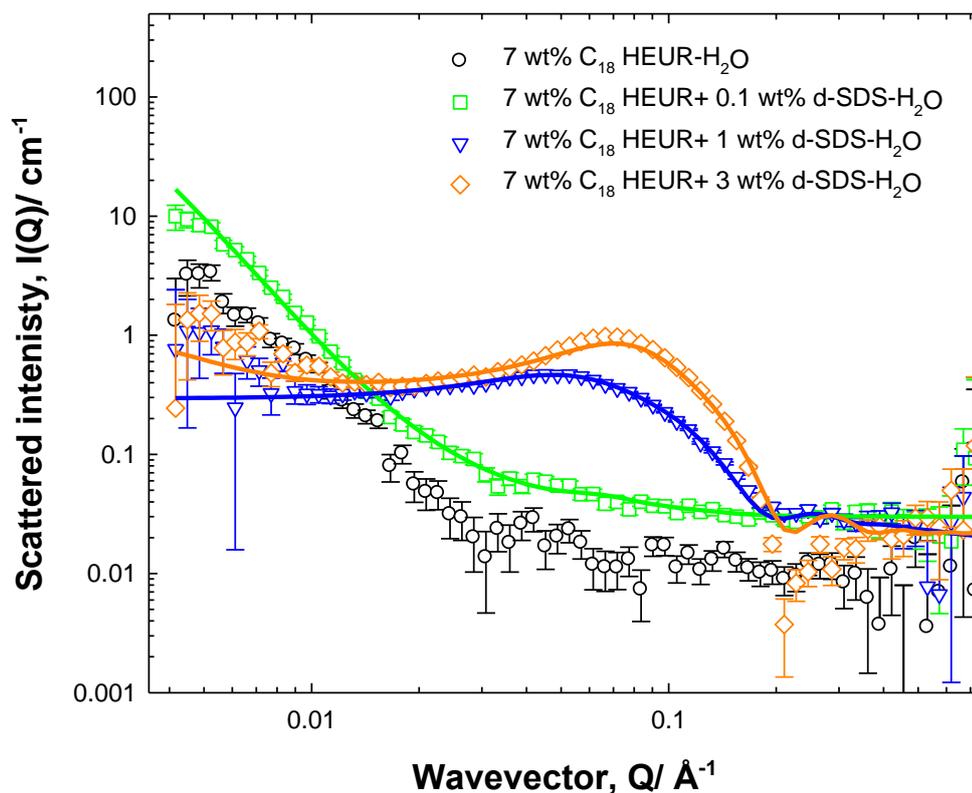
Figure A.21. Small-angle neutron scattering from h-C_{18}-L-(EO_{200}-L)$_7$-C_{18}/d-surfactant/H_2O; $C_{polymer}$ = 7 wt% with SDS 0 (circles), 0.1 (squares), 1 (triangles) and 3 (diamonds) wt% (last three points have been omitted for clarity). The scattering contribution is from the SDS only in polymer/SDS blend. Measurements were carried out at 25 °C, pH 9, and ionic strength 100 mM. The solid lines are fits for sphere and gel model. Key fitting parameters value are presented in Table A.15.

Appendix A.

Fit parameters/ Units	7 % HEUR + 0 % SDS	7 % HEUR + 0.1 % SDS	7 % HEUR + 0.5 % SDS	7 % HEUR + 1 % SDS	7 % HEUR + 3 % SDS
Intensity of radius term	3.4×10^{-6}	5.1×10^{-6}	2.4×10^{-6}	1.8×10^{-6}	4.1×10^{-5}
Radius (Å)	74 ± 5	69 ± 5	56 ± 2	21 ± 1	20 ± 1
e	n.d.	n.d.	n.d.	10	10
K^{-1} (Å)	0.3	0.29	0.28	0.27	0.23
φ	0.07	0.071	0.075	0.08	0.1
l_1	2.6	2.6	2.6	2.6	0.8
ξ (Å)	33 ± 1	30 ± 1	32 ± 1	27 ± 1	21 ± 1
l_2	2680	2600	2600	2600	2000
A (Å)	320 ± 5	330 ± 5	320 ± 5	330 ± 5	334 ± 5

Table A.10. SANS key parameters from the sphere and network model for h-C$_{10}$-L-(EO$_{200}$-L)$_4$-C$_{10}$/h-SDS/D$_2$O at $C_{polymer}$ = 7 wt%.

Fit parameters/ Units	7 % HEUR + 0 % SDS	7 % HEUR + 0.1 % SDS	7 % HEUR + 0.5 % SDS	7 % HEUR + 1 % SDS	7 % HEUR + 3 % SDS
Intensity of radius term	3.4×10^{-6}	4.0×10^{-6}	2.4×10^{-6}	2.3×10^{-6}	1.7×10^{-5}
Radius (Å)	74 ± 5	70 ± 5	56 ± 2	21 ± 1	20 ± 1
e	n.d.	n.d.	n.d.	10	10
K^{-1} (Å)	0.3	0.29	0.28	0.27	0.23
φ	0.07	0.071	0.075	0.08	0.1
l_1	2.6	2.6	2.6	1.5	0.9
ξ (Å)	33 ± 1	32 ± 1	32 ± 1	27 ± 1	21 ± 1
l_2	2680	2600	2600	2200	2200
A (Å)	320 ± 5	305 ± 5	305 ± 5	334 ± 5	334 ± 5

Table A.11. SANS key parameters from the sphere and network model for h-C$_{10}$-L-(EO$_{200}$-L)$_4$-C$_{10}$/d-SDS/D$_2$O $C_{polymer}$ = 7 wt%.

Appendix A.

Fit parameters/ Units	7 % HEUR + 0.5 % SDS	7 % HEUR + 1 % SDS	7 % HEUR + 3 % SDS
Intensity of radius term	1.5×10^{-6}	3.9×10^{-6}	2.2×10^{-5}
Radius (Å)	23 ± 1	22 ± 1	20 ± 0.5
e	n.d.	10	10
K^{-1} (Å)	0.28	0.27	0.23
φ	0.075	0.08	0.1
l_1	0.08	0.08	0.1
ξ (Å)	13 ± 1	13 ± 1	6 ± 1
l_2	23	20	25
A (Å)	300 ± 5	299 ± 5	299 ± 5

Table A.12. SANS key parameters from the sphere and network model for h-C$_{10}$-L-(EO$_{200}$-L)$_4$-C$_{10}$/d-SDS/H$_2$O C$_{polymer}$ = 7 wt%.

Fit parameters/ Units	7 % HEUR + 0 % SDS	7 % HEUR + 0.1 % SDS	7 % HEUR + 0.5 % SDS	7 % HEUR + 1 % SDS	7 % HEUR + 3 % SDS
Intensity of radius term	1.2×10^{-6}	5.3×10^{-6}	4.5×10^{-6}	2.4×10^{-6}	7.9×10^{-5}
Radius (Å)	70 ± 5	70 ± 5	38 ± 2	25 ± 1	20 ± 1
e	n.d.	n.d.	n.d.	10	10
K^{-1} (Å)	0.3	0.29	0.28	0.27	0.23
φ	0.07	0.071	0.075	0.08	0.1
l_1	8.9	3.8	4	4.3	2
ξ (Å)	66 ± 2	66 ± 2	66 ± 2	45 ± 2	45 ± 2
l_2	1106	200	230	400	250
A (Å)	217 ± 5	224 ± 5	217 ± 5	200 ± 5	200 ± 5

Table A.13. SANS key parameters from the sphere and network model for for h-C$_{18}$-L-(EO$_{200}$-L)$_7$-C$_{18}$/h-SDS/D$_2$O at C$_{polymer}$ = 7 wt%.

Appendix A.

Fit parameters/ Units	7 % HEUR + 0 % SDS	7 % HEUR + 0.1 % SDS	7 % HEUR + 0.5 % SDS	7 % HEUR + 1 % SDS	7 % HEUR + 3 % SDS
Intensity of radius term	1.2×10^{-6}	5.3×10^{-6}	4.5×10^{-6}	3.7×10^{-5}	8.9×10^{-5}
Radius (Å)	70 ± 5	70 ± 5	38 ± 2	30 ± 1	25 ± 1
e	0	0	0	10	10
K^{-1} (Å)	0.3	0.29	0.28	0.27	0.23
φ	0.07	0.071	0.075	0.08	0.1
l_1	8.9	10	10	4.3	3
ξ (Å)	66 ± 2	66 ± 2	66 ± 2	45 ± 2	80 ± 2
l_2	1106	500	450	400	216
A (Å)	217 ± 5	217 ± 5	217 ± 5	190 ± 5	337 ± 5

Table A.14. SANS key parameters from the sphere and network model for for h-C$_{18}$-L-(EO$_{200}$-L)$_7$-C$_{18}$/d-SDS/D$_2$O $C_{polymer}$ = 7 wt%.

Fit parameters/ Units	7 % HEUR + 1 % SDS	7 % HEUR + 3 % SDS
Intensity of radius	9.8×10^{-6}	2.8×10^{-5}
Radius (Å)	25 ± 1	20 ± 1
e	10	10
K^{-1} (Å)	0.27	0.23
φ	0.08	0.1
l_1	n.d.	n.d.
ξ (Å)	n.d.	n.d.
l_2	n.d.	1
A (Å)	n.d.	200 ± 5

Table A.15. SANS key parameters from the sphere and network model for h-C$_{18}$-L-(EO$_{200}$-L)$_7$-C$_{18}$/d-SDS/H$_2$O $C_{polymer}$ = 7 wt%.

B. Supplemental figures for Chapter 3
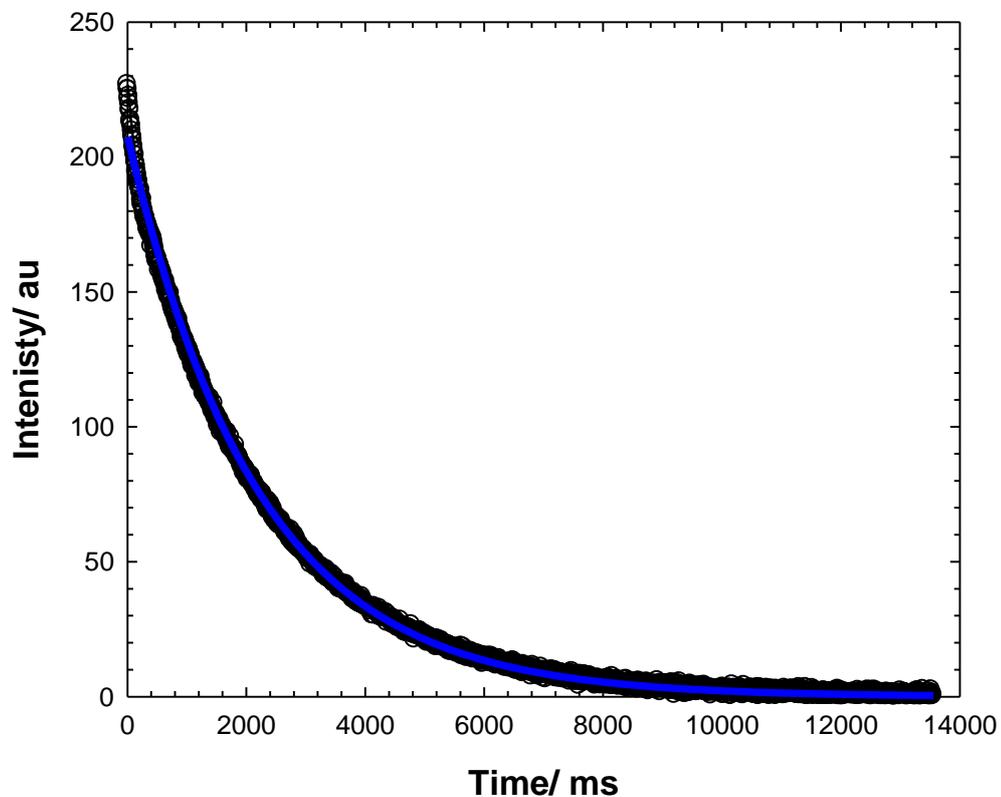
Figure B.1. Magnetisation decay as a function of time for 2 wt% C$_6$-L-(EO$_{100}$-L)$_9$-C$_6$/5 wt% PS-BAL in Hydroin buffered H$_2$O, pH 9.Measurements were carried out at 25°C.

Appendix B.

Linearised data
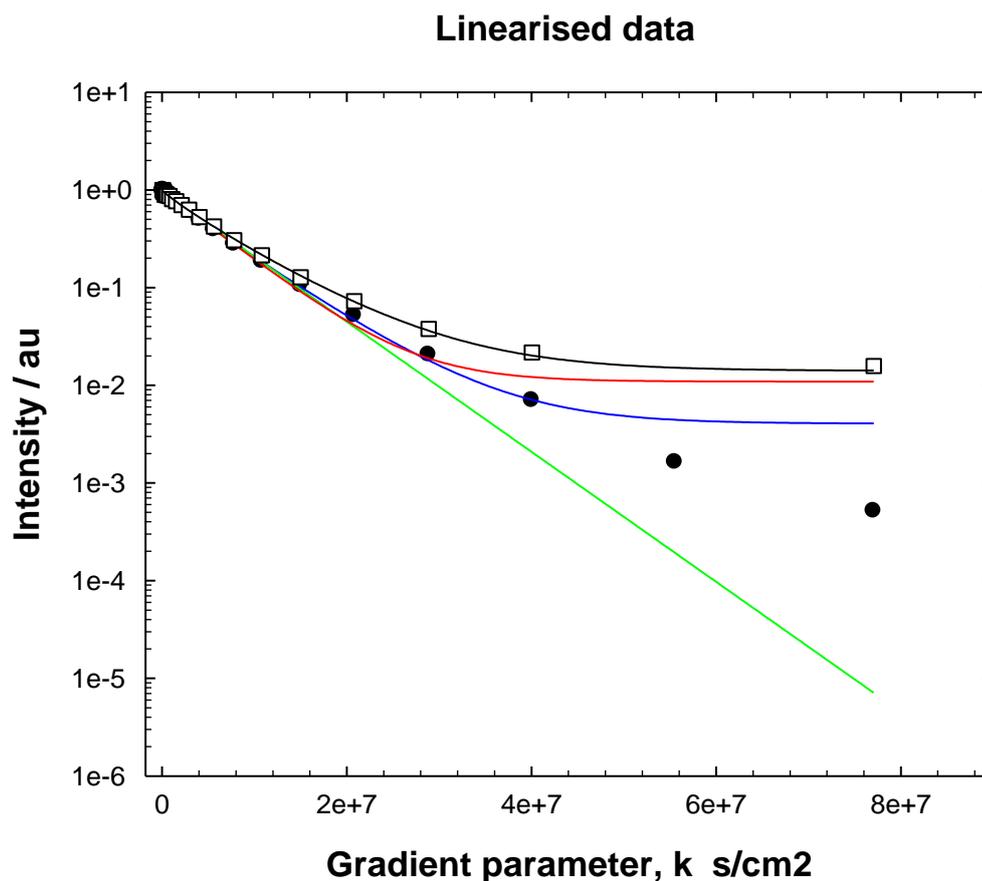
Figure B.2. Signal decay as a function of gradient parameter for 2 wt% C$_6$-L-(EO$_{100}$-L)$_9$-C$_6$ (●) in Hydroin buffered D$_2$O, pH 9,single exponential (-), single stretched (-), and single stretched with base line fit (-). The blue line seems to be the best fit of all. The beta parameter is 0.92 for the pure polymer. The signal decay as a function of gradient parameter for 2 wt% C$_6$-L-(EO$_{100}$-L)$_9$-C$_6$/ 5 wt% PS-BAL (□), and single stretched with baseline fit (-). Beta parameter is 0.892 for the polymer in the polymer/latex mixture.

C. Supplemental figures and tables for Chapter 5
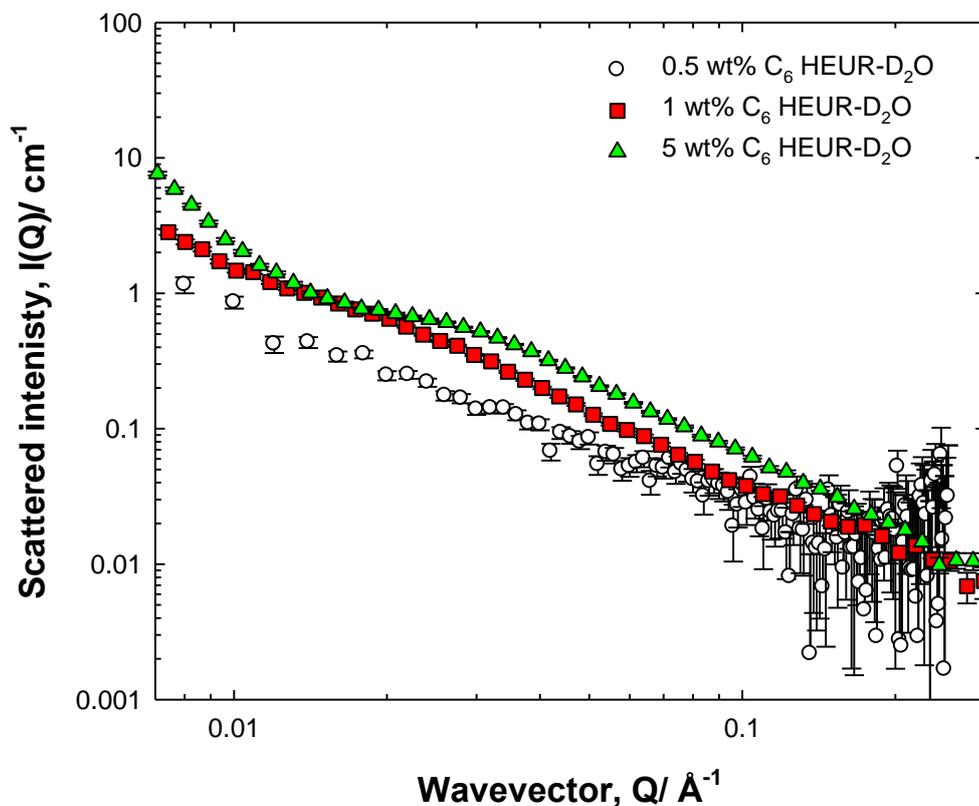
Figure C.1. Small-angle neutron scattering from 0.5 (white circles), 2 (red squares), and 5 (green triangles) wt% C_6-L-(EO_{100}-L)$_9$-C_6 in 92 %(v/v) D_2O. Measurements were carried out at 25 °C.

Parameters/units	0.5 % polymer/ 20 % dodecane	2 % polymer/20 % dodecane	5 % polymer/20 % dodecane
Intensity of radius term	n.d.	n.d.	n.d.
Radius (Å)	n.d.	n.d.	n.d.
Q	n.d.	n.d.	n.d.
R_g (Å)	n.d.	n.d.	n.d.
I_1	2.5	9	16
ξ (Å)	110 ± 2	110 ± 2	110 ± 2
I_2	7	6	6
A (Å)	110 ± 2	110 ± 2	110 ± 2

Table C.1. SANS key parameters from the sphere and network model for 20 wt% dodecane as a function of C_6-L-(EO_{100}-L)$_9$-C_6 concentration.

Appendix. C

Parameters/units	0.5 % polymer/ 0 % dodecane	0.5 % polymer/ 20 % dodecane
Intensity of radius term	n.d.	n.d.
Radius (Å)	n.d.	n.d.
Q	n.d.	n.d.
R_g (Å)	n.d.	n.d.
l_1	1	2.5
ξ (Å)	80 ± 2	110 ± 2
l_2	0	7
A (Å)	0	110 ± 2

Table C.2. SANS key parameters from the sphere and network model for 0.5 wt% C_6-L-(EO_{100}-L)$_9$-C_6 as a function of dodecane concentration.
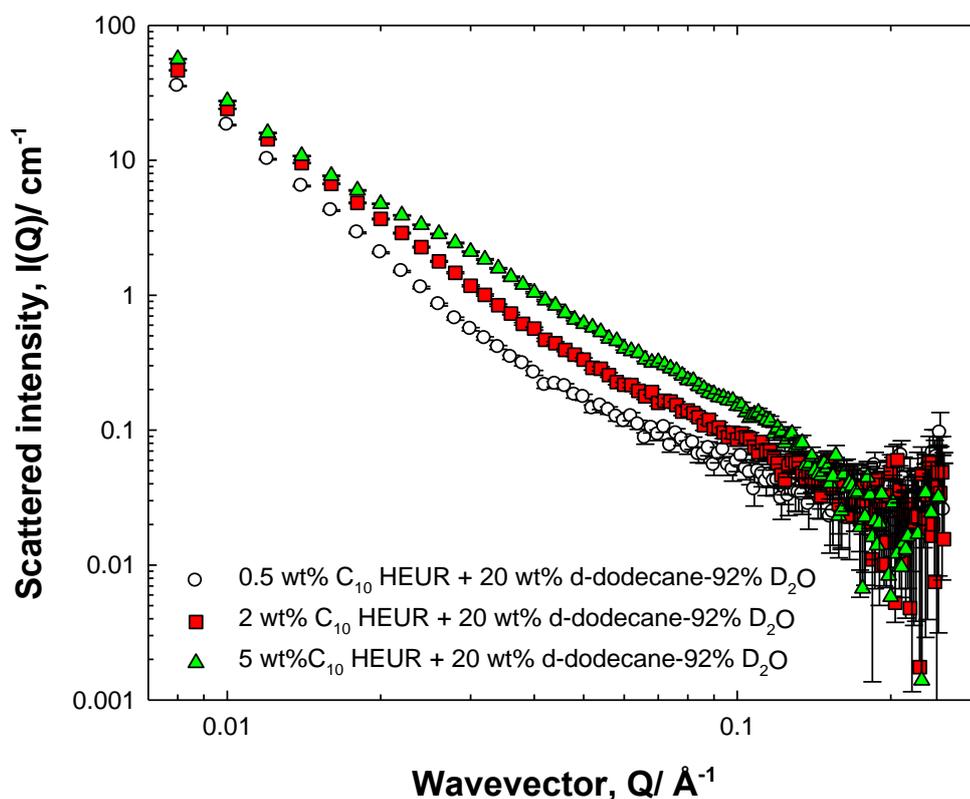
Figure C.2. Small-angle neutron scattering from 20 wt% d-dodecane in the presence of 0.5 (white circles), 2 (red squares), and 5 (green triangles) wt% h-C_{10}-L-(EO_{200}-L)$_4$-C_{10} in 92 %(v/v) D_2O. Measurements were carried out at 25 °C.
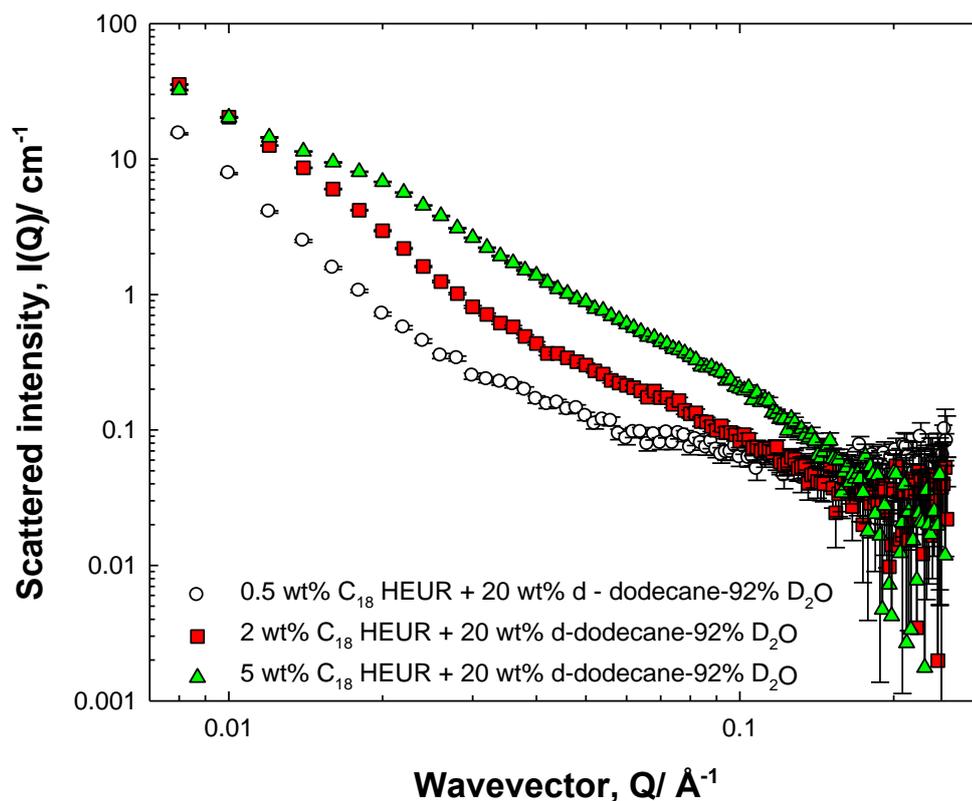
Figure C.3. Small-angle neutron scattering from 20 wt% d-dodecane in the presence of 0.5 (white circles), 2 (red squares), and 5 (green triangles) wt% h-C₁₈-L-(EO₂₀₀-L)₇-C₁₈ in 92 %(v/v) D₂O. Measurements were carried out at 25 °C.
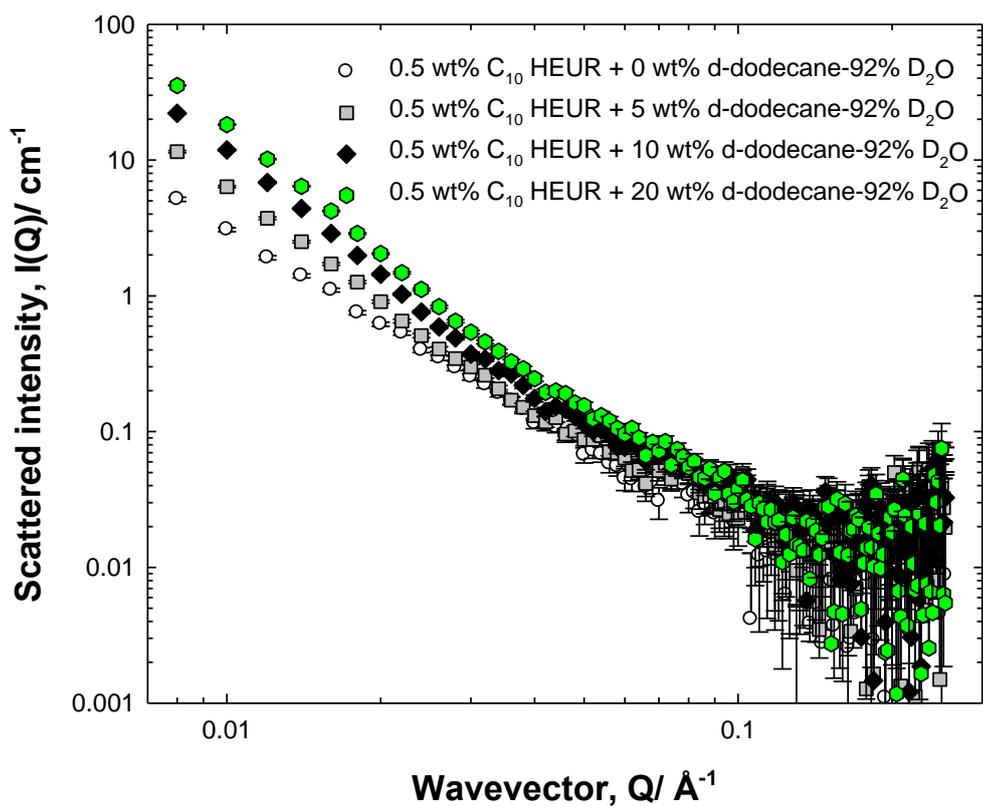
Figure C.4. Small-angle neutron scattering from 0.5 wt% h-C_{10}-L-(EO_{200}-L)$_4$-C_{10} in the absence (white circles) and presence of 5 (grey squares), 10 (black diamonds), and 20 (green hexagons) wt% d-dodecane in 92 %(v/v) D_2O. Measurements were carried out at 25 °C.
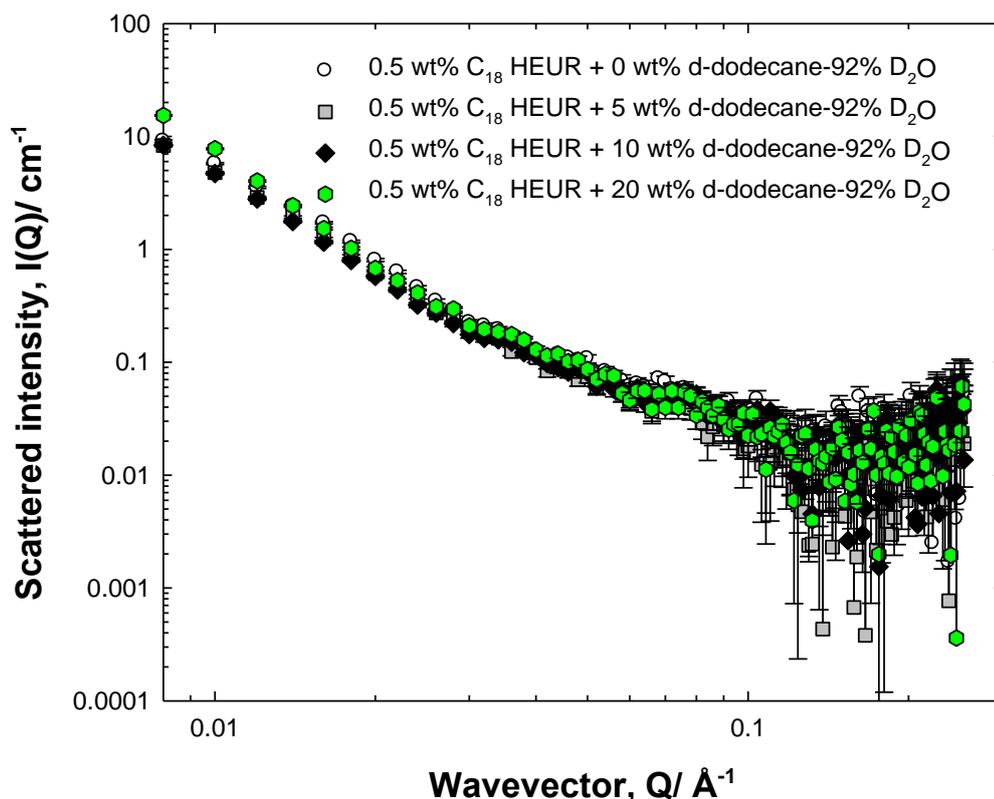
Figure C.5. Small-angle neutron scattering from 0.5 wt% h-C₁₈-L-(EO₂₀₀-L)₇-C₁₈ in the absence (white circles) and presence of 5 (grey squares), 10 (black diamonds), and 20 (green hexagons) wt% d-dodecane in 92 %(v/v) D₂O. Measurements were carried out at 25 °C.

Parameters/units	0.5 % polymer/0.1 % SDS/20 % dodecane	0.5 % polymer/0.5 % SDS/20 % dodecane	0.5 % polymer/1 % SDS/20 % dodecane
Intensity of radius term	n.d.	n.d.	2×10^{-5}
Radius (Å)	n.d.	n.d.	18 ± 1
Q	n.d.	n.d.	10
R_g (Å)	n.d.	n.d.	n.d.
l_1	0.5	1	1
ξ (Å)	40 ± 2	25 ± 2	25 ± 2
l_2	45	150	150
A (Å)	110 ± 2	140 ± 2	150 ± 2

Table C.3. SANS key parameters from the sphere and network model for 0.5 wt% C₆-L-(EO₁₀₀-L)₉-C₆ /20 wt% dodecane as a function of SDS concentration.
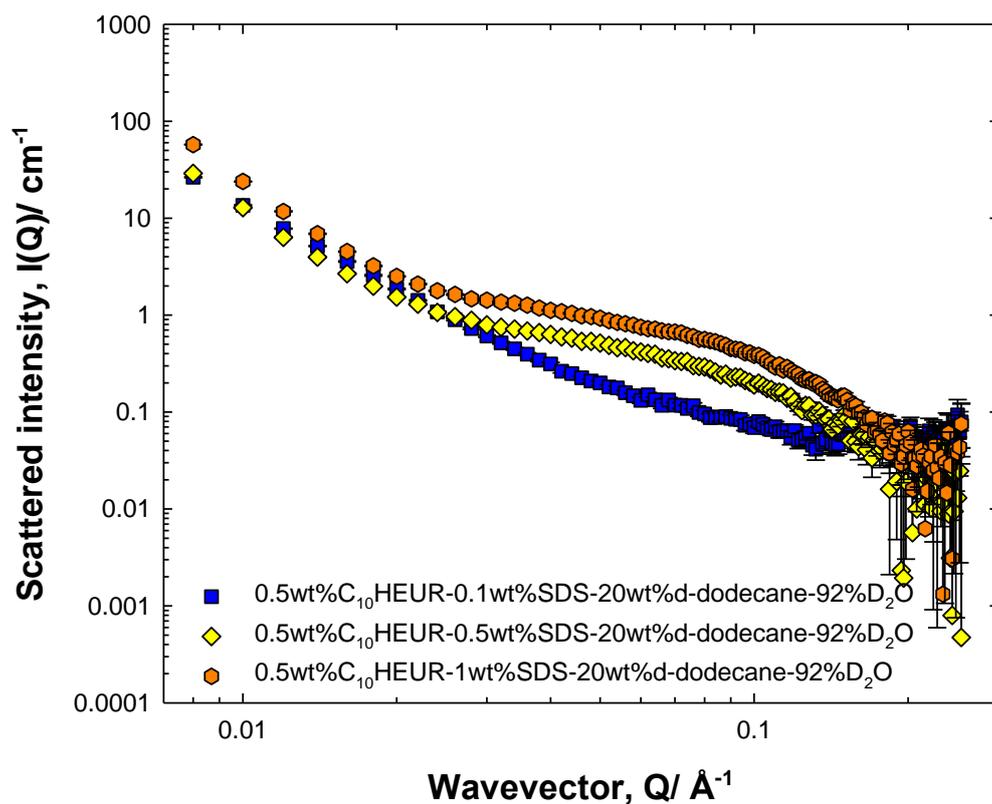
Figure C.6. Small-angle neutron scattering from 0.5 wt% h-C$_{10}$-L-(EO$_{200}$-L)$_4$-C$_{10}$/20 wt% d-dodecane in the presence of 0.1 (blue squares), 0.5 (yellow diamonds), and 1 (orange hexagons) wt% h-SDS in 92 %(v/v) D$_2$O. Measurements were carried out at 25 °C.
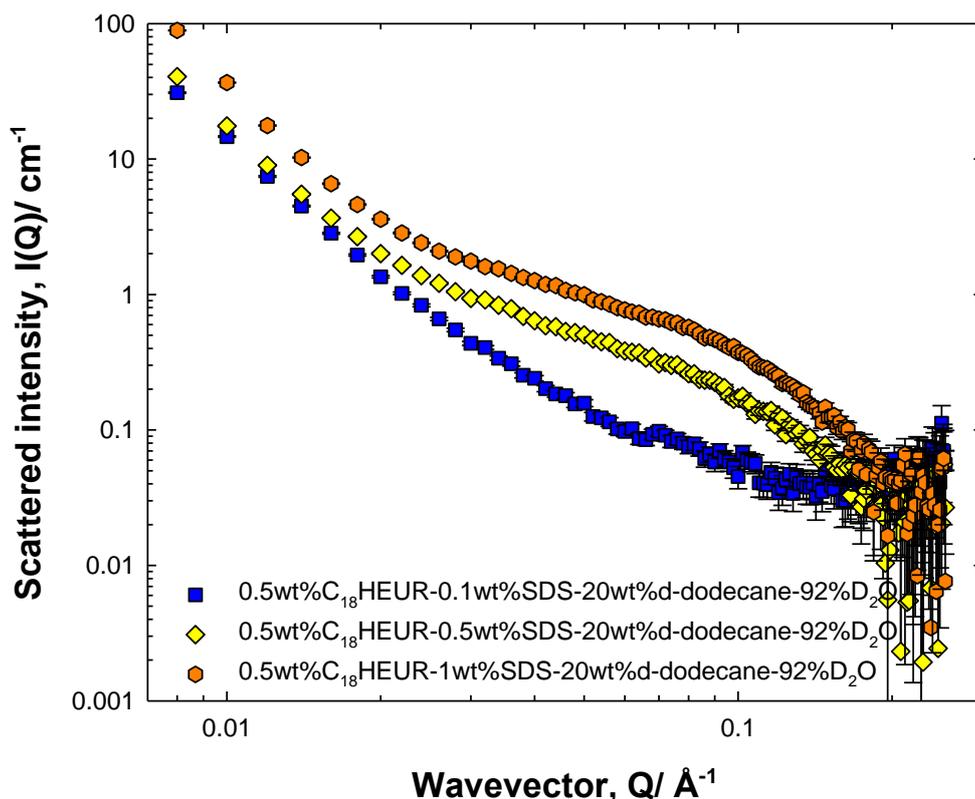
Figure C.7.Small-angle neutron scattering from 0.5 wt% C_{18}-L-(EO$_{200}$-L)$_7$-C_{18}/20 wt% d-dodecane in the presence of 0.1 (blue squares), 0.5 (yellow diamonds), and 1 (orange hexagons) wt% h-SDS in 92 %(v/v) D$_2$O. Measurements were carried out at 25 °C.

Parameters/units	0.5 % polymer/0.1 % d-SDS/20 % dodecane	0.5 % polymer/0.5 % d-SDS/20 % dodecane	0.5 % polymer/1 % d-SDS/20 % dodecane
Intensity of radius term	n.d.	n.d.	n.d.
Radius (Å)	n.d.	n.d.	n.d.
Q	n.d.	n.d.	n.d.
R_g (Å)	n.d.	n.d.	n.d.
I_1	0.2	0.2	0.1
ξ (Å)	40 ± 2	25 ± 2	25 ± 2
I_2	40	25	150
A (Å)	110 ± 2	140 ± 2	150 ± 2

Table C.4. SANS key parameters from the sphere and network model for 0.5 wt% C_6-L-(EO$_{100}$-L)$_9$-C_6/20 wt% dodecane as a function of d-SDS concentration.
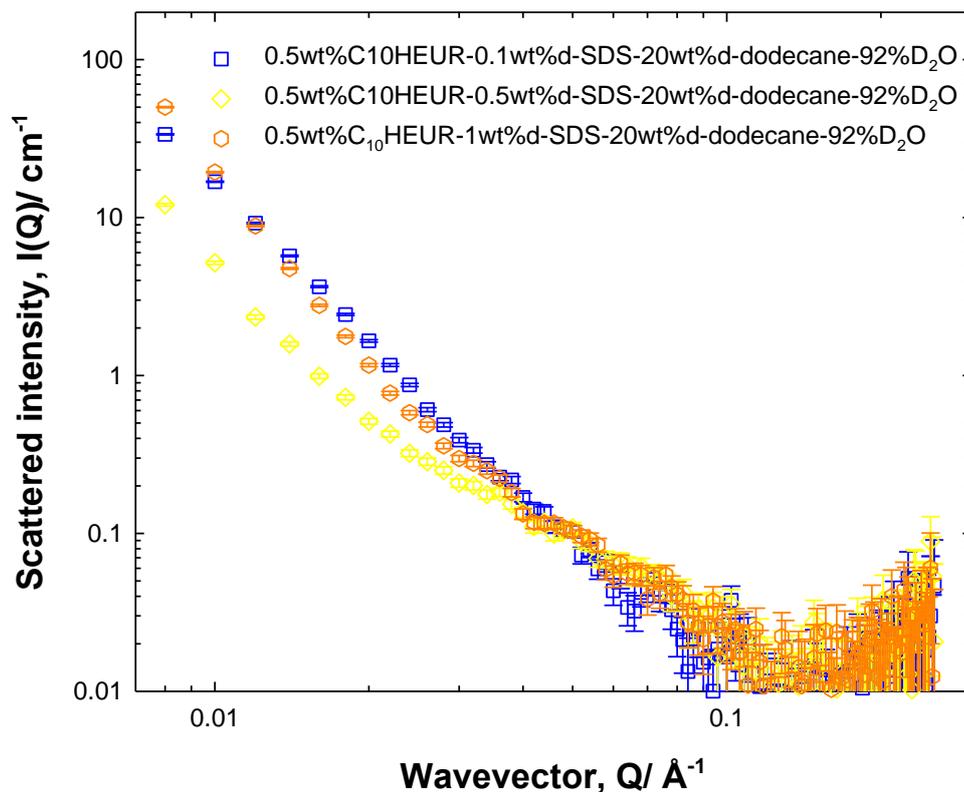
Figure C.8. Small-angle neutron scattering from 0.5 wt% h-C$_{10}$-L-(EO$_{200}$-L)$_4$-C$_{10}$/20 wt% d-dodecane in the presence of 0.1 (blue squares), 0.5 (yellow diamonds), and 1 (orange hexagons) wt% d-SDS in 92 %(v/v) D$_2$O. Measurements were carried out at 25 °C.
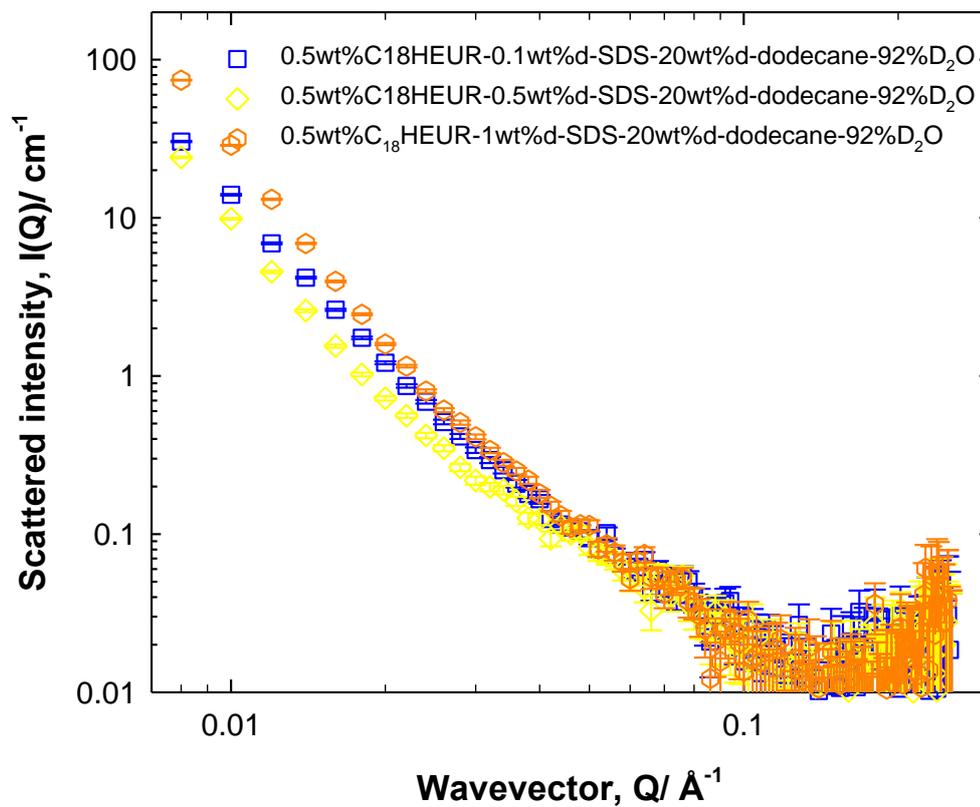
Figure C.9. Small-angle neutron scattering from 0.5 wt% h-C$_{18}$-L-(EO$_{200}$-L)$_7$-C$_{18}$/20 wt% d-dodecane in the presence 0.1 (blue squares), 0.5 (yellow diamonds), and 1 (orange hexagons) wt% d-SDS in 92 %(v/v) D$_2$O. Measurements were carried out at 25 °C.
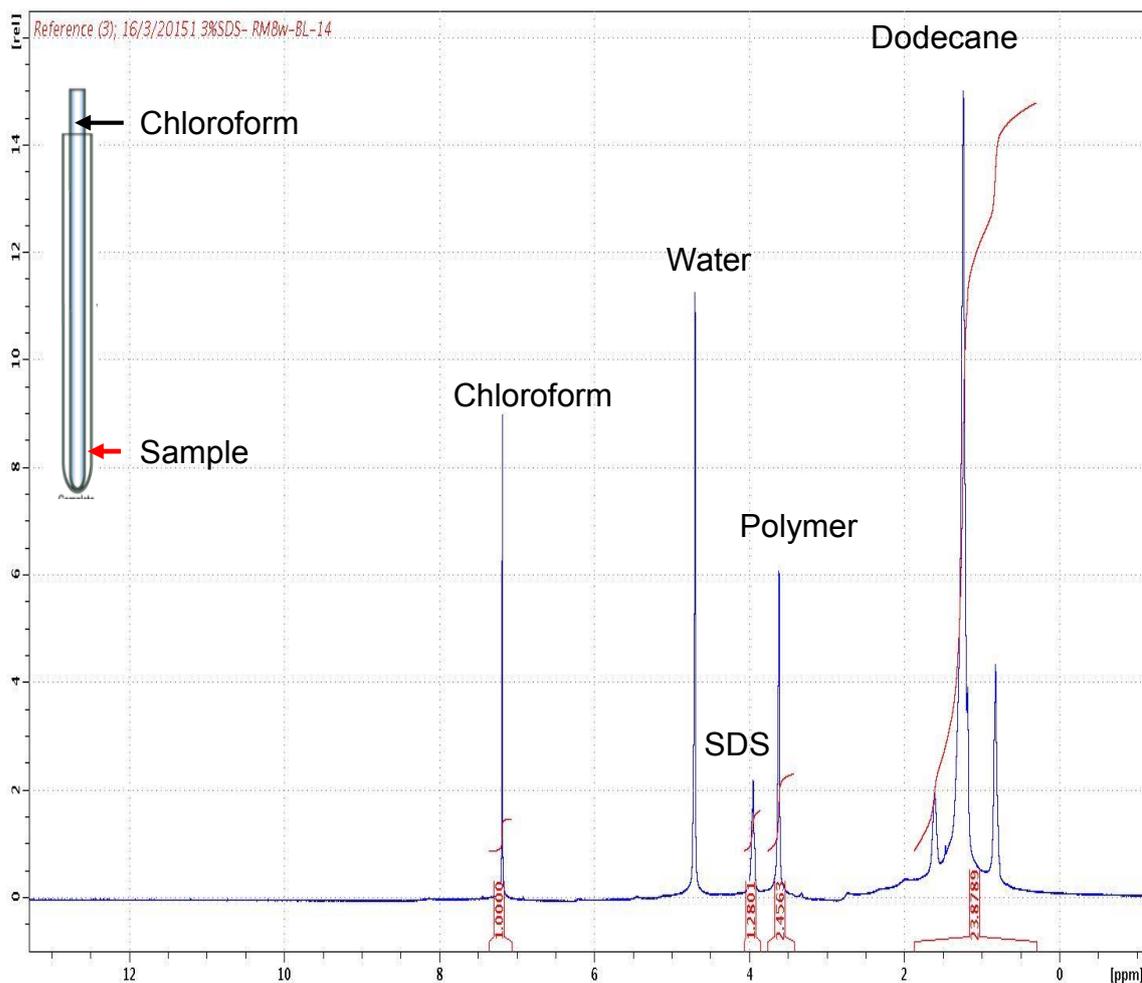
Figure C.10. ^{1}H spectrum of HEUR/SDS/dodecane emulsion.

Sample name	chloroform	SDS ± 0.2	Polymer ± 0.2	Dodecane ± 0.2
5 % SDS/0.5 % polymer	1	2.5	2.3	67
3 % SDS/0.5 % polymer	1	1.3	2.5	24
1 % SDS/0.5 % polymer	1	0.6	3	9
0.1 % SDS/0.5 % polymer	1	n.d.	3.5	20

Table C.5. Integration of C_{10}-(EO_{200}-L)$_4$-C_{10}, SDS and dodecane peaks relative to the chloroform (external probe) peak in aqueous layer of phase separated emulsions.

Appendix. C

Sample name	Chloroform	SDS ± 0.2	Polymer ± 0.2	Dodecane ± 0.2
5 % SDS/0.5 % polymer	1	5	5	89
4 % SDS/0.5 % polymer	1	5	7.3	102

Table C.6. Integration of C$_{18}$-(EO$_{200}$-L)$_7$-C$_{18}$, SDS and dodecane peaks relative to the chloroform (external probe) peak in aqueous layer of phase separated emulsions.

Sample name	Chloroform	SDS ± 0.2	Polymer ± 0.2	Dodecane ± 0.2
5 % SDS/0.5 % polymer	1	2.5	2	558
3 % SDS/0.5 % polymer	1	0.4	2	458
1 % SDS/0.5 % polymer	1	0.5	2.6	64
0.1 % SDS/0.5 % polymer	1	n.d.	2.4	20.4

Table C.7. Integration of C$_{10}$-(EO$_{200}$-L)$_4$-C$_{10}$, SDS and dodecane peaks relative to the chloroform (external probe) peak in oil layer of phase separated emulsions.

Sample name	Chloroform	SDS ± 0.2	Polymer ± 0.2	Dodecane ± 0.2
5 % SDS/0.5 % polymer	1	27.3	23.4	1404.6
4 % SDS/0.5 % polymer	1	6.2	8.8	571

Table C.8. Integration of C$_{18}$-(EO$_{200}$-L)$_7$-C$_{18}$, SDS and dodecane peaks relative to the chloroform (external probe) peak of sample component peaks in oil layer in phase separated emulsions.

D. Purity of chemicals

D.1. Polymers

The samples employed here were gifts from Dow, and the manufacturer's information suggested that the HEUR polymer used here may be described as C_n-L-$(EO_x$-L$)_y$-C_n where C_n denotes the length of the hydrophobic end group and L is a urethane linker (the polymers studied here possess 4, 4'-methylene dicyclohexyl diisocyanate (H_{12}MDI) linkers, Figure D.1), x is the number of ethylene oxide units per segment, and y is the number of segments per polymer. Three polymers are used in this study C_6-L-$(EO_{100}$-L$)_9$-C_6, C_{10}-L-$(EO_{200}$-L$)_4$-C_{10}, and C_{18}-L-$(EO_{200}$-L$)_7$-C_{18}. HEUR polymers are generally synthesised in two steps: (a) reaction between PEG and hexamethylene diisocyanate using step polymerization technique that yields ethoxylated urethane prepolymer, (b) the modification occurs by reacting the prepolymer with alcohol that provides the hydrophobic end-group (1,2).
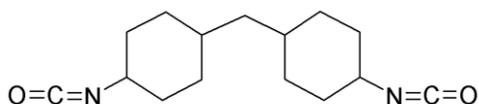
Figure D.1. Structure of 4, 4'-methylene dicyclohexyl diisocyanate (H_{12}MDI).

HEUR manufacturers usually add cyclodextrin to incorporate the hydrophobic end-group in the cyclodextrin cavity to decrease the polymer viscosity since that the polymer may be easily pumped. The AkzoNobel team shared the percentage of the added cyclodextrin to C_6-L-$(EO_{100}$-L$)_9$-C_6 which is equivalent to 0.2 %. The ^{1}H NMR spectra were recorded for the 2 wt% C_6-L-$(EO_{100}$-L$)_9$-C_6 as supplied and compared to the C_6-L-$(EO_{100}$-L$)_9$-C_6 with added 5 wt% α-, β- and γ-cyclodextrin, Figure D.2, Figure D.3, and Figure D.4, respectively. Samples were dissolved in dimethyl sulfoxide (DMSO) to prevent the aggregation of the polymer hydrophobes. The three NMR spectra show no evidence of cyclodextrin presence in the sample.

To exclude the inability to detect the cyclodextrin as a result of its low concentration in the C_6-L-$(EO_{100}$-L$)_9$-C_6 samples, the C_{10}-L-$(EO_{200}$-L$)_4$-C_{10} was studied which contains 2 wt% cyclodextrin. The polymer sample was shaken with chloroform for one hour, to

enable the polymer to partition into the chloroform phase and the cyclodextrin into the aqueous phase. The chloroform layer was retrieved where the chloroform was then evaporated leaving a polymer film which was resuspended in water or deuterium oxide depending on the experiment to be conducted. The absence of chloroform was checked by ^{1}H NMR. Samples for parent C_{10}-L-$(EO_{200}$-L$)_4$-C_{10} (as supplied), purified in chloroform were resuspended in DMSO, to be compared to purified samples with added α- (Figure D.5), β- (Figure D.6), and γ-cyclodextrin (Figure D.7). The concentration of the polymer and cyclodextrin in the mixtures were 2 and 5 wt%, respectively. The presence of cyclodextrins were not detected in the as supplied material purified C_{10}-L-$(EO_{200}$-L$)_4$-C_{10} samples.
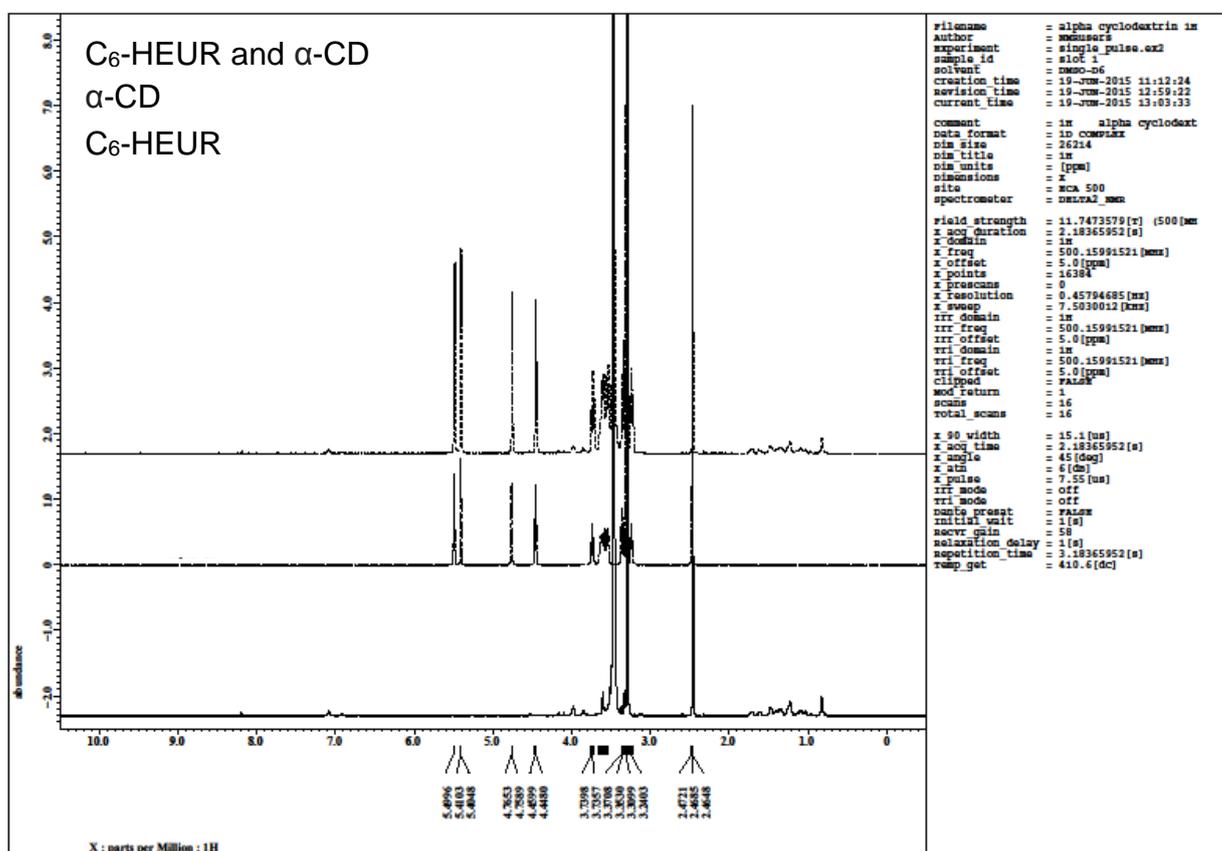
Figure D.2. The ^{1}H spectra arranged from top to bottom are for C_6-L-$(EO_{100}$-L$)_9$-C_6/α-cyclodextrin (α-CD), α-CD, and C_6-L-$(EO_{100}$-L$)_9$-C_6 (C_6-HEUR) as supplied. Measurements were carried out at 25°C.
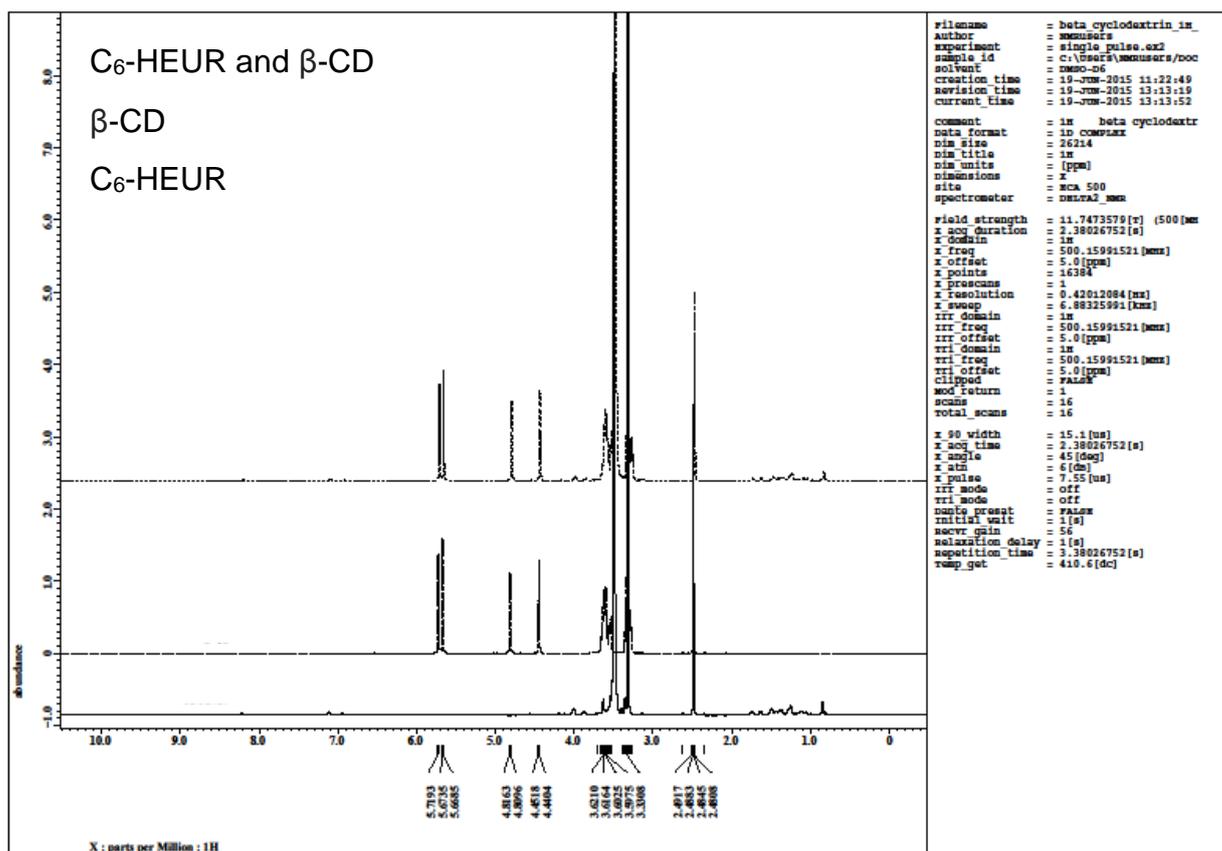
Appendix D.

Figure D.3. The ^{1}H spectra arranged from top to bottom and C_6-L-(EO_{100}-L)$_9$-C_6/β-cyclodextrin (β-CD), β-CD, and C_6-L-(EO_{100}-L)$_9$-C_6 (C_6-HEUR) as supplied. Measurements were carried out at 25°C.
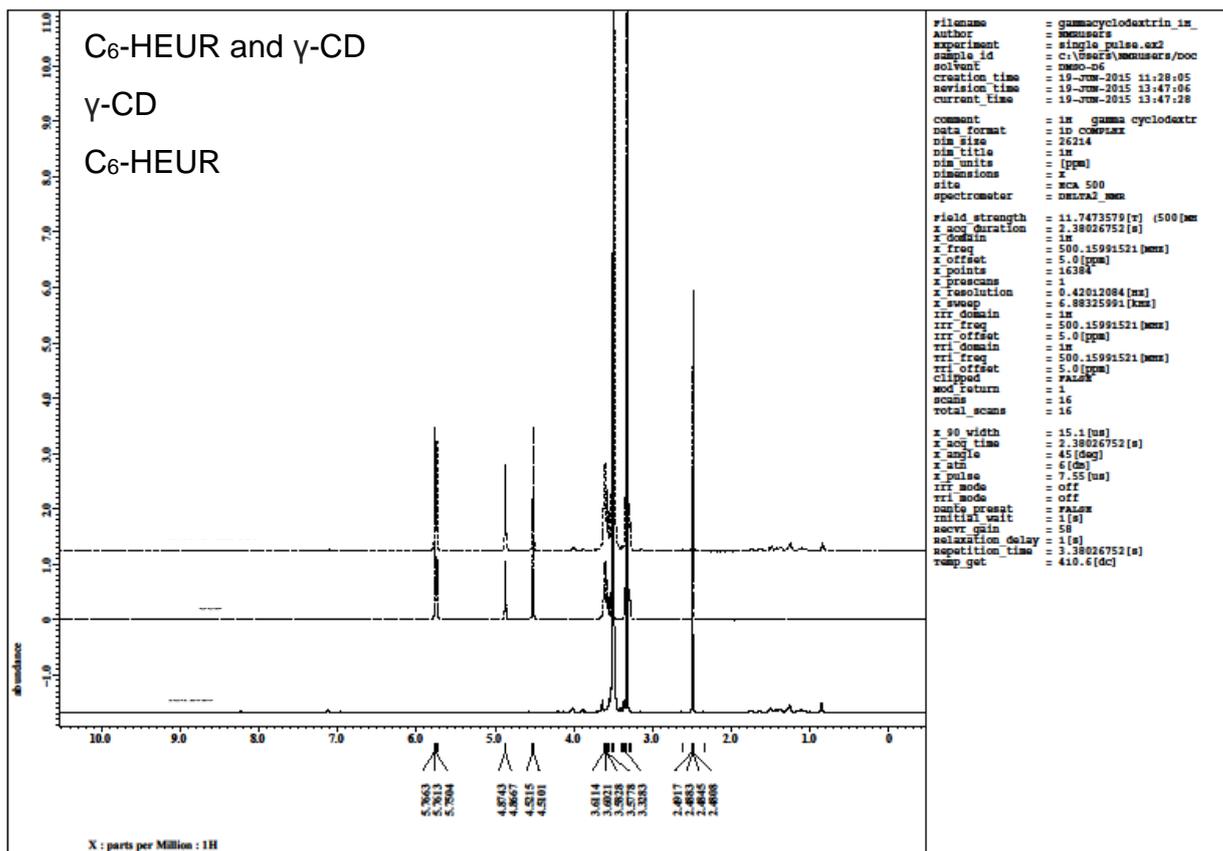
Figure D.4. The ^{1}H spectra arranged from top to bottom and C$_6$-L-(EO$_{100}$-L)$_9$-C$_6$/γ-cyclodextrin (γ-CD), γ-CD, and C$_6$-L-(EO$_{100}$-L)$_9$-C$_6$ (C$_6$-HEUR) as supplied. Measurements were carried out at 25°C.
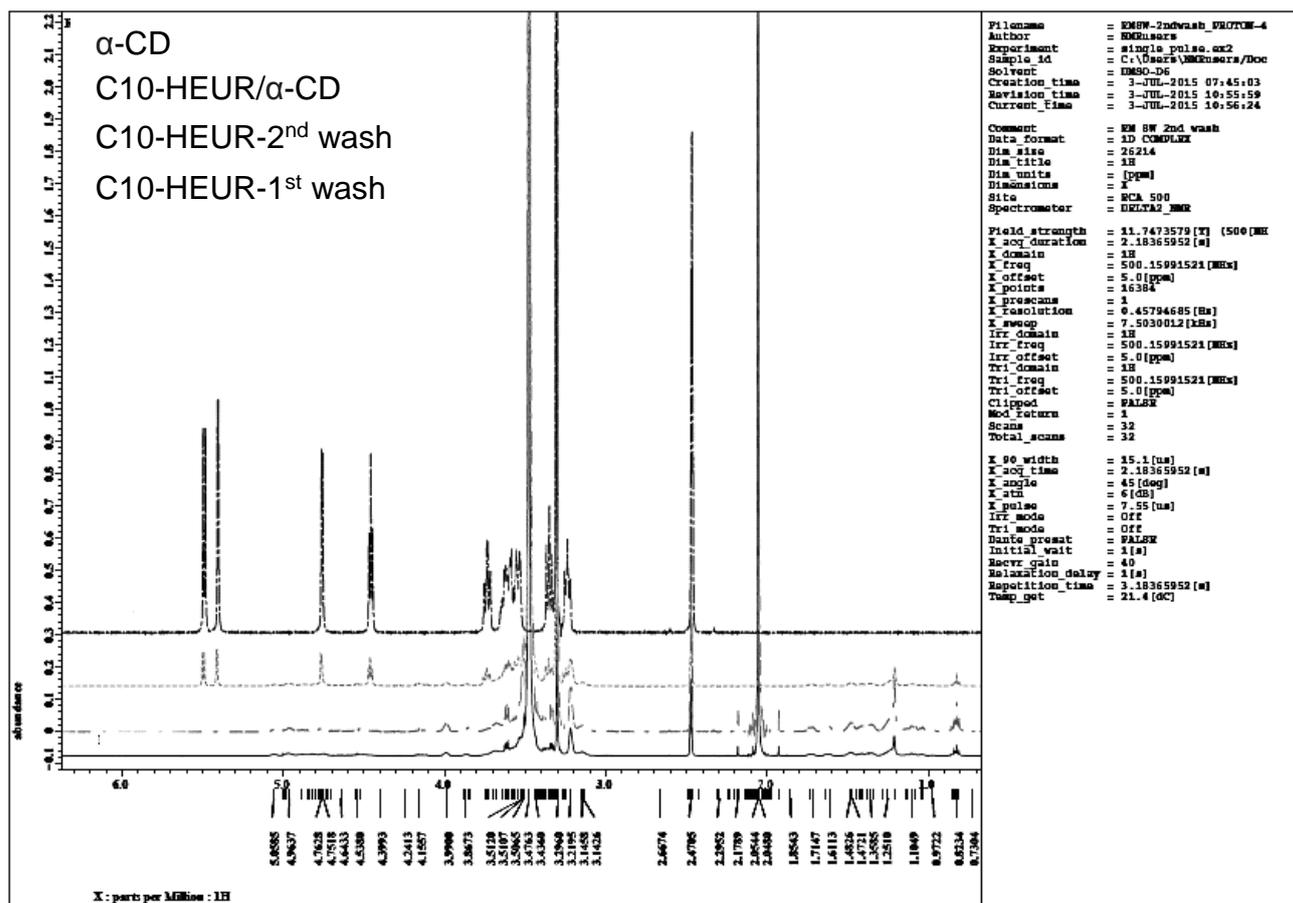
Figure D.5. The ^{1}H spectra from top to bottom for α-cyclodextrin (α-CD), C_{10}-L-$(EO_{200}$-L$)_4$-C_{10}/α-CD, C_{10}-L-$(EO_{200}$-L$)_4$-C_{10} second wash, and C_{10}-L-$(EO_{200}$-L$)_4$-C_{10} (C_{10}-HEUR) first wash. Measurements were carried out at 25°C.
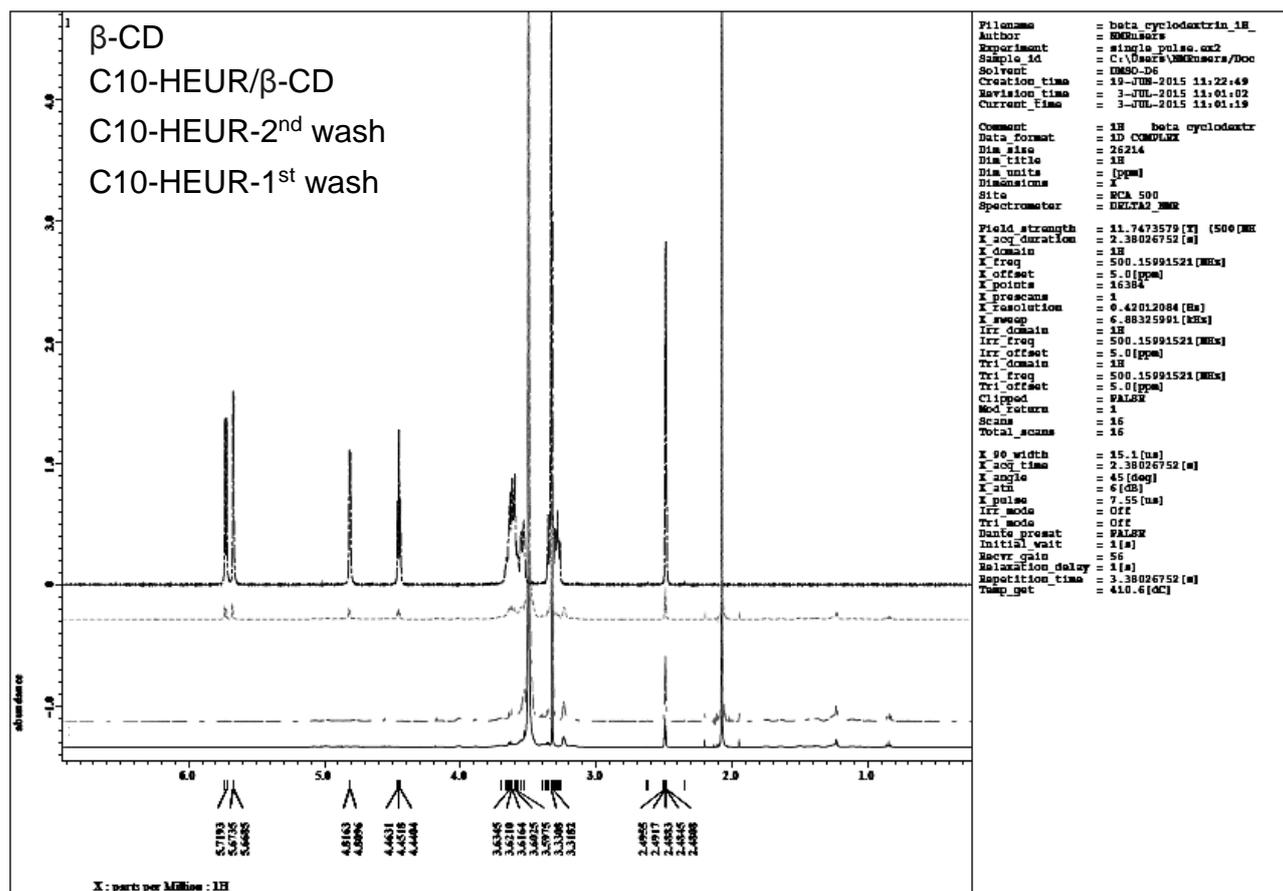
Figure D.6. The ^{1}H spectra from top to bottom for β-cyclodextrin (β-CD), C_{10}-L-(EO_{200}-L)$_4$-C_{10}/β-CD, C_{10}-L-(EO_{200}-L)$_4$-C_{10} second wash, and C_{10}-L-(EO_{200}-L)$_4$-C_{10} (C_{10}-HEUR) first wash. Measurements were carried out at 25°C.

Appendix D.
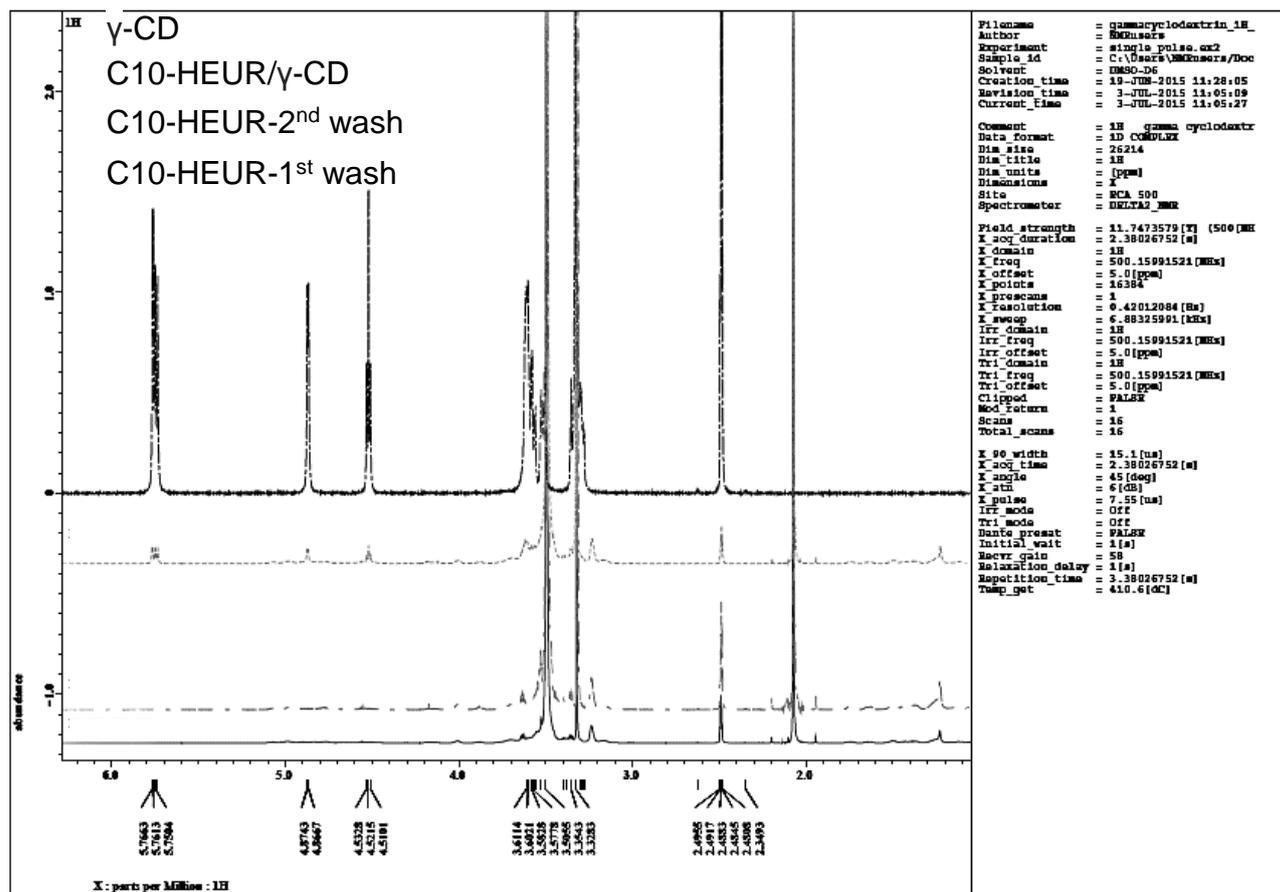
Figure D.7. The ^{1}H spectra from top to bottom for γ-cyclodextrin (γ-CD), C_{10}-L-$(EO_{200}$-L$)_4$-C_{10}/γ-CD, C_{10}-L-$(EO_{200}$-L$)_4$-C_{10} second wash, and C_{10}-L-$(EO_{200}$-L$)_4$-C_{10} (C_{10}-HEUR) first wash. Measurements were carried out at 25°C.

D.2. Sodium dodecyl sulphate (SDS)

SDS was purchased from Aldrich. SDS is produced by esterification of lauryl alcohol (dodecanol) with sulphuric acid followed by neutralization with NaOH (3). SDS could be contaminated with dodecanol as a result of SDS hydrolysis. The presence of dodecanol in SDS sample is usually identified by the presence of a minimum in surface tension curve just prior to the CMC, *e.g.* Figure D.8. The dodecanol is more surface active than SDS thus it adsorbs at the liquid/air interface and the surface tension decreases. When micelles are formed in solution dodecanol becomes solubilised into the hydrophobic core and SDS substitutes the alcohol at liquid/air surface, reflected by an increase in the surface tension. The purity of the SDS was checked by measuring the surface tension as a function of ln SDS concentration the absence of minimum and the correct CMC value,

Appendix D.

0.22 wt% or 8 mM at 25 °C in deionized water(4), suggests the purity of the sample, Figure D.9.
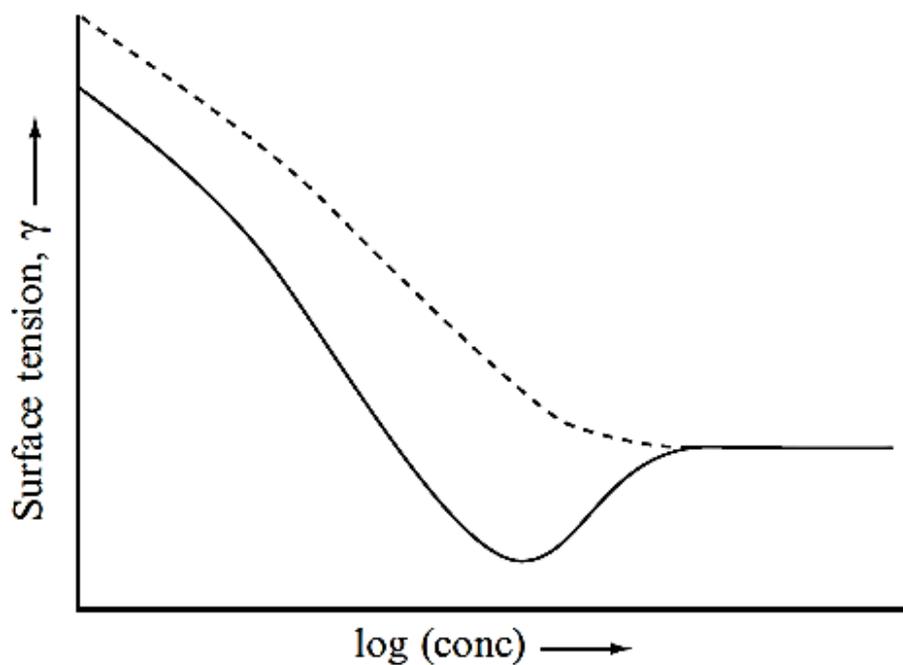
Figure D.8. Surface tension (γ) of SDS in presence (solid line) and absence (dashed line) of dodecanol as a function of SDS concentration (4).

Appendix D.
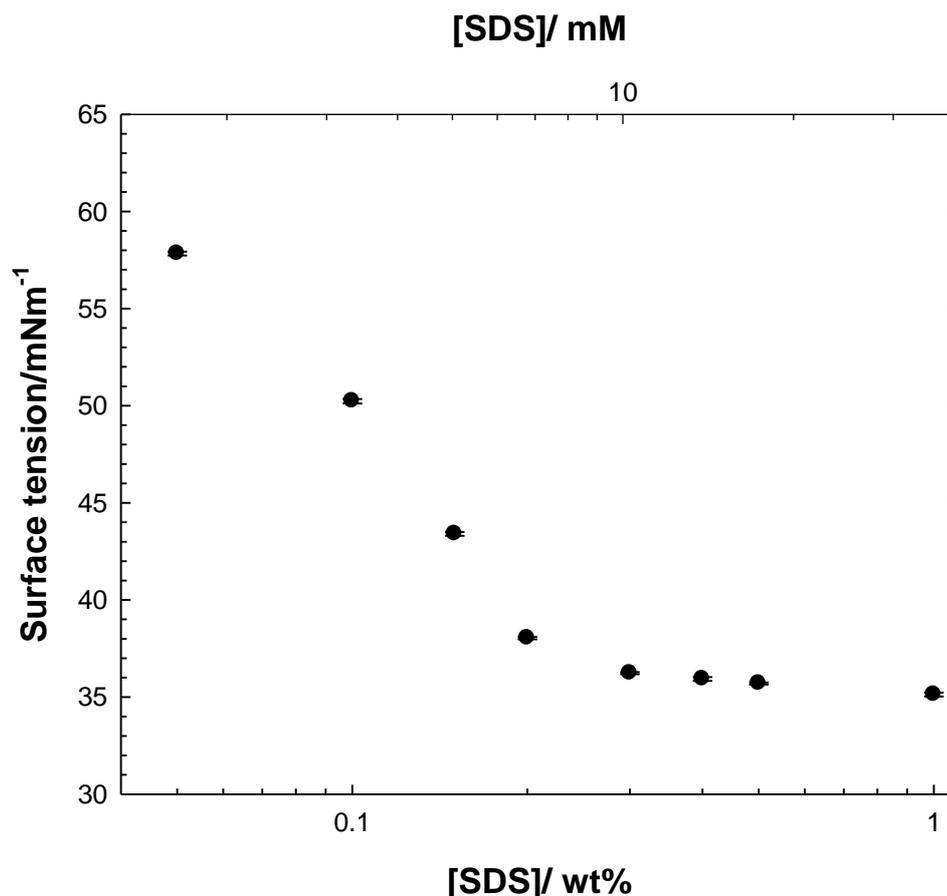
Figure D.9. Surface tension (γ) of SDS in deionized water as a function of SDS concentration showing the CMC of SDS at 0.22 wt%, which is equivalent to 8 mM, indicative of the purity of sample and absence of dodecanol contamination. Measurements were carried out at 25°C.

D.3. References

1. Najafi F, Pishvaei M. Synthesis and characterization of nonionic urethane based linker. *Prog Color Color Coat.* **2011**;*4*:71–77.

2. Barmar M, Barikani M, Kaffashi B. Synthesis of ethoxylated urethane and modification with cetyl alcohol as thickener. *Iran Polym J.* **2001**;*10*(5):331–335.

3. PubChem Compound Database. Available from: https://pubchem.ncbi.nlm.nih.gov/compound/Sodium_dodecyl_sulfate#section=Top, (accessed January 2017).

4. Jonsson B, Lindman B, Holmberg K, Kronberg B. Surfactants, and Polymers in Aqueous Solution. Chichester,UK:*Wiley*;**1998**.

Appendix E.

E. Techniques

E.1. Nuclear magnetic resonance (NMR)

For an atom to be NMR active it should have a nuclear spin quantum number of ½, -½ or multiples thereof. Generally, molecules have a magnetic moment, therefore, when an external magnetic field is applied the molecules arrange themselves with or against the external magnetic field. For NMR to occur the nucleus has to change spin state by absorption of a quantum of energy (radio frequency) which matches the Larmor frequency. The number of spins in each state will return to the equilibrium population upon cessation of the radio frequency pulse (1,2).

The molecules can relax by the interaction between the nucleus and surroundings and the equilibrium magnetization is restored in the z-axis direction, this is known as spin-lattice or longitudinal relaxation. The time required for the nucleus to restore equilibrium magnetization in the z-axis is known as T_1. If the nuclei relax by exchanging the energy amongst themselves without loss of energy to the surrounding, this relaxation is known as spin-spin or transverse relaxation. It is characterised by T_2, where T_2 is the decay of the phase coherence of magnetization formed in the x-y phase (3).

E.1.1. Solvent relaxation NMR spectroscopy

This technique is based on measuring the relaxation of protons in water molecules within a sample. The protons of the water molecules bind to the surface of particles and show a restricted motion compared with the atoms in the bulk, hence the efficiency of the relaxation is improved. As the concentration of discrete particles increases, the surface area available for water molecules to bind to also increases, hence more relaxation enhancement is observed. Therefore, this technique can be used to study the changes of the particle surface area at a fixed concentration, *i.e.* aggregation or enhanced dispersion of the particle. The adsorption of a polymer to the particles can enhance the relaxation of the water molecules due to the entrapment of water molecules between the adsorbed polymer layer and the particle surface, Figure E.1 (3).
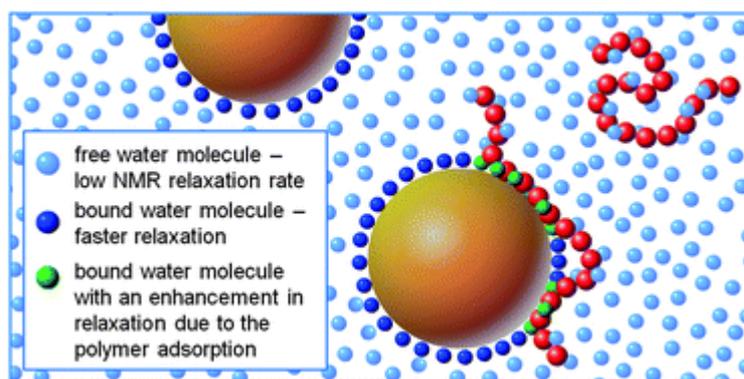
Figure E.1. Illustration of the relaxation of the water molecules in the bulk, bound to particles and entrapped between adsorbed polymer layer and particles (3).

If the exchange between the solvent molecules adsorbed at the surface and those in the bulk is slow compared to the measurement time, a multi-exponential decay of the signal is observed hence two relaxation rates are present. However, a single exponential decay is observed if the exchange is fast and the observed relaxation rate is an average rate (3).

To measure the T_2 a Carr-Purcell-Meiboom-Gill (CPMG) pulse sequence is used to reduce the effect of diffusion. A 90° pulse is applied where the magnetization is tipped to the *x-y* plan, followed by a train of 180° pulses to measure the T_2, Figure E.2 (4).
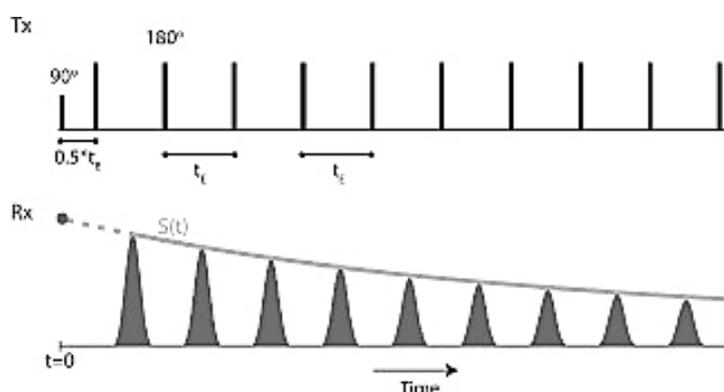
Figure E.2. CPMG pulse sequence, the top panel shows the transmitted pulses timing, the bottom panel shows the received NMR echo signals, and the grey line illustrates the signal decay (5).

The relaxation time can be determined from the signal decay as a function of time from Equation E.1:

$$M_y(t) = M_y(0)e^{\left(-\frac{t}{T_2}\right)}$$
<div align="right">Equation E.1</div>

where $M_y(t)$ is the magnetization at a specific time, $M_y(0)$ the transverse magnetization after 90° pulse, t the time in ms and T_2 the transverse relaxation.

Appendix E.

The relaxation rate for two water environments with fast (T_{2f}) and short (T_{2s}) relaxation time in a sample that shows a fast exchange between the two environments can be described by Equation E.2:

$$\frac{1}{T_2} = \frac{1-P_b}{T_{2f}} + \frac{P_b}{T_{2s}}$$
Equation E.2

where T_2 is the transverse relaxation, $1-P_b$ the water environment that has the fast relaxation time T_{2f}, and P_b the water environment with the slow relaxation time T_{2s} (4). The average relaxation rate (R) of the protons can be calculated from T_2,

$$R = \frac{1}{T_2}$$
Equation 3

A more convenient way of presenting the data is to calculate the specific relaxation rate (R_{2sp}) by normalizing the relaxation rate of the sample (R_2) to the solvent (R_2^0),

$$(R_{2sp} = \frac{R_2}{R_2^\circ} - 1)$$
Equation 4

E.1.2. Pulsed-Gradient Spin-Echo Nuclear Magnetic Resonance (PGSE-NMR)

Diffusion NMR can be used to probe the size, shape, aggregation, encapsulation, complexation, and H-bonding. Self-diffusion coefficient (D_s) arises from the Brownian motion of molecules and measures the rate of mean square displacement of a molecule, therefore, has a unit of $m^2\,s^{-1}$. The Stoke-Einstein equation can be used to calculate the size of the molecule from the extracted D_s:

$$D_s = \frac{k_B T}{f}$$
Equation E.5

where D_s is the self-diffusion coefficient, k_B the Boltzmann constant, T the absolute temperature and f the friction factor. The friction factor for a sphere can be described by Equation E.6:

$$f = 6\pi\eta r$$
Equation E.6

the η is the viscosity of the sample, and r the sphere radius (1).

Field gradient function is used to encode the physical location of a molecule in solution to characterise its diffusion along the direction of the applied gradient field. This can be described by Equation E.7:

$$B(r) = B_0 + \gamma G(r)$$
Equation E.7

Appendix E.

where *B(r)* is the effective field in the presence of field gradients, B_0 the static field strength and γ the gyromagnetic ratio, *G(r)* the applied magnetic field-gradients that encodes into the NMR signal the position of the molecule (*r*) (6).

The PGSE-NMR sequence involves applying 90° pulse, after which the net magnetization is tipped in the *x-y* plane, after which a gradient is then applied to defocus (dephase) the spins. Another 90° pulse is applied to tip the magnetization to the *z* axis. Finally, the magnetization returns to the *x-y* plane by a third 90° pulse. The sample is refocused by application of a second identical gradient pulse and then the acquisition of signal occurs, Figure E.3. Therefore, if a molecule diffuses in the time Δ, the signal will partially refocus as the molecule is experiencing a different gradient.
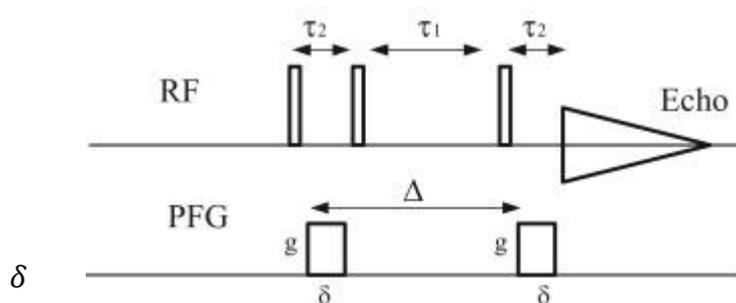
Figure E.3. Pulsed-Gradient Spin-Echo Nuclear Magnetic Resonance (PGSE-NMR) sequence (7).

To measure diffusion rates, it is possible to increase the diffusion time (Δ), the length of the gradient pulse (δ) or the gradient strength (*G*). Increasing the Δ allow more time for the molecules to move within the samples, whilst increasing δ or *G* increases the signal dephasing across the sample. The signal decay is plotted as a function of the gradient parameter *K* ($K = \gamma^2 G^2 \delta^2 \left(\Delta - \frac{\delta}{3}\right)$) and the diffusion is extracted from the slope of the curve. The intensity of the signal is correlated to diffusion using Equation E.8:

$$I = I_0 \, e^{-D_s \gamma^2 G^2 \delta^2 \left(\Delta - \frac{\delta}{3}\right)} \qquad\qquad \text{Equation E.8}$$

where I_0 is the signal intensity in absence of gradient pulses, D_s the diffusion coefficient, γ the gyromagnetic ratio of protons, *G* the gradient, Δ the diffusion time, and δ the pulse duration (1).

Appendix E.

E.2. Small angle neutron scattering

The aim of a small-angle neutron scattering (SANS) experiment is to determine the shape and organization, averaged in time, of particles or aggregates dispersed in a continuous medium (8). The schematic representation of a small-angle scattering experiment is illustrated in Figure E.4.
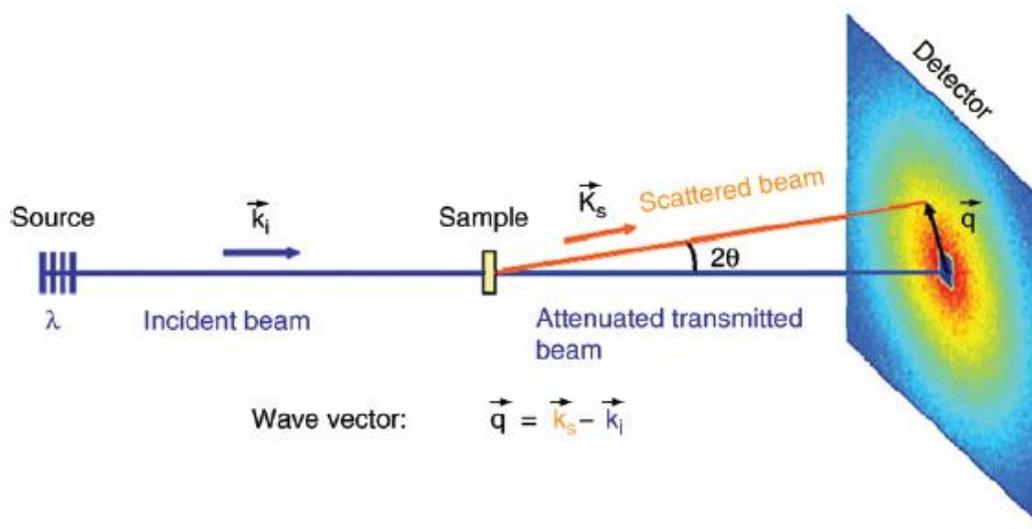
Figure E.4. schematic representation of a scattering experiment and representation of the scattering vector *q* in the detector plane (9).

The neutron beam can be viewed as an assembly of particles flying at the same speed in parallel directions. In SANS, only the coherent elastic interaction between the neutron beam and the sample is considered, such that the variable is the direction of the wave vector k_s.

The scattering vector q is the difference between incident and scattered wave vectors ($q = k_s − k_i$). By definition, the angle between k_s and k_i is called 2θ. The magnitude of q quantifies the lengths in the reciprocal space and is expressed in $Å^{-1}$ or nm^{-1}

$$q = \frac{4\pi}{\lambda} sin\theta \qquad \qquad \text{Equation E.9}$$

where λ is the wavelength of the beam, and θ the scattering angle. If Equation E.9 is introduced in the Bragg law ($\sin \theta = n\lambda/2d$) n is an integer, Equation E.10 is obtained:

$$q = \frac{2\pi}{d} \qquad \qquad \text{Equation E.10}$$

This simple relation links the lengths in direct (*d*) and reciprocal spaces and allows the definition of the observation window during the experiment. The intensity of scattering of

neutrons is correlated to the number of scattering species N_p, volume of scattering species V_p, difference of scattering length density between molecules and the solvent $\Delta\rho$, form factor $P(q)$, structure factor $S(q)$, and B_{inc} incoherent background (9):

$$I(Q) = N_p V_P^2 \Delta\rho^2 P(Q)S(Q) + B_{inc} \qquad\qquad \text{Equation E.11}$$

E.2.1. Scattering length density (SLD) and contrast variation

The degree of interaction between the neutron and a molecule consisting of atoms, i, is given by the scattering length density ρ:

$$\rho = \sum_i b_i \left(\frac{\delta N_A}{M_W}\right) \qquad\qquad \text{Equation E.12}$$

where b is the scattering length, δ the bulk density, N_A the Avogadro's number and M_W the molecular weight of the scattering species. The contrast is the difference in ρ value between the molecule of interest ρ_p, and the surrounding medium ρ_m squared *i.e. $(\Delta\rho)^2$.* So if this equals zero there is little/no SANS and the scattering bodies are said to be contrast-matched. The contrast term is very useful as different isotopes have different scattering length densities. The scattering length densities of hydrogen and deuterium exhibit a large difference in their ρ values. The scattering length of H_2O is -0.56×10^{10} cm^{-2} and D_2O 6.38×10^{10} cm^{-2}. This makes it very easily to distinguish proton-containing hydrocarbon material dissolved in D_2O. If the level of H/D substitution is controlled in the system it is possible to resolve different parts of a multi-component system by contrast variation (10).

E.3. Electron-paramagnetic resonance

The EPR is used to study materials with unpaired electrons. However, if the sample does not have an unpaired electron (*e.g.* polymers and surfactants) a stable free radical probe can be used. One of the most commonly used probes is the 16-doxylstearic acid methyl ester (16-DSE), Figure E.5, which has a surfactant-like structure. 16-DSE is water-insoluble, hence has no EPR signal in water. However, in presence of hydrophobic aggregates of the polymer or surfactant micelle the probe is solubilised in the hydrophobic core giving an EPR signal (11,12).

Appendix E.
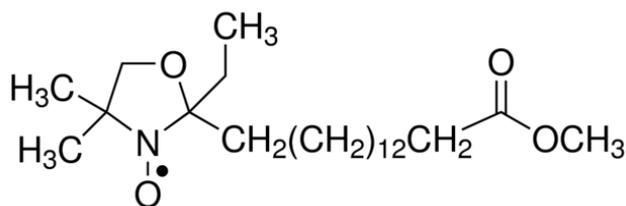
Figure E.5. Structure of 16-doxylstearic acid methyl ester (16-DSE).

E.3.1. Rotational correlation times

The rotational correlation time (τ_c) and micropolarity are determined from the analysis of the EPR spectra, where it can be calculated from Equation E.13:

$$\tau_{c\,uncorrected} = 6.6 * 10^{-10} \Delta H_\circ \left[\sqrt{\left(\frac{V_0}{V_{-1}}\right)} + \sqrt{\left(\frac{V_0}{V_{+1}} - 2\right)} \right] \quad \text{Equation E.13}$$

where ΔH_0 is the overall line-width of the central line, *V -1, 0, 1* are the peak-to-peak intensities of the high-, middle- and low-field lines, respectively. Alternatively, Equation E.14 can be used to calculate the approximation:

$$\tau_{c\,uncorrected} = 6.6 * 10^{-10} \Delta H_\circ \left[\sqrt{\left(\frac{V_0}{V_{+1}}\right)} + \sqrt{\left(\frac{V_0}{V_{-1}}\right)} \right] \qquad \text{Equation E.14}$$

The superscript "*uncorrected*" in Equations E.13 and E.14 refers to the fact that the lines are not a perfect Lorentzian or Gaussian distribution, therefore, a Voigt approximation is used to correct the equations (11,12). This correction is applied in the Lowfit program used to fit the data in Chapter 2.

E.3.2. Polarity determination

The polarity is determined by the magnetic interaction between the electron and nuclear spins of the neighboring atoms. The ^{14}N in the aminoxyl free radical has three spin states (m = 1, 0, -1), hence three lines are observed in the spectrum. Half the separation of the low and high field peak determines the hyperfine coupling constant. The hyperfine coupling constant varies according to the polarity sensed by the probe due to the shifting in the aminoxyl radical form. In polar solvents, form 1 of the aminoxyl radical is stabilised, however, as the probe is solubilized in the hydrophobic aggregates form 2 is formed, Figure E.6. Therefore, information regarding polarity experienced by the probe can be revealed (11,12).

Appendix E.
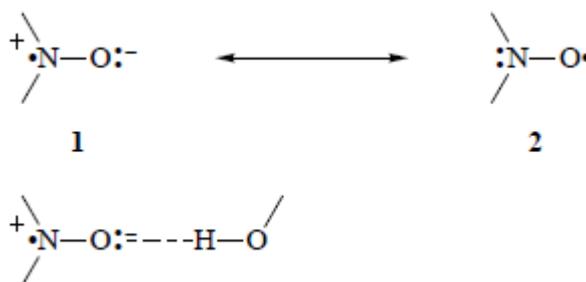
Figure E.6. Scheme illustrating the two forms of the probe aminoxyl group (11)**.**

E.4. Fluorescence Spectroscopy

Fluorescent compounds usually have one or more aromatic group (fluorophore). Fluorescence occurs during molecular relaxation from electronic excited states. These photonic processes involve a transition between electronic and vibrational states of the fluorescent molecule. If the molecule does not carry a chromophore a fluorescent probe can be added to the sample *e.g.* 8-anilinonapthalene-1-sulphonic acid (ANS) dye. ANS is a dye used to assess surface hydrophobicity as it is very weakly fluorescent in water but more fluorescent in presence of apolar solvent or hydrophobic surface (13).

ANS can undergo twisted intramolecular charge transfer (TICT) where a charge transfer from the electron donating amino-aryl group to the sulfonated naphthalene group with a subsequent twist of the molecule. The high polarity of the structure after the TICT favors its formation in the polar environment resulting in a low quantum yield of fluorescence. The ANS fluorescence is sensitive to viscosity and temperature change, the TICT decreases in high viscosity media which in turn increases the ANS fluorescence. On the other hand, an increase of temperature enhances the loss of energy by a non-radiative vibrational process which decreases the ANS intensity (13,14).

E.5. Maximum bubble pressure tensiometer

The maximum bubble pressure tensiometer is a useful tool to study the surface tension of solutions. Air bubbles are produced by the tensiometer at a constant controlled rate through a capillary with a known radius. As the air bubble is produced at the tip of the capillary in the sample, the curvature increases initially, to the point where a maximum in the pressure is observed, the bubble curvature then increases exponentially with time and the pressure inside decreases. Finally, the bubble detached from the capillary and another cycle starts. Pressure is converted to surface tension, using the Young-Laplace equation:

Appendix E.

$$P = \frac{2\sigma}{r}$$
<div align="right">Equation E.15</div>

where P is the internal pressure of the bubble, σ surface tension, and r the radius of curvature. As the capillary is immersed in the liquid, the hydrostatic pressure P_0 resulting from the immersion depth and the density of the liquid must be subtracted. Therefore, Equation E.15 is modified to Equation E.16:

$$\sigma = \frac{(P_{max} - P_0).r}{2}$$
<div align="right">Equation E.16</div>

where the r in Equation E.16 is the radius of the capillary. The measured value corresponds to the surface tension at a certain bubble lifetime, the time from the start of the bubble formation to the occurrence of the pressure maximum (15).

E.6. References

1. Claridge TDW. High-Resolution NMR techniques in organic chemistry. Second Edition. Oxford,UK:*Elsevier*, **2009**.

2. Horst Friebolin. Basic One and two Dimention NMR spectroscopy. Fifth Edition. Heidelberg,Germany:*Wiley*; **1990**.

3. Cooper CL, Cosgrove T, Duijneveldt JS Van, Murray M, Prescott SW. The use of solvent relaxation NMR to study colloidal suspensions. *Soft Matter*. **2013**;*9*(30):7211–7228.

4. Larsen FH, Jakobsen HJ, Ellis PD, Nielsen NC. Sensitivity-enhanced quadrupolar-echo NMR of half-integer quadrupolar nuclei. Magnitudes and relative orientation of chemical shielding and quadrupolar coupling tensors. *J Phys Chem A*. **1997**;*46*(101):8597–8606.

5. Walsh D, Turner P, Grunewald E, Zhang H, Bulter J, Reboulet E, Knobbe S, Christy T, Lane JW, Johnson CD, Munday T, Fitzpatrick A. A small-diameter NMR logging tool for groundwater investigations. *Groundwater*. **2013**;*51*(6):914–926.

6. Occhipinti P, Griffiths PC. Quantifying diffusion in mucosal systems by pulsed-gradient spin-echo NMR. *Adv Drug Deliv Rev*. **2008**;*60*(15):1570–1582.

7. Hayamizu K, Matsuda Y, Matsui M, Imanishi N. Lithium ion diffusion measurements on a garnet-type solid conductor $Li_{6.6}$ La_3 $Zr_{1.6}$ $Ta_{0.4}$ O_{12} by using a pulsed-gradient spin-echo NMR method. *Solid State Nucl Magn Reson*. **2015**;*70*:21–27.

Appendix E.

8.   Zemb T, Linder P. Neutrons, X-rays and light scattering methods applied to soft condensed matter. First edition. North Holland: *Elsevier*; **2002**.

9.   Grillo I. Small-angle neutron scattering and applications in soft condensed matter. Berlin, Germany: *Springer-Verlag*; **2008**.

10.   Crichton RR, Engleman DM, Haas J, Koch MH, Moore PB, Parfait R, Stuhrmann HB. Contrast variation study of specifically deuterated Escherichia coli ribosomal subunits. *Proc Natl Acad Aci USA*. **1977**;*74*(12):5547–5550.

11.   Griffiths PC, Rowlands CC, Goyffon P, Howe AM, Bales BL. EPR insights into aqueous solutions of gelatin and sodium dodecyl sulfate. *J Chem Soc Perkin Trans. 2*, **1997**;*0*(12): 2473-2478.

12.   Persson K, Bales BL. EPR study of an associative polymer in solution: determination of aggregation number and interactions with surfactants. *J Chem Soc Faraday Trans*. **1995**;*91*(17):2863.

13.   Hawe A, Sutter M, Jiskoot W. Extrinsic fluorescent dyes as tools for protein characterization. *Pharm Res*. **2008**;*25*(7):1487–1499.

14.   Gasymov OK, Glasgow BJ. ANS fluorescence: potential to augment the identification of the external binding sites of proteins. *Biochim Biophys Acta - Proteins Proteomics*. **2007**;*1774*(3):403–411.

15.   Mandy P, Sharma HK. An investigation of the different application and techniques of maximum pressure tensiometer. *J of Adv in Sci and Tech.* **2011**;*II*(II):1-6.